日中笹川医学奨学金制度(学位取得コース)評価書
課程博士：指導教官用

第 43 期　　研究者番号：G4304　　作成日　：2023 年 3 月 10 日

氏　名	張 茂芮	Zhang　Maorui	性別	F	生年月日　1993.06.23
所属機関（役職）	西南医科大学附属口腔医院インプラント科（医師）				
研究先（指導教官）	東京医科歯科大学大学院医歯学総合研究科口腔機能再構築学講座生体補綴歯科学分野（若林　則幸教授）				
研究テーマ	歯科疾患に対する mRNA を用いた治療戦略の確立 Establishment of mRNA therapy for dental disease				
専攻種別	□論文博士		☑課程博士		

研究者評価（指導教官記入欄）

成績状況	優 学業成績係数=3．75	取得単位数 30／30
学生本人が行った研究の概要	本研究は，歯科口腔外科・歯周外科分野において，大規模に骨欠損を生じた症例における効率的な骨再生を促進する治療方法を提案するために，①mRNA を用いて投与する骨誘導治療因子の選定および最適化,②ラットを用いた動物モデルにおける骨再生治療効果を明らかにすることを目的としている． 本年度は，ラット顎骨にクリティカルサイズの骨欠損を作製し，前年度に最適化した 2 種の骨誘導治療因子を投与し，骨再生の促進を検討した．初めに投与するキャリアの部位および経時的代謝を評価するために，Gluc mRNA を内包するキャリアを投与したところ，投与した骨欠損部に一致した発光を認め，96 時間まで持続した発現を認めた．次に 2 種の治療因子を投与し骨形成量をマイクロ CT により評価を行った．投与 1 週間後では骨増生は認められなかったが，投与 2 週間後より母床骨より骨再生が生じた．また，単一因子の投与と比較して，2 種の因子を同時に投与した際に有意に骨再生の促進が認められた．このことは，複数の治療因子を同時投与することにより治療の短期間化が望めることを示唆している．	
総合評価	【良かった点】 本年度は，昨年度行った in vitro の実験を発展させ，臨床応用に向けた in vivo の実験を行った．動物事件に関わる研究スキルの習得と実験データの解析を行い，十分な研究活動を行ったと評価できる．また，論文作成にあたり，十分な過去の知見を引用しながら自分の考えと新たな知見を記載できたことは特筆すべき点であると考える．また，研究室の移動に伴い，新たなチームとも協調性をもって活動することができ，十分な討論も行っている． 【改善すべき点】 今後，自立した研究者として活躍するためには，後輩への教育も必要と考えられる．現在の所，直接指導する後輩がいないため難しいが，次年度以降に学生が配属されるため，教育係としても活躍を期待している． 【今後の展望】 治療因子の投与による骨再生の促進が達成されたが,他の手法による骨再生速度と比較すると，未だ十分でない事が問題とされる．治療因子の生体内での拡散が原因の一つとして考えられるため，新たなキャリアや東洋方法の検討など，次年度より新たな実験を開始する予定である．	
学位取得見込	研究は順調に進捗しており，本学が定める学位取得の単位も到達している．論文執筆が完了し，本年度中に学術雑誌への投稿を予定しており，十分に学位取得の要件を満たすと考える．	
	評価者　若林　則幸	

日中笹川医学奨学金制度(学位取得コース)報告書
研究者用

第43期　　研究者番号: G4304　　作成日:2023年 2 月 28 日

氏名	張 茂芮	ZHANG　Maorui	性別	F	生年月日 1993. 06. 23
所属機関(役職)	西南医科大学附属口腔医院インプラント科(医師)				
研究先(指導教官)	東京医科歯科大学 大学院医歯学総合研究科 口腔機能再構築学講座 生体補綴歯科学分野(若林　則幸 教授)				
研究テーマ	骨誘導因子Runx2 mRNAとVEGF mRNA医薬を用いた顎骨再生 Co-delivery of VEGF and RUNX2 Messenger RNA by Polyplex Nanomicelles improves the process of mandibular bone regeneration				
専攻種別	論文博士	☐	課程博士	☑	

1. 研究概要(1)

1）目的（Goal）

The combine use of different kinds of osteogenic proteins (Runx2 and VEGF) may have some positive implications on the treatment of bone regeneration who suffers from bone fractures and bone defects. Using Runx2 and VEGF for bone repair and regeneration is feasible for mRNA delivery treatment strategies in future. The objective of this study is to explore whether local delivering of Runx2 and VEGF mRNA would enhance mandibular defects repair of rat by in vivo and in vitro study. From this study, I hope to find evidence that Runx2 and VEGF mRNA promote bone repair and provide reliable experimental results for mRNA treatment in the field of bone regeration.

2）戦略（Approach）

From the literature reviews, there are a lot of evidences that Runx2 and VEGF are important promoters of osteogenic differentiation[1,2]. But the intrinsic interactions among Runx2 and VEGF in bone regeration still needs to be well documented. In this study, I plan to use mRNA encoding Runx2 and VEGF sequences as the method of osteogenic factor transmission, establish an mandibular defect model of SD rat, and explore the effect of Runx2 and VEGF mRNA on bone repair. By comparing the different effects of two factors and their combination of mRNA on mandibular bone defect using histological and molecular biological analysis, I want to find one candidate one mRNA or one mRNA pair which has the most effective osteo-induction effect.

3）材料と方法（Materials and methods）

Materials: VEGFa165 mRNA, Runx2 mRNA, Gluc mRNA, Luc2 mRNA, pladmid, Lipofectamin MessengerMAX, Renilla-Glo™ Luciferase Assay System, NIPPON GENETICS mRNA extraction, TOYOBO Reverse transcription kit, GeneAce SYBR® qPCR Mix α, PEG-PAspDET(43-63) polymer, Hepes aqueous solution, Masson golden staining, CD-31 antibody, ALP antibody, OCN antibody, 8-week-old male SD rat, low speed minimotor and handpiece, 4-mm circle drill, micro-CT, n vivo imaging system(IVIS).

Methods:

a) mRNA transfection Lipofectamin MessengerMAX: Seeding primary-osteoblasts(POBs) to be 70% confluent at transfection at day0. 24 hours later, dilute MessengerMAX Reagent(5μl) in Opti-MEM Medium(175μl) and prepare diluted mRNA master mix by adding mRNA(2μg) to OptiMEM Medium(175μl). Then mixing diluted mRNA to each tube of Diluted MessengerMAX Reagent(1:1 ratio). Finally, change the medium 24 hours later.

b) Gluc expression analyze: Add 100μl of Renilla Luciferase Assay Reagent to the luminometer tube. Add 20μl of cell lysate. Mix quickly by flicking the tube or vortexing for 1-2 seconds.Place the tube in a luminometer and initiate measurement. Luminescence should be integrated over 10 seconds with a 2-second delay. Other integration times may be used. If the luminometer is not connected to a printer or computer, record the Renilla luciferase activity measurement.

c) Runx2 and VEGF mRNA transfetion: P4-primary cells are seeding into 6-well-plate(1×10^5 cells/well)，group setting：A-only medium, B-Lipofectamine+Luc2, C-Lipofectamine+RUNX2, D-Lipofectamine+VEGF, E-Lipofectamine +RUNX2 (1 μg/well)+VEGF(1 μg/well),F-Lipofectamine+osteogenic medium.

d) Realtime PCR: mRNA extraction by fastGene™ RNA Basic Kit. Reverse transfection the RNA by ReverTra AceTM qPCR RT Master Mix kit.Target gene(ocn and opn) are anlyzed by real-time qPCR using SYBR Green I dye method. All the data are calculated by 2ΔΔCT method.　　e)

Mandiblular defect: 8-week-old male rats are conducted mandibular defect surgery(4mm defect hole) under anesthesia.

f) IVIS: Luc2 mRNA(10μg)+PEG-PAspDET(43-63) polymer with total 50μl volume is injected into mandibular defect area. 4h, 24h, 48h, 72, 96h, 1week after injection, Luciferase expression is imaged by IVIS.

g) Runx2 and VEGF mRNA in vivo treatment: group: A-Hepes solution, B-Runx2(10μg), C-VEGF(10μg), E-RUNX2 (10μg)+VEGF(10μg), from post-surgury 1week, conduct mRNA injection treatment every week.

h) micro-CT: post-surgury 4week, conduct microCT to analyze the bone mineral density and bone volume for new bone formation.

i) Immunofluorescence staining: 8week mandibular samples are collected to making frozen slides, then using CD-31 antibody to mark the angeogenesis and ALP and OCN antibody to mark the osteogenesis of the bone defect area by immunofluorescence staining.

1．研究概要(2)

4)実験結果(Results)

a) mRNA synthesis and validity verification: western blot image showed that Runx2 and Vegf mRNA made in our lab successfully produced protein in Hela cells (Figure1a). successful Gluc mRNA transfection: Gluc expression curve demonstrated that the mRNA expression peaked at 24 hours post-transfection and gradually decrease with time.

b) Runx2 mRNA and VEGF mRNA promoted the osteogenic markers in vitro: After transfected with mRNA in different groups,the RT-PCR results showed that expression of osteoprotin and osteocalcin were relatively highest in RUNX2+VEGF group, while using RUNX2 or VEGF mRNA alone weakly stimulates osteogenic differentiation compared with blank group and Luc2 group(Figure 1d-f). The β-catenin, Lef1, and Osterix mRNA expression at 7 days also showed a slight increase in Runx2 mRNA/VEGF mRNA transfection group than the Blank and Luc2 group. These in vitro data revealed that the use of Runx2 mRNA or VEGF mRNA alone only upregulated the expression of OCN at 11 days.

d) PEG-PAsp(DET)-nanomicelles successfully delivered Luc2 mRNA into target area: IVIS observed tha luciferase signal 4 hours after Luc2 mRNA injection. The images demonstrated the luciferase expression peaked at 24 h then decreased with time. The distribution of ZsGreen1 from microscopic images verified that ZsGreen1 mRNA-loaded by polyplex nanomicelles was nonspecifically delivered into multiple cells in vivo. And the ZsGreen1 signal was dispersed in the mandibular defect area.

e) mandibular defect model identification and mRNA treament by microCT: 3D construction image showed a clear⌀4mm-circle bone defect was established. The results showed local co-administration of Runx2/VEGF mRNA accelerated the new bone regeneration and bone mineralization in the early phase of mandible bone healing. After the first mRNA injection, the new bone tissue was observed in the Runx2 mRNA group, VEGF mRNA, and Runx2/VEGF mRNA group, and the process of bone regeneration continued after weekly administration. The ROI of mandible defect showed a large amount of new bone tissue was produced in the Runx2/VEGF mRNA group, followed by VEGF mRNA group.

5）考察（Discussion）

The combination of Runx2 and VEGF mRNA treatment in bone tissue regeneration is an exploration of an mRNA-based therapeutic strategy. In this study, Runx2 and VEGF mRNA transfection enhanced the expression of osteogenic differentiation genes in osteoblasts, which was confirmed by in vitro experiments. The subsequent in vivo animal experiments provided strong evidence that co-delivery of Runx2 and VEGF mRNA by polyplex nanomicelles accelerated mandibular defect healing and enhanced new bone formation over the Runx2 or VEGF mRNA single-administration groups. The morpho-histological analyses of ALP, OCN, and CD31 proteins expression revealed that osteogenesis and angiogenesis coupling was activated by co-administration in the early phase of bone repair. Our in vitro and in vivo results substantiated that the co-administration of Runx2 and VEGF mRNA has the advantage of synergistic effect on bone tissue regeneration and osteogenesis and angiogenesis coupling compared with the single factor administration within a mandibular defect model. In the complicated bone healing period, not only bone mesenchymal progenitors and osteoblasts lineages but also endothelial progenitors are recruited into the bone defect area, and the cellular interactions between different types of cells participate in the process of osteogenesis and angiogenesis[3]. Based on this concept of co-administration therapy, our study provides a feasible approach to add more candidates of osteogenic factors for combination therapy in bone regeneration medicine.

The mRNA delivery achieves the combined administration of Runx2 and VEGF in the mandible defect area based on its characteristics of efficiently, low cost, and safely stimulating cells to produce activity proteins. As a protein-replacement therapy, IVT mRNA is designed to be structurally similar to those that occur naturally in eukaryotic cells and stimulates cells to produce the target bioactive protein, which overcomes the difficulties such as the high cost of artificial recombinant protein synthesis and strict manufacturing conditions[4]. And it is also easy to evaluate the optimal dose by adjusting different mRNA doses and dosage ratios, hence achieving better efficacy in bone regeneration treatment.[5].

mRNA therapeutics have made rapid progress in the fields of cancer immunotherapies and infectious disease vaccines in recent years, but their application in bone tissue regeneration is still in its infancy. In our study, the dose ratio and administration time of Runx2 and VEGF mRNA in the treatment of mandibular defects need to be further optimized. And the mechanism of synergistic effect between RUNX2 and VEGF mRNA in osteogenesis and angiogenesis coupling also requires our in-depth exploration. Although this study has some limitations, the successful application of co-delivery Runx2 and VEGF mRNA for early bone healing in our research has expanded the idea of mRNA medicine. Our results provide a reliable experimental basis for the treatment of bone regeneration based on mRNA administration and support the feasibility of mRNA-loaded polyplex nanomicelles drugs for bone regeneration.

6）参考文献（References）

[1] Komori T. R. International journal of molecular sciences. 2019;20
[2] Hu K，Olsen BR. Bone. 2016;91:30-38.
[3] Liu WC CS, Zheng L, et al. Adv Healthc Mater. 2017;6(5);1600434.
[4] Sahin U, Karikó K, Türeci Ö. Nature Reviews Drug Discovery 2014; 13:759-780.
[5] Lee E KJ, Kim J, et al. Biomater Sci. 2019;7(11);4588-602.

2. 執筆論文 Publication of thesis ※記載した論文を添付してください。Attach all of the papers listed below.

論文名 1 Title	Metformin Rescues the Impaired Osteogenesis Differentiation Ability of Rat Adipose-Derived Stem Cells in High Glucose by Activating Autophagy				
掲載誌名 Published journal	Stem Cells and Development				
	2021 年 9 月	30 巻(号)	1017 頁 ～ 1027 頁	言語 Language	English
第1著者名 First author	Maorui ZHANG	第2著者名 Second author	Bo YANG	第3著者名 Third author	Shuanglin PENG
その他著者名 Other authors	Jingang XIAO				
論文名 2 Title	Downregulation of DNA methyltransferase-3a ameliorates the osteogenic differentiation ability of adipose-derived stem cells in diabetic osteoporosis via Wnt/β-catenin signaling pathway				
掲載誌名 Published journal	Stem Cell Research & Therapy				
	2022 年 8 月	13 巻(号)	397 頁 ～ 414 頁	言語 Language	English
第1著者名 First author	Maorui ZHANG	第2著者名 Second author	Yujin GAO	第3著者名 Third author	Qing LI
その他著者名 Other authors	Huayue CAO, Jianghua YANG, Xiaoxiao CAI, Jingang XIAO				
論文名 3 Title					
掲載誌名 Published journal					
	年 月	巻(号)	頁 ～ 頁	言語 Language	
第1著者名 First author		第2著者名 Second author		第3著者名 Third author	
その他著者名 Other authors					
論文名 4 Title					
掲載誌名 Published journal					
	年 月	巻(号)	頁 ～ 頁	言語 Language	
第1著者名 First author		第2著者名 Second author		第3著者名 Third author	
その他著者名 Other authors					
論文名 5 Title					
掲載誌名 Published journal					
	年 月	巻(号)	頁 ～ 頁	言語 Language	
第1著者名 First author		第2著者名 Second author		第3著者名 Third author	
その他著者名 Other authors					

3. 学会発表 Conference presentation ※筆頭演者として総会・国際学会を含む主な学会で発表したものを記載してください

※Describe your presentation as the principal presenter in major academic meetings including general meetings or international meetin

学会名 Conference	第22回日本再生医療学会総会								
演 題 Topic	mRNA Therapeutics for the Treatment of Mandibular Bone Defect: Co-administration of Runx2/VEGF mRNA								
開催日 date	2023 年	3 月	24 日	開催地 venue	京都 国立京都国際会館1階（Event Hall）				
形式 method	☐ 口頭発表 Oral	☑ ポスター発表 Poster		言語 Language	☐ 日本語	☑ 英語	☐ 中国語		
共同演者名 Co-presenter									
学会名 Conference									
演 題 Topic									
開催日 date	年	月	日	開催地 venue					
形式 method	☐ 口頭発表 Oral	☐ ポスター発表 Poster		言語 Language	☐ 日本語	☐ 英語	☐ 中国語		
共同演者名 Co-presenter									
学会名 Conference									
演 題 Topic									
開催日 date	年	月	日	開催地 venue					
形式 method	☐ 口頭発表 Oral	☐ ポスター発表 Poster		言語 Language	☐ 日本語	☐ 英語	☐ 中国語		
共同演者名 Co-presenter									
学会名 Conference									
演 題 Topic									
開催日 date	年	月	日	開催地 venue					
形式 method	☐ 口頭発表 Oral	☐ ポスター発表 Poster		言語 Language	☐ 日本語	☐ 英語	☐ 中国語		
共同演者名 Co-presenter									

4. 受賞（研究業績） Award (Research achievement)

名 称 Award name					
	国名 Country		受賞年 Year of award	年	月
名 称 Award name					
	国名 Country		受賞年 Year of award	年	月

5. 本研究テーマに関わる他の研究助成金受給 Other research grants concerned with your resarch theme

受給実績 Receipt record	■ 有　□ 無
助成機関名称 Funding agency	国立研究開発法人科学技術振興機構
助成金名称 Grant name	次世代研究者挑戦的研究プログラム[東京医科歯科大学卓越大学院生制度（Ⅱ）]
受給期間 Supported period	2021　年　10　月　～　2024　年　3　月
受給額 Amount received	月額16万 円
受給実績 Receipt record	□ 有　□ 無
助成機関名称 Funding agency	
助成金名称 Grant name	
受給期間 Supported period	年　月　～　年　月
受給額 Amount received	円

6. 他の奨学金受給 Another awarded scholarship

受給実績 Receipt record	□ 有　□ 無
助成機関名称 Funding agency	
奨学金名称 Scholarship name	
受給期間 Supported period	年　月　～　年　月
受給額 Amount received	円

7. 研究活動に関する報道発表 Press release concerned with your research activities

※記載した記事を添付してください。Attach a copy of the article described below

報道発表 Press release	□ 有　□ 無	発表年月日 Date of release	
発表機関 Released medium			
発表形式 Release method	・新聞　・雑誌　・Web site　・記者発表　・その他（　　）		
発表タイトル Released title			

8. 本研究テーマに関する特許出願予定 Patent application concerned with your research theme

出願予定 Scheduled	□ 有　□ 無	出願国 Application	
出願内容（概要） Application contents			

9. その他 Others

指導責任者（記名）　若林　則幸

STEM CELLS AND DEVELOPMENT
Volume 30, Number 20, 2021

DOI: 10.1089/scd.2021.0181

Metformin Rescues the Impaired Osteogenesis Differentiation Ability of Rat Adipose-Derived Stem Cells in High Glucose by Activating Autophagy

Maorui Zhang,[1–3,i] Bo Yang,[4] Shuanglin Peng,[1,2] and Jingang Xiao[1,2]

The incidence and morbidity of diabetes osteoporosis (DOP) are increasing with each passing year. Patients with DOP have a higher risk of bone fracture and poor healing of bone defects, which make a poor quality of their life. Bone tissue engineering based on autologous adipose-derived stem cells (ASCs) transplantation develops as an effective technique to achieve tissue regeneration for patients with bone defects. With the purpose of promoting auto-ASCs transplantation, this research project explored the effect of metformin on the osteogenic differentiation of ASCs under a high-glucose culture environment. In this study, we found that 40 mM high glucose inhibited the physiological function of ASCs, including cell proliferation, migration, and osteogenic differentiation. Indicators of osteogenic differentiation were all downregulated by 40 mM high glucose, including alkaline phosphatase activity, runt-related transcription factor 2, and osteopontin gene expression, and Wnt signaling pathway. At the same time, the cell autophagy makers BECLIN1 and microtubule-associated protein 1 light chain 3 (LC3 I/II) were decreased. While 0.1 mM metformin upregulated the expression of BECLIN1 and LC3 I/II gene and inhibited the expression of mammalian target of rapamycin (mTOR) and GSK3β, it contributed to reverse the osteogenesis inhibition of ASCs caused by high glucose. When 3-methyladenine was used to block the activity of metformin, metformin could not exert its protective effect on ASCs. All the findings elaborated the regulatory mechanism of metformin in the high-glucose microenvironment to protect the osteogenic differentiation ability of ASCs. Metformin plays an active role in promoting the osteogenic differentiation of ASCs with DOP, and it may contribute to the application of ASCs transplantation for bone regeneration in DOP.

Keywords: metformin, adipose-derived stem cells, autophagy, Wnt signaling pathway, GSK3β, osteogenic differentiation

Introduction

THE BONE TISSUE complication caused by a persistent high blood glucose of diabetes mellitus (DM) is called diabetic osteoporosis (DOP), which is characterized by bone loss, destruction of the bone microstructure, increased bone fragility, and high fracture risk [1]. Hyperglycemia is one of the main manifestations of DM patients, and the abnormal glucose metabolism in the internal environment leads to osteogenesis disorder in bone tissue. Literature showed that the number of mesenchymal stem cells and osteoblasts decreased, and the synthesis and secretion of regulatory factors of osteogenic differentiation were also impeded in DM [1,2]. The insufficient osteogenic differentiation and bone formation in DM made it difficult to repair and regenerate bone tissue. The poor bone healing and remaining bone defects in DOP patients after the bone defect or fracture leading to a decline in the quality of life of patients. So it is of great significance and urgent necessity to explore the treatment to improve the osteogenesis differentiation process in DOP.

In recent years, the induction of autologous mesenchymal stem cells for tissue regeneration and cell-based tissue-engineered bone provides a new therapy for promoting DOP bone defect repair. Adipose-derived stem cells (ASCs) are a type of adult mesenchymal stem cells from fat tissue that have a capacity for self-renewal [3]. ASCs can be directionally differentiated into osteogenesis, adipogenesis, and chondrogenesis, which have a wide application prospect in the research fields of bone regeneration, bone healing, and bone integration. Under somatic osteogenic induction conditions, ASCs differentiate into osteogenic precursors expressing genes and proteins related to osteogenic differentiation such

[1]Department of Oral Implantology and [2]Oral & Maxillofacial Reconstruction and Regeneration Laboratory, The Affiliated Stomatology Hospital of Southwest Medical University, Luzhou, People's Republic of China.
[3]Division of Oral Health Sciences, Department of Fixed Prosthodontics, Graduate School of Medical and Dental Sciences, Tokyo Medical and Dental University, Tokyo, Japan.
[4]Department of Anesthesiology, The Affiliated Hospital of Southwest Medical University, Luzhou, People's Republic of China.
[i]ORCID ID (https://orcid.org/0000-0002-1420-6515).

as runt-related transcription factor 2 (Runx2), osteopontin (Opn), DLX5, and Osterix. However, studies have proved that the internal environment disturbance caused by diabetic hyperglycemia had an impact on the metabolism of ASCs, leading to significantly impaired ASCs bone-orientation differentiation ability under the DOP microenvironment. However, the reasons for the osteogenic differentiation injury of ASCs in the diabetes microenvironment are not fully understood, and the treatment of bone repair and regeneration using autologous ASCs from DOP still needs further exploration.

Metformin (MF) is one of the first-line drugs for type 2 diabetes treatment. Recent studies presented that metformin maintained the stability of cell metabolism, activate autophagy, and also had a relieving effect on osteoporosis [4–6]. Autophagy is a process in which cells self-regulate and degrade intracellular macromolecules and damaged organelles. The cell degradation products are recycled by cell autophagy, which maintains the homeostasis of the intracellular environment [7]. Researchers found an increasing number of autophagic vesicles in femur tissue during postnatal development, while the femur and tibia were underdeveloped in $Fgf18^{+/-}$ transgenic mice [8]. Gao et al. demonstrated that metformin regulated the development of bone marrow cells and promoted the differentiation of bone marrow mesenchymal stem cells to osteogenesis by regulating the expression of Cbfa1, LRP5, and COL1 genes [9]. Although studies have shown that metformin promoted the osteogenic differentiation of mesenchymal stem cell lines, the regulatory mechanism of metformin on ASCs osteogenic differentiation under the high-glucose environment is still not clear, and the relationship between autophagy and ASCs osteogenic differentiation needs to be clarified.

Our previous study found that the DOP microenvironment significantly inhibited the osteogenic differentiation of ASCs; then, we want to further study the effect of metformin in the osteogenic differentiation process of ASCs. Therefore, in this project, rat ASCs from fat tissue were cultured in vitro and treated with high glucose, metformin, and 3-methyladenine (3-MA) to explore whether metformin can activate cell autophagy level to promote the process of bone orientation differentiation of ASCs, as well as the molecular mechanism and signaling pathway involved.

Materials and Methods

Isolation of ASCs

This animal research was approved by the Animal Ethics Committee of Southwest Medical University, Luzhou, China. All the procedures, including anesthesia, surgery, nursing, and euthanasia, were conducted according to the guidelines of the National Institutes of Health of China.

The Sprague-Dawley male rats were given general anesthesia. After removing the inguinal adipose tissue, the skin wound was sutured and resuscitated. The tissue sample was cultured by the tissue block culture method under aseptic conditions. First, adipose tissue was washed by phosphate-buffered solution (PBS; HyClone) containing 1% penicillin–streptomycin solution (FBS; HyClone). Then, it was carefully cut into mince and laid on the bottom of the culture flask. Next, we gently added alpha-modified eagle's medium (α-MEM; HyClone) medium containing 10% fetal bovine serum (FBS; HyClone), and cultured in an incubator in 5% CO_2 at 37°C for primary cell culture. The culture medium was changed every 3 days. The multilineage differentiation capacity of ASCs was proved by our previous article [10]. The cells were passed to third-generation for the following experiments.

Cell proliferation analysis after reagents treatment

Cell Counting Kit-8 (CCK-8; Dojindo, China) was used to detect the toxicity of different glucose concentration of ASCs. The third-passage ASCs (5×10^4 cells/mL, 100 μL/well) were cultured in 96-well plates with α-MEM for 24 h. Then, ASCs were treated with different concentrations of glucose (10, 25, 50, 75, and 100 mM; MedChemExpress). After 48 and 96 h, we added a reagent of the CCK-8 into medium and incubated for 2–3 h. The optical densities of the incubated medium in different groups were measured at 450 nm by an automatic microplate reader (Spectra Thermo, Switzerland).

Cell wound healing assay

The third-passage ASCs (5×10^4 cells/well) were seeded into 6-well plates, and then, ASCs were treated with 40 mM glucose and 0.1 mM metformin (MedChemExpress) [11,12]. When the cell density reached 95%–100%, a 100 μL pipette tip (Thermo Scientific) was used to make a straight scratch in the center of each plate. Images were collected at 6-h intervals to observe the wound healing ability of ASCs.

Alizarin red-S staining

ASCs (5×10^4 cells/well) were seeded into 6-well plates and cultured in an osteogenic medium (Cyagen Biosciences, Inc.) with high glucose, metformin, and 3-MA. The components of osteogenic medium were as follows: basal medium (175 mL), FBS (20 mL), glutamine (2 mL), penicillin–streptomycin (2 mL), ascorbate (400 μL), β-glycerophosphate (2 mL), and dexamethasone (20 μL). After 21 days, the number of mineralized nodes with alizarin red stain was used to demonstrate the osteogenic differentiation ability of ASCs. After 21 days, PBS was used to wash cells thrice, and 4% paraformaldehyde was used to fix ASCs for 30 min. Then ASCs with mineralized matrix was stained with Alizarin red-S dye for 1 h and the images were collected by inverted light microscope (Olympus, Japan).

Alkaline phosphatase staining

After drug treatment cultured with osteogenic induction medium in 7 days, ASCs were fixed by 4% paraformaldehyde and washed by PBS thrice. The activity of alkaline phosphatase (ALP) was examined by 5-bromo-4-chloro-3-indolyl phosphate/Nitro Blue Tetrazolium Color Development Kit (Beyotime, China) overnight. Also, the stained cells were observed by an inverted light microscope.

Western blot assay

Total protein of ASCs was lysed using the Total Protein Extraction Kit (Keygen Biotech, China) after drug treatment. Then, we detected the concentration of total protein by Bicinchoninic Acid Protein Assay Kit (Thermo Scientific). Then, different proteins among each group were divided by 8% or 10% or 12% (v/v) sodium dodecyl sulfate–polyacrylamide gel electrophoresis (SDS-PAGE) gel

(Beyotime) with 90 V for 1 h and 120 V for 1 h. Also, the SDS-PAGE gel was transferred to polyvinylidene difluoride (PVDF) membranes (Bio-Rad) at a constant current of 100 mA for 1 h. All PVDF strips were blocked with 5% skim milk (Bio-Rad), which was diluted in 0.05% (v/v) Tween-20 Tris-buffer saline (TBST) and incubated with target primary antibodies (1:1,000) overnight at 4°C, including glyceraldehyde 3-phosphate dehydrogenase (GAPDH; ab181602), OPN (ab91655), GSK3β (ab32391), mammalian target of rapamycin (mTOR) (ab32028) and BECLIN1 (ab62557; Abcam, United Kingdom), and RUNX2 (12556s), LEF1 (2230p), β-catenin (D10A8), and light chain 3 (LC3) I/II (12741T; Cell Signaling Technology). Membranes were washed with TBST thoroughly for 30 min and immersed in goat-anti-rabbit secondary antibodies (Beyotime) for 1 h. The image results were visualized using an Enhanced Chemiluminescence Detection System (Bio-Rad).

Immunofluorescence staining and confocal laser scanning

ASCs (1×10^4 cells) were inoculated on confocal dishes (Corning) and treated as previously described with high glucose and metformin for 4 days. Cells were gently washed with PBS and fixed with 4% paraformaldehyde for 15 min. Permeabilized the cytomembrane of ASCs by 0.5% Triton X-100 and immersed them in 5% goat serum (Beyotime) for 1 h. Next, rabbit primary antibodies of BECLIN1 and GSK3β (1:200) were used to incubate ASC samples overnight at 4°C, and a fluorescence-conjugated goat-anti-rabbit secondary antibody (Beyotime) was used to combine the primary antibody for 1 h. Finally, the nucleus of ASCs was stained by 4′,6-diamidino-2-phenylindole (Beyotime). The fluorescence images were captured by the inverted fluorescence microscope (Olympus).

RNA extraction and real-time fluorescent polymerase chain reaction

Total RNA of ASCs in each group was extracted by Total RNA Extraction Kit (BioFlux, China). The mRNAs were reverse transcribed into cDNA by PrimeScript RT Reagent Kit (Takara Bio, Japan). Then real-time polymerase chain reaction (RT-PCR) was conducted by SYBR Premix ExTaq kit (Takara Bio) with ABI 7900 system machine (Applied Biosystems) as follows: 95°C for 45 s; then 40 cycles of 95°C for 5 s; and finally 60°C for 30 s. All the primer sequences details are shown in Table 1. The quality of the PCR product was examined by melting curve, while the gene cycle threshold (CT) values from all groups were calibrated with Gapdh CT values and calculated by the $2^{-\Delta\Delta Ct}$ method.

Statistical analysis

Experimental results were repeated over three times independently, and the data were calculated by SPSS 19.0 software (SPSS, Inc.) with Student's *t*-test or one-way ANOVA. Differences were marked as statistically significant if $P < 0.05$.

Results

High glucose restrained cell proliferation and cell migration

Cultured with different differentiation induction mediums, ASCs derived from adipose tissue were induced into osteoblasts, adipocytes, and chondrocytes, which demonstrated the multidirectional differentiation ability of ASCs (Fig. 1A). After osteogenic induction, ASCs changed their morphology from spindle shape of fibroblasts to typical polygon shape of osteoblast, and mineralized matrix accumulates around the cells. While in the adipogenic medium, the shape of ASCs became ovoid and filled with lipid, which was dyed orange by Oil Red O. When ASCs differentiate into chondroblasts, they secreted proteoglycan, collagen, and other extracellular matrices to make the cells stick together.

Excessive glucose concentrations are toxic to the proliferation, migration, and differentiation of ASCs. The CCK-8 results showed that the cell proliferation ability of ASCs was gradually

Table 1. Primer Sequences Information for Amplification of Genes

Gene name	*RefSeq transcripts*	*Sequence (5′→3′)*
Gapdh	NM_017008.4	Forward: ACAGCAACAGGGTGGTGGAC Reverse: TTTGAGGGTGCAGCGAACTT
Runx2	NM_001278483.1	Forward: AGGGACTATGGCGTCAAACA Reverse: GGCTCACGTCGCTCATCTT
Opn	NM_012881.2	Forward: CACTCCAATCGTCCCTACA Reverse: CTTAGACTCACCGCTCTTCAT
β-Catenin	NM_053357.2	Forward: AAGTTCTTGGCTATTACGACA Reverse: ACAGCACCTTCAGCACTCT
Gsk3β	NM_019827.7	Forward: AACTCCACCAGAGGCAATCG Reverse: CGTTGCACTCTTAGCCCTGT
Lef1	NM_130429.1	Forward: CAGACCTGTCACCCTTCAGC Reverse: GTGAGACGGATTGCCAAACG
mTOR	NM_019906.2	Forward: AGTGGGAAGATCCTGCACATT Reverse: TGGAAACTTCTCTCGGGTCAT
Beclin1	NM_053739.2	Forward:AGCACGCCATGTATAGCAAAGA Reverse: GGAAGAGGGAAAGGACAGCAT
LC3 II	NM_022867.2	Forward: GAGTGGAAGATGTCCGGCTC Reverse: CCAGGAGGAAGAAGGCTTGG

Gapdh, glyceraldehyde 3-phosphate dehydrogenase; LC3, light chain 3; mTOR, mammalian target of rapamycin; Opn, osteopontin; Runx2, runt-related transcription factor 2.

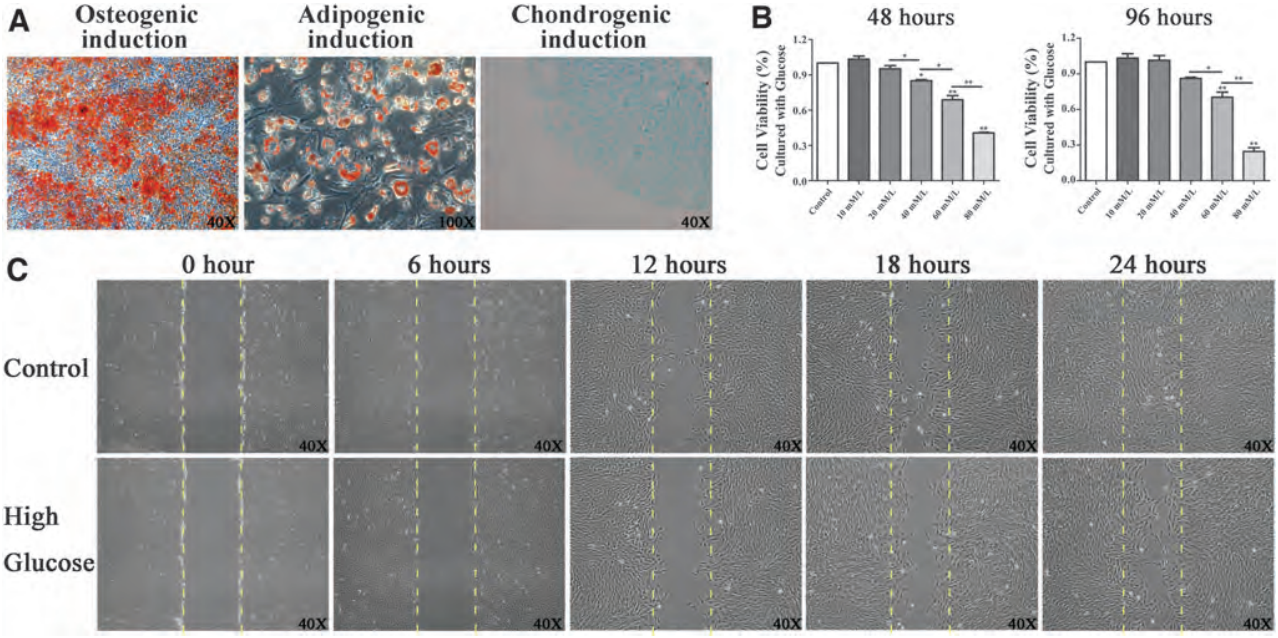

FIG. 1. ASCs had multidirectional differentiation ability, but high-glucose inhibited the cell proliferation and migration of ASCs. **(A)** ASCs multidirectional differentiation was analyzed by Alizarin red-S staining (in *red*), Oil Red O staining (in *orange*), and Alcian blue assay (in *blue*) after induction culture; **(B)** CCK-8 assay data showed that the high-glucose concentration inhibited the cell proliferation activity at 48 and 96 h. At 40 mM high glucose, the cell proliferation activity was reduced to 80% which was statistically different from the control group; **(C)** cell wound healing progress was detected every 6 h with an inverted light microscope, the images showed that the cell migration ability was suppressed in the high-glucose group and its scratch was not healed within 24 h. The yellow dotted line shows the initial boundary of the scratch. $*P < 0.05$, $**P < 0.01$. ASC, adipose-derived stem cell; CCK-8, Cell Counting Kit-8. Color images are available online.

declined with the increase of glucose concentration in 48 and 96 h (Fig. 1B). Also, the cell migration ability of ASCs was depressed under 40 mM glucose treatment compared with the control group at different time points (Fig. 1C). Then, we studied the inhibiting effect of high glucose on osteogenic differentiation of ASCs in the following part of our research.

High glucose inhibited osteogenic differentiation capacity and Wnt signaling pathway in ASCs

To explore the relationship between high glucose and ASCs osteogenic differentiation, we treated ASCs with 40 mM glucose and 0.1 mM metformin and detected the changes of cell mineralization, ALP activity, osteogenic factors, and Wnt signaling pathway. After osteogenic differentiation induction for 21 days, the mineralized external matrix produced by ASCs was stained by Alizarin red-S staining. The staining results demonstrated that high-glucose treatment caused the lower formation of mineralized nodules in the high-glucose group, while the addition of metformin in high glucose promoted the formation of mineralized nodules to a certain extent (Fig. 2A). The ALP staining results of ASCs after osteogenic differentiation for 7 days also proved that a high-glucose environment inhibited ALP activity, while metformin upregulated its expression (Fig. 2C). RUNX2 and OPN were the represent proteins for osteogenic differentiation, β-CATENIN and LEF1 represented the activity of the Wnt signaling pathway. After 4 days of ASCs osteogenic differentiation, the western blot and RT-PCR results were consistent with the results of Alizarin red-S staining and ALP staining (Fig. 2B, D).

High glucose suppressed the autophagy level and metformin modulated autophagy inhibition induced by high glucose

Our results showed a correlation between osteogenic differentiation potential damage of ASCs and the inhibition of autophagy level by high glucose. After being cultured under high glucose and metformin condition, the protein and mRNA of ASCs in different groups were analyzed. The western blot images showed that high glucose inhibited the expression of two key proteins in autophagy: BECLIN1 and LC3 I/II, while they were upregulated by metformin (Fig. 3A, B). However, the expression of mTOR and GSK3β, which negatively regulated the autophagy signaling pathway, was increased in the high-glucose group. The gene expression results detected by RT-PCR were consistent with western blot results (Fig. 3D). Then, the fluorescence signal images showed that the expression of Beclin1 was the weakest in the high glucose group, while metformin activated the expression of Beclin1 and showed the strongest fluorescence (Fig. 3C).

3-MA antagonized the effect of metformin on osteogenic differentiation and cell autophagy in ASCs

To further prove the important role of autophagy in promoting osteogenic differentiation of ASCs, we added 3-MA, an inhibitor of metformin, to verify that once inhibited by 3-MA, metformin was not able to recover the damaged osteogenic differentiation potential of ASCs by high

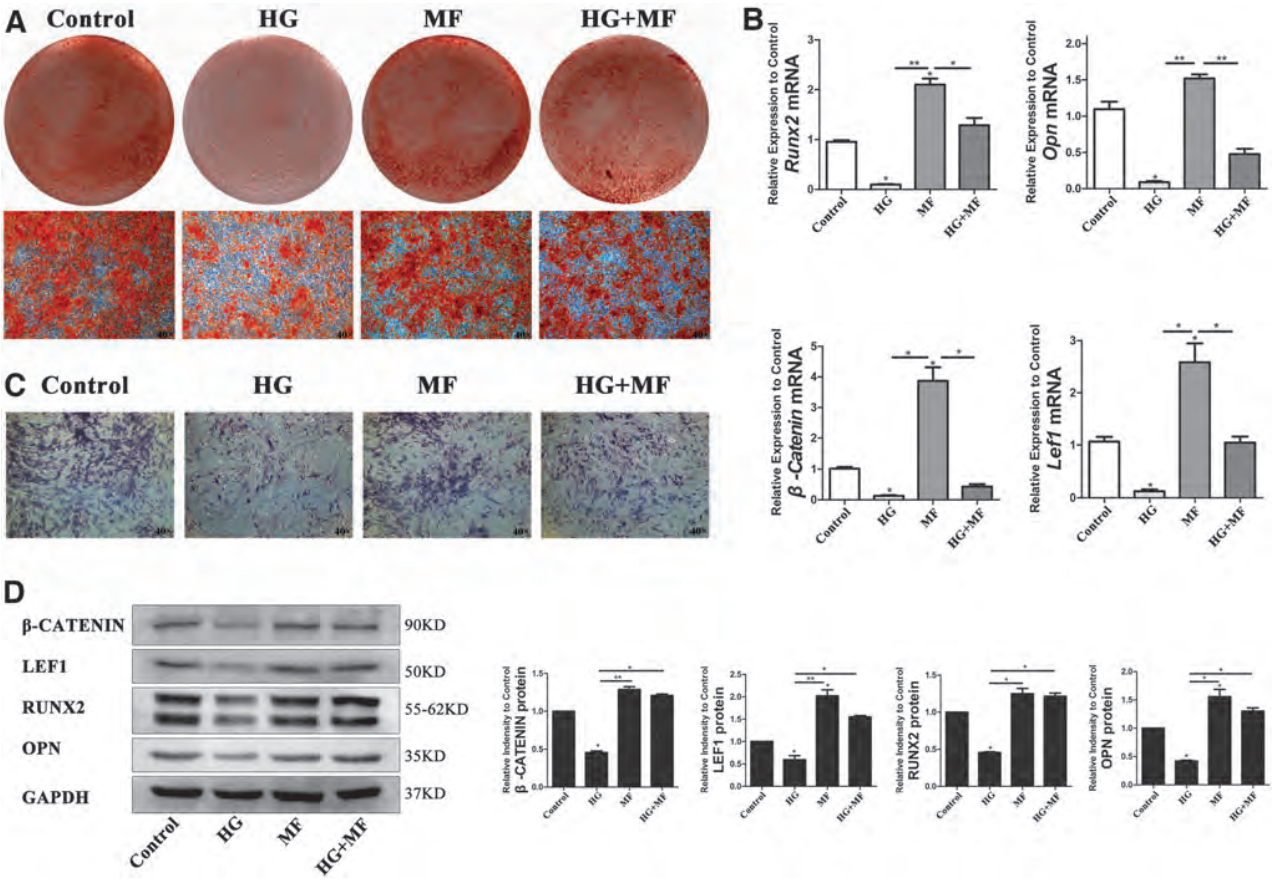

FIG. 2. The osteogenic differentiation capacity of ASCs and the Wnt signaling pathway were detected after glucose and metformin treatment. **(A)** Osteogenesis cultured for 21 days, mineralized nodules were stained by Alizarin red-S; **(C)** osteogenesis cultured for 7 days, and the active ALP in ASCs was dyed *purple*. Metformin group had the highest of mineralized nodules formation and ALP activity; **(B, D)** RT-PCR and western blot data showed that the expression of typical osteogenic genes *Runx2* and *Opn* and Wnt signaling pathway genes *β-catenin* and *Lef1* was higher in the metformin group than that of the high-glucose group. Although the expression level of the HG+MF group was not as good as that of the metformin group, it was also higher than that of the HG group. The difference was statistically significant. All the results showed that metformin resisted the negative effect of high glucose and promoted bone formation. $*P < 0.05$, $**P < 0.01$. ALP, alkaline phosphatase; MF, metformin; Opn, osteopontin; RT-PCR, real-time polymerase chain reaction; Runx2, runt-related transcription factor 2. Color images are available online.

glucose. The Alizarin red-S staining images demonstrated that after the addition of 3-MA, the ability of metformin to promote osteogenic differentiation was offset by 3-MA (Fig. 4A). The results of western blot and RT-PCR demonstrated that the expression of Beclin1 and LC3 I/II was successfully inhibited by 3-MA, and metformin could not upregulate their expression (Fig. 4B, C). The expression of RUNX2 and OPN was higher in the HG+MF group than in the HG group. When 3-MA inhibited the effect of metformin, the expression of RUNX2 and OPN was downregulated in the 3-MA+MF+HG group compared with the MF+HG group (Fig. 4B, C). The results meant that the positive effect of metformin on ASCs osteogenesis was inhibited by 3-MA.

Metformin-modulated autophagy activated Wnt signaling pathway in the process of osteogenic differentiation

So far, we have proved that high glucose inhibited the osteogenic differentiation potential of ASCs through autophagy, while metformin reversed this negative effect. However, we still need to find the clues behind the osteogenesis damage of ASCs and autophagy. The literature review found that GSK3β could not only negatively regulate the level of autophagy but also targeted to bind the β-CATENIN to inhibit the Wnt signaling pathway [13,14]. Therefore, we were committed to exploring whether GSK3β is a link between the Wnt signaling pathway and cell autophagy. After treatment with high glucose, metformin, and 3-MA, we detected the expression activity of mTOR, GSK3β, β-CATENIN, and LEF1 among each group (Fig. 5A, C). The protein expression of mTOR and GSK3β was upregulated in the high-glucose group, and metformin could not depress them in the HG +3-MA+MF group. The expression of β-CATENIN and LEF1 was higher in the HG+MF group than that in the HG group and the HG +3-MA+MF group. The results demonstrated that the Wnt signaling was activated when the cell autophagy level was upregulated by metformin, which promoted the progress of osteogenic differentiation. The fluorescence staining of GSK3β showed that it was highly

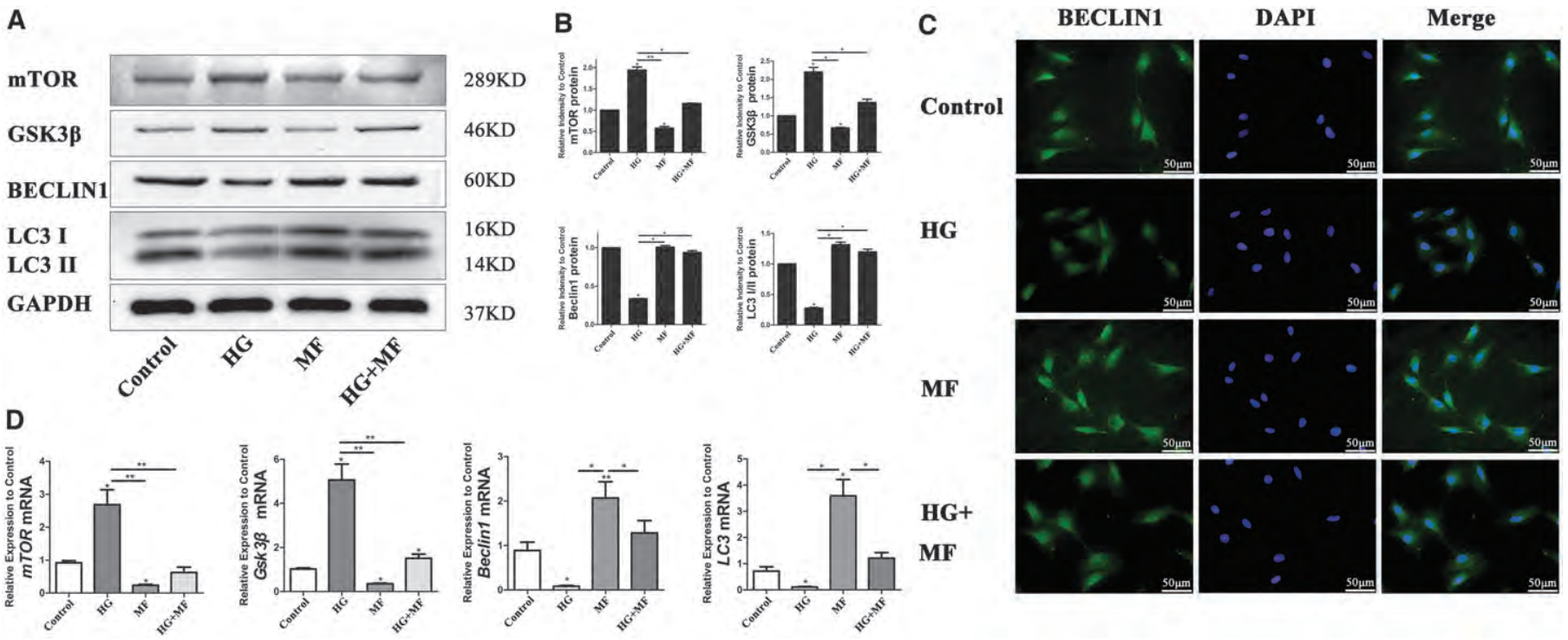

FIG. 3. Metformin upregulated the expression level of autophagy suppressed by high glucose. **(A, B)** The expression of autophagy protein BECLIN1 and LC3 I/II was significantly less at 0.5 times in the high-glucose group than that of the control group, while metformin was able to upregulate them in the HG+MF group. The expression of mTOR and GSK3β was suppressed in the metformin group compared with the high-glucose group, which was the opposite results of BECLIN1 and LC3 I/II; **(C)** fluorescence staining image of BECLIN1 showed the weakest expression in the high-glucose group, while it was strongest in the HG+MF group; **(D)** the gene expression trend of *Beclin1*, *LC3 II*, *mTOR*, and *Gsk3β* in each group was consistent with that of western blot. $*P<0.05$, $**P<0.01$. LC3, light chain 3; mTOR, mammalian target of rapamycin. Color images are available online.

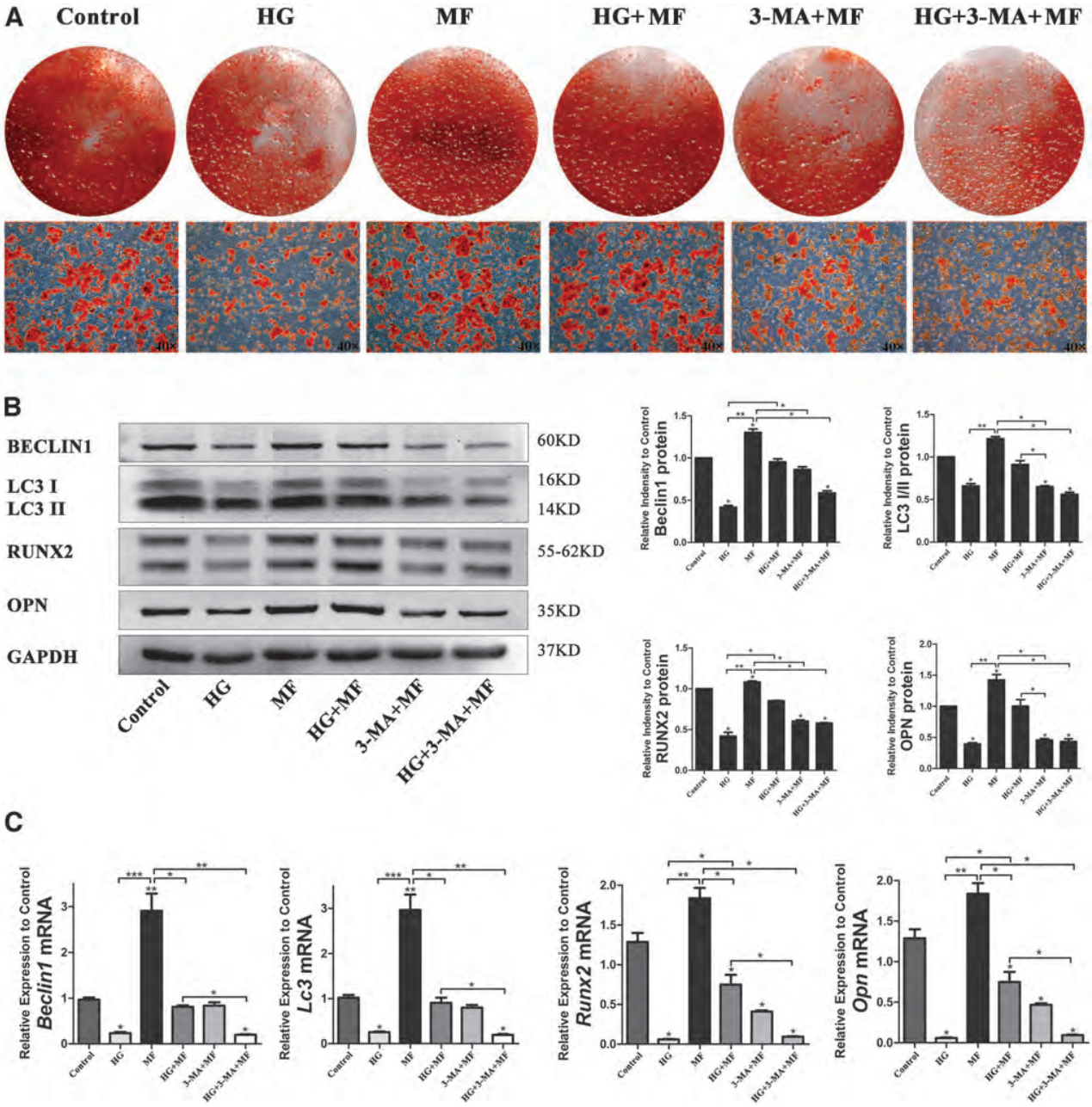

FIG. 4. Metformin alleviated the high glucose-induced damage to the osteogenic capacity of ASCs by activating autophagy. **(A)** The Alizarin red-S staining images showed that metformin was helpful for osteogenesis and promoted the production of mineralized nodules even in the HG+MF group. But after adding 3-MA, the size and the number of mineralized nodules were reduced, especially in the HG +3-MA+MF group; **(B, C)** the protein and gene expression of Beclin1 and LC3 I/II was downregulated in the 3-MA+MF group and the HG +3-MA+MF group. The expression of Runx2 and Opn was also decreased and could not recover in the HG +3-MA+MF group. $*P<0.05$, $**P<0.01$, $***P<0.001$. 3-MA, 3-methyladenine. Color images are available online.

FIG. 5. Metformin regulated Wnt signaling pathway. **(A)** Western blot image and bar graph showed that the expression of mTOR and GSK3β was the lowest in the MF group, but was increased under the treatment of 3-MA. Because of the inhibitory effect of 3-MA on metformin, the expression of β-CATENIN and LEF1 was suppressed in the HG +3-MA+MF group. The activation effect of metformin on the expression of β-CATENIN and LEF1 was negatively influenced by 3-MA. **(B)** The *red* fluorescence showed the expression of GSK3β of ASCs. It was obvious that the fluorescence signal of GSK3β was weakest in the MF group, and it was weaker in the HG+MF group than the HG group and HG +3-MA+MF group. These images showed that GSK3β was significantly inhibited by metformin. **(C)** The mRNA expression results of *β-Catenin*, *LEF1*, *mTOR*, and *GSK3β* were consistent with western blot analysis, which demonstrated that the depress effect of metformin on *GSK3β* activated the Wnt signaling pathway. $*P<0.05$, $**P<0.01$, $***P<0.001$. Color images are available online.

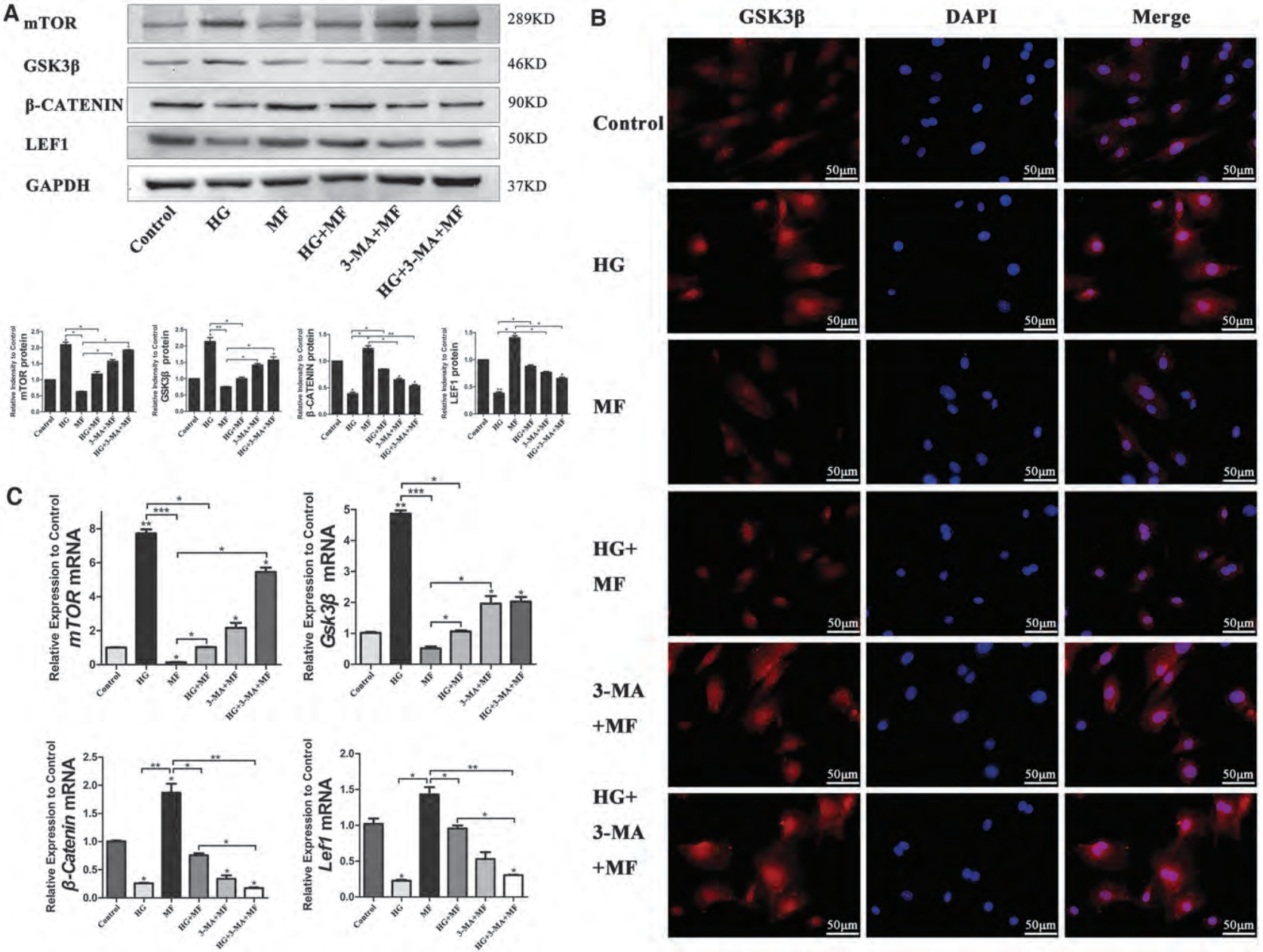

expressed in the HG group and downregulated by metformin in the HG+MF group. But metformin failed to work on GSK3β in the presence of 3MA in the 3-MA+MF group and HG +3-MA+MF group (Fig. 5B).

Discussion

Although studies have reported that the risk of bone metabolic disease due to diabetes is not consistent across ethnic groups, it has become a global public health issue affecting over 422 million individuals all over the world [15–19]. It was found that skeletal fragility in diabetes caused an increased incidence of osteoporosis, a higher risk of fracture and poor bone healing [20]. Rodent models of diabetes proved that obesity, insulin resistance, and hyperglycemia of the T2D diabetes model caused skeletal abnormalities, including lower femoral cortical thickness, decreased stiffness, and abnormalities of multiple trabecular and cortical microarchitectural [21]. Studies of osteoblast cell lines based on diabetes and hyperglycemia environment also showed that diabetes has a significant negative effect on cell physiological function. Previous studies in my research group showed that the osteogenic differentiation ability of ASCs was significantly suppressed by advanced glycation end products, which is a kind of glucose and protein metabolites due to hyperglycemia [10,22]. In this study, we used high-dose glucose to simulate a hyperglycemia environment, and the results showed that the proliferation, migration, and osteogenic differentiation of ASCs are significantly inhibited, which is consistent with the published literature.

To solve the problem of osteogenic differentiation inhibition of ASCs with high glucose, we set our sights on the first-line hypoglycemic drugs, trying to find the positive effect of metformin on osteogenic differentiation of ASCs. Numerous researches give experimental evidence for a promising benefit of metformin for skeletal metabolism [23,24]. In vitro studies (Wang P et al.) found that metformin contributed to the differentiation of human-induced pluripotent stem cell-derived mesenchymal stem cell to osteoblast cell line by mediating the LKB1/AMPK pathway [25]. Agnieszka S et al. proposed that low concentration metformin promoted the metabolic activity of ASCs, while high-concentration metformin inhibited it [26]. On the flip side, high-concentration metformin had a stronger effect on osteogenesis, while low-concentration metformin appeared to have a weak effect. According to existing literatures, 0.1 mM metformin is a nontoxic concentration for different types of cells and showed good effects on osteogenic differentiation [11,12]. Therefore, the 0.1 mM metformin was used in our study as the treatment concentration. Our research data based on ASCs proved a positive effect of 0.1 mM metformin in expediting the osteogenic differentiation of ASCs. Most intuitively, there is a significant increase in the production of mineralized nodules visible to the naked eye after 0.1 mM metformin treatment. In addition, the expression of osteogenic markers and the Wnt signaling pathway was upregulated by metformin.

In recent years, the role of metformin as an autophagy activator has been gradually discovered. Our study analyzed the expression of autophagy key proteins Beclin1 and LC3 I/II, which was significantly inhibited under high-glucose conditions while was rescued by metformin. At the same time, metformin decreased the expression of the negative regulatory factors of autophagy, mTOR, and p-GSK3β (Fig. 3). Some research work has demonstrated that the disturbance of physiological activity of cells in a high-glucose environment is closely related to the change of autophagy level [27,28]. Metformin prominently regulates the osteoprotegerin-mediated inhibition of osteoclasts differentiation by upregulating the level of autophagy [29]. Another study on metformin showed that the autophagic capacity, antiaging ability, and osteogenic differentiation were positively improved after being treated with metformin every day [6]. In this study, we demonstrated that the high expression of autophagy-related genes and proteins altered by adding metformin, and their changes are positively correlated with osteogenic differentiation of ASCs. Therefore, the activating effect of metformin on autophagy maybe its key mechanism to promote osteogenesis.

With the development of autophagy study, researchers revealed that the negative regulator of autophagy is also an important factor affecting autophagy. A close relationship between autophagy level and cell osteogenesis was found not only in osteoblasts and osteoclasts but also in hematopoietic progenitors and macrophagocyte [30,31]. GSK3β was reported to have negative regulatory effects on the autophagy pathway in cancer cells but also in other diseases [32,33]. Azoulay-Alfaguter et al. reported that a high level of GSK3α and GSK3β activated mTORC1 and suppressed Beclin1 expression in MCF-7 human breast cancer cells, contributing to cancer therapy [34]. It was also showed a negative correlation between Akt/GSK3β/β-catenin signaling and autophagy in atrial fibrosis of human atrial fibroblasts [32]. Our data found that the inhibition of high glucose on the autophagy pathway was related to the overexpression of GSK3β and mTOR1 in ASCs. Metformin appeared to inhibit the expression of GSK3β while activating autophagy.

As we know, GSK3β is also an important protein that inhibited the key factor, β-Catenin, in the Wnt signaling pathway [10,14,22,35]. Glucagon-like peptide-1 improved the glucose tolerance and insulin tolerance in a diabetic mouse model and promoted the expression of osteogenic markers via the Wnt/GSK3β/β-catenin pathway [14]. The osteogenic differentiation ability of human BMSCs was activated by Ginsenoside Rg1 because of its inhibitory effect on GSK3β [35]. What's more, it is worth noting that direct evidence showed that GSK3β is a link factor between the autophagy pathway and the Wnt signaling pathway [36]. The authors proved that electroacupuncture pretreatment provided neuroprotective effects and ischemic stroke prevention by upregulating autophagy and β-catenin through the inhibition of GSK3β in the cerebral ischemia injury model. Therefore, based on the literature and our research, we believe GSK3β might be an important connection point on the impetus of metformin on osteogenic differentiation of ASCs. When metformin activated the cell autophagy of ASCs, it also gave a negative feedback effect on GSK3β. The expression suppression of GSK3β by metformin relieved its inhibiting effect on the cell autophagy and Wnt signaling pathway ultimately promoted the recovery of osteogenic differentiation ability of ASCs. In our next stage, we will continue to in-depth study about the molecular mechanisms of metformin and GSK3β regulating the osteogenic

differentiation of ASCs in the diabetic microenvironment and provide more experimental evidence to promote the application of metformin in bone repair and regeneration with diabetic osteoporosis.

Conclusion

Current results demonstrated that the expression of autophagy and the Wnt signaling pathway was significantly inhibited under the high-glucose culture environment, resulting in the damage of the osteogenic differentiation ability of ASCs. As an autophagy agonist, metformin resisted the negative effects of high glucose and restored the activity of autophagy and the Wnt signaling pathway, playing a positive role in the osteogenic differentiation process of ASCs. This study elaborated a mechanism of metformin reducing the inhibitory effect of high glucose on the osteogenic differentiation of ASCs by activating cellular autophagy and the Wnt signaling pathway, which provided a possibility for the application of metformin in transplantation of ASCs for bone repair under diabetes osteoporosis conditions.

Acknowledgments

The authors thank Oral & maxillofacial Reconstruction and Regeneration Laboratory, The Affiliated Stomatology Hospital of Southwest Medical University for experimental equipments in this research.

Author Disclosure Statement

No competing financial interests exist.

Funding Information

This work was funded by National Natural Science Foundation of China (81870746), Program of Southwest Medical University (2019ZQN167, 2019ZQN143), Program of The Affiliated Stomatology Hospital of Southwest Medical University (202017), Climb Plan Project of The Affiliated Stomatology Hospital of Southwest Medical University (2020QY04), and Open Project of the State Key Laboratory of Oral Disease Research (SKLOD2021OF08).

References

1. Hofbauer LC, CC Brueck, SK Singh and H Dobnig. (2007). Osteoporosis in patients with diabetes mellitus. J Bone Miner Res 22:1317–1328.
2. Tan J, L Zhou, Y Zhou, P Xue, G Wu, G Dong, H Guo and Q Wang. (2017). The influence of diabetes mellitus on proliferation and osteoblastic differentiation of MSCs. Curr Stem Cell Res Ther 12:388–400.
3. Wallner C, S Abraham, JM Wagner, K Harati, B Ismer, L Kessler, H Zöllner, M Lehnhardt and B Behr. (2016). Local application of isogenic adipose-derived stem cells restores bone healing capacity in a type 2 diabetes model. Stem Cells Transl Med 5:836–844.
4. Aung M, S Amin, A Gulraiz, FR Gandhi, JA Pena Escobar and BH Malik. (2020). The future of metformin in the prevention of diabetes-related osteoporosis. Cureus 12:e10412–e10418.
5. Bahrambeigi S, B Yousefi, M Rahimi and V Shafiei-Irannejad. (2019). Metformin; an old antidiabetic drug with new potentials in bone disorders. Biomed Pharmacother 109:1593–1601.
6. Lin J, R Xu, X Shen, H Jiang and S Du. (2020). Metformin promotes the osseointegration of titanium implants under osteoporotic conditions by regulating BMSCs autophagy, and osteogenic differentiation. Biochem Biophys Res Commun 531:228–235.
7. Djajadikerta A, S Keshri, M Pavel, R Prestil, L Ryan and DC Rubinsztein. (2020). Autophagy induction as a therapeutic strategy for neurodegenerative diseases. J Mol Biol 432:2799–2821.
8. Greenhill C. (2016). Bone: autophagy regulates bone growth in mice. Nat Rev Endocrinol 12:4.
9. Gao Y, Y Li, J Xue, Y Jia and J Hu. (2010). Effect of the anti-diabetic drug metformin on bone mass in ovariectomized rats. Eur J Pharmacol 635:231–236.
10. Zhang M, Y Li, P Rao, K Huang, D Luo, X Cai and J Xiao. (2018). Blockade of receptors of advanced glycation end products ameliorates diabetic osteogenesis of adipose-derived stem cells through DNA methylation and Wnt signaling pathway. Cell Prolif 51:e12471–e12482.
11. Ma J, Z-L Zhang, X-T Hu, X-T Wang and AM Chen. (2018). Metformin promotes differentiation of human bone marrow derived mesenchymal stem cells into osteoblast via GSK3β inhibition. Eur Rev Med Pharmacol Sci 22: 7962–7968.
12. Jia L, Y Xiong, W Zhang, X Ma and X Xu. (2020). Metformin promotes osteogenic differentiation and protects against oxidative stress-induced damage in periodontal ligament stem cells via activation of the Akt/Nrf2 signaling pathway. Exp Cell Res 386:111717.
13. Ren J, T Liu, Y Han, Q Wang, Y Chen, G Li and L Jiang. (2018). GSK-3beta inhibits autophagy and enhances radiosensitivity in non-small cell lung cancer. Diagn Pathol 13:33–43.
14. Li Y, H Fu, H Wang, S Luo, L Wang, J Chen and H Lu. (2020). GLP-1 promotes osteogenic differentiation of human ADSCs via the Wnt/GSK-3beta/beta-catenin pathway. Mol Cell Endocrinol 515:110921.
15. Koromani F, L Oei, E Shevroja, K Trajanoska, J Schoufour, T Muka, OH Franco, MA Ikram, MC Zillikens, et al. (2020). Vertebral fractures in individuals with type 2 diabetes: more than skeletal complications alone. Diabetes Care 43:137–144.
16. Moayeri A, M Mohamadpour, SF Mousavi, E Shirzadpour, S Mohamadpour and M Amraei. (2017). Fracture risk in patients with type 2 diabetes mellitus and possible risk factors: a systematic review and meta-analysis. Ther Clin Risk Manag 13:455–468.
17. Looker AC, MS Eberhardt and SH Saydah. (2016). Diabetes and fracture risk in older U.S. adults. Bone 82:9–15.
18. Hothersall EJ, SJ Livingstone, HC Looker, SF Ahmed, S Cleland, GP Leese, RS Lindsay, J McKnight, D Pearson, et al. (2014). Contemporary risk of hip fracture in type 1 and type 2 diabetes: a national registry study from Scotland. J Bone Miner Res 29:1054–1060.
19. World Health Organization. (2016). *World Health Organization: Global Report on Diabetes*. World Health Organization, Geneva, Switzerland.
20. Rubin MR. (2017). Skeletal fragility in diabetes. Ann N Y Acad Sci 1402:18–30.
21. Gimble JM. (2011). Leptin's balancing act between bone and fat. J Bone Miner Res 26:1694–1697.

22. Li Y, L Wang, M Zhang, K Huang, Z Yao, P Rao, X Cai and J Xiao. (2020). Advanced glycation end products inhibit the osteogenic differentiation potential of adipose-derived stem cells by modulating Wnt/beta-catenin signalling pathway via DNA methylation. Cell Prolif 53: e12834-e12847.
23. Hampp C, V Borders-Hemphill, DG Moeny and DK Wysowski. (2014). Use of antidiabetic drugs in the U.S., 2003-2012. Diabetes Care 37:1367–1374.
24. Jang WG, EJ Kim, IH Bae, KN Lee, YD Kim, DK Kim, SH Kim, CH Lee, RT Franceschi, HS Choi and JT Koh. (2011). Metformin induces osteoblast differentiation via orphan nuclear receptor SHP-mediated transactivation of Runx2. Bone 48:885–893.
25. Wang P, T Ma, D Guo, K Hu, Y Shu, HHK Xu and A Schneider. (2017). Metformin induces osteoblastic differentiation of human induced pluripotent stem cell-derived mesenchymal stem cells. J Tissue Eng Regen Med 12:437–446.
26. Agnieszka S, AT Krzysztof, K Katarzyna and M Krzysztof. (2018). Metformin promotes osteogenic differentiation of adipose-derived stromal cells and exerts pro-osteogenic effect stimulating bone regeneration. J Clin Med 7:482–507.
27. Zhou DM, F Reng, HZ Ni, LL Sun, LXiao, XQ Li, WD Li. (2020). Metformin inhibits high glucose-induced smooth muscle cell proliferation and migration. Aging 12:5352–5361.
28. Zhao K, H Hao, J Liu, C Tong, Y Cheng, Z Xie, L Zang, Y Mu and W Han. (2015). Bone marrow-derived mesenchymal stem cells ameliorate chronic high glucose-induced beta-cell injury through modulation of autophagy. Cell Death Dis 6:e1885–e1898.
29. Tong X, C Zhang, D Wang, R Song, Y Ma, Y Cao, H Zhao, J Bian, J Gu and Z Liu. (2020). Suppression of AMP-activated protein kinase reverses osteoprotegerin-induced inhibition of osteoclast differentiation by reducing autophagy. Cell Prolif 53:e12714–e12730.
30. Li Z, X Liu, Y Zhu, Y Du, X Liu, L Lv, X Zhang, Y Liu, P Zhang and Y Zhou. (2019). Mitochondrial phosphoenolpyruvate carboxykinase regulates osteogenic differentiation by modulating AMPK/ULK1-dependent autophagy. Stem Cells 37:1542–1555.
31. Chen Z, S Ni, S Han, R Crawford, S Lu, F Wei, J Chang, C Wu and Y Xiao. (2017). Nanoporous microstructures mediate osteogenesis by modulating the osteo-immune response of macrophages. Nanoscale 9:706–718.
32. Lin R, S Wu, D Zhu, M Qin and X Liu. (2020). Osteopontin induces atrial fibrosis by activating Akt/GSK-3beta/beta-catenin pathway and suppressing autophagy. Life Sci 245:117328.
33. Mancinelli R, G Carpino, S Petrungaro, CL Mammola, L Tomaipitinca, A Filippini, A Facchiano, E Ziparo and C Giampietri. (2017). Multifaceted roles of GSK-3 in cancer and autophagy-related diseases. Oxid Med Cell Longev 2017:4629495.
34. Azoulay-Alfaguter I, R Elya, L Avrahami, A Katz and H Eldar-Finkelman. (2015). Combined regulation of mTORC1 and lysosomal acidification by GSK-3 suppresses autophagy and contributes to cancer cell growth. Oncogene 34: 4613–23.
35. Peng S, S Shi, G Tao, Y Li, D Xiao, L Wang, Q He, X Cai and J Xiao. (2021). JKAMP inhibits the osteogenic capacity of adipose-derived stem cells in diabetic osteoporosis by modulating the Wnt signaling pathway through intragenic DNA methylation. Stem Cell Res Ther 12:120–135.
36. Chen C, Q Yu, K Xu, L Cai, BM Felicia, L Wang, A Zhang, Q Dai, W Geng, J Wang and Y Mo. (2020). Electroacupuncture pretreatment prevents ischemic stroke and inhibits Wnt signaling-mediated autophagy through the regulation of GSK-3beta phosphorylation. Brain Res Bull 158:90–98.

Address correspondence to:
Dr. Jingang Xiao
Department of Oral Implantology
The Affiliated Stomatology Hospital
of Southwest Medical University
No. 2 Jiangyang South Road
Luzhou 646000
People's Republic of China

E-mail: drxiaojingang@163.com

Received for publication July 23, 2021
Accepted after revision August 30, 2021
Prepublished on Liebert Instant Online September 5, 2021

Zhang *et al. Stem Cell Research & Therapy* (2022) 13:397
https://doi.org/10.1186/s13287-022-03088-4

Stem Cell Research & Therapy

RESEARCH Open Access

Downregulation of DNA methyltransferase-3a ameliorates the osteogenic differentiation ability of adipose-derived stem cells in diabetic osteoporosis via Wnt/β-catenin signaling pathway

Maorui Zhang[1,2†], Yujin Gao[1,3†], Qing Li[4], Huayue Cao[1], Jianghua Yang[4], Xiaoxiao Cai[2*] and Jingang Xiao[1,3,4*]

Abstract

Background: Diabetes-related osteoporosis (DOP) is a chronic disease caused by the high glucose environment that induces a metabolic disorder of osteocytes and osteoblast-associated mesenchymal stem cells. The processes of bone defect repair and regeneration become extremely difficult with DOP. Adipose-derived stem cells (ASCs), as seed cells in bone tissue engineering technology, provide a promising therapeutic approach for bone regeneration in DOP patients. The osteogenic ability of ASCs is lower in a DOP model than that of control ASCs. DNA methylation, as a mechanism of epigenetic regulation, may be involved in DNA methylation of various genes, thereby participating in biological behaviors of various cells. Emerging evidence suggests that increased DNA methylation levels are associated with activation of Wnt/β-catenin signaling pathway. The purpose of this study was to investigate the influence of the diabetic environment on the osteogenic potential of ASCs, to explore the role of DNA methylation on osteogenic differentiation of DOP-ASCs via Wnt/β-catenin signaling pathway, and to improve the osteogenic differentiation ability of ASCs with DOP.

Methods: DOP-ASCs and control ASCs were isolated from DOP C57BL/6 and control mice, respectively. The multipotency of DOP-ASCs was confirmed by Alizarin Red-S, Oil Red-O, and Alcian blue staining. Real-time polymerase chain reaction (RT-PCR), immunofluorescence, and western blotting were used to analyze changes in markers of osteogenic differentiation, DNA methylation, and Wnt/β-catenin signaling. Alizarin Red-S staining was also used to confirm changes in the osteogenic ability. DNMT small interfering RNA (siRNA), shRNA-Dnmt3a, and LVRNA-Dnmt3a were used to assess the role of Dnmt3a in osteogenic differentiation of control ASCs and DOP-ASCs. Micro-computed

†Maorui Zhang and Yujin Gao contributed equally to this work

*Correspondence: xcai@scu.edu.cn; drxiaojingang@163.com

[1] Department of Oral Implantology, The Affiliated Stomatological Hospital of Southwest Medical University, Luzhou 646000, China
[2] State Key Laboratory of Oral Diseases, West China Hospital of Stomatology, Sichuan University, Chengdu 610041, China
Full list of author information is available at the end of the article

tomography, hematoxylin and eosin staining, and Masson staining were used to analyze changes in the osteogenic capability while downregulating Dnmt3a with lentivirus in DOP mice in vivo.

Results: The proliferative ability of DOP-ASCs was lower than that of control ASCs. DOP-ASCs showed a decrease in osteogenic differentiation capacity, lower Wnt/β-catenin signaling pathway activity, and a higher level of Dnmt3a than control ASCs. When Dnmt3a was downregulated by siRNA and shRNA, osteogenic-related factors Runt-related transcription factor 2 and osteopontin, and activity of Wnt/β-catenin signaling pathway were increased, which rescued the poor osteogenic potential of DOP-ASCs. When Dnmt3a was upregulated by LVRNA-Dnmt3a, the osteogenic ability was inhibited. The same results were obtained in vivo.

Conclusions: Dnmt3a silencing rescues the negative effects of DOP on ASCs and provides a possible approach for bone tissue regeneration in patients with diabetic osteoporosis.

Keywords: DNA methyltransferase-3a, Diabetic osteoporosis, Adipose-derived stem cells, Osteogenic differentiation, Wnt/β-catenin signaling pathway

Background

Diabetic osteoporosis (DOP) is a systemic metabolic bone disease that involves bone mass reduction, destruction of the bone tissue microstructure, and prone fractures [1, 2]. The high glucose environment and metabolic disorders caused by diabetes disrupt physiological activities such as cell growth, proliferation, and differentiation [3]. Glucose metabolism disorders break the balance between osteogenesis and osteoclast processes, which reduces the numbers of osteoblasts and mesenchymal stem cells (MSCs), and activation of osteoclasts [4, 5]. The imbalance of bone metabolism also reduces the bone differentiation ability and makes it difficult to repair bone tissue and regenerate bone [6].

In recent years, bone tissue engineering technology has provided a new approach for regeneration of bone defects. Adult stem cells are a major element of bone regeneration and have become a major research topic [7–9]. Adipose-derived mesenchymal stem cells (ASCs), as a type of MSC, have a multi-directional differentiation potential for osteogenic, cartilage, and adipose cell lineages [10–12]. They are widely used in studies of bone defect repair and regeneration, and have positive application prospects. However, the proliferation and differentiation of ASCs may be affected in the diabetic environment. Therefore, it is worth exploring whether DOP-ASCs have a normal osteogenic differentiation ability.

DNA methylation is a mechanism of epigenetic regulation. It is generally believed that the hypermethylation status of DNA sequences is related to inhibition of gene expression [13, 14]. There are three kinds of DNA methyltransferases (DNMTs) in animals, namely DNMT1, DNMT3a, and DNMT3b [15–17]. Studies have shown that DNMT3a is essential for establishment of mammalian DNA methylation during development [18, 19]. Scholars believe that the increased expression of DNMT3a regulates the increased DNA methylation level [19, 20]. Under catalysis mediated by DNMTs, the cytosines of two nucleotides of CG in DNA are selectively conjugated with methyl groups to form 5-methylcytosine (5-MC). The occurrence of various skeletal diseases, which include osteoporosis and osteoarthritis, is closely related to impaired DNA methylation in stem cells [10, 13, 21].

The canonical Wnt pathway is activated when β-catenin transfers to the nucleus and binds to TCF/LEF in the nucleus to regulate target genes [22]. β-catenin and LEF1 may reflect the status of Wnt/β-catenin pathway [23, 24]. Emerging evidence indicates that increased DNA methylation levels are associated with activation of Wnt/β-catenin pathway [25–28]. Liu T et al. [26] reported that miR708-5p inhibits the expression of Dnmt3a, resulting in the reduced global DNA methylation and, preventing β-catenin nuclear transport, thereby inhibiting Wnt/β-catenin signaling pathway. Exploring the role of DNA methylation in osteogenic differentiation of DOP-ASCs via Wnt/β-catenin signaling is not only conducive to elucidate the mechanism of DOP, but also to develop bone tissue engineering.

In our previous study, we found that advanced glycation end products inhibit the osteogenic differentiation ability of normal ASCs with a high level of DNA methylation [5]. This suggested that DNA methylation is a cause of the decline in the osteogenic differentiation ability of DOP-ASCs in the diabetic environment. In this study, we isolated ASCs from control and DOP C57BL/6 mice and compared their osteogenic differentiation potentials. Moreover, we investigated whether DNA methylation inhibits the osteogenic differentiation potential of DOP-ASCs by modulating Wnt/β-catenin signaling pathways.

Methods

Isolation and culture of ASCs and DOP-ASCs

All procedures that involved animals were reviewed and approved by the Southwest Medical University

Ethical Committee. Anesthesia and animal care were implemented by following the guidelines for the Care and Use of Laboratory Animals (Ministry of Science and Technology of China, 2006). Adipose tissue in the inguinal region was collected from C57BL/6 DOP and control mice under sterile conditions. The adipose tissue was cut finely and fragments were seeded in 25-cm^2 culture flasks (Corning Inc., NY) and cultured in alpha-modified Eagle's medium (α-MEM, Hyclone, USA) supplemented with 10% fetal bovine serum (FBS, Hyclone) and 1% penicillin/streptomycin (Hyclone) at 37 °C with 5% CO_2. The medium was changed every 3 days. Adherent cells were cultured and non-adherent cells were removed.

DOP-ASCs were passaged three times to obtain relatively pure ASCs. Osteogenic, adipogenic, and cartilage media (Cyagen, USA) were used to define the multipotential differentiation capacity of DOP-ASCs. DOP-ASCs (5×10^4 cells) were seeded in a 6-well plate for osteogenic induction. DOP-ASCs (1×10^5 cells) were also seeded for adipogenic induction. All cells were cultured for 21 days. Then, the cells were washed three times with PBS and fixed with 4% paraformaldehyde for 1 h. Alizarin Red-S (osteogenic dye) and 0.3% Oil Red-O (adipogenic dye) were used to stain mineralized nodules and lipid droplets, respectively, for 30 min. The stained cells were imaged under an inverted phase contrast microscope (Nikon, Japan). For cartilage induction, DOP-ASCs (2.5×10^5 cells) were centrifuged and cell aggregates were cultured in cartilage medium. After 21 days, the cell aggregates were washed three times with PBS and fixed with 4% paraformaldehyde. The cartilage pellets were imaged under a stereo fluorescence microscope (Carl Zeiss Microscopy, Germany). Then, they were embedded in paraffin and sections were stained with Alcian blue. Cartilage matrix was imaged under an optical microscope (Nikon).

Proliferation assay

A Cell Counting Kit-8 (CCK-8) assay (Sigma-Aldrich, St Louis, Missouri, USA) and xCelligence system for real-time cellular analysis (RTCA) (Roche Diagnostics GmbH, Basel, Switzerland) were used to assess cell proliferation. For the CCK-8 assay, cells were seeded in 96-well plates (Corning Inc.) at a density of 3×10^3 cells per well and cultured in α-MEM with 10% FBS for 5 days. A BioTek ELX800 (Bio-Tek, USA) was used to measure absorbance at 450 nm. For RTCA, cells were seeded in 96-well E-plates (Roche Diagnostics GmbH) at 3×10^3 cells per well. Cell proliferation in the RTCA SP xCelligence system was monitored in real-time as the impedance value over 5 days. Data were analyzed by the provided RTCA software.

Alizarin red-S staining

Mineralized nodule formation in ASCs was stained by Alizarin Red-S (Cyagen). DOP-ASCs and control ASCs (5×10^4 cells) in 6-well plates were treated with osteogenic medium for 21 days. Cells were then washed with PBS three times, fixed in 4% paraformaldehyde for 1 h, and stained with Alizarin Red-S for 30 min.

Real-time polymerase chain reaction (RT-PCR)

Total RNA was extracted using a Total mRNA Extraction Kit (Takara Bio, Japan). cDNA was synthesized by reverse transcription using a Prime Script Reverse Transcription Reagent Kit (Takara Bio). Then, RT-PCR was conducted to measure the gene expression of Runt-related transcription factor 2 (*Runx2*), osteopontin (*Opn*), DNA methyltransferase 1/3a/3b (*Dnmt1/3a/3b*), *β-catenin*, and lymphoid enhancer-binding factor-1 (*Lef1*). Primer sequences are shown in Table 1. Samples were analyzed using a SYBR Premix ExTaq kit (Takara Bio), following the standard procedure, in an ABI 7900 system (Applied Biosystems, USA), which included melting curve analysis and obtaining CT values. The results were normalized to *Gapdh* CT values and the $2^{-\Delta\Delta Ct}$ method was used to calculate gene expression.

Western blot assay

A Total Protein Extraction Kit (Keygen Biotech, China) was used to extract total cellular proteins. A bicinchoninic acid protein assay kit (Thermo Fisher Scientific, MA, USA) was used to measure the protein concentration. Proteins were separated by 10% (v/v) sodium dodecyl sulfate–polyacrylamide gel electrophoresis and then

Table 1 Primer sequences for RT-PCR

Genes		Sequence (5′ → 3′)
Gapdh	Forward	GGTGAAGGTCGGTGTGAACG
	Reverse	CTCGCTCCTGGAAGATGGTG
Runx2	Forward	CCGAACTGGTCCGCACCGAC
	Reverse	CTTGAAGGCCACGGGCAGGG
Opn	Forward	GGATTCTGTGGACTCGGATG
	Reverse	CGACTGTAGGGACGATTGGA
Dnmt1	Forward	CCGAACTGGTCCGCACCGAC
	Reverse	CTTGAAGGCCACGGGCAGGG
Dnmt3a	Forward	GAGGGAACTGAGACCCCAC
	Reverse	CTGGAAGGTGAGTCTTGGCA
Dnmt3b	Forward	AGCGGGTATGAGGAGTGCAT
	Reverse	GGGAGCATCCTTCGTGTCTG
β-Catenin	Forward	AAGTTCTTGGCTATTACGACA
	Reverse	ACAGCACCTTCAGCACTCT
Lef1	Forward	ACAGATCACCCCACCTTCTTG
	Reverse	TGATGGGAAAACCTGGACAT

transferred onto a polyvinylidene difluoride membrane at 200 mA for 1 h. Tris-buffered saline with 0.05% (v/v) Tween-20 (TBST) was used to dissolve dry skimmed milk (Keygen Biotech). PVDF membranes were blocked with 5% dry skimmed milk for 1 h and then incubated with antibodies against GAPDH (ab181602), DNMT3a (ab188470), DNMT3b (ab79822), and OPN (ab91655) (Abcam, UK), RUNX2 (12556 s), DNMT1 (5032S), β-catenin (D10A8), or LEF1 (2230p) (Cell Signaling Technology, USA) for 1 day at 4 °C. Then, PVDF membranes were washed three times with TBST and incubated with a goat anti-rabbit secondary antibody (Beyotime, Shanghai, China) for 1 h. They were then washed again with TBST and developed with an enhanced chemiluminescence detection system (Bio-Rad, USA).

Immunofluorescence staining

Cells were seeded on round coverslips (Corning Inc.) and cultured for 4 days. After various treatments, the cells were carefully washed three times with PBS, fixed with 4% paraformaldehyde for 1 h, and permeabilized with 0.5% Triton X-100 for 10 min. Then, they were blocked with 5% goat serum (Beyotime) for 1 h and incubated for 1 day at 4 °C with antibodies against RUNX2, OPN, DNMT1, DNMT3a, DNMT3b, 5-MC (28692S), β-catenin, or LEF1. The next day, the samples were incubated with a fluorescent dye-conjugated secondary antibody (Beyotime) for 1 h. Nuclei were counterstained with 4′6-diamidino-2-phenylindole (Beyotime) for 10 min and phalloidin (Beyotime) was used to stain microfilaments for 10 min. Cells were imaged under a laser scanning confocal microscope (Olympus, Japan).

Table 2 siRNA sequences for gene silencing

siRNA		Sequence (5′ → 3′)
Dnmt1	Sense	CCGAAGAUCAACUCACCAATT
	Antisense	UUGGUGAGUUGAUCUUCGGTT
Dnmt3a	Sense	CCAUGUACCGCAAAGCCAUTT
	Antisense	AUGGCUUUGCGGUACAUGGTT
Dnmt3b	Sense	CCUCAAGACAAAUAGCUAUTT
	Antisense	AUAGCUAUUUGUCUUGAGGTT
Negative control	Sense	UUCUUCGAACGUGUCACGUTT
	Antisense	ACGUGACACGUUCGGAGAATT

Transfection of small interfering RNA (siRNA)

Small interfering RNA (siRNA) that targeted *Dnmt1*, *Dnmt3a*, and *Dnmt3b* was designed and provided by GenePharma Co., Ltd (Shanghai, China). siRNA sequences are shown in Table 2. DOP-ASCs (5×10^4 cells) were seeded in a 12-well plate before siRNA transfection. The transfection reagent (Lipofectamine 2000; Thermo Fisher Scientific) was diluted with Opti-MEM I Reduced Serum Medium (Hyclone) and incubated at room temperature for 5 min. The siRNA was added to the diluted Lipofectamine 2000 and gently mixed to form the siRNA-lipofectamine-Opti-MEM complex. Then, the mixture was added to cells at 1 ml per well and incubated at 37 °C with 5% CO_2.

Transduction of shRNA-*Dnmt3a* and LVRNA-*Dnmt3a*

The *Dnmt3a* overexpression lentiviral vector (pLenti-EF1a-EGFP-P2A-Puro-CMV-*Dnmt3a*-3Flag) and *Dnmt3a*-silencing lentiviral vector (pLDK-CMV-EGFP-2A-Puro-U6-shRNA*Dnmt3a*) were designed and manufactured by OBiO Technology Corp., Ltd. (Shanghai, China). The oligonucleotide sequences of shRNA with Dnmt3a RNA interference targets are shown in Table 3. Various virus concentrations were used to determine the multiplicity of infection (MOI). The transduction efficiency was evaluated by analyzing the percentage of green fluorescent protein (GFP)-positive cells under a fluorescence microscope. ASCs at a density of 5×10^4/ml were seeded in a 6-well plate at 2 ml per well. After 12 h of culture, the medium was replaced with a lentivirus suspension medium (MOI:80; 0.6 μg/ml puromycin; 5 μg/ml polybrene). The gene and protein expression were analyzed by RT-PCR and western blotting, respectively, after 4 days of osteogenic induction and their osteogenic ability was assessed by Alizarin Red-S staining after induction for 21 days.

Analysis of DOP-ASCs seeded on BCP by scanning electron microscopy (SEM)

Before seeding DOP-ASCs, scaffolds sterilized by ultraviolet light were placed in 12-well plates. Then, 1 ml of

Table 3 Dnmt3a shRNA sequences

5′		STEM	Loop	STEM	3′
sh-Dnmt3a-F	Ccgg	CCACCAGGTCAAACTCTAT	TTCAAGAGA	ATAGAGTTTGACCTGGTGG	TTTTTTg
sh-Dnmt3a-R	aattcaaaaaa	CCACCAGGTCAAACTCTAT	TCTCTTGAA	ATAGAGTTTGACCTGGTGG	
sh-NC-F	CCGG	TTCTCCGAACGTGTCACGT	TTCAAGAGA	ACGTGACACGTTCGGAGAA	TTTTTTG
sh-NC-R	AATTCAAAAAA	TTCTCCGAACGTGTCACGT	TCTCTTGAA	ACGTGACACGTTCGGAGAA	

passage 2 DOP-ASCs at a density of 5×10^4/ml was seeded on the surface of BCP in each well. After culture at 37 °C with 5% CO_2 for 3 days, samples were fixed with paraformaldehyde. After alcohol gradient dehydration, critical point drying, and spraying the cells with gold, scaffolds were observed by SEM.

Implantation of BCP seeded with DOP-ASCs transduced with shRNA into a DOP mouse model with critically sized calvarial defects

DOP-ASCs were divided into DOP-blank, negative control, and Dnmt3a shRNA groups. DOP-ASCs infected with the silence-Dnmt3a lentivirus were cultured in osteogenic induction medium. A1-ml cell suspension (5×10^4 cells/ml) was added to the surface of BCP in a 12-well plate and cultured for 48 h. Nine DOP mice received calvarial surgery to establish critically sized calvarial defect models. After anaesthetization, the DOP mice were subjected to prone fixation, skin preparation, and disinfection at the top of the skull. An incision was made along the median of the calvarium and the periosteum was bluntly separated to expose the calvarial bone surface. Then, a 4-mm diameter trephine bur was applied to drill a standardized round defect on the side of the sagittal suture. A 0.9% saline solution was used to irrigate the skull surface during drilling. Subsequently, the BCP seeded with DOP-ASCs was implanted into the skull defect area and the periosteum and dermis were sutured in position. After 8 weeks, mice were euthanized and skull specimens were obtained.

Micro-computed tomography (Micro-CT), hematoxylin and eosin staining (HE) staining, and Masson staining

At 8 weeks, the calvarium was removed intact and fixed in freshly prepared 4% formaldehyde for 24 h at 4 °C. Micro-CT scans of skull defects were performed to observe new bone formation. Then, three-dimensional reconstructed images were analyzed. The ratio of the bone volume to total volume available in the scaffold (BV/TV) was calculated. A high ratio indicated that more bone had grown into the scaffolds. Then, tissue samples of the mouse skull defect were decalcified for HE and Masson staining. Next, the samples were dehydrated in an alcohol gradient, clarified, and embedded in paraffin for sectioning. Lastly, the sections were stained with hematoxylin and eosin and Masson trichrome.

Statistical analysis

All experiments were repeated at least three times independently. Two group comparisons were made by the independent-samples t-test and multiple comparisons were made by one-way ANOVA with SPSS 18.0 software (SPSS Inc., Chicago, USA). $P < 0.05$ was regarded to be statistically significant.

Results

Cell proliferation and multipotent differentiation of DOP-ASCs

ASCs from inguinal adipose tissue were isolated and passaged three times (Fig. 1A). RTCA (Fig. 1B) and CCK-8 assays (Fig. 1D) showed that the proliferation rate of the DOP group was relatively lower than that of the control group. After culture in osteogenic and adipogenic media, the morphology of DOP-ASCs had distinctly changed to osteogenic-like in osteogenic medium and adipose-like in adipogenic medium (Fig. 1C). In cartilage medium, ASCs were aggregated to culture for 21 days and then stained with Alcian blue to indicate cartilage-like cells. The findings demonstrated the multipotency of DOP-ASCs (Fig. 1C).

Osteogenic differentiation capacity decreases in DOP-ASCs

To investigate the osteogenic differentiation capacity, we cultured control ASCs and DOP-ASCs to analyze mineralized nodule formation as well as gene and protein expression of OPN and RUNX2. Alizarin Red-S staining showed that the degree of mineralized nodule formation was reduced in DOP-ASCs compared with control ASCs (Fig. 2A). RT-PCR showed that the mRNA levels of *Runx2* and *Opn* in DOP-ASCs were significantly lower than those in control ASCs at 3 and 7 days (Fig. 2B). The protein levels of OPN and RUNX2 were analyzed by immunofluorescence and western blotting, which showed that the fluorescence signals (Fig. 2C) and band intensities (Fig. 2D) at 4 days in DOP-ASCs were weaker compared with those in control ASCs.

DNA methylation increases in DOP-ASCs

DNMT1, DNMT3a, and DNMT3b are major enzymes in DNA methylation and 5-MC is the product of this process. We analyzed the expression of these factors by RT-PCR, western blotting, and immunofluorescence. The expression of *Dnmt1*, *Dnmt3a*, and *Dnmt3b* in DOP-ASCs increased compared with that in control ASCs (Fig. 3A, B). Immunofluorescence confirmed the increases in 5-MC, DNMT1, DNMT3a, and DNMT3b at 4 days (Fig. 3C–F).

Wnt/β-Catenin signaling pathway is suppressed in DOP-ASCs

The Wnt/β-Catenin signaling pathway is a major regulatory pathway in the process of osteogenic differentiation [29, 30]. Therefore, the main factors, which included *β-catenin* and *Lef1*, were detected to demonstrate the activation level of Wnt/β-Catenin signaling pathway.

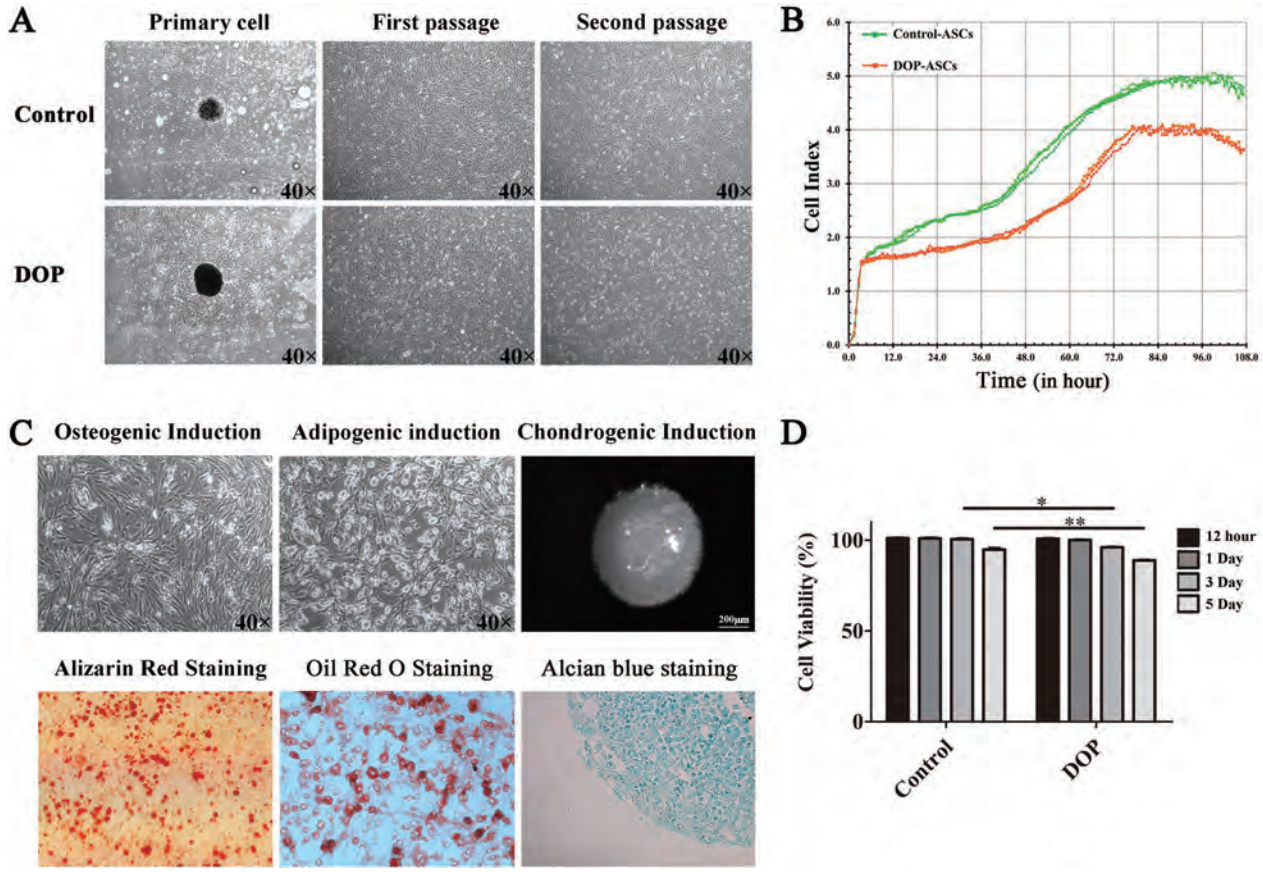

Fig. 1 Cell proliferation and multipotent differentiation of ASCs. **A**: Normal morphology of primary, first, and second passages of control ASCs and DOP-ASCs under light microscopy. **B**, **D**: RTCA and CCK-8 assays showed that the proliferation rate of the DOP group was lower than that of the control group. **C**: Multipotent differentiation of DOP-ASCs into osteogenic cell-like, adipose-like, and cartilage-like cells

RT-PCR showed that the expression of *β-catenin* and *Lef1* decreased in DOP-ASCs compared with that in CON-ASCs, and the results of western blotting were consistent with those of RT-PCR (Fig. 4A, B). Immunofluorescence confirmed that the expression of β-catenin and LEF1 was low in DOP-ASCs (Fig. 4C, D).

Inhibiting DNA methyltransferases rescues loss of the osteogenic potential in DOP-ASCs

The results showed that the reduced osteogenic differentiation capacity of DOP-ASCs was related to increases in DNA methylation levels and suppression of Wnt/β-Catenin signaling pathway. Next, we used siRNA to inhibit the expression of DNA methylation enzymes and explored the relationship between DNA methylation and the osteogenic differentiation ability of DOP-ASCs. After siRNA treatment, the formation of mineralized nodules was increased when the DNA methylation level was downregulated (Fig. 5A). RT-PCR and western blotting showed that RUNX2 was increased in Dnmt1-siRNA, Dnmt3a-siRNA, and Dnmt3b-siRNA groups, and OPN was particularly increased in the Dnmt3a-siRNA group (Fig. 5B, C). In terms of Wnt/β-Catenin signaling pathway, β-catenin and LEF1 were upregulated after siRNA treatment and their expression was the highest in the Dnmt3a-siRNA group compared with the other groups (Fig. 5D, E). These data suggested that downregulation of Dnmt3a inhibited osteogenic differentiation and activity of Wnt/β-Catenin signaling pathway.

Knockdown of Dnmt3a promotes osteogenic differentiation of DOP-ASCs

To further demonstrate the effect of Dnmt3a on osteogenic differentiation of DOP-ASCs, we used lentiviruses to knockdown or overexpress Dnmt3a in DOP-ASCs. The cells were successfully infected by the lentiviruses and showed green fluorescence at an MOI of 80 (Fig. 6A). RT-PCR and western blotting showed that Dnmt3a was successfully knocked down by Dnmt3a shRNA and overexpressed by Dnmt3a LVRNA. 3-Flag was a marker of positive overexpression (Fig. 6B, D). Immunofluorescence confirmed the differences in expression of

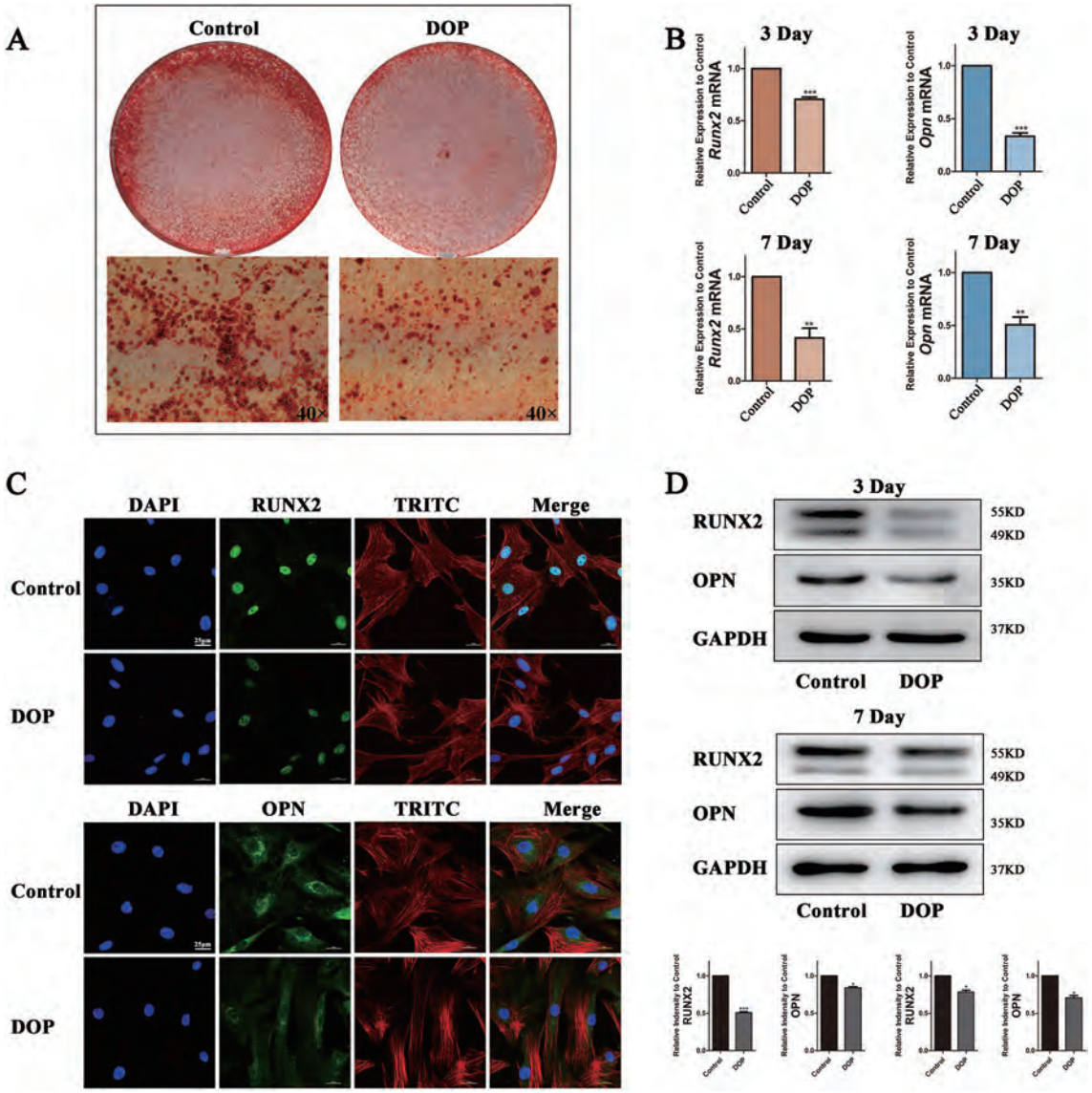

Fig. 2 Decrease of the osteogenic differentiation capacity in DOP-ASCs. **A**: Alizarin Red-S staining of control ASCs and DOP-ASCs. **B**: mRNA levels of osteogenesis-related molecules *Runx2* and *Opn* after 3 and 7 days of osteoinduction. **C**: Immunofluorescence staining of RUX2 and OPN proteins in control ASCs and DOP-ASCs after 4 days of osteoinduction. **D**: Protein levels of osteogenesis-related molecules RUNX2 and OPN after 3 and 7 days of osteoinduction. Data represent the mean ± SD of at least three independent experiments, $^{*}P < 0.05$, $^{**}P < 0.01$

DNMT3a among the DOP-blank group, Negative Control, Dnmt3a shRNA and Dnmt3a LVRNA. (Fig. 6C).

Next, we found that the formation of mineralized nodules was the highest in the Dnmt3a shRNA group and the lowest in the Dnmt3a LVRNA group (Fig. 7A). Expression of *Opn* and *Runx2* was upregulated in the Dnmt3a shRNA group compared with the other three groups and the results of western blot assays were consistent with those of RT-PCR (Fig. 7B–D). Detection of osteogenic differentiation by Alizarin Red-S staining, RT-PCR, and western blotting showed that knockdown of Dnmt3a rescued the osteogenic differentiation capacity of DOP-ASCs. Although Dnmt3a LVRNA treatment decreased the expression of *β-catenin* and *Lef1* compared with DOP-ASC and negative control groups, the expression of these factors was recovered by Dnmt3a shRNA treatment. This suggested that the low activity of the Wnt signaling pathway in DOP-ASCs was recovered by knocking down Dnmt3a (Fig. 7E–G). Taken together, these results suggested that knockdown of Dnmt3a decreased the DNA methylation level, alleviated inhibition of Wnt by DNA methylation,

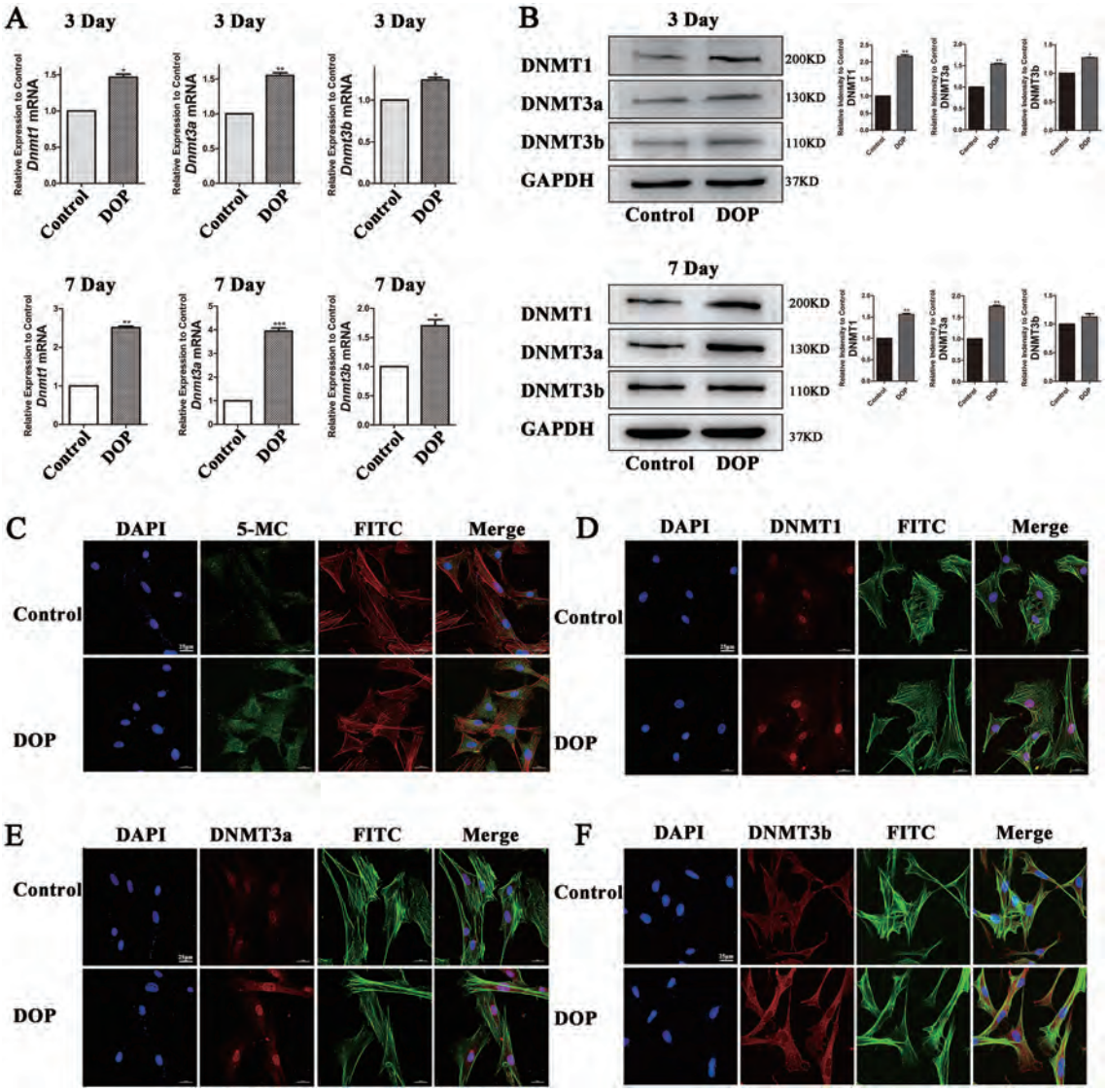

Fig. 3 Increase of the DNA methylation level in DOP-ASCs. **A**, **B**: RT-PCR and western blot analyses showing that the expression of Dnmt1, Dnmt3a, and Dnmt3b in DOP-ASCs was increased compared with that in control ASCs. **C**, **D**: Immunofluorescence showing increases in 5-MC, DNMT1, DNMT3a, and DNMT3b after 4 days of osteoinduction. Data represent the mean ± SD of at least three independent experiments, $^{*}P < 0.05$, $^{**}P < 0.01$

and rescued the loss of the osteogenic capacity of DOP-ASCs.

Downregulation of Dnmt3a promotes the osteogenic capacity of DOP-ASCs in vivo

RT-PCR and western blotting showed that Dnmt3a was successfully knocked down by Dnmt3a shRNA (Fig. 8A, B). SEM and fluorescence microscopy showed that DOP-ASCs grew adherently on the surface and pores of BCP (Fig. 8C). The DOP mouse model with critically sized calvarial defects was successfully established and BCP seeded with transfected DOP-ASCs were implanted into the defect area (Fig. 8D). Eight weeks later, Micro-CT showed new bone matrix on BCP at sagittal and coronal levels. Three-dimensional reconstruction showed that the amount of new bone matrix in the Dnmt3a shRNA group was significantly larger than that in DOP-ASC and negative control groups.BV/TV, BS/BV, and TbTh analyses further demonstrated that the osteogenic capacity was greatly increased when Dnmt3a was downregulated by shRNA in vivo (Fig. 9A, B). HE and Masson staining were also used to observe the osteogenic capacity of DOP-ASCs in vivo. HE staining showed new bone matrix as red and Masson staining showed new bone matrix as

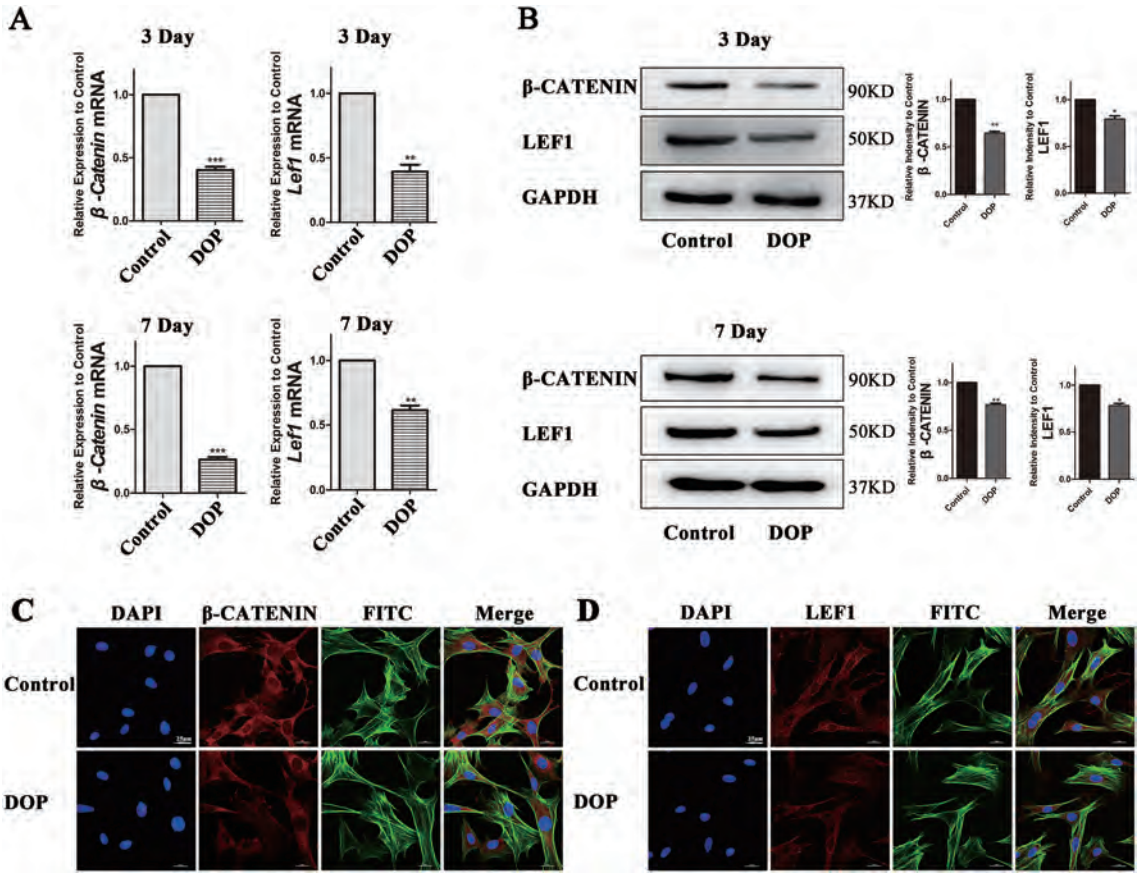

Fig. 4 Wnt/β-Catenin signaling pathway is suppressed in DOP-ASCs. **A**, **B**: RT-PCR and western blot analyses showing that the expression of β-catenin and LEF1 was decreased compared with that in CON-ASCs. **C**, **D**: Immunofluorescence staining of β-catenin and LEF1. Data represent the mean ± SD of at least three independent experiments, $^{*}P < 0.05$, $^{**}P < 0.01$

blue. Both staining showed that the staining degree in the Dnmt3a shRNA group was stronger than that in DOP-ASC and negative control groups (Fig. 9C). These results suggested that knockdown of Dnmt3a rescued the loss of the osteogenic capacity of DOP-ASCs.

Discussion

Many studies have shown that hyperglycemia and the glycolytic metabolites of diabetes decrease cell viability and proliferation, and even promote apoptosis of MSCs, which impairs osteogenic differentiation [29–33]. Heilmeier et al. found that serum miR-550a-5p inhibited the osteogenic differentiation of ASCs in postmenopausal women with type 2 diabetes [34]. Liu et al. reported that osteogenic differentiation of hPDLSCs was significantly inhibited in a high glucose environment and the levels of osteoblast-related factors expressed by cells were reduced significantly [35]. In this study, DOP-ASCs were isolated from DOP mice by the tissue block method, which had osteogenic, adipogenic, and chondrogenic differentiation abilities. However, the expression of osteogenic-related genes *Runx2* and *Opn* was downregulated in DOP-ASCs compared with control ASCs, which demonstrated inhibition of the differentiation process of DOP-ASCs to osteoblasts.

The differentiation of MSCs into osteogenic progenitor cells is regulated by various growth factors and signaling pathways [36, 37]. The Wnt/β-Catenin signaling pathway plays a major role in regulating the proliferation and differentiation of MSCs. Activation of Wnt/β-Catenin signaling pathway promotes osteogenic differentiation of ASCs [38, 39]. Moldes et al. reported that β-catenin expression was higher in 3T3-L1 precursor adipocytes and the expression level of β-catenin was significantly reduced during adipogenesis [40]. In our previous studies, after activation of Wnt/β-Catenin signaling pathway, the expression of Wnt-related signaling molecules, such as β-catenin and LEF1, was upregulated in normal ASCs, which promoted the expression of osteogenic differentiation factors such as Opn and Runx2 [5, 41]. In this

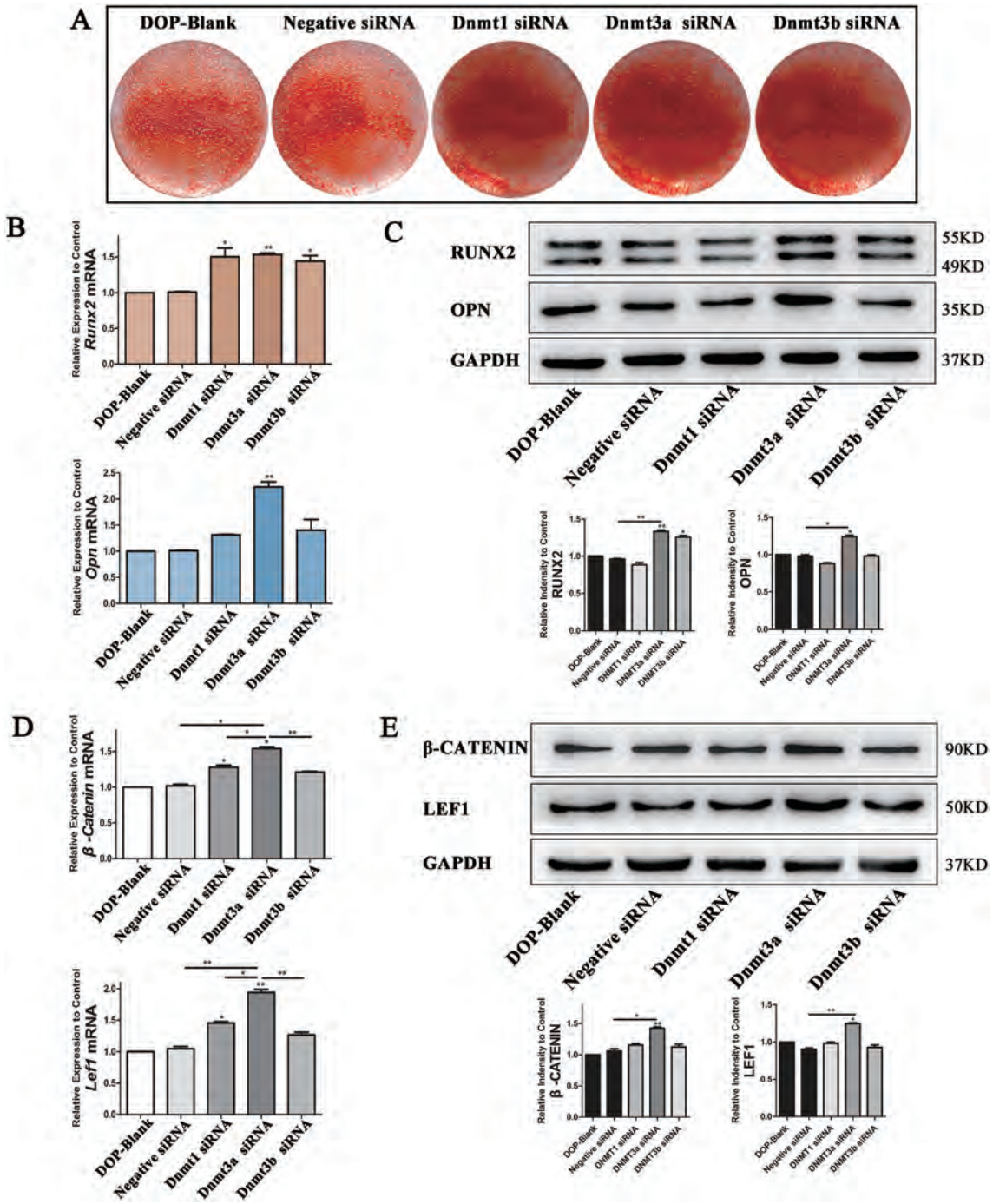

Fig. 5 *Dnmt* siRNAs increase the osteogenic potential of DOP-ASCs. **A**: Alizarin Red-S staining showing that the formation of mineralized nodules in Dnmt3a shRNA was increased compared with that in Negative Control after *Dnmt* siRNA treatment of DOP-ASCs (osteoinduction for 21 days). **B**–**E**: mRNA and protein levels of Wnt/β-Catenin signaling pathway markers and osteogenesis-related molecules were upregulated after *Dnmt* siRNA transfection into DOP-ASCs (osteoinduction for 4 days). Data represent the mean ± SD of at least three independent experiments, $^{*}P < 0.05$, $^{**}P < 0.01$

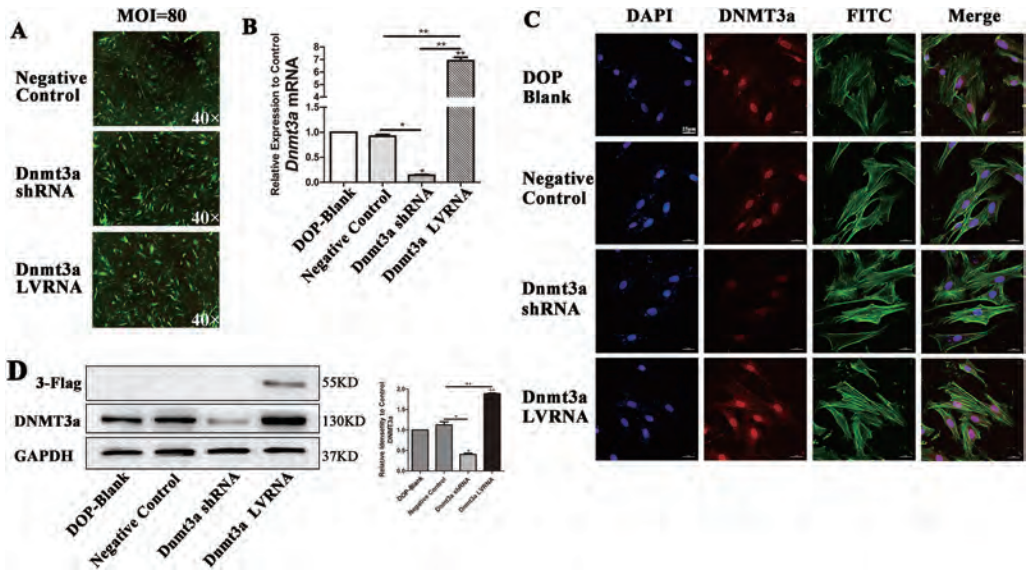

Fig. 6 Dnmt3a shRNA and Dnmt3a LVRNA were successfully transduced into DOP-ASCs. **A**: Cells were successfully infected with lentiviruses and exhibited green fluorescence at an MOI of 80. **B**, **D**: mRNA levels of *Dnmt3a* and protein levels of 3-Flag showed that Dnmt3a was knocked down by Dnmt3a shRNA and overexpressed by Dnmt3a LVRNA. **C**: Immunofluorescence staining of Dnmt3a. Data represent the mean ± SD of at least three independent experiments, $^{*}P < 0.05$, $^{**}P < 0.01$

study, we compared DOP-ASCs and control ASCs and demonstrated that osteogenic differentiation and Wnt/β-Catenin signaling pathway were suppressed in ASCs of DOP mice.

The high glucose environment caused by diabetes increases DNA methylation in cells, which affects their differentiation processes [42, 43]. Many studies have suggested that DNA methylation is involved in the osteogenic differentiation of stem cells [44–48]. Wang et al. reported that KDM6A promoted chondrogenic differentiation of periodontal ligament stem cells by demethylation of SOX9 [49]. Zhang et al. reported that a demethylated Runx2 gene in bone marrow mesenchymal stem cells promoted their differentiation into osteoblasts [47]. These studies showed that, during the process of osteogenic differentiation of ASCs, the DNA methylation levels of osteogenesis-specific genes Dlx5 and Runx2, and the CpG island region of the Osterix promoter were downregulated significantly, and the expression of these genes was upregulated. Seman et al. found that the DNA methylation level of the promoter region of the SLC30A8 gene in a diabetic population was higher than that in non-diabetic patients, which suggested that high DNA methylation of the SLC30A8 gene affects the occurrence of diabetes [50]. We observed that the DNA methylation levels and expression of DNMT genes in DOP-ASCs were upregulated significantly. After decreasing DNMTs by siRNA, we found that the expression of osteogenic differentiation factors RUNX2 and OPN was relatively increased, which indicated that DNA methylation had a close relationship with the osteogenic differentiation process of ASCs.

DNA methylation at specific sites is catalyzed by DNMTs, which might play various roles in cell differentiation. Dnmt3a, as the main methyltransferase in embryonic development and differentiation, is mainly located in the chromatin region and is highly expressed in oocytes, spermatogonia, and stem cells [51, 52]. Mark A. Casillas Jr NL et al. found that the expression of Dnmt3a was highly abundant in oocytes, but gradually decreased during maturation [53]. They observed that the overall methylation level of genomic DNA in senescent cells was reduced, which corresponded to the decrease in expression of Dnmt1, while some genes were hypermethylated with high expression of Dnmt3a and Dnmt3b [53]. Disturbances in epigenetic regulation may be a factor that contributes to diseases [54, 55]. In our study, RNA interference was used to silence the expression of Dnmt1, Dnmt3a, and Dnmt3b. Silencing of Dnmt3a promoted the expression of bone-related genes and Wnt/β-Catenin signaling pathway-related genes were induced, thereby promoting the osteogenic differentiation of DOP-ASCs. Overexpression of Dnmt3a by lentivirus infection confirmed that Dnmt3a significantly inhibited the expression of osteogenic-related genes and Wnt/β-Catenin signaling pathway in DOP-ASCs and the osteogenic differentiation ability of DOP-ASCs was restored after inhibition of Dnmt3a.

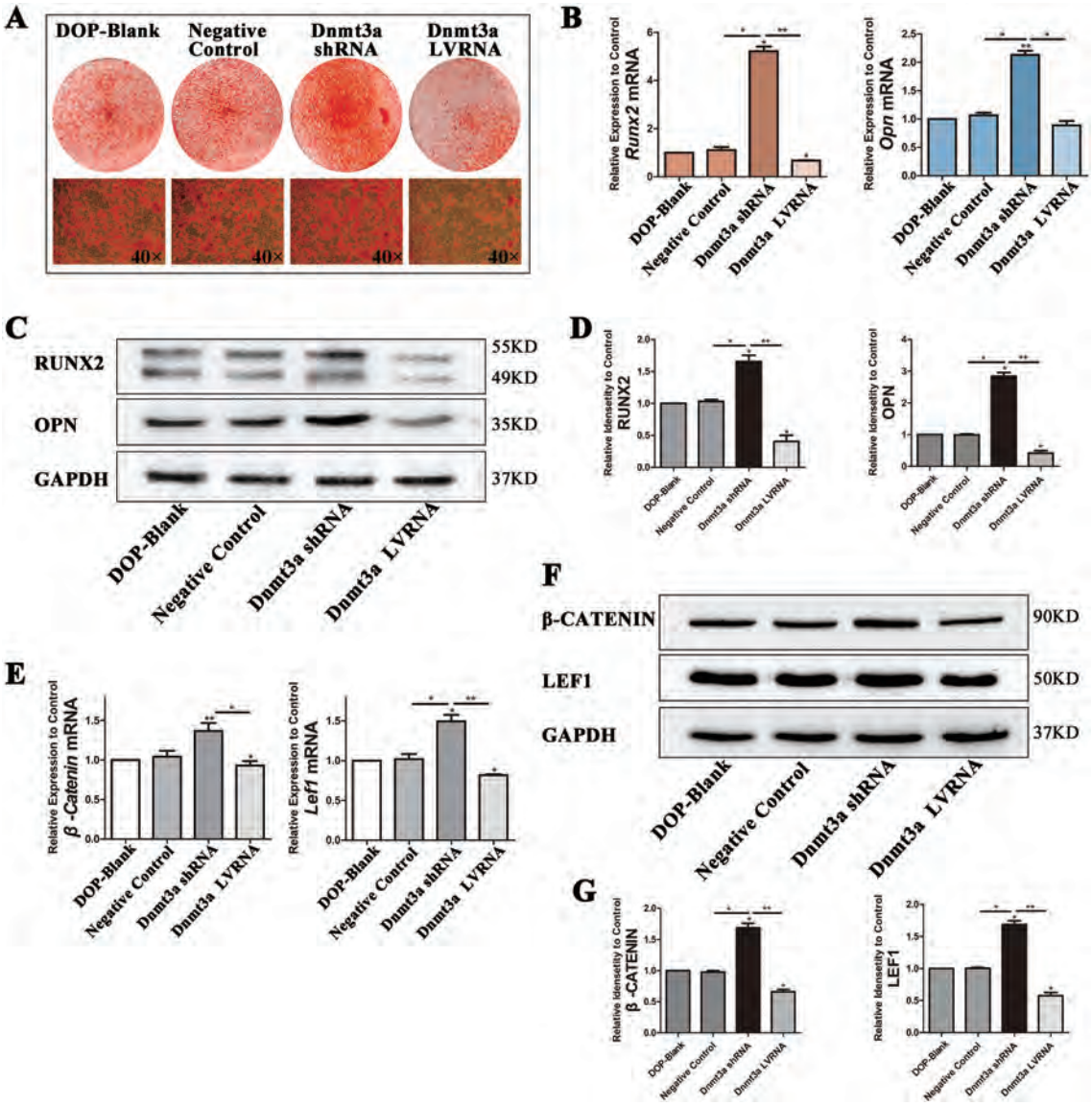

Fig. 7 Knockdown of Dnmt3a promotes osteogenic differentiation of DOP-ASCs. **A**: Alizarin Red-S staining showing that the formation of mineralized nodules was the highest in the Dnmt3a shRNA group and the lowest in the Dnmt3a LVRNA group (osteoinduction for 21 days). **B**–**D**: mRNA and protein levels of osteogenesis-related molecules were upregulated in the Dnmt3a shRNA group compared with the other three groups (osteoinduction for 4 days). **E**–**G**: mRNA and protein levels of Wnt signaling pathway markers were recovered by knockdown of Dnmt3a. Data represent the mean ± SD of at least three independent experiments, $^{*}P < 0.05$, $^{**}P < 0.01$

We also confirmed the osteogenic effects of Dnmt3a in DOP mice in vivo. BCP is considered to be a biomaterial with high porosity and penetration, which creates a favorable microenvironment for bone regeneration [56, 57]. Tang et al. implanted various BCP scaffolds into a critically sized bone defect model in OVX rats and applied Micro-CT to analyze new bone formation [58–60]. In our study, we seeded DOP-ASCs on BCP and implanted the scaffold into a mouse critically sized skull defect to assess the osteogenic capacity in vivo. Three-dimensional reconstruction of Micro-CT images showed that new bone formation in the Dnmt3a shRNA group had obviously increased compared with that in DOP-ASC and negative control groups. Furthermore, histology of the corresponding tissue samples was consistent with the results of Micro-CT, i.e., the amount of new bone formation in the Dnmt3a shRNA group was more obvious than that in DOP-blank and Negative Control.

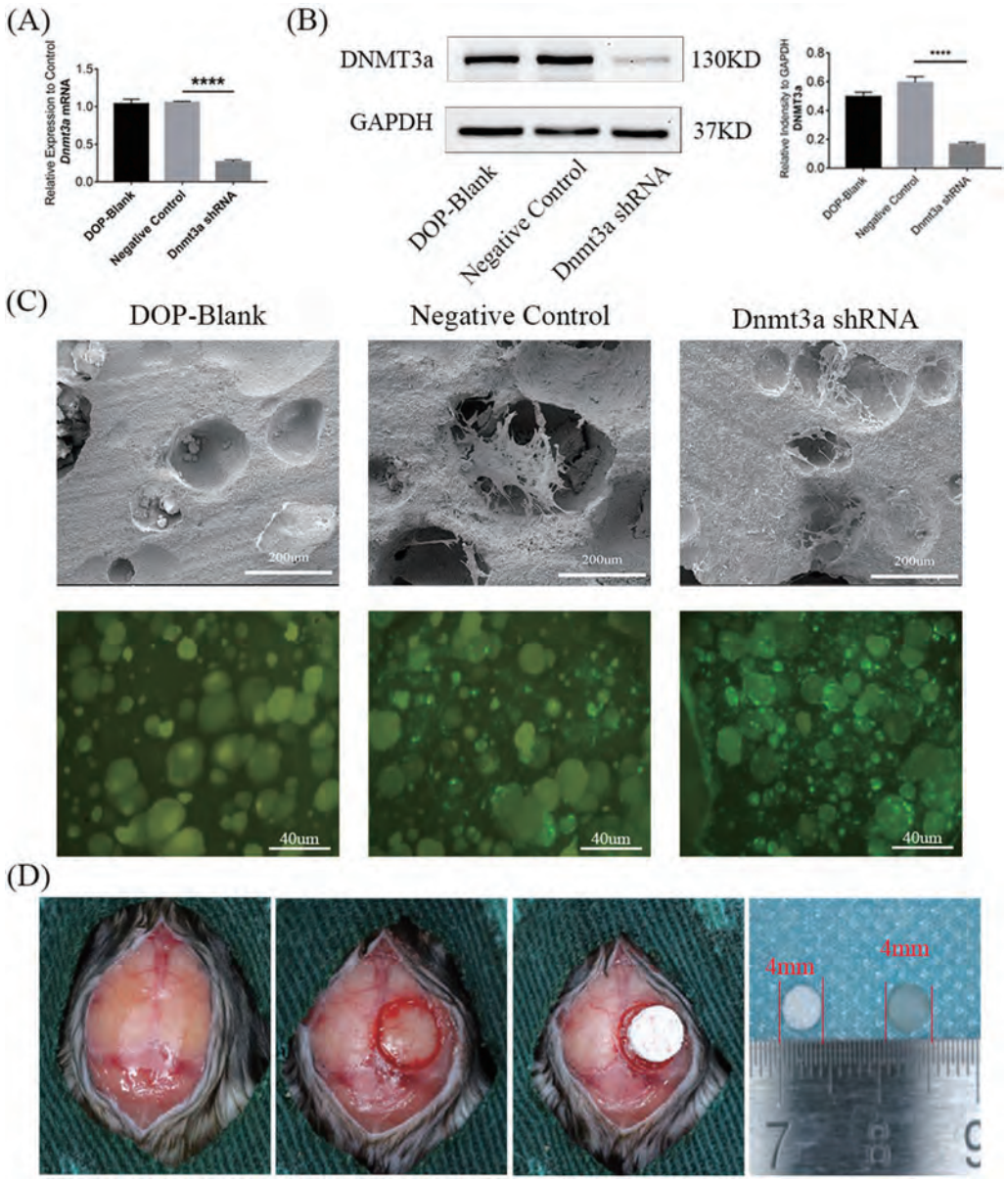

Fig. 8 BCP was successfully implanted into the skull defect of mice. BCP seeded with transfected DOP-ASCs were implanted into critically sized calvarial defects in DOP mouse models. **A**, **B**: mRNA and protein levels of Dnmt3a were successfully knocked down by Dnmt3a shRNA (osteoinduction for 3 days). **C**: SEM and fluorescence microscopy showing that DOP-ASCs grew adherently on the surface and pores of BCP. **D**: The DOP mouse model with critically sized calvarial defects was successfully established and BCP seeded with transfected DOP-ASCs were implanted into the defect area

DOP has become a severe public health problem. DNA methylation as a kind of stable epigenetic alteration is involved in bone formation and resorption [61]. Epigenetic modifications play an implant role in cell differentiation and development [62]. Many studies have demonstrated that DNA methylation is a therapeutic target for bone diseases [61]. Our study demonstrated that a high level of Dnmt3a may impair the osteogenic ability of ASCs, and the osteogenic differentiation ability of DOP-ASCs was restored after inhibition of Dnmt3a. Therefore, this study explains the decrease in the osteogenic capacity of DOP-ASCs from the viewpoint of epigenetics and provides a potential therapeutic target for the prevention and treatment of DOP.

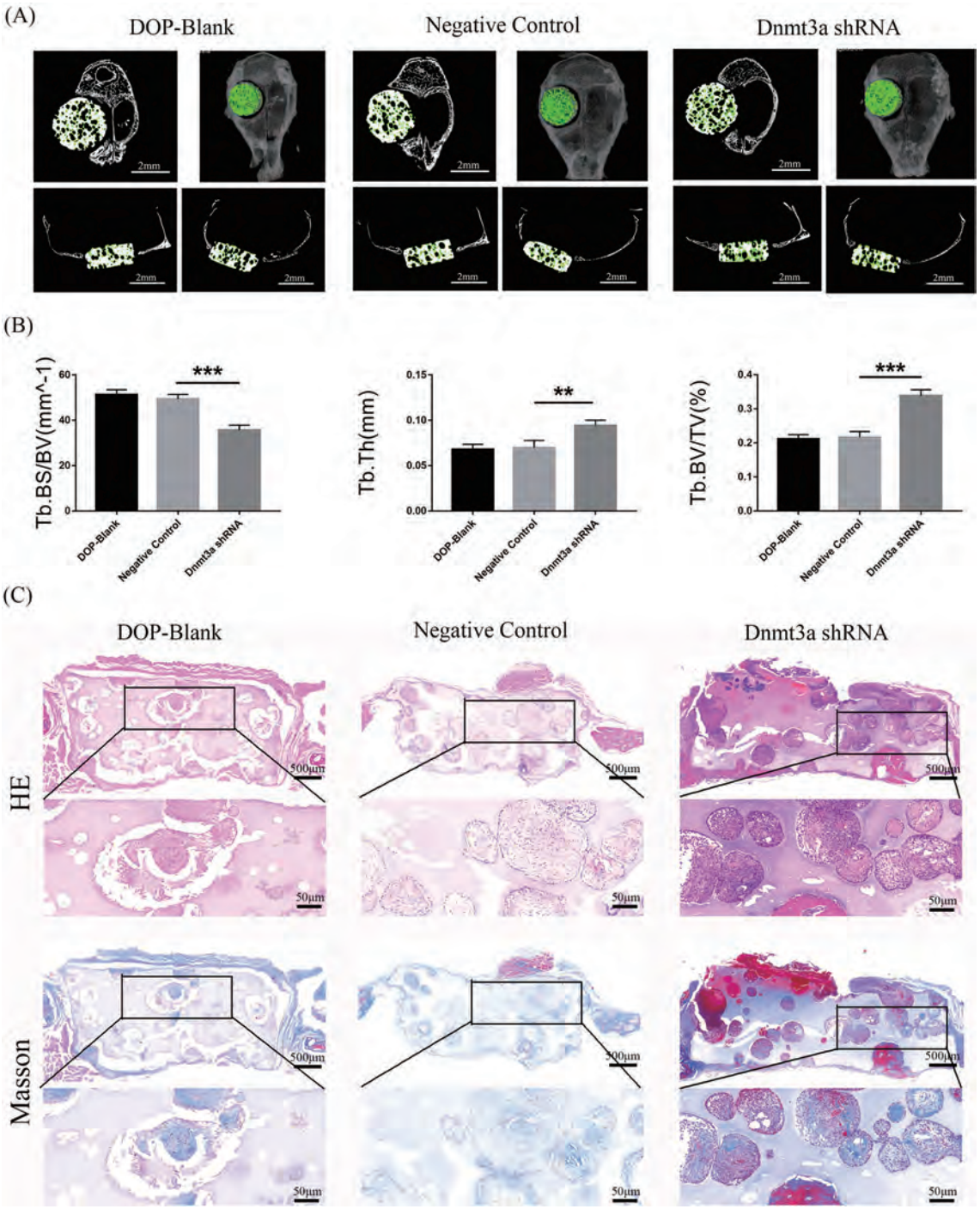

Fig. 9 Downregulation of Dnmt3a promotes the osteogenic capacity of DOP-ASCs in vivo. **A** Micro-CT showed that the amount of new bone matrix (green) in the Dnmt3a shRNA group was significantly higher than that in DOP-ASC and negative control groups. **B** BV/TV, BS/BV, and TbTh analysis demonstrated that the osteogenic capacity was greatly increased when Dnmt3a was downregulated by shRNA in vivo. Data represent the mean ± SD of at least three independent experiments, $^{*}P < 0.05$, $^{**}P < 0.01$. **C**: HE and Masson staining of BCP showed that the staining degree in the Dnmt3a shRNA group was stronger than that in DOP-ASC and negative control groups

Conclusions

Our study showed that Wnt/β-catenin signaling pathway is a major player in the process of osteogenic differentiation of DOP-ASCs and DNA methylation is an important factor that affects the osteogenic differentiation of DOP-ASCs, which has significance for bone regeneration in DOP. Downregulation of Dnmt3a activated Wnt/β-catenin pathway, and promoted the osteogenic differentiation of DOP-ASCs. These findings indicate that Dnmt3a knockdown rescues the impaired osteogenic ability of DOP-ASCs *in vitro* and *in vivo*, thereby providing a possible approach for bone regeneration using DOP-ASCs in DOP patients.

Abbreviations

DOP: Diabetic osteoporosis; DM: Diabetes mellitus; ASCs: Adipose-derived stem cells; PCR: Quantitative real-time polymerase chain reaction; ALP: Alkaline phosphatase; β-Catenin: Cadherin associated protein; Runx2: Runt-related transcription factor 2; Opn: Osteopontin; GAPDH: Glyceraldehyde phosphate dehydrogenase; DNMT1: DNA methyltransferases 1; DNMT3a: DNA methyltransferases 3a; DNMT3b: DNA methyltransferases 3b; BV/TV: Ratio of bone volume to tissue volume; BS/BV: The area of bone tissue per unit volume; TbTh: Trabecular thickness .

Acknowledgements

Not applicable.

Author contributions

All authors have made important contributions to this research. MZ conducted in vitro experiments, executed the analysis of the data, and wrote the main manuscript. YG conducted in vivo experiments and wrote the main manuscript. QL reviewed and revised the manuscript. HC collected the data. JY established the animal model of diabetic osteoporosis. XC designed the experimental project, analyzed data, and revised the manuscript. JX conceived and designed the experiment, analyzed data, revised the manuscript, and provided funding. All authors have read and approved the final manuscript.

Funding

This work was funded by National Natural Science Foundation of China (81870746, 81970986, 81771125), Open Project of the State Key Laboratory of Oral Disease Research (SKLOD2021OF08), Joint project of Luzhou Municipal People's Government and Southwest Medical University (2020LZXNYDZ09), Program of Southwest Medical University (2019ZQN167), Program of The Affiliated Stomatological Hospital of Southwest Medical University (202017), Climb Plan Project of The Affiliated Stomatological Hospital of Southwest Medical University (2020QY04), Key Program of Southwest Medical University (2021ZKZD009), and Project of Stomatological Institute of Southwest Medical University (2021XJYJS01).

Availability of data and materials

The datasets generated or analyzed during the current study can be obtained from the corresponding author in accordance with reasonable requirements.

Declarations

Ethics approval and consent to participate

The Ethics Committee of Southwest Medical University reviewed and approved the experimental animal procedures, and we conducted animal care and anesthesia in accordance with the guidelines of the Care and Use of Laboratory Animals (Ministry of Science and Technology of China, 2006).

Consent for publication

Not applicable.

Competing interests

The authors declare that there is no conflict of interests regarding the publication of this paper.

Author details

[1]Department of Oral Implantology, The Affiliated Stomatological Hospital of Southwest Medical University, Luzhou 646000, China. [2]State Key Laboratory of Oral Diseases, West China Hospital of Stomatology, Sichuan University, Chengdu 610041, China. [3]Department of Oral and Maxillofacial Surgery, The Affiliated Hospital of Southwest Medical University, Luzhou 646000, China. [4]Luzhou Key Laboratory of Oral & Maxillofacial Reconstruction and Regeneration, The Affiliated Stomatological Hospital of Southwest Medical University, Luzhou 646000, China.

Received: 20 March 2022 Accepted: 23 July 2022
Published online: 04 August 2022

References

1. Motyl KJ, Mccauley LK, Mccabe LR. Amelioration of type I diabetes-induced osteoporosis by parathyroid hormone is associated with improved osteoblast survival. J Cell Physiol. 2012;227(4):1326–34.
2. Zheng HX, Chen J, Zu YX, Wang EZ, Qi SS. Chondroitin sulfate prevents STZ induced diabetic osteoporosis through decreasing blood glucose, antioxidative stress, anti-inflammation and OPG/RANKL expression regulation. Int J Mol Sci. 2020;21(15):5303.
3. Wang N, Xu P, Wang X, Yao W, Wang B, Wu Y, Shou D. Timosaponin AIII attenuates inflammatory injury in AGEs-induced osteoblast and alloxan-induced diabetic osteoporosis zebrafish by modulating the RAGE/MAPK signaling pathways. Phytomedicine. 2020;75: 153247.
4. Chen S, Du K, Zou C. Current progress in stem cell therapy for type 1 diabetes mellitus. Stem Cell Res Ther. 2020;11(1):275.
5. Zhang M, Li Y, Rao P, Huang K, Luo D, Cai X, Xiao J. Blockade of receptors of advanced glycation end products ameliorates diabetic osteogenesis of adipose-derived stem cells through DNA methylation and Wnt signalling pathway. Cell Prolif. 2018;51(5): e12471.
6. Oliveira PAD, Oliveira AMSD, Pablos AB, Costa FO, Silva GA, Santos JN, Cury PR. Influence of hyperbaric oxygen therapy on peri-implant bone healing in rats with alloxan-induced diabetes. J Clin Periodontol. 2012;39(9):879–86.
7. Wallner C, Abraham S, Wagner JM, Harati K, Ismer B, Kessler L, Zöllner H, Lehnhardt M, Behr B. Local application of isogenic adipose-derived stem cells restores bone healing capacity in a type 2 diabetes model. Stem Cells Transl Med. 2016;5(6):836–44.
8. Wu R, Ruan J, Sun Y, Liu M, Sha Z, Fan C, Wu Q. Long non-coding RNA HIF1A-AS2 facilitates adipose-derived stem cells (ASCs) osteogenic differentiation through miR-665/IL6 axis via PI3K/Akt signaling pathway. Stem Cell Res Ther. 2018;9(1):348.
9. Li S, Liu Y, Tian T, Zhang T, Lin S, Zhou M, Zhang X, Lin Y, Cai X. Bioswitchable delivery of microRNA by framework nucleic acids: application to bone regeneration. Small. 2021;17(47): e2104359.
10. Vanhatupa S, Ojansivu M, Autio R, Juntunen M, Miettinen S. Bone Morphogenetic protein-2 induces donor-dependent osteogenic and adipogenic differentiation in human adipose stem cells. Stem Cells Transl Med. 2015;4(12):1391–402.
11. Zhou N, Li Q, Lin X, Hu N, Liao JY, Lin LB, Zhao C, Hu ZM, Liang X, Xu W, Chen H, Huang W. BMP2 induces chondrogenic differentiation, osteogenic differentiation and endochondral ossification in stem cells. Cell Tissue Res. 2016;366(1):101–11.
12. Uccelli A, Moretta L, Pistoia V. Mesenchymal stem cells in health and disease. Nat Rev Immunol. 2008;8(9):726–36.
13. Vrtacnik P, Marc J, Ostanek B. Hypoxia mimetic deferoxamine influences the expression of histone acetylation- and DNA methylation-associated genes in osteoblasts. Connect Tissue Res. 2015;56(3):228–35.
14. Chen Q, Yan W, Duan E. Epigenetic inheritance of acquired traits through sperm RNAs and sperm RNA modifications. Nat Rev Genet. 2016;17(12):733–43.
15. Portela A, Esteller M. Epigenetic modifications and human disease. Nat Biotechnol. 2010;28(10):1057–68.

16. Moore LD, Le T, Fan G. DNA methylation and its basic function. Neuropsychopharmacology. 2013;38(1):23–38.
17. Law PP, Holland ML. DNA methylation at the crossroads of gene and environment interactions. Essays Biochem. 2019;63(6):717–26.
18. Deplus R, Denis H, Putmans P, Calonne E, Fourrez M, Yamamoto K, Suzuki A, Fuks F. Citrullination of DNMT3A by PADI4 regulates its stability and controls DNA methylation. Nucleic Acids Res. 2014;42(13):8285–96.
19. Veland N, Lu Y, Hardikar S, Gaddis S, Zeng Y, Liu B, Estecio MR, Takata Y, Lin K, Tomida MW, Shen J, Saha D, Gowher H, Zhao H, Chen T. DNMT3L facilitates DNA methylation partly by maintaining DNMT3A stability in mouse embryonic stem cells. Nucleic Acids Res. 2019;47(1):152–67.
20. Anteneh H, Fang J, Song J. Structural basis for impairment of DNA methylation by the DNMT3A R882H mutation. Nat Commun. 2020;11(1):2294.
21. Ghayor C, Weber FE. Epigenetic regulation of bone remodeling and its impacts in osteoporosis. Int J Mol Sci. 2016;17(9):1446.
22. Liu J, Xiao Q, Xiao J, Niu C, Li Y, Zhang X, Zhou Z, Shu G, Yin G. Wnt/β-catenin signalling: function, biological mechanisms, and therapeutic opportunities. Signal Transduct Target Ther. 2022;7(1):3.
23. Peng S, Gao Y, Shi S, Zhao D, Cao H, Fu T, Cai X, Xiao J. LncRNA-AK137033 inhibits the osteogenic potential of adipose-derived stem cells in diabetic osteoporosis by regulating Wnt signaling pathway via DNA methylation. Cell Prolif. 2022;55(1): e13174.
24. Yu AX, Xu ML, Yao P, Kwan KK, Liu YX, Duan R, Dong TT, Ko RK, Tsim KW. Corylin, a flavonoid derived from Psoralea Fructus, induces osteoblastic differentiation via estrogen and Wnt/β-catenin signaling pathways. FASEB J. 2020;34(3):4311–28.
25. Svedlund J, Aurén M, Sundström M, Dralle H, Akerström G, Björklund P, Westin G. Aberrant WNT/β-catenin signaling in parathyroid carcinoma. Mol Cancer. 2010;9:294.
26. Liu T, Wu X, Chen T, Luo Z, Hu X. Downregulation of DNMT3A by miR-708-5p inhibits lung cancer stem cell-like phenotypes through repressing Wnt/β-catenin signaling. Clin Cancer Res. 2018;24(7):1748–60.
27. Wong CC, Xu J, Bian X, Wu JL, Kang W, Qian Y, Li W, Chen H, Gou H, Liu D, Yat Luk ST, Zhou Q, Ji F, Chan LS, Shirasawa S, Sung JJ, Yu J. In colorectal cancer cells with mutant KRAS, SLC25A22-mediated glutaminolysis reduces DNA demethylation to increase WNT signaling, stemness, and drug resistance. Gastroenterology. 2020;159(6):2163-2180.e6.
28. Wu B, Li Y, Li B, Zhang B, Wang Y, Li L, Gao J, Fu Y, Li S, Chen C, Surani MA, Tang F, Li X, Bao S. DNMTs play an important role in maintaining the pluripotency of leukemia inhibitory factor-dependent embryonic stem cells. Stem Cell Rep. 2021;16(3):582–96.
29. Luo W, Zhang L, Huang B, Zhang H, Zhang Y, Zhang F, Liang P, Chen Q, Cheng Q, Tan D, Tan Y, Song J, Zhao T, Haydon RC, Reid RR, Luu HH, Lee MJ, El Dafrawy M, Ji P, He TC, Gou L. BMP9-initiated osteogenic/odontogenic differentiation of mouse tooth germ mesenchymal cells (TGMCS) requires Wnt/β-catenin signalling activity. J Cell Mol Med. 2021;25(5):2666–78.
30. Kim JH, Liu X, Wang J, Chen X, Zhang H, Kim SH, Cui J, Li R, Zhang W, Kong Y, Zhang J, Shui W, Lamplot J, Rogers MR, Zhao C, Wang N, Rajan P, Tomal J, Statz J, Wu N, Luu HH, Haydon RC, He TC. Wnt signaling in bone formation and its therapeutic potential for bone diseases. Ther Adv Musculoskelet Dis. 2013;5(1):13–31.
31. Wang C, Wang M, Xu T, Zhang X, Lin C, Gao W, Xu H, Lei B, Mao C. Engineering bioactive self-healing antibacterial exosomes hydrogel for promoting chronic diabetic wound healing and complete skin regeneration. Theranostics. 2019;9(1):65–76.
32. Abdulameer SA, Sulaiman SA, Hassali MA, Subramaniam K, Sahib MN. Osteoporosis and type 2 diabetes mellitus: what do we know, and what we can do? Patient Prefer Adherence. 2012;6:435–48.
33. Heilmeier U, Hackl M, Skalicky S, Weilner S, Schroeder F, Vierlinger K, Patsch JM, Baum T, Oberbauer E, Lobach I, Burghardt AJ, Schwartz AV, Grillari J, Link TM. Serum mirna signatures are indicative of skeletal fractures in postmenopausal women with and without type 2 diabetes and influence osteogenic and adipogenic differentiation of adipose tissue-derived mesenchymal stem cells in vitro. J Bone Miner Res. 2016;31(12):2173–92.
34. Tencerova M, Figeac F, Ditzel N, Taipaleenmäki H, Nielsen TK, Kassem M. High-fat diet-induced obesity promotes expansion of bone marrow adipose tissue and impairs skeletal stem cell functions in mice. J Bone Miner Res. 2018;33:1154–65.
35. Liu Z, Chen T, Sun W, Yuan Z, Yu M, Chen G, Guo W, Xiao J, Tian W. DNA demethylation rescues the impaired osteogenic differentiation ability of human periodontal ligament stem cells in high glucose. Sci Rep. 2016;6:27447.
36. Fan T, Qu R, Yu Q, Sun B, Jiang X, Yang Y, Huang X, Zhou Z, Ouyang J, Zhong S, Dai J. Bioinformatics analysis of the biological changes involved in the osteogenic differentiation of human mesenchymal stem cells. J Cell Mol Med. 2020;24(14):7968–78.
37. Saidova AA, Vorobjev IA. Lineage commitment, signaling pathways, and the cytoskeleton systems in mesenchymal stem cells. Tissue Eng Part B Rev. 2020;26(1):13–25.
38. Wang CG, Hu YH, Su SL, Zhong D. LncRNA DANCR and miR-320a suppressed osteogenic differentiation in osteoporosis by directly inhibiting the Wnt/β-catenin signaling pathway. Exp Mol Med. 2020;52(8):1310–25.
39. Hang K, Ying L, Bai J, Wang Y, Kuang Z, Xue D, Pan Z. Knockdown of SERPINB2 enhances the osteogenic differentiation of human bone marrow mesenchymal stem cells via activation of the Wnt/β-catenin signalling pathway. Stem Cell Res Ther. 2021;12(1):525.
40. Moldes M, Zuo Y, Morrison RF, Silva D, Park BH, Liu J, Farmer SR. Peroxisome-proliferator-activated receptor γ suppresses Wnt/β-catenin signalling during adipogenesis. Biochem J. 2003;376:607–13.
41. Li Y, Wang L, Zhang M, Huang K, Yao Z, Rao P, Cai X, Xiao J. Advanced glycation end products inhibit the osteogenic differentiation potential of adipose-derived stem cells by modulating Wnt/β-catenin signalling pathway via DNA methylation. Cell Prolif. 2020;53(6): e12834.
42. Davegårdh C, García-Calzón S, Bacos K, Ling C. DNA methylation in the pathogenesis of type 2 diabetes in humans. Mol Metab. 2018;14:12–25.
43. Ling C, Rönn T. Epigenetics in human obesity and type 2 diabetes. Cell Metab. 2019;29(5):1028–44.
44. An Y, Zhang H, Wang C, Jiao F, Xu H, Wang X, Luan W, Ma F, Ni L, Tang X, Liu M, Guo W, Yu L. Activation of ROS/MAPKs/NF-kappaB/NLRP3 and inhibition of efferocytosis in osteoclast-mediated diabetic osteoporosis. FASEB J. 2019;33(11):12515–27.
45. Sun B, Shi Y, Yang X, Zhao T, Duan J, Sun Z. DNA methylation: a critical epigenetic mechanism underlying the detrimental effects of airborne particulate matter. Ecotoxicol Environ Saf. 2018;161:173–83.
46. Kornicka K, Szlapka-Kosarzewska J, Śmieszek A, Marycz K. 5-Azacytydine and resveratrol reverse senescence and ageing of adipose stem cells via modulation of mitochondrial dynamics and autophagy. J Cell Mol Med. 2019;23:237–59.
47. Zhang RP, Shao JZ, Xiang LX. GADD45A protein plays an essential role in active DNA demethylation during terminal osteogenic differentiation of adipose-derived mesenchymal stem cells. J Biol Chem. 2011;286:41083–94.
48. Ma W, Zhan Y, Zhang Y, Mao C, Xie X, Lin Y. the biological applications of DNA nanomaterials: current challenges and future directions. Signal Transduct Target Ther. 2021;6(1):351.
49. Li ZF, Meng DD, Liu YY, Bi FG, Tian K, Xu JZ, Sun JG, Gu CX, Li Y. Hypoxia inducible factor-3α promotes osteosarcoma progression by activating KDM3A-mediated demethylation of SOX9. Chem Biol Interact. 2021;351: 109759.
50. Seman NA, Mohamud WN, Östenson CG, Brismar K, Gu HF. Increased DNA methylation of the SLC30A8 gene promoter is associated with type 2 diabetes in a Malay population. Clin Epigenetics. 2015;7(1):30.
51. Ko YG, Nishino K, Hattori N, Arai Y, Tanaka S, Shiota K. Stage-by-stage change in DNA methylation status of Dnmt1 locus during mouse early development. J Biol Chem. 2005;280(10):9627–34.
52. Zhang ZM, Lu R, Wang P, Yu Y, Chen D, Gao L, Liu S, Ji D, Rothbart SB, Wang Y, Wang GG, Song J. Structural basis for DNMT3A-mediated de novo DNA methylation. Nature. 2018;554(7692):387–91.
53. Casillas MA Jr, Lopatina N, Andrews LG, Tollefsbol TO. Transcriptional control of the DNA methyl-transferases is altered in aging and neoplastically-transformed human fibroblasts. Mol Cell Biochem. 2003;252(1–2):33–43.
54. Lyko F. The DNA methyltransferase family: a versatile toolkit for epigenetic regulation. Nat Rev Genet. 2018;19(2):81–92.
55. Jung YD, Park SK, Kang D, Hwang S, Kang MH, Hong SW, Moon JH, Shin JS, Jin DH, You D, Lee JY, Park YY, Hwang JJ, Kim CS, Suh N. Epigenetic regulation of miR-29a/miR-30c/DNMT3A axis controls SOD2 and mitochondrial oxidative stress in human mesenchymal stem cells. Redox Biol. 2020;37: 101716.

56. Mofakhami S, Salahinejad E. Biphasic calcium phosphate microspheres in biomedical applications. J Control Release. 2021;338:527–36.
57. Liao J, Cai X, Tian T, Shi S, Xie X, Ma Q, Li G, Lin Y. The fabrication of biomimetic biphasic CAN-PAC hydrogel with a seamless interfacial layer applied in osteochondral defect repair. Bone Res. 2017;5:17018.
58. Wu T, Yao Z, Tao G, et al. Role of Fzd6 in regulating the osteogenic differentiation of adipose-derived stem cells in osteoporotic mice. Stem Cell Rev Rep. 2021;17(5):1889–904.
59. Tang Q, Hu Z, Jin H, Zheng G, Yu X, Wu G, Liu H, Zhu Z, Xu H, Zhang C, Shen L. Erratum: Microporous polysaccharide multilayer coated BCP composite scaffolds with immobilised calcitriol promote osteoporotic bone regeneration both *in vitro* and *in vivo*: Erratum. Theranostics. 2021;11(13):6524–5.
60. Wu J, Chen T, Wang Z, Chen X, Qu S, Weng J, Zhi W, Wang J. Joint construction of micro-vibration stimulation and BCP scaffolds for enhanced bioactivity and self-adaptability tissue engineered bone grafts. J Mater Chem B. 2020;8(19):4278–88.
61. Yu L, Xia K, Cen X, Huang X, Sun W, Zhao Z, Liu J. DNA methylation of noncoding RNAs: new insights into osteogenesis and common bone diseases. Stem Cell Res Ther. 2020;11(1):109.
62. Qi Q, Wang Y, Wang X, Yang J, Xie Y, Zhou J, Li X, Wang B. Histone demethylase KDM4A regulates adipogenic and osteogenic differentiation via epigenetic regulation of C/EBPα and canonical Wnt signaling. Cell Mol Life Sci. 2020;77(12):2407–21.

Publisher's Note

日中笹川医学奨学金制度＜学位取得コース＞評価書
論文博士：指導教官用

第 43 期　　研究者番号：G4305　　作成日　：2024 年 3 月 10 日

氏　名	江 傑	JIANG JIE	性別	M	生年月日　1982/05/15
所属機関（役職）	東莞市人民医院腎内科（副主任医師）				
研究先（指導教官）	日本医科大学医学部解析人体病理学（清水 章　教授）				
研究テーマ	腎疾患の進展機序の解明とその制御 The elucidation of the mechanism of the development of renal disease, and its control				
専攻種別	☑論文博士		□課程博士		

研究者評価（指導教官記入欄）

成績状況	優 (良) 可　不可	取得単位数 取得単位数／取得すべき単位総数
学生本人が行った研究の概要	IgA 腎症自然発症モデルマウスとして知られている HIGA マウスに Lipopolysaccharides (LPS)や Zymosan を投与して炎症反応を増強し、糸球体腎炎の進展や糸球体障害の機序や様式を検討している。その過程で、Gasdermin D (GSDMD)の免疫染色から highly inflammatory form of lytic programmed cell death として知られているパイロトーシス(Pyroptosis)が誘導されていることを示した。炎症反応の増強で糸球体内への浸潤マクロファージに接着した係蹄内皮細胞にパイロトーシスが誘導され、浸潤炎症細胞による係蹄傷害が糸球体腎炎の進展に関わっていることを示した。係蹄内皮細胞障害からの係蹄上皮細胞障害や係蹄基底膜障害への進展について検討を進めている。	
総合評価	【良かった点】 糸球体腎炎の進展過程で壊死やアポトーシスの細胞死は知られているが、新たに炎症性に誘導されるパイロトーシス細胞死が糸球体腎炎の過程で誘導されていることを示すことができた。パイロトーシスの制御により糸球体腎炎の進展を抑制することができ、新規治療戦略につながると期待している。パイロトーシス細胞死は広く炎症性疾患に関わっている可能性もあり、多くの炎症性疾患に応用が可能で、今後の展開に期待が持てる。 【改善すべき点】 得られた結果の考察が不十分で、得られた結果の積み重ねからの次の研究への発展が十分に導かれていない。自身の研究結果を大切に、その考察から連続する研究の大切さを実感され、継続的な研究に進める必要がある。 【今後の展望】 IgA 腎症のモデルマウスへの炎症反応増強による糸球体腎炎の進展過程でパイロトーシス細胞死が誘導されている結果が得られた。このモデルマウスでのパイロトーシス誘導機序を明らかにするとともに、臨床腎生検検体で IgA 腎症を含む多くの糸球体腎炎での、炎症性パイロトーシスの誘導を検討し、さらにその細胞死と糸球体腎炎の進展との関連を明らかにする必要がある。	
学位取得見込	現在の研究結果、および今後の展望の研究を丁寧に進めることにより、十分に学位論文の作成は可能であり、かつ、学位の取得は可能であると考える。日本医科大学での論文博士の取得には、研究歴が５年必要であり、中国に帰国後も研究を継続しながら、論文の作成を行うが、研究から得られた結果に基づき、学位論文の作成は可能で、学位の取得は可能であると考える。	
	評価者（指導教官名）　清水　章	

日中笹川医学奨学金制度<学位取得コース>報告書
研究者用

第43期　　研究者番号：G4305　　作成日：2024年3月10日

氏名	江 杰	JIANG JIE	性別	M	生年月日 1982/05/15
所属機関(役職)	東莞市人民医院腎内科(副主任医師)				
研究先(指導教官)	日本医科大学医学部解析人体病理学(清水 章　教授)				
研究テーマ	腎疾患の進展機序の解明とその制御 The elucidation of the mechanism of the development of renal disease, and its control				
専攻種別	論文博士	☑	課程博士	☐	

1．研究概要(1)

1)目的(Goal)
Hematuria and proteinuria after infection is the most common clinical manifestation of IgA nephropathy (IgAN). However, the pathophysiological mechanisms is not fully studied because lacking of animal models similar to the patient. Although inflammasome are reported to contribute to immunomodulation following injury, proinflammatory cytokine manufacturing and microvascular barrier dysfunction are unclear, we hypothesized that innate immune-induced HIGA mice will set one active and progressive IgAN model.

2)戦略(Approach):
Immunoglobulin A nephropathy (IgAN) is the most common form of primary glomerulonephritis worldwide among patients undergoing renal biopsy, especially in the Asian Pacific region. It's recognized that 20-50% of affected patients progress to kidney failure over 10 to 20 years.(1,2) The most characteristic clinical feature of this disease is hematuria and proteinuria coinciding with or immediately following an upper respiratory or gastrointestinal tract infection. Thus, a dysregulation of innate immunity has been extensively postulated in IgAN.(3) Recent progress in understanding of how metabolic regulation relates to type 2 immunity firstly by considering specifics of metabolism within type 2 immune cells and type 2 immune cells are integrated more broadly into the metabolism of the organism as a whole.(4) Here, recent reports have both confirmed and analyzed in more detail the importance of glycolysis and fatty acid metabolism for the development and airway inflammation initiated by epithelial cells.(5) Glucose metabolism was shown to be essential for the function, proliferation, and differentiation capacity of airway progenitor cells.(6) In contrast, complete inhibition of glycolysis inhibited both the differentiation and proliferation of the progenitor cells.(7) Type 2 immunity has been noticed by researchers in the field of IgAN. Chintalacharuvu S. reported that the glycosylation of IgA produced by murine B cells is altered by Th2 cytokines.(8) Yamada K also find that down-regulation of core 1 β 1,3-galactosyltransferase and Cosmc by Th2 cytokine alters O-glycosylation of IgA1.(9) However, the effects of type 2 immune-related glycolysis metabolic reprogramming on renal epithelial cells have not been studied in IgAN. Podocytes and proximal tubular epithelial cells (PTECs) is important in the pathogenesis of IgAN.(10) Segmental sclerotic lesions are commonly seen in glomeruli in IgAN, which regarded as a form of podocyte dysregulation and transdifferentiation. In the Oxford Classification, the presence of segmental sclerosis was found to predict an adverse outcome.(11,12) However, evidence has shown that in many cases the sclerotic lesions in IgAN are more like those found in primary focal segmental glomerulosclerosis (FSGS).(13) Detailed biopsy examinations from a homogeneous group of IgAN patients has shown that it was very common to find capsular adhesion without any inflammation in the underlying glomerular tuft. This was present in 41% of cases of IgAN studied, compared with only 8% of cases of lupus glomerulonephritis. In primary FSGS, this figure was 69%.(14) Therefore, in terms of adhesions and segmental sclerosis, IgAN behaves more like primary FSGS than like an immune complex glomerulonephritis. Shimizu's study demonstrated that there was an association between severity of glomerular endothelial cells (GEC) damage and FSGS activity. GEC injury contributes to the process of sclerosis and may be a potential therapeutic target in the future. And GEC injury is associated with the formation of necrotizing and crescentic lesions in crescentic glomerulonephritis.(15,16) They also proved that the severity of GEC injury is associated with infiltrating macrophage heterogeneity in endocapillary proliferative glomerulonephritis.(17) Shimizu's found that GEC injury in acute and chronic glomerular lesions in patients with IgA nephropathy.(18) Hou Fanfan discovered glomerular macrophage can predict IgAN patients' response to subsequent immunosuppression.(19) But the relationship and mechanism of macrophage and GEC injure in IgAN still unknown. Therefore, it's important to focus on type 2 immunity mediates innate immune and develops inflammation in glomeruli and renal tubules in IgAN. A high IgA strain (HIGA) of ddY mice have been reported to constantly increase serum levels of IgA and IL-4 from the age of 10-60 weeks.(20,21) We hypothesis that the innate immune responses of LPS-induced play an important role in activate and progressive pathophysiology due to their metabolism change respond to type 2 cytokines in this inbred murine model of IgAN.

3)材料と方法(Materials and methods)
3.1. Experimental animals and in vivo mouse models.
3.2. Histopathological examination, Light microscopy.
3.3. Electron microscopy.
3.4. Immunohistochemistry and OPAL IHC, imaging and quantifications.
3.5. RNA sequencing, library construction and analysis.
3.6. Enzyme-linked immunosorbent assays.
3.7. Low vacuum scanning electron microscopy.
3.8. Statistical analysis.

1．研究概要(2)

4)実験結果(Results)

4.1. A model of IgA nephropathy similar to human phenotype was successfully established. During day3-35, proteinuria increased significantly in 36w LPS-induced HIGA mice and part of them accompanied by hematuria. Compared to age matching HIGA mice, under light microscopy, IgA deposition in mesangial region increased significantly, complement activate and mesangial cells proliferated. Under electron microscope, foot process effacement with focal detaching from glomerular basement membrane (GBM).

4.2. Immunohistochemistry showed that CD68+WT1+ cells pyropotosis mediated inflammation and injury with much higher iNOS express in HIGA mice after LPS stimulation at 36w old. But only co-deposition with Arg1 in hematuric HIGA mice.

4.3. CD68+WT1+ cells is aerobic glycolysis metabolic and epigenetic reprogramming after type 2 inflammatory primer.

4.4. After the intervention of LPS in vivo, mitochondrial ROS mediated the pyroptosis of CD68+WT1+ cells, showing significantly enhanced glycolytic and oxidative phosphorylation metabolism, and expressing obvious pro-inflammatory phenotypes of H3K4me3 and H3K27ac. By electron microscopy abnormal mitochondria and lysosome swelling were observed in both podocytes and tubular epithelial cells, and endoplasmic reticulum meshing in endothelial cells.

4.5. NT-GSDMD mediated GBM holes caused hematuria and tubular injury significantly aggravated after GBM broken.

4.6. Blocking GSDMD by disulfiram significantly aggravate proteinuria, activation of the inflammasome promotes CASPAS8(C362S)-mediated apoptosis and tissue pathology in LPS-HIGA mice.

4.7. CD68+WT1+ cells is distinguished to be yolk sac macrophage of kidney resident macrophages based on their expression of Lyve1 but not MHC-II.

4.8. Zymosan induced monocytes transformed into F4/80 macrophages in the glomeruli in C57B/6 and 36w HIGA mice, but not BALAB/C and 12w HIGA mice.

4.9. F4/80 macrophage expressing iNOS triggered pyroptosis in GEC of zym-primered 36w HIGA mice with high serum IFN-γ.

4.10. To further verify which subtypes of human IgAN have the pyroptosis phenotype. And macrophage infiltration predicted the progressive histological change in human kidney biopsy specimen.

5)考察(Discussion)

In this work, we find that a hallmark of pro-inflammatory CD68+WT1+ cells is the upregulation of aerobic glycolysis in 36w HIGA mice. Type 2 inflammatory induce this kind of cells proliferation and transdifferentiation by increasing glycolytic metabolism and epigenetic reprogramming. LPS stimulates macrophage-like responses by enhancing the state of aerobic glycolysis and oxidative phosphorylation in CD68+WT1+ cells.CD68+WT1+ cells in tubular area is distinguished to be yolk sac macrophage of kidney resident macrophages based on their expression of Lyve1.Pyroptosis is induced CD68+WT1+ cells when ROS levels rise beyond the cellular lysosomal processing capacity, mediate inflammation and podocyte damage. Progressive histological change of segmental sclerosis related to IFNγ and CD68+iNOS+ macrophage induced TNF-α mediated impaired angiogenesis and GEC pyroptosis. The epigenetic state of IL-4-polarized macrophages enables inflammatory cistromic expansion and extended synergistic response to TLR ligands.22The glycolysis/HIF-1a axis defines the inflammatory role of IL-4-primed macrophages.23Glycolysis-dependent phagocytic activity of LPS/IL-4-induced macrophages was strongly enhanced as was that of M1 macrophages; however, the energy metabolism of LPS/IL-4-induced macrophages, such as activation state of glycolytic and oxidative phosphorylation, was quite different from that of M1 or M2 macrophages.24We found the resident macrophage CD68+WT1+LYVE1+ show proinflammatory phenotype upon LPS stimulation in the HIGA mice with high IL-4.LPS/IL-4-induced CD68+WT1+LYVE1+ cell have a higher ROS production capacity induced pyroptosis. Glycolytic ATP serving as a rheostat to gauge PI3K-Akt-Foxo1 signaling in T cell immunity control CD8+ T cell expansion and differentiation.25Aerobic glycolysis promotes T helper 1 cell differentiation through an epigenetic mechanism.26 IFN-gamma and IL-4 gene polymorphisms could influence disease susceptibility and disease progression in IgA nephropathy in Japanese patients.27IFN-γ exposure inhibited basal glycolysis of quiescent primary human coronary artery endothelial cells by 20% through the global transcriptional suppression of glycolytic enzymes resulting from decreased basal HIF1α.28TNF and IFNγ synergistically inhibited endothelial-cell proliferation by up to 80%.29When we indued M1 macrophage in the glomeruli, causing GFB barrier both in C57BL/6 and HIGA mice. However, vascular repair and angiogenesis were impaired only in HGA mice with high IFNγ. It showes TNF-α and IFNγ synergistically inhibits angiogenesis following vascular injury induced progessive IgAN tissue change.

In conclusion, CD68+WT1+cell is progenitor pro-inflammation cell of IgA nephropathy, by which LPS-induced pyropotosis mediates innate immune and developes inflammation state in glomeruli and renal tubules, and the inhibition of its activation is not a safe therapeutic method. F4/80 macrophage induced pyroptosis in GEC relate to progressive histological change in IgAN.

6)参考文献(References)

1. Manno C, et al. Am J Kidney Dis 2007; 49: 763-775.
2. McGrogan A, et al. Nephrol Dial Transplant 2011;26(2):414-30.
3. Coppo R, et al. J Nephrol 2010; 23: 626-632.
4. Agnieszka M, et al. Immunity 2023 ;56(4):723-741.
5. Lin Y, et al. Curr Allergy Asthma Rep 2023;23(1):41-52.
6. Li K, et al. Cell Death Dis 2019;10:875.
7. Hammad H, et al. Immunity 2015;43:29-40.
8. Chintalacharuvu S.J Immunol 1997;159(5):2327-33.
9.Yamada K , et al. Nephrol Dial Transplant 2010;25: 3890-3897.
10.Joseph CKL, et al. Semin Nephrol 2018;38(5):485-495.
11. Menon MC, et al. Contribute Nephrol 2013;181:41-51.
12. Cook HT. Kidney Int 2011;79:581-3.
13. El Karoui K, et al. Kidney Int 2011;79:643-54.
14. Hill GS, et al. Kidney Int 2011;79:635-42.
15. Morita M, et al. Kidney Int Rep 2022;7(6):1229-1240.
16. Fujita E, et al. J Nippon Med Sch 2015;82(1):27-35.
17. Arai M,et al. Sci Rep 2021;11(1):13339.
18. Kusano T. Hum Pathol 2016;49:135-44.
19.Xie D, et al. J Am Soc Nephrol 2021;32(12):3187-3196.
20. Imai H, et al. Kidney Int1985; 27: 756-761.
21. Nogaki F, et al. Nephrol Dial Transplant 2000 ;15(8):1146-54.
22. Czimmerer Z, et al. Immunity 2022;55(11):2006-2026.e6.
23. Dang B, et al. Cell Rep 2023;42(5):112471.
24. Ishida K, et al. Front Immunol. 2023 ;14:1111729.
25. Xu K, et al. Science 2021;371(6527):405-410.
26. Peng M.Science 2016 ;354(6311):481-484.
27. Masutani K, et al. Am J Kidney Dis 2003 ;41(2):371-9.
28. Lee LYH, et al. Circulation 2021;144(20):1612-1628.

2. 執筆論文 Publication of thesis ※記載した論文を添付してください。Attach all of the papers listed below.

論文名 1 Title							
掲載誌名 Published journal							
	年 月	巻(号)	頁 ～ 頁	言語 Language			
第1著者名 First author		第2著者名 Second author		第3著者名 Third author			
その他著者名 Other authors							
論文名 2 Title							
掲載誌名 Published journal							
	年 月	巻(号)	頁 ～ 頁	言語 Language			
第1著者名 First author		第2著者名 Second author		第3著者名 Third author			
その他著者名 Other authors							
論文名 3 Title							
掲載誌名 Published journal							
	年 月	巻(号)	頁 ～ 頁	言語 Language			
第1著者名 First author		第2著者名 Second author		第3著者名 Third author			
その他著者名 Other authors							
論文名 4 Title							
掲載誌名 Published journal							
	年 月	巻(号)	頁 ～ 頁	言語 Language			
第1著者名 First author		第2著者名 Second author		第3著者名 Third author			
その他著者名 Other authors							
論文名 5 Title							
掲載誌名 Published journal							
	年 月	巻(号)	頁 ～ 頁	言語 Language			
第1著者名 First author		第2著者名 Second author		第3著者名 Third author			
その他著者名 Other authors							

3. 学会発表　Conference presentation　※筆頭演者として総会・国際学会を含む主な学会で発表したものを記載してくだ

※Describe your presentation as the principal presenter in major academic meetings including general meetings or international me

学会名 Conference					
演　題 Topic					
開催日 date	年　　月　　日	開催地 venue			
形式　method	□　口頭発表　Oral　□　ポスター発表　Poster	言語　Language	□　日本語	□　英語	□　中国語
共同演者名 Co-presenter					
学会名 Conference					
演　題 Topic					
開催日 date	年　　月　　日	開催地 venue			
形式　method	□　口頭発表　Oral　□　ポスター発表　Poster	言語　Language	□　日本語	□　英語	□　中国語
共同演者名 Co-presenter					
学会名 Conference					
演　題 Topic					
開催日 date	年　　月　　日	開催地 venue			
形式　method	□　口頭発表　Oral　□　ポスター発表　Poster	言語　Language	□　日本語	□　英語	□　中国語
共同演者名 Co-presenter					
学会名 Conference					
演　題 Topic					
開催日 date	年　　月　　日	開催地 venue			
形式　method	□　口頭発表　Oral　□　ポスター発表　Poster	言語　Language	□　日本語	□　英語	□　中国語
共同演者名 Co-presenter					

4. 受賞（研究業績） Award (Research achievement)

名　称 Award name				
	国名 Country		受賞年 Year of	年　　月
名　称 Award name				
	国名 Country		受賞年 Year of	年　　月

5. 本研究テーマに関わる他の研究助成金受給 Other research grants concerned with your resarch theme

受給実績 Receipt record	□ 有　■ 無
助成機関名称 Funding agency	
助成金名称 Grant name	
受給期間 Supported period	年　月 ～　年　月
受給額 Amount received	円
受給実績 Receipt record	□ 有　■ 無
助成機関名称 Funding agency	
助成金名称 Grant name	
受給期間 Supported period	年　月 ～　年　月
受給額 Amount received	円

6. 他の奨学金受給 Another awarded scholarship

受給実績 Receipt record	□ 有　■ 無
助成機関名称 Funding agency	
奨学金名称 Scholarship name	
受給期間 Supported period	年　月 ～　年　月
受給額 Amount received	円

7. 研究活動に関する報道発表 Press release concerned with your research activities

※記載した記事を添付してください。Attach a copy of the article described below

報道発表 Press release	□ 有　■ 無	発表年月日 Date of release	
発表機関 Released medium			
発表形式 Release method	・新聞　・雑誌　・Web site　・記者発表　・その他（　　）		
発表タイトル Released title			

8. 本研究テーマに関する特許出願予定 Patent application concerned with your research theme

出願予定 Scheduled	□ 有　■ 無	出願国 Application	
出願内容（概要） Application contents			

9. その他 Others

指導責任者（記名）　清水 章

日中笹川医学奨学金制度＜学位取得コース＞中間評価書
論文博士：指導教官用

第 43 期　　研究者番号：G4306　　作成日　：2024 年 3 月 10 日

氏　名	王 晴	WANG QING	性別	F	生年月日　1985/12/20
所属機関（役職）	中国医科大学附属第四医院胸部外科(主治医師)				
研究先（指導教官）	順天堂大学医学部消化器外科講座上部消化管外科学(峯 真司　教授)				
研究テーマ	食道癌に対する基礎的臨床的研究 Basic and clinical researches of esophageal cancer				
専攻種別	☑論文博士		□課程博士		

研究者評価（指導教官記入欄）

成績状況	優　良　可　不可	取得単位数 取得単位数／取得すべき単位総数
学生本人が行った研究の概要	1　食道癌に対する食道切除術において High volume center は low volume center と比べて全生存期間に差があるということは知られているが症例数の適切な cutoff 値は知られていない。この件について Meta-analysis を行った。Cutoff 値は示せなかったが、症例数が増えると一貫して生存期間が改善するということを示し論文化した。 2　食道癌手術においてリンパ節郭清個数と予後が相関することは知られているが、この事実はある程度のリンパ節郭清が必要でることを示していると考えられている。しかし、同程度の手術でもリンパ節個数に個人差があることも多く、同じ手術を行った場合の個人差が予後と関連するかということについて検討し、同程度の郭清を行った場合にはリンパ節個数と予後に関連はないことを示した（論文作成中） 3　食道癌検体を用いてオルガノイドを作成し、cancer-associated fibroblast の機能解析を行った	
総合評価	【良かった点】 毎日熱心に基礎的研究を行った。 臨床研究においても論文作成も早く、論文や研究の改善点を指摘した場合も Response も早く修正できた。 【改善すべき点】 Covid 19 感染症流行期に来日したためであるが、研究以外ではあまり交流が持てなかった。基礎研究についてはやや時間が短く十分な成果が出なかった。 【今後の展望】 中国に戻られたあとに食道癌手術や研究について中国を引っ張っていっていただきたいし、我々とも keep in touch できればと思う。	
学位取得見込	博士審査も終了し、取得予定である	
評価者（指導教官名）峯　真司		

日中笹川医学奨学金制度<学位取得コース>報告書
研究者用

第43期　　研究者番号：G4306　　作成日：2024年3月10日

氏名	王 晴	WANG QING	性別	F	生年月日 1985/12/20
所属機関(役職)	中国医科大学附属第四医院胸部外科(主治医師)				
研究先（指導教官）	順天堂大学医学部消化器外科講座上部消化管外科学(峯 真司　教授)				
研究テーマ	食道癌に対する基礎的臨床的研究 Basic and clinical researches of esophageal cancer				
専攻種別	論文博士	☑	課程博士	☐	

1．研究概要(1)

1)目的(Goal)

Esophageal cancer is the eighth most commonly diagnosed cancer and the sixth most common cause of cancer death in the world [1]. In addition to esophagectomy, there are neoadjuvant chemotherapy, chemoradiotherapy molecular targeted therapy, immunotherapy, or a combination of modalities, but the prognosis for esophageal cancer is extremely poor, with a 5-year survival rate of less than 30% [2, 3]. Therefore, it is urgent to identify biomarkers that can predict treatment effects and to find new molecular targets.

Fibroblasts present in tumors are called cancer-associated fibroblasts (CAFs), which have been shown to promote cancer cell proliferation and malignant transformation [4]. Research on CAFs' function has been active in breast cancer, pancreatic cancer, and other areas, and some reports suggest that they contribute to tumor growth, metastasis, and treatment resistance in esophageal cancer [5].

In this study, we used immortalized fibroblasts to create CAFs using semi-artificial methods. CAFs produced by this method are called experimental CAFs, which have long-term stability and can be cultured on a large scale. They can also be used in in vitro co-culture experiments of cancer cells and CAFs, as well as in in vivo co-implantation experiments of cancer cells and CAFs. By creating these experimental CAFs and using them in various experiments, we will elucidate the characteristics and functions of CAFs in esophageal cancer. In addition to cancer cell lines, we also aim to create experimental CAFs that are more similar to in vivo CAFs by using cancer organoids in this study.

2)戦略(Approach)

To create experimental CAF and analyze it, two different types of cells (immortalized normal esophageal fibroblasts and patient-derived esophageal cancer organoids) were co-transplanted into immunodeficient mice.

3)材料と方法(Materials and methods)

①Immortalization of normal esophageal fibroblasts:

Immortalized fibroblasts are obtained by introducing the hTERT (telomerase) gene into fibroblasts derived from human esophagus. The fibroblasts are obtained from Cell Biologics and normal human esophagus specimens.

②Establishing patient-derived esophageal cancer organoids

Organoids derived from human esophageal cancer samples provide a novel and unique platform to model esophageal development, homeostatic regenerative differentiation, and benign and malignant esophageal diseases.

③Creation of experimental CAFs using esophageal cancer cells (cell lines/organoids):

CAF can be obtained by primary culture from surgical samples, but there are reports that their properties change after several passages and they become unstable, and it is difficult to use them as stable experimental materials due to cell aging. The method for creating experimental CAFs was developed in this course. This cell can be massively propagated and its properties are stable. Immortalized fibroblasts with antibiotic resistance are mixed with cancer cells and co-transplanted into immunodeficient mice to convert fibroblasts into CAFs within the tumor.

④Analysis using established experimental CAFs:

By comparing the gene expression of normal fibroblasts and established experimental CAFs, signal pathways that are upregulated in CAFs are identified, and the mechanism of CAF formation is predicted. In addition, functional evaluation is performed by mixing experimental CAFs with cancer cells and transplanting them into mice (to investigate tumor growth and cancer malignancy function).

4)実験結果(Results)

①Immortalization of normal esophageal fibroblasts:

By detecting the population doubling level (PDL) of the cells, it was determined that the normal esophageal fibroblasts had become immortalized normal esophageal fibroblasts (by introduction of hTERT gene (hygromycin resistance)).

②Establishing patient-derived esophageal cancer organoids

Esophageal cancer organoids have been established using patient-derived esophageal cancer tissue. These are three-dimensional culture systems that can be grown in vitro to form miniaturized, self-organizing structures that mimic the architecture and function of the original tumor. These organoids are composed of different types of cells, including cancer cells, stromal cells, and immune cells, and can recapitulate the heterogeneity and complexity of the original tumor.

③Establishing an esophageal cancer patient-derived xenograft (PDX) model by co-transplanting esophageal cancer

1．研究概要(2)

organoids or esophageal cancer cell lines with immortalized esophageal fibroblast. Inject subcutaneous injections into both sides of the mice, and tumor were resected 2 weeks, 1 month, 2 month, and 3 months after co-transplantation, respectively. Then culture the cells in medium containing hygromycin. Only hygromycin-resistance fibroblast can survive and proliferate.

④Performing Immunohistochemistry on the resected tumor, we found that the expression of human vimentin 9 was very little.

⑤Immunofluorescent staining revealed that human vimentin 9 was expressed in counterpart fibroblasts, and exp-CAFs. α-SMA was expressed in counterpart fibroblasts, exp-CAFs and 10T1/2.

⑥Examing maker expression of CAF subtypes mCAF and iCAF by RT-qPCR.

KYSE150 esophageal cancer+ Normal hTERT fibroblast cells tend to express SDF1 (CXCL12).): KYSE270 esophageal cancer + Normal hTERT fibroblast cells can be seen upregulation of inflammatory cytokines.

5)考察(Discussion)

This study represents the first establishment of experimental cancer-associated fibroblasts (CAFs) related to esophageal cancer. Experimental CAFs can be used to simulate the microenvironment surrounding esophageal cancer cells, providing researchers with a more physiologically relevant experimental platform.

CAFs are stromal cells that are mainly induced in tumor microenvironment, and are involved in cancer cell proliferation and invasion, angiogenesis, inflammation, immunosuppress, and extracellular matrix remodeling [6]. There are 2 main subtypes of CAFs: myofibroblastic CAFs (mCAFs), which is a subtype that expresses α-SMA and exhibits myofibroblast phenotype, and inflammatory CAFS (iCAFs), which is a subtype that produces inflammotry cytokines [7]. In our study, we successfully established two subtypes of CAFS respectively.

CAFs can be used to simulate the microenvironment surrounding cancer cells, providing researchers with a more physiologically relevant experimental platform. CAFs can also be utilized for screening potential drugs targeting the cancer microenvironment, as well as assessing the effects of these drugs on the microenvironment. Research on CAFs can aid in the development of therapeutic strategies targeting the cancer microenvironment to improve cancer treatment outcomes [6, 8].

Experimental cancer-associated fibroblasts (CAFs) are CAFs created using immortalized fibroblasts through semi-artificial methods. CAFs produced using this method have long-term stability and can be cultivated on a large scale. They can also be used in in vitro co-culture experiments of cancer cells and CAFs, as well as in in vivo co-implantation experiments of cancer cells and CAFs. By creating these experimental CAFs and using them in various experiments, we will elucidate the characteristics and functions of CAFs in esophageal cancer.

In our study, we also use establish patient-derived esophageal cancer organoids. Organoid technology can cultivate gastrointestinal tumors in a way that preserves their genetic, phenotypic, and behavioral characteristics, which is far superior to traditional tumor cell cultures [9].

In subsequent experiments, we need to conduct another round of animal transplant experiments to ensure that the performance of experimental CAF is more stable. Then study the mechanism of CAF's influence on esophageal cancer tumorigenesis.

6)参考文献(References)

1. Sung H, Ferlay J, Siegel RL, Laversanne M, Soerjomataram I, Jemal A, Bray F. Global Cancer Statistics 2020: GLOBOCAN Estimates of Incidence and Mortality Worldwide for 36 Cancers in 185 Countries. CA Cancer J Clin. 2021;71(3):209-249.

2. Allemani C, Matsuda T, Di Carlo V, Harewood R, Matz M, Nikšić M, Bonaventure A, Valkov M, Johnson CJ, Estève J, Ogunbiyi OJ, Azevedo E Silva G, Chen WQ, Eser S, Engholm G, Stiller CA, Monnereau A, Woods RR, Visser O, Lim GH, Aitken J, Weir HK, Coleman MP; CONCORD Working Group. Global surveillance of trends in cancer survival 2000-14 (CONCORD-3): analysis of individual records for 37 513 025 patients diagnosed with one of 18 cancers from 322 population-based registries in 71 countries. Lancet. 2018;391(10125):1023-1075.

3. Siegel RL, Miller KD, Fuchs HE, Jemal A. Cancer statistics, 2022. CA Cancer J Clin. 2022;72(1):7-33.

4. Orimo A, Gupta PB, Sgroi DC, Arenzana-Seisdedos F, Delaunay T, Naeem R, Carey VJ, Richardson AL, Weinberg RA. Stromal fibroblasts present in invasive human breast carcinomas promote tumor growth and angiogenesis through elevated SDF-1/CXCL12 secretion. Cell. 2005;121(3):335-348.

5. Qiao Y, Zhang C, Li A, Wang D, Luo Z, Ping Y, Zhou B, Liu S, Li H, Yue D, Zhang Z, Chen X, Shen Z, Lian J, Li Y, Wang S, Li F, Huang L, Wang L, Zhang B, Yu J, Qin Z, Zhang Y. IL6 derived from cancer-associated fibroblasts promotes chemoresistance via CXCR7 in esophageal squamous cell carcinoma. Oncogene. 2018;37(7):873-883.

6. Biffi G, Tuveson DA. Diversity and Biology of Cancer-Associated Fibroblasts. Physiol Rev. 2021;101(1):147-176.

7. Lavie D, Ben-Shmuel A, Erez N, Scherz-Shouval R. Cancer-associated fibroblasts in the single-cell era. Nat Cancer. 2022;3(7):793-807.

8. Chen X, Song E. Turning foes to friends: targeting cancer-associated fibroblasts. Nat Rev Drug Discov. 2019;18(2):99-115.

9. Lau HCH, Kranenburg O, Xiao H, Yu J. Organoid models of gastrointestinal cancers in basic and translational research. Nat Rev Gastroenterol Hepatol. 2020;17(4):203-222.

2. 執筆論文 Publication of thesis ※記載した論文を添付してください。Attach all of the papers listed below.

論文名 1 Title	Association of Hospital Volume and Long-term Survival After Esophagectomy: A Systematic Review and Meta-Analysis					
掲載誌名 Published journal	Front Surg					
	2023 年 4 月	10 巻(号)	1E+06 頁 ～ 頁	言語 Language	English	
第1著者名 First author	Qing Wang	第2著者名 Second author	Shinji Mine	第3著者名 Third author	Motomi Nasu	
その他著者名 Other authors	Tetsu Fukunaga , Shuko Nojiri, Chun-Dong Zhang					
論文名 2 Title	Effect of the number of dissected lymph nodes on the survival of patients who underwent the same extent of lymphadenectomy for esophageal cancer					
掲載誌名 Published journal	The article is being submitted.					
	年 月	巻(号)	頁 ～ 頁	言語 Language		
第1著者名 First author	Qing Wang	第2著者名 Second author	Shinji Mine	第3著者名 Third author	Takashi Hashimoto	
その他著者名 Other authors	Hajime Orita, Motomi Nasu, Tadasuke Hashiguchi, Sanae Kaji, Daisuke Fujiwara, Yukinori Yube, Asako Ozaki, Kohei Yoshino, Yuki Sugahara, Akira Kubota, Hiroki Egawa, Tetsu Fukunaga, Yoshiaki Kajiyama, Masahiko Tsurumaru					
論文名 3 Title						
掲載誌名 Published journal						
	年 月	巻(号)	頁 ～ 頁	言語 Language		
第1著者名 First author		第2著者名 Second author		第3著者名 Third author		
その他著者名 Other authors						
論文名 4 Title						
掲載誌名 Published journal						
	年 月	巻(号)	頁 ～ 頁	言語 Language		
第1著者名 First author		第2著者名 Second author		第3著者名 Third author		
その他著者名 Other authors						
論文名 5 Title						
掲載誌名 Published journal						
	年 月	巻(号)	頁 ～ 頁	言語 Language		
第1著者名 First author		第2著者名 Second author		第3著者名 Third author		
その他著者名 Other authors						

3. 学会発表 Conference presentation ※筆頭演者として総会・国際学会を含む主な学会で発表したものを記載してください

※Describe your presentation as the principal presenter in major academic meetings including general meetings or international meetin

学会名 Conference	No								
演 題 Topic									
開催日 date	年 月 日		開催地 venue						
形式 method	□ 口頭発表 Oral	□ ポスター発表 Poster	言語 Language	□ 日本語	□ 英語	□ 中国語			
共同演者名 Co-presenter									
学会名 Conference									
演 題 Topic									
開催日 date	年 月 日		開催地 venue						
形式 method	□ 口頭発表 Oral	□ ポスター発表 Poster	言語 Language	□ 日本語	□ 英語	□ 中国語			
共同演者名 Co-presenter									
学会名 Conference									
演 題 Topic									
開催日 date	年 月 日		開催地 venue						
形式 method	□ 口頭発表 Oral	□ ポスター発表 Poster	言語 Language	□ 日本語	□ 英語	□ 中国語			
共同演者名 Co-presenter									
学会名 Conference									
演 題 Topic									
開催日 date	年 月 日		開催地 venue						
形式 method	□ 口頭発表 Oral	□ ポスター発表 Poster	言語 Language	□ 日本語	□ 英語	□ 中国語			
共同演者名 Co-presenter									

4. 受賞（研究業績） Award (Research achievement)

名 称 Award name	No			
	国名 Country		受賞年 Year of award	年 月
名 称 Award name				
	国名 Country		受賞年 Year of award	年 月

5. 本研究テーマに関わる他の研究助成金受給 Other research grants concerned with your resarch theme

受給実績 Receipt record	□ 有　■ 無
助成機関名称 Funding agency	
助成金名称 Grant name	
受給期間 Supported period	年　月 ～　年　月
受給額 Amount received	円
受給実績 Receipt record	□ 有　■ 無
助成機関名称 Funding agency	
助成金名称 Grant name	
受給期間 Supported period	年　月 ～　年　月
受給額 Amount received	円

6. 他の奨学金受給 Another awarded scholarship

受給実績 Receipt record	□ 有　■ 無
助成機関名称 Funding agency	
奨学金名称 Scholarship name	
受給期間 Supported period	年　月 ～　年　月
受給額 Amount received	円

7. 研究活動に関する報道発表 Press release concerned with your research activities

※記載した記事を添付してください。Attach a copy of the article described below

報道発表 Press release	□ 有　■ 無	発表年月日 Date of release	
発表機関 Released medium			
発表形式 Release method	・新聞　・雑誌　・Web site　・記者発表　・その他（　　）		
発表タイトル Released title			

8. 本研究テーマに関する特許出願予定 Patent application concerned with your research theme

出願予定 Scheduled	□ 有　■ 無	出願国 Application	
出願内容（概要） Application contents			

9. その他 Others

指導責任者（記名） 峯 真司

frontiers | Frontiers in Surgery

TYPE Systematic Review
PUBLISHED 21 April 2023
DOI 10.3389/fsurg.2023.1161938

OPEN ACCESS

EDITED BY
Atalel Fentahun Awedew,
Addis Ababa University, Ethiopia

REVIEWED BY
François Dépret,
Assistance Publique Hopitaux De Paris, France
Yasuhiro Tsubosa,
Shizuoka Cancer Center, Japan

*CORRESPONDENCE
Shinji Mine
✉ s.mine.gv@juntendo.ac.jp

SPECIALTY SECTION
This article was submitted to Visceral Surgery, a section of the journal Frontiers in Surgery

RECEIVED 13 February 2023
ACCEPTED 27 March 2023
PUBLISHED 21 April 2023

CITATION
Wang Q, Mine S, Nasu M, Fukunaga T, Nojiri S and Zhang C-D (2023) Association of hospital volume and long-term survival after esophagectomy: A systematic review and meta-analysis.
Front. Surg. 10:1161938.
doi: 10.3389/fsurg.2023.1161938

Association of hospital volume and long-term survival after esophagectomy: A systematic review and meta-analysis

Qing Wang[1,2], Shinji Mine[1]*, Motomi Nasu[1], Tetsu Fukunaga[1], Shuko Nojiri[3] and Chun-Dong Zhang[4]

[1]Department of Esophageal and Gastroenterological Surgery, Juntendo University Graduate School of Medicine, Tokyo, Japan, [2]Department of Thoracic Surgery, The Fourth Affiliated Hospital of China Medical University, Shenyang, China, [3]Medical Technology Innovation Center, Juntendo University, Tokyo, Japan, [4]Department of Gastrointestinal Surgery, Graduate School of Medicine, The University of Tokyo, Tokyo, Japan

Background: It remains controversial whether esophageal cancer patients may benefit from esophagectomy in specialized high-volume hospitals. Here, the effect of hospital volume on overall survival (OS) of esophageal cancer patients post esophagectomy was assessed.
Methods: PubMed, Embase, and Cochrane Library were systematically searched for relevant published articles between January 1990 and May 2022. The primary outcome was OS after esophagectomy in high- vs. low-volume hospitals. Random effect models were applied for all meta-analyses. Subgroup analysis were performed based on volume grouping, sample size, study country, year of publication, follow-up or study quality. Sensitivity analyses were conducted using the leave-one-out method. The Newcastle-Ottawa Scale was used to assess the study quality. This study followed the Preferred Reporting Items for Systematic Reviews and Meta-analysis guidance, and was registered (identifier: INPLASY202270023).
Results: A total of twenty-four studies with 113,014 patients were finally included in the meta-analysis. A significant improvement in OS after esophagectomy was observed in high-volume hospitals as compared to that in their low-volume counterparts (HR: 0.77; 95% CI: 0.71–0.84, $P < 0.01$). Next, we conducted subgroup analysis based on volume grouping category, consistent results were found that high-volume hospitals significantly improved OS after esophagectomy than their low-volume counterparts. Subgroup analysis and sensitivity analyses further confirmed that all the results were robust.
Conclusions: Esophageal cancer should be centralized in high-volume hospitals.

KEYWORDS

esophageal carcinoma, esophagectomy, hospital volume, overall survival, centralization

1. Introduction

Centralization of demanding cancer surgeries to improve the safety and effectiveness of cancer treatment is a topic of ongoing concern in many countries around the world (1–4). Esophagectomy is one of the most complex surgery with high morbidity and mortality, and whether it should be centralized in high-volume hospitals remains controversial (5–9).

Abbreviations
CI, confidence interval; HR, hazard ratio; HV, hospital volume; HVH, high-volume hospital; LVH, low-volume hospital; No., number; NR, not reported; ref, reference; USA, United States of America.

Clinical long-term outcomes of esophageal cancer after surgery are usually affected by standardization of surgical procedures, chemotherapy, radiation therapy, molecular targeted therapy and immunotherapy (10–12); moreover, hospital volume also influences mortality after esophagectomy (13). Some previous studies have been reported that esophagectomy for cancer centralized in high-volume hospitals benefited long-term prognosis outcomes (6, 7, 14, 15), whereas, there are also some reports showing inconsistent results (5, 8, 9, 16). Therefore, whether a better long-term overall survival after esophagectomy showing high-volume hospitals remains to be established.

In the present study, we evaluated the influence of high- vs. low-volume hospitals on the long-term OS of patients with esophageal cancer after esophagectomy.

2. Materials and methods

2.1. Literature search strategy

This systematic review was registered in https://doi.org/10.37766/inplasy2022.7.0023 (identifier: INPLASY202270023) (17). We conducted a systematic search for all relevant articles on the relationship between hospital volume of esophagectomies and long-term OS (17). The search was performed in PubMed, Embase, and Cochrane Library. For example, we combined Medical Subject Headings (MeSH) terms and text terms for the search in PubMed. The following search terms were used: ("esophagectomy" OR "esophageal surgery " OR "esophageal cancer surgery" OR "esophageal resection" OR "esophageal cancer resection") AND ("hospital volume" OR "high volume" OR "low volume" OR "healthcare institution size" OR "surgical volume"). We also searched the references of the included studies to search for potentially eligible articles. The last search was completed on May 30, 2022. This study followed the Preferred Reporting Items for Systematic Reviews and Meta-analysis guidance (PRISMA) (17, 18).

2.2. Study selection and eligibility criteria

As we previously described, after the retrieval of the relevant articles, they were screened to remove the duplicates (17). All studies were published in English. Search results were screened by two authors (Q.W. and C.D.Z.) independently according to the titles and abstracts. To better reflect modern surgical practices and perioperative management, this study focuses only on articles published after 2002. Next, the retained studies were searched for their full text and further were screened according to the following eligibility criteria: publication in English language; surgery for esophageal carcinoma as the theme; primary outcomes included hospital volume and long-term OS; comparison of OS between high- and low-volume hospitals; original articles with informative data; articles reporting adjusted hazard ratios (HRs) in multivariate analysis; publication before 2002; and articles in which procedural volume was an exact cutoff. Any disagreements were resolved through consultation with the third author (17).

2.3. Data extraction

Two authors (QW and CDZ) independently extracted data from the included studies and collated the following information: author, published year, country, study period, population, the unit of exposure (hospital volume), volume classification for hospitals, volume grouping (dichotomies, tertiles, quartiles, quintiles or others) and the longest follow-up and clinical outcomes (OS) (17). Any disagreements were resolved by discussion with the third author. We further assessed the extent of risk adjustment (17).

2.4. Study quality evaluation

All included studies were rigorously assessed for methodological quality and risk of bias by two authors (QW and CDZ) by using the Newcastle-Ottawa Scale (17, 19). This scale assesses the quality of studies from three aspects: selection of study population (0–4 points), comparability between groups (0–2 points), and outcome measurement (0–3 points) (17). The total score is 9 points.

2.5. Data integration

High-volume hospitals or low-volume hospitals were defined by the authors of the included studies. We used hazard ratios (HRs) in low-volume groups as the reference. If an included study reported more than two surgical volume groups, only the lowest and highest volume groups were compared in the analysis. The primary outcome was OS at the last follow-up, excluding 30-day mortality, 90-day mortality, in-hospital mortality, and postoperative mortality (17).

2.6. Statistical analyses

The results were calculated by HRs with 95% confidence intervals (CIs) for long-term outcomes. Heterogeneity among the studies was quantified by the I^2 test, and studies with a statistic of 25%–50% of I^2 were regarded as low heterogeneous, 51%–75% as moderate, and more than 75% as highly heterogeneous (20). Regarding the clinical heterogeneity (inconsistency in pathological staging, therapeutic regimens, and other confounding factors among the studies), we applied random-effect models for all the analyses. To obtain adequate statistical power, subgroup analysis was conducted based on volume grouping category. Then meta-analyses of at least five included studies were performed for different cutoff values (high-volume hospital vs. low-volume hospital). In addition, subgroup analyses in relation to volume group, sample size, study country, year of

publication, follow-up or study quality and sensitivity analyses of a leave-one-out method were conducted to verify the results. Funnel plots were used to evaluate potential publication bias. $P < 0.05$ was considered to be statistically significant. All statistical analyses were performed by Review Manager 5.4.1 and Stata 13.1.

3. Results

3.1. Study selection and characteristics

This systematic review was registered in https://doi.org/10.37766/inplasy2022.7.0023 (identifier: INPLASY202270023). Figure 1 shows the process of literature selection. We retrieved 115 articles from PubMed and 66 from Embase; of these, 136 studies were retained for primary selection after 59 duplicate studies were excluded. After screening of titles and abstracts, 30 studies were excluded. Among the remaining 106 articles, which were related to the volume-outcome relationship in esophageal cancer surgery, we further excluded 24 reviews without primary data, three articles not related to esophagectomy, 23 articles without data of long-term survival, 10 articles without data of hospital volume, three articles without data of low-volume hospitals, four articles published before 2002. Finally, 24 studies published from 2002 to May 2022 with 113,014 participants were included in the meta-analysis.

Among the 24 included studies, six were from the United States (6–8, 21–23), four from Sweden (9, 15, 24, 25), three each from Australia (26–28) and Netherlands (29–31), two each from Japan (32, 33) and England (14, 34), and one each from China (35), Korea (36), Brazil (37), and Canada (38) (Table 1). The longest follow-up period was 24 years.

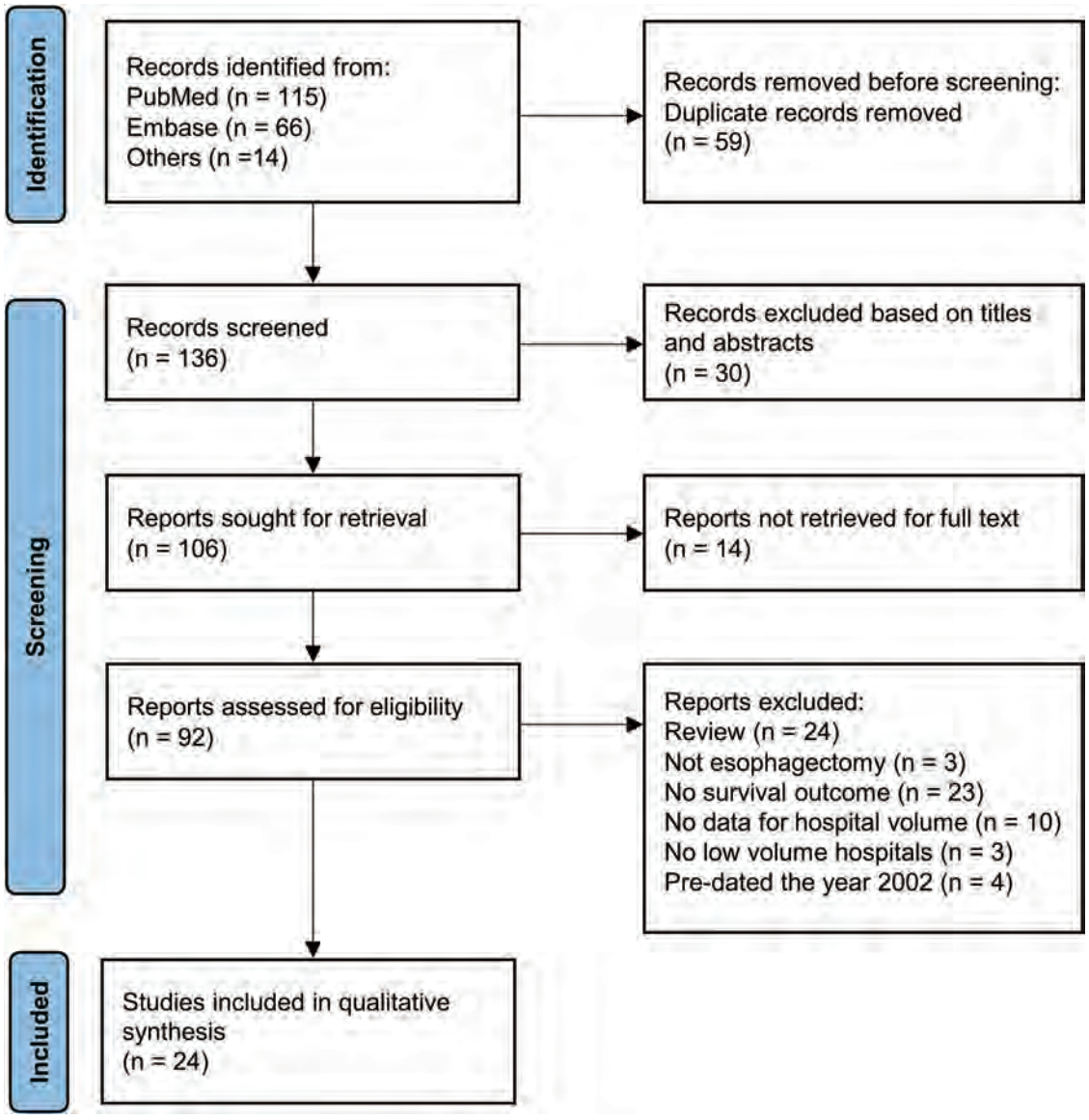

FIGURE 1
The PRIMSA flow diagram for included studies.

TABLE 1 Basic characteristics of all included studies for meta-analysis on the relation between hospital volume and outcome of esophagectomies for cancer.

Author, year	Year	Country	Study	Population	Age, years	Male	Exposure	Hospital volume		Volume grouping	The longest	Survival	Hospital
[Ref]			*P*eriod			(%)		High	Low	Category	Follow-up, year	After	Number
Dikken (4)	2012	Netherlands	1989–2009	10,025	NR	76.0%	HV	≥21	≤5	Quartiles	3 years	Surgery	44
Van de Poll-Fanse (5)	2011	Netherlands	1995–2006	638	66.0	76.5%	HV	15–20	<4	Tertiles	3 years	Surgery	NR
Yang (10)	2018	USA	2004–2013	2445	62.0	90.6%	HV	3.1–15.8	0.1–1.0	Tertiles	11 years	Surgery	450
Coupland (11)	2013	England	2004–2008	5403	NR	71.9%	HV	≥80	<20	Quintiles	6 years	Surgery	NR
Derogar (13)	2013	Sweden	1987–2005	1335	66.0	74.0%	HV	≥17	≤8	Tertiles	24 years	Surgery	NR
Patel (26)	2021	USA	2006–2013	11,739	62.0–63.0	85.1%	HV	>6	≤6	Dichotomies	5 years	Surgery	1018
Han (27)	2020	USA	2004–2016	37,695	NR	NR	HV	≥25	<5	Quintiles	5 years	Surgery	NR
Gasper (28)	2009	USA	1995–2004	2404	NR	75.9%	HV	>6	<2	Quintiles	5 years	Surgery	NR
Bilimoria (29)	2008	USA	1994–1999	12,246	64.0–65.0	NR	HV	>15	<3	Quintiles	6 years	Surgery	1154
Birkmeyer (30)	2007	USA	1992–2002	822	NR	79.6%	HV	>14	<4	Tertiles	5 years	Surgery	206
Sundelof (31)	2008	Sweden	1994–1997	232	67.0	83.2%	HV	≥10	6–9	Dichotomies	10 years	Surgery	33
Rouvelas (32)	2007	Sweden	1987–2000	1199	65.0–66.0	71.9%	HV	≥10	<10	Dichotomies	17 years	Surgery	53
Wenner (33)	2005	Sweden	1987–1996	1429	66.0–67.0	72.8%	HV	>15	<5	Tertiles	13 years	Surgery	74
Narendra (34)	2021	Australia	2001–2015	1167	NR	NR	HV	≥6	NR	Dichotomies	5 years	Surgery	24
Smith (35)	2014	Australia	2001–2008	908	NR	80.5%	HV	>6	≤6	Dichotomies	9 years	Surgery	42
Stavrou (36)	2010	Australia	2000–2005	321	NR	74.0%	HV	>20	≤10	Tertiles	3 years	Surgery	NR
Verhoef (37)	2007	Netherlands	1994–2002	213	NR	69.1%	HV	≥20	<20	Dichotomies	10 years	Surgery	18
Taniyama (38)	2021	Japan	2006–2013	3578	NR	83.5%	HV	54–70	≤10	Tertiles	10 years	Surgery	96
Ioka (39)	2007	Japan	1994–1998	2961	NR	NR	HV	>43	<8	Quartiles	5 years	Surgery	143
Bachmann (40)	2002	England	1996–1997	781	NR	NR	HV	60–83	7–32	Tertiles	3 years	Surgery	23
Hsu (41)	2014	China	2008–2011	2151	55.2	94.1%	HV	>22	≤22	Dichotomies	3 years	Surgery	58
Kim (42)	2021	Korea	2004–2017	11,346	64.2	92.6%	HV	≥48	<12	Tertiles	5 years	Surgery	122
Duarte (43)	2020	Brazil	2000–2013	1347	NR	84.9%	HV	>8	<5	Dichotomies	5 years	Surgery	NR
Simunovic (44)	2006	Canada	1990–2000	629	63.0–65.0	NR	HV	≥44	≤7	Quartiles	10 years	Surgery	68

Ref, reference.

10.3389/fsurg.2023.1161938

3.2. Quality assessment

The quality of the included studies was assessed using the Newcastle-Ottawa Scale. The median Newcastle-Ottawa Scale score of the included studies was 7, with a range of 6–9 (Table 2).

3.3. Long-term os in relation to hospital volume

A total of 24 studies was included to assess the impact of high-volume vs. low-volume hospitals on long-term overall survival after esophagectomy. Regarding to the longest period of follow-ups, high-volume hospitals showed significantly better overall survival than low-volume hospitals (HR: 0.77; 95% CI: 0.71–0.84, $P < 0.01$) (Figure 2).

Next, we analyzed the pooled HRs of OS (high-volume hospital vs. low-volume hospital) for multiple cutoff values (Table 3). Consistent results were found that high-volume hospitals showed a significant improvement in OS after esophagectomy than their low-volume counterparts (all $P \leq 0.05$).

3.4. Subgroup analysis

Subgroup analysis was conducted based on volume grouping category in Figure 2. A significant improvement in OS after esophagectomy was observed in high-volume hospitals as compared to that in their low-volume counterparts in each volume grouping category. The pooled HRs were 0.76 (95% CI: 0.71–0.81) for quintiles, 0.72 (95% CI: 0.61–0.85) for quartiles, 0.77 (95% CI:0.62–0.96) for tertiles, and 0.82 (95% CI:0.78–0.87) for dichotomies, respectively (Figure 2, Table 4).

In addition, we carried out subgroup analyses in relation to sample size, study country, year of publication, follow-up or study quality. Overall, the results were robust and that patients with esophagectomy significantly benefited from high-volume hospitals than from low-volume hospitals (Table 3).

3.5. Sensitivity analyses

Sensitivity analyses with the leave-one-out method further revealed the consistent results, which were observed a significant improvement in OS after esophagectomy in high-volume hospitals as compared to that in their low-volume counterparts, with HRs ranging from 0.75 (95% CI: 0.68–0.83) to 0.79 (95% CI: 0.73–0.85) (Table 5).

3.6. Publication bias

We further assessed the publication bias (Figure 3). Because of the relatively small number of included studies in some volume

TABLE 2 Quality assessment of all included studies by Newcastle-Ottawa scale.

Study	Selection				Comparability	Outcome			Total score
	I	II	III	IV	V	VI	VII	VIII	
Dikken 2012 (29)		★	★	★	★★	★	★	★	8
Van de Poll-Fanse 2011 (30)	★	★	★		★★	★	★	★	8
Yang 2019 (21)	★	★	★		★	★	★	★	7
Coupland 2013 (14)	★	★	★	★	★★	★	★	★	9
Derogar 2013 (15)	★	★	★	★	★★	★	★	★	9
Patel 2022 (6)	★	★	★		★★	★	★	★	8
Han 2021 (7)	★	★	★	★	★★	★	★	★	9
Gasper 2009 (8)	★	★	★	★	★★	★	★	★	9
Bilimoria 2008 (22)	★	★	★	★	★★	★	★	★	9
Birkmeyer 2007 (23)	★	★	★	★	★★	★	★	★	9
Sundelof 2008 (24)			★	★	★★	★	★	★	7
Rouvelas 2007 (9)			★	★	★★	★	★		6
Wenner 2005 (25)		★	★	★	★★		★		6
Narendra 2021 (26)		★	★	★	★	★	★		6
Smith 2014 (27)		★	★	★	★★	★	★	★	8
Stavrou 2010 (28)			★	★	★★	★	★	★	7
Verhoef 2007 (31)	★	★	★	★	★★	★	★		8
Taniyama 2021 (32)	★	★		★	★★	★	★		7
Ioka 2007 (33)			★	★	★★		★	★	6
Bachmann 2002 (34)	★	★	★	★	★	★	★	★	8
Hsu 2014 (35)			★	★	★★	★	★	★	7
Kim 2021 (36)	★	★	★	★	★	★	★		7
Duarte 2020 (37)		★	★	★	★	★	★		6
Simunovic 2006 (38)		★	★	★	★	★	★		6

*One score. I, representativeness of the exposed cohorts; II, selection of the non-exposed cohorts; III, ascertainment of exposure; IV, demonstration that outcome of interest was not present at start of study of interest; V, comparability of cohorts on the basis of the design or analysis; VI, assessment of outcomes; VII, was follow-up long enough for outcomes to occur; VIII, adequacy of follow-up of cohorts.

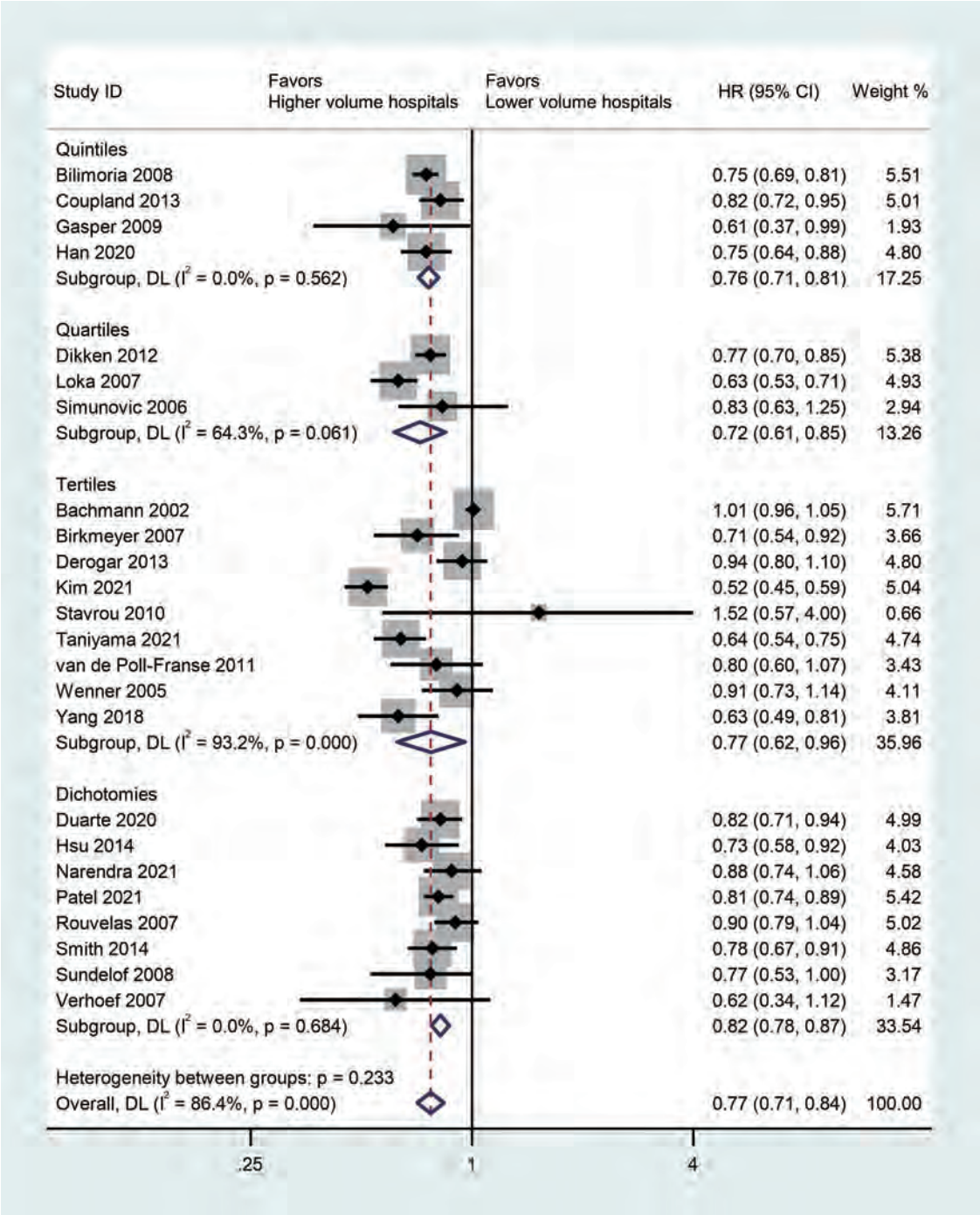

FIGURE 2
Forest plot of long-term survivals following esophagectomy comparing high- with low-volume hospitals (reference) according to volume grouping.

grouping category meta-analyses, we consider that publication bias should exist.

4. Discussion

This meta-analysis outlined the most up-to-date evidence on the relationship between hospital volume and long-term survival outcomes in esophagectomy. We found for the first time that centralization of esophagectomy in high-volume hospitals improved OS as compared to that in low-volume hospitals and patients with esophageal cancer will benefit from an esophagectomy conducted in a higher volume hospital than in a lower one, whether in total or in volume grouping category. However, we were still unable to decide the optimal cutoff value of dividing high- and low-volume hospitals in current study.

Centralization of esophageal cancer surgery has been common in the Netherlands, England, and Canada (18, 39, 40), Comparing a

TABLE 3 Comparisons of the overall survivals between high- and low-volume hospitals by different cutoff values of hospital volume.

Cutoff values of hospital volume (CV) HVH (≥CV) vs. LVH (<CV)	No. of studies	No. of patients	Effect estimate		
			HR	(95% CI)	*P* value
5	6	55,152	0.76	0.71–0.80	<0.001
6	11	80,408	0.79	0.75–0.84	<0.001
7	8	66,606	0.79	0.73–0.85	<0.001
8	9	67,261	0.79	0.74–0.84	<0.001
9	10	68,596	0.78	0.74–0.83	<0.001
10	12	74,347	0.77	0.72–0.83	<0.001
11	11	73,148	0.77	0.72–0.83	<0.001
12–14	12	84,494	0.75	0.68–0.83	<0.001
15	11	83,672	0.75	0.68–0.84	<0.001
16	9	80,741	0.72	0.65–0.80	<0.001
17	8	68,494	0.72	0.63–0.81	<0.001
18–19	7	67,159	0.71	0.61–0.82	<0.001
20	9	77,976	0.71	0.63–0.81	<0.001
21	8	71,427	0.72	0.63–0.82	<0.001
22	7	63,232	0.64	0.56–0.73	<0.001
23–25	6	61,081	0.70	0.60–0.82	<0.001
26–32	5	23,386	0.69	0.57–0.84	<0.001
33–43	6	24,167	0.75	0.59–0.95	0.02
44	5	21,737	0.74	0.55–1.00	0.05

CI, confidence interval; HR, hazard ratio; HVH, high-volume hospital; LVH, low-volume hospital; No., number.

TABLE 4 Subgroup analyses of comparisons of the overall survivals between high- and low-volume hospitals.

Subgroup HVH vs. LVH	No. of studies	No. of patients	Effect estimate	
			HR (95% CI)	*P* value
Total	24	113,014	0.77 (0.71–0.84)	<0.001
Volume group				
Dichotomies	8	18,956	0.82 (0.78–0.87)	<0.001
Tertiles	9	22,695	0.77 (0.62–0.96)	0.02
Quartiles	3	13,615	0.72 (0.61–0.85)	<0.001
Quintiles	4	57,748	0.76 (0.71–0.81)	<0.001
Sample size				
>5,000	6	88,454	0.73 (0.65–0.82)	<0.001
<5,000	18	24,560	0.79 (0.72–0.87)	<0.001
Study country				
Western countries	20	98,381	0.82 (0.76–0.88)	<0.001
Eastern countries	4	20,036	0.61 (0.53–0.70)	<0.001
Year of publication				
2002–2012	13	33,900	0.80 (0.70–0.90)	<0.001
2013–2022	11	79,114	0.75 (0.67–0.83)	<0.001
Follow-up				
Longest follow-up ≥10 years	8	11,060	0.79 (0.69–0.91)	<0.001
Longest follow-up <10 years	16	101,954	0.76 (0.69–0.85)	<0.001
Study quality				
High	19	107,243	0.74 (0.67–0.83)	<0.001
Moderate	5	5771	0.87 (0.80–0.94)	<0.001

CI, confidence interval; HR, hazard ratio; HVH, high-volume hospital; LVH, low-volume hospital; No., number.

centralized country (England) with a non-centralized country (U.S.), a previous study of 13,291 patients illustrated a lower in-hospital mortality in England hospitals than those in the U.S. (4.2% vs. 5.5%) (41). Regarding this, centralization is urgently required, in terms of high-volume hospitals with sufficient surgical volumes, skillful interdisciplinary teams, to provide the optimal treatment for patients with esophageal cancer.

TABLE 5 Sensitivity analysis using leave-one-out method for overall survival of high-volume hospitals vs. low-volume hospitals.

Given named study is omitted	Hazard ratio	95% CI	*P* value
Dikken (29)	0.77	0.70–0.84	<0.001
Van de Poll-Fanse (30)	0.77	0.71–0.84	<0.001
Yang (21)	0.78	0.71–0.85	<0.001
Coupland (14)	0.77	0.70–0.84	<0.001
Derogar (15)	0.76	0.70–0.83	<0.001
Patel (6)	0.77	0.70–0.84	<0.001
Han (7)	0.77	0.71–0.84	<0.001
Gasper (8)	0.75	0.68–0.83	<0.001
Bilimoria (22)	0.77	0.70–0.85	<0.001
Birkmeyer (23)	0.77	0.71–0.84	<0.001
Sundelof (24)	0.77	0.70–0.84	<0.001
Rouvelas (9)	0.76	0.70–0.84	<0.001
Wenner (25)	0.77	0.70–0.84	<0.001
Narendra (26)	0.77	0.70–0.84	<0.001
Smith (27)	0.77	0.70–0.84	<0.001
Stavrou (28)	0.77	0.70–0.84	<0.001
Verhoef (31)	0.77	0.71–0.84	<0.001
Taniyama (32)	0.78	0.71–0.85	0.02
Ioka (33)	0.78	0.72–0.85	0.05
Bachmann (34)	0.76	0.71–0.81	<0.001
Hsu (35)	0.77	0.71–0.84	<0.001
Kim (36)	0.79	0.73–0.85	<0.001
Duarte (37)	0.77	0.70–0.84	<0.001
Simunovic (38)	0.77	0.70–0.84	<0.001

CI, confidence interval.

Although the reasons why high-volume hospitals are associated with better long-term survival are still not fully understood, high-volume hospitals may provide patients with better multidisciplinary teams, more comprehensive preoperative examinations, more accurate preoperative diagnosis, perioperative management, and high-quality surgical care, more specialized surgeons who have more consistent skills of performing curable operations for esophageal cancer patients (42–45). Compared with low-volume hospitals, high-volume hospitals not only have a lower complication rate after esophagectomies, but also the ability of managing complications (46). In addition, the applications of neoadjuvant chemoradiation, perioperative chemotherapy, and postoperatively follow-up can improve long-term outcomes after esophagectomies; therefore, high-volume hospitals are more likely to provide a better overall cancer therapy and care, and the size of hospital volume may serve as a significant indicator of the overall medical quality and health care (47).

Unfortunately, it is difficult for patients to know the overall quality of nearby hospitals. Based on the main findings of current study, patients can select relatively higher volume hospitals nearby. Considering the importance of such knowledges, policy makers should make efforts to educate people for selecting the optimal hospitals for the treatments of specific diseases (e.g., esophagectomy for esophageal cancer), through public reporting systems.

Our study still has limitations. First, this study has the potential for selection bias of individual studies because of

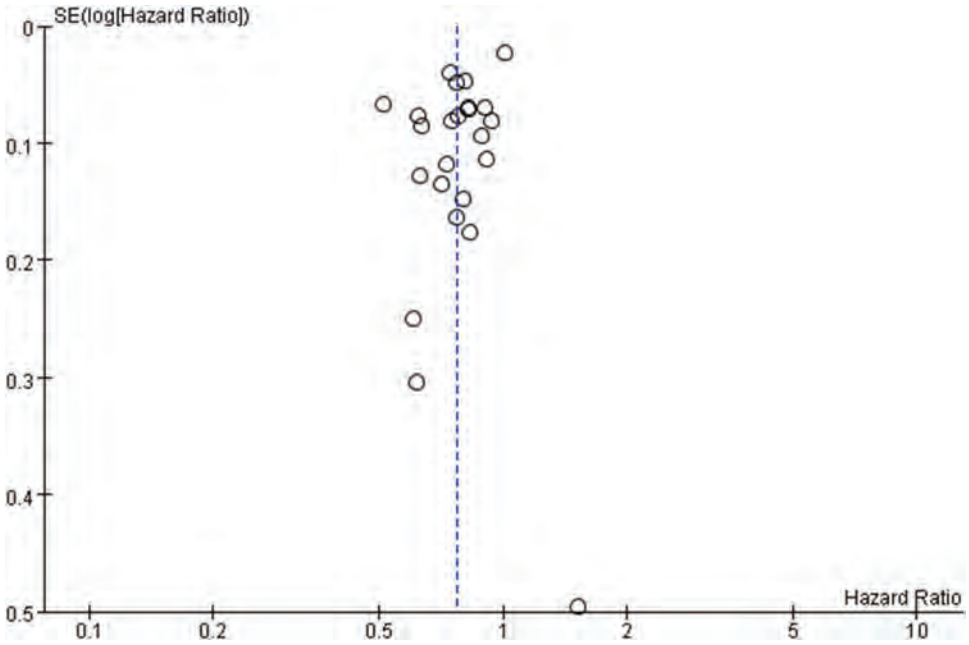

FIGURE 3
Funnel plot of survival benefit following esophagectomy comparing high- with low-volume hospital (reference).

the original data, even with case mix adjustment. Second, all the included studies were observational and retrospective. Third, some of the included studies used the same database (e.g., Sweden), and some participants might be overlapped, even though the study period were different; however, sensitivity analyses of a leave-one-out method confirmed that all the current results were robust. Fourth, as some of the data in the included studies were obtained from the National Cancer Registry, some details of the surgery, such as surgical approach and the extent of lymph nodes dissection, were unknown. Fifth, the volume grouping categories of the annual hospital volumes across the included studies varied greatly, and there was still no optimal threshold, and the main findings of current study thus need to be verified in further studies.

5. Conclusion

In summary, high-volume hospitals significantly improved long-term OS of patients with esophageal cancer after esophagectomy as compared to their low-volume counterparts. Esophagectomy should be centralized in high-volume hospitals.

Data availability statement

The original contributions presented in the study are included in the article, further inquiries can be directed to the corresponding author.

Author contributions

Conceptualization: QW, CDZ. Methodology: QW, SN. Software: QW. Validation: QW, MN, TF, SN, CDZ, SM. Formal analysis: QW, CDZ. Investigation: QW, MN, TF, SN, CDZ, SM. Resources: QW, CDZ. Data curation: QW, CDZ. Writing—original draft preparation: QW. Writing—review and editing: MN, SM. Visualization: QW. Supervision: SM. Reading and approving the final manuscript: QW, MN, TF, SN, CDZ, SM. All authors contributed to the article and approved the submitted version.

Acknowledgments

The authors thank the members of the Department of Esophageal and Gastroenterological Surgery, Juntendo University Graduate School of Medicine, for their thoughtful discussion and helpful advice. The authors also thank all participants and study authors in this study. QW was partly supported by the Japan China Sasakawa Medical Fellowship. CDZ was partly supported by the China Scholarship Council (201908050148).

Conflict of interest

The authors declare that the research was conducted in the absence of any commercial or financial relationships that could be construed as a potential conflict of interest.

Publisher's note

References

1. Sheetz KH, Dimick JB, Nathan H. Centralization of high-risk cancer surgery within existing hospital systems. *J Clin Oncol*. (2019) 37(34):3234–42. doi: 10.1200/JCO.18.02035

2. Balzano G, Guarneri G, Pecorelli N, Paiella S, Rancoita PMV, Bassi C, et al. Modelling centralization of pancreatic surgery in a nationwide analysis. *Br J Surg*. (2020) 107(11):1510–9. doi: 10.1002/bjs.11716

3. van Putten M, Nelen SD, Lemmens VEPP, Stoot JHMB, Hartgrink HH, Gisbertz SS, et al. Overall survival before and after centralization of gastric cancer surgery in The Netherlands. *Br J Surg*. (2018) 105(13):1807–15. doi: 10.1002/bjs.10931

4. Asplund J, Mattsson F, Plecka-Ostlund M, Markar SR, Lagergren J. Annual surgeon and hospital volume of gastrectomy and gastric adenocarcinoma survival in a population-based cohort study. *Acta Oncol*. (2022) 61(4):425–32. doi: 10.1080/0284186X.2022.2025612

5. Lagergren J, Lagergren P. Recent developments in esophageal adenocarcinoma. *CA Cancer J Clin*. (2013) 63(4):232–48. doi: 10.3322/caac.21185

6. Patel DC, Jeffrey Yang CF, He H, Liou DZ, Backhus LM, Lui NS, et al. Influence of facility volume on long-term survival of patients undergoing esophagectomy for esophageal cancer. *J Thorac Cardiovasc Surg*. (2022) 163(4):1536–1546 e1533. doi: 10.1016/j.jtcvs.2021.05.048

7. Han S, Kolb JM, Hosokawa P, Friedman C, Fox C, Scott FI, et al. The volume-outcome effect calls for centralization of care in esophageal adenocarcinoma: results from a large national cancer registry. *Am J Gastroenterol*. (2021) 116(4):811–5. doi: 10.14309/ajg.0000000000001046

8. Gasper WJ, Glidden DV, Jin C, Way LW, Patti MG. Has recognition of the relationship between mortality rates and hospital volume for major cancer surgery in California made a difference?: a follow-up analysis of another decade. *Ann Surg*. (2009) 250(3):472–83. doi: 10.1097/SLA.0b013e3181b47c79

9. Rouvelas I, Lindblad M, Zeng W, Viklund P, Ye W, Lagergren J. Impact of hospital volume on long-term survival after esophageal cancer surgery. *Arch Surg*. (2007) 142(2):113–7; discussion 118. doi: 10.1001/archsurg.142.2.113

10. Yang H, Liu H, Chen Y, Zhu C, Fang W, Yu Z, et al. Long-term efficacy of neoadjuvant chemoradiotherapy plus surgery for the treatment of locally advanced esophageal squamous cell carcinoma: the NEOCRTEC5010 randomized clinical trial. *JAMA Surg*. (2021) 156(8):721–9. doi: 10.1001/jamasurg.2021.2373

11. Yu S, Zhang W, Ni W, Xiao Z, Wang Q, Zhou Z, et al. A propensity-score matching analysis comparing long-term survival of surgery alone and postoperative treatment for patients in node positive or stage III esophageal squamous cell carcinoma after R0 esophagectomy. *Radiother Oncol*. (2019) 140:159–66. doi: 10.1016/j.radonc.2019.06.020

12. He S, Xu J, Liu X, Zhen Y. Advances and challenges in the treatment of esophageal cancer. *Acta Pharm Sin B*. (2021) 11(11):3379–92. doi: 10.1016/j.apsb.2021.03.008

13. Lagergren J, Smyth E, Cunningham D, Lagergren P. Oesophageal cancer. *Lancet*. (2017) 390(10110):2383–96. doi: 10.1016/S0140-6736(17)31462-9

14. Coupland VH, Lagergren J, Luchtenborg M, Jack RH, Allum W, Holmberg L, et al. Hospital volume, proportion resected and mortality from oesophageal and gastric cancer: a population-based study in England, 2004-2008. *Gut*. (2013) 62(7):961–6. doi: 10.1136/gutjnl-2012-303008

15. Derogar M, Sadr-Azodi O, Johar A, Lagergren P, Lagergren J. Hospital and surgeon volume in relation to survival after esophageal cancer surgery in a population-based study. *J Clin Oncol*. (2013) 31(5):551–7. doi: 10.1200/JCO.2012.46.1517

16. Gillison E. W., Powell J., McConkey C. C., Spychal R. T. Surgical workload and outcome after resection for carcinoma of the oesophagus and cardia. *Br J Surg*. (2002) 89(3):344–8. doi: 10.1046/j.0007-1323.2001.02015.x

17. Wang Q, Nasu M, Fukunaga T, Nojiri S, Zhang C-D, Mine S. Association of hospital volume and long-term survival after esophagectomy: a systematic review and meta-analysis. *INPLASY*. (2022). doi: 10.37766/inplasy2022.7.0023

18. Page MJ, McKenzie JE, Bossuyt PM, Boutron I, Hoffmann TC, Mulrow CD, et al. The PRISMA 2020 statement: an updated guideline for reporting systematic reviews. *Br Med J*. (2021) 372:n71. doi: 10.1136/bmj.n71

19. Stang A. Critical evaluation of the Newcastle-Ottawa scale for the assessment of the quality of nonrandomized studies in meta-analyses. *Eur J Epidemiol*. (2010) 25(9):603–5. doi: 10.1007/s10654-010-9491-z

20. Higgins J, Thompson S, Deeks J, Altman D. Measuring inconsistency in meta-analyses. *Br Med J*. (2003) 327(7414):557–60. doi: 10.1136/bmj.327.7414.557

21. Yang GQ, Mhaskar R, Rishi A, Naghavi AO, Frakes JM, Almhanna K, et al. Intensity-modulated radiotherapy at high-volume centers improves survival in patients with esophageal adenocarcinoma receiving trimodality therapy. *Dis Esophagus*. (2019) 32(8):doy124. doi: 10.1093/dote/doy124

22. Bilimoria KY, Bentrem DJ, Feinglass JM, Stewart AK, Winchester DP, Talamonti MS, et al. Directing surgical quality improvement initiatives: comparison of perioperative mortality and long-term survival for cancer surgery. *J Clin Oncol*. (2008) 26(28):4626–33. doi: 10.1200/JCO.2007.15.6356

23. Birkmeyer JD, Sun Y, Wong SL, Stukel TA. Hospital volume and late survival after cancer surgery. *Ann Surg*. (2007) 245(5):777–83. doi: 10.1097/01.sla.0000252402.33814.dd

24. Sundelof M, Lagergren J, Ye W. Surgical factors influencing outcomes in patients resected for cancer of the esophagus or gastric cardia. *World J Surg*. (2008) 32(11):2357–65. doi: 10.1007/s00268-008-9698-2

25. Wenner J, Zilling T, Bladström A, Alvegård T. The influence of surgical volume on hospital mortality and 5-year survival for carcinoma of the oesophagus and gastric cardia. *Anticancer Res*. (2005) 25(1B):419–24.

26. Narendra A, Baade PD, Aitken JF, Fawcett J, Leggett B, Leggett C, et al. Hospital characteristics associated with better "quality of surgery" and survival following oesophagogastric cancer surgery in Queensland: a population-level study. *ANZ J Surg*. (2021) 91(3):323–8. doi: 10.1111/ans.16397

27. Smith RC, Creighton N, Lord RV, Merrett ND, Keogh GW, Liauw WS, et al. Survival, mortality and morbidity outcomes after oesophagogastric cancer surgery in New South Wales, 2001-2008. *Med J Aust*. (2014) 200(7):408–13. doi: 10.5694/mja13.11182

28. Stavrou EP, Smith GS, Baker DF. Surgical outcomes associated with oesophagectomy in New South Wales: an investigation of hospital volume. *J Gastrointest Surg*. (2010) 14(6):951–7. doi: 10.1007/s11605-010-1198-7

29. Dikken JL, Dassen AE, Lemmens VE, Putter H, Krijnen P, van der Geest L, et al. Effect of hospital volume on postoperative mortality and survival after oesophageal and gastric cancer surgery in The Netherlands between 1989 and 2009. *Eur J Cancer*. (2012) 48(7):1004–13. doi: 10.1016/j.ejca.2012.02.064

30. van de Poll-Franse LV, Lemmens VE, Roukema JA, Coebergh JW, Nieuwenhuijzen GA. Impact of concentration of oesophageal and gastric cardia cancer surgery on long-term population-based survival. *Br J Surg*. (2011) 98(7):956–63. doi: 10.1002/bjs.7493

31. Verhoef C, van de Weyer R, Schaapveld M, Bastiaannet E, Plukker JT. Better survival in patients with esophageal cancer after surgical treatment in university hospitals: a plea for performance by surgical oncologists. *Ann Surg Oncol*. (2007) 14(5):1678–87. doi: 10.1245/s10434-006-9333-0

32. Taniyama Y, Tabuchi T, Ohno Y, Morishima T, Okawa S, Koyama S, et al. Hospital surgical volume and 3-year mortality in severe prognosis cancers: a population-based study using cancer registry data. *J Epidemiol*. (2021) 31(1):52–8. doi: 10.2188/jea.JE20190242

33. Ioka A, Tsukuma H, Ajiki W, Oshima A. Hospital procedure volume and survival of cancer patients in Osaka, Japan: a population-based study with latest cases. *Jpn J Clin Oncol*. (2007) 37(7):544–53. doi: 10.1093/jjco/hym052

34. Bachmann M, Alderson D, Edwards D, Wotton S, Bedford C, Peters T, et al. Cohort study in south and west England of the influence of specialization on the management and outcome of patients with oesophageal and gastric cancers. *Br J Surg*. (2002) 89(7):914–22. doi: 10.1046/j.1365-2168.2002.02135.x

35. Hsu PK, Chen HS, Wu SC, Wang BY, Liu CY, Shih CH, et al. Impact of hospital volume on long-term survival after resection for oesophageal cancer: a population-based study in taiwandagger. *Eur J Cardiothorac Surg*. (2014) 46(6):e127–135; discussion e135. doi: 10.1093/ejcts/ezu377

36. Kim BR, Jang EJ, Jo J, Lee H, Jang DY, Ryu HG. The association between hospital case-volume and postoperative outcomes after esophageal cancer surgery: a population-based retrospective cohort study. *Thorac Cancer*. (2021) 12(18):2487–93. doi: 10.1111/1759-7714.14096

37. Duarte MBO, Pereira EB, Lopes LR, Andreollo NA, Carvalheira JBC. Chemoradiotherapy with or without surgery for esophageal squamous cancer according to hospital volume. *JCO Glob Oncol*. (2020) 6:828–36. doi: 10.1200/JGO.19.00360

38. Simunovic M, Rempel E, Thériault M, Coates A, Whelan T, Holowaty E, et al. Influence of hospital characteristics on operative death and survival of patients after major cancer surgery in Ontario. *Can J Surg*. (2006) 49(4):251–8.

39. Varghese TK Jr., Wood DE, Farjah F, Oelschlager BK, Symons RG, MacLeod KE, et al. Variation in esophagectomy outcomes in hospitals meeting leapfrog volume outcome standards. *Ann Thorac Surg*. (2011) 91(4):1003–9; discussion 1009–1010. doi: 10.1016/j.athoracsur.2010.11.006

40. Chang AC. Centralizing esophagectomy to improve outcomes and enhance clinical research: invited expert review. *Ann Thorac Surg*. (2018) 106(3):916–23. doi: 10.1016/j.athoracsur.2018.04.004

41. Munasinghe A, Markar SR, Mamidanna R, Darzi AW, Faiz OD, Hanna GB, et al. Is it time to centralize high-risk cancer care in the United States? Comparison of outcomes of esophagectomy between England and the United States. *Ann Surg*. (2015) 262(1):79–85. doi: 10.1097/SLA.0000000000000805

42. Van den Broeck T, Oprea-Lager D, Moris L, Kailavasan M, Briers E, Cornford P, et al. A systematic review of the impact of surgeon and hospital caseload volume on oncological and nononcological outcomes after radical prostatectomy for nonmetastatic prostate cancer. *Eur Urol*. (2021) 80(5):531–45. doi: 10.1016/j.eururo.2021.04.028

43. Khanna A, Saarela O, Lawson K, Finelli A, Haber GP, Lee B, et al. Hospital quality metrics for radical cystectomy: disease specific and correlated to mortality outcomes. *J Urol*. (2019) 202(3):490–7. doi: 10.1097/JU.0000000000000282

44. Wright JD, Chen L, Hou JY, Burke WM, Tergas AI, Ananth CV, et al. Association of hospital volume and quality of care with survival for ovarian cancer. *Obstet Gynecol*. (2017) 130(3):545–53. doi: 10.1097/AOG.0000000000002164

45. Ghaferi AA, Birkmeyer JD, Dimick JB. Complications, failure to rescue, and mortality with major inpatient surgery in medicare patients. *Ann Surg*. (2009) 250(6):1029–34. doi: 10.1097/sla.0b013e3181bef697

46. Ghaferi A, Birkmeyer J, Dimick J. Hospital volume and failure to rescue with high-risk surgery. *Med Care*. (2011) 49(12):1076–81. doi: 10.1097/MLR.0b013e3182329b97

47. Eskander A, Irish J, Groome PA, Freeman J, Gullane P, Gilbert R, et al. Volume-outcome relationships for head and neck cancer surgery in a universal health care system. *Laryngoscope*. (2014) 124(9):2081–8. doi: 10.1002/lary.24704

日中笹川医学奨学金制度＜学位取得コース＞評価書
課程博士：指導教官用

第 43 期　　研究者番号：G4307　　作成日　：2024 年 3 月 10 日

氏　名	張 瑛	ZHANG YING	性別	F	生年月日　1985/08/14
所属機関（役職）	寧波市医療中心李恵利医院超音波科（主治医師）				
研究先（指導教官）	横浜市立大学大学院 医学研究科消化器内科学（前田 愼　主任教授）				
研究テーマ	肝胆膵疾患・炎症性腸疾患における超音波を主体とした画像診断と治療 Ultrasound-based multi-modality imaging and therapy for hepatobiliary and pancreatic oncology and inflammatory bowel disease				
専攻種別	□論文博士		☑課程博士		

研究者評価（指導教官記入欄）

成績状況	優　(良)　可　不可 学業成績係数=	取得単位数 取得単位数 40／取得すべき単位総数 60
学生本人が行った研究の概要	1. 超音波造影剤と CT/MRI 造影剤についての総説を記載し、受理された(Frontiers in Oncology 2022 Jun 2;12:921667). 2. 多施設で後ろ向き検討ではあるが、Intermediate stage の切除不能肝癌に対して肝癌の抗がん剤である Lenvatinib 投与後にラジオ波を実施し腫瘍量を減らし、さらに再度 Lenvatinib を投与する群と Lenvatinib 群の baseline を matching させて全生存期間を比較した。Lenvatinib とラジオ波逐次治療群は有意に全生存期間を延長した. Hepatology research に投稿した. 3. Sonazoid 造影超音波後血管相でクッパー細胞がない中分化・低分化肝癌は低エコー病変として検出される. 従来の低音圧造影では超音波の減衰のため十分に評価できないが、高音圧に切り替えることで有意には低エコー病変として検出できることを統計学的に証明し、その論文をアメリカの超音波学会雑誌(Journal of Ultrasound in Medicine)に投稿した.	
総合評価	【良かった点】 超音波造影剤と CT/MRI 造影剤についての総説を最初に記載したので、造影超音波に関する知見が深まったと考える. 肝細胞癌の対する診断と治療についての論文を、統計を含め、真摯な態度で詳細に記載しましたので、今後の診療に役立つと思われる. 【改善すべき点】 コロナの時期も重なっていたが、対面で、もっと一緒に造影超音波やラジオ波治療を体験してもらいたかった. 【今後の展望】原著論文が revise になれば、accept するために修正していく予定.	
学位取得見込	原著論文を２つ投稿しており、いずれも質が高い内容なので、accept されると期待している。Accept されれば、残りの 20 単位が加算され、学位は取得されると考える. その阿知はすでに中間審査は済み、最終審査に進む予定.	
評価者（指導教官名）　前田 愼		

日中笹川医学奨学金制度<学位取得コース>報告書
研究者用

第43期　　研究者番号：G4307　　作成日：2024年3月6日

氏名	张 瑛	ZHANG YING	性別	F	生年月日 1985/08/14
所属機関(役職)	寧波市医療中心李恵利医院超音波科（主治医師）				
研究先（指導教官）	横浜市立大学大学院 医学研究科消化器内科学（前田 愼　主任教授）				
研究テーマ	肝胆膵疾患・炎症性腸疾患における超音波を主体とした画像診断と治療 Ultrasound-based multi-modality imaging and therapy for hepatobiliary and pancreatic oncology and inflammatory bowel disease				
専攻種別	論文博士	☐	課程博士	☑	

1．研究概要（1）

Lenvatinib radiofrequency ablation sequential therapy offers survival benefits for patients with unresectable hepatocellular carcinoma at intermediate stage and the liver reserve of Child-Pugh A category: A Multicenter Study

1）目的（Goal）

This study aims to evaluate the efficacy and safety of lenvatinib radiofrequency ablation (RFA) sequential therapy for certain hepatocellular carcinoma (HCC) patients.

2）戦略（Approach）

As a multi-targeted TKI for systemic pharmacotherapy, lenvatinib acts as an antiangiogenic treatment to slow tumor growth, demonstrating non-inferiority in OS but superiority in PFS, time to progression, and ORR compared to sorafenib1, 2. The combined effect of lenvatinib-induced reduction in tumor blood flow and tumor growth, along with additional RFA, was observed to effectively reduce viable tumor volume3. With the reduction in tumor volume achieved through additional local therapy, the resumption of lenvatinib at a reduced dose was contemplated to mitigate AEs and extend the duration of administration, rendering patients apt for prolonged lenvatinib treatment4.

3）材料と方法（Materials and methods）

Unresectable HCC patients in the intermediate stage with a liver reserve of Child-Pugh A were retrospectively recruited in a multicenter setting. Those in the lenvatinib RFA sequential therapy group received lenvatinib initially, followed by RFA and the re-administration of lenvatinib. The study compared overall survival (OS), progression-free survival (PFS), tumor response, and adverse events (AEs) between patients undergoing sequential therapy and lenvatinib monotherapy.

4）実験結果（Results）

A total of 119 patients from nine institutions were included. After propensity score matching, independent factors influencing OS were identified as sequential therapy and modified Albumin-Bilirubin (mALBI) grade with hazard ratios (HR) of 0.426 (95% confidence intervals, CI: 0.221-0.824) and 1.672 (95% CI: 1.158-2.414), respectively. Stratified analysis based on mALBI grades confirmed the independent influence of treatment strategy across all mALBI grades for OS (HR: 0.443, 95% CI: 0.226-0.869). Furthermore, sequential therapy was identified as an independent factor of PFS (HR: 0.363, 95% CI: 0.212-0.621). Sequential therapy significantly outperformed monotherapy on survival benefits (OS: 38.27 vs. 19.38 months for sequential therapy and monotherapy, respectively, p=0.012; PFS: 13.80 vs. 5.32 months for sequential therapy and monotherapy, respectively, p<0.001). The sequential therapy significantly associated with objective response by modified Response Evaluation Criteria in Solid Tumors (mRECIST) (odds ratio: 10.060). Regarding safety, ten out of 119 experienced grade 3 AEs, with no AE beyond grade 3 observed.

5）考察（Discussion）

The findings in the current research affirmed that the lenvatinib RFA sequential therapy serves as a protective measure for uHCC patients' survival benefits. The effectiveness of lenvatinib RFA sequential therapy appears to be primarily attributed to volume reduction induced by both lenvatinib and RFA, and the sustained administration of lenvatinib with tolerable dose adjustments. Meanwhile, as a strong inhibitor of vascular endothelial growth factor receptor and fibroblast growth factor receptor, lenvatinib has also been reported being involved in the cancer immune cycle5, 6. The demonstrated superior antitumor efficacy of lenvatinib, attributable to its underlying immunomodulatory activity, surpasses that of sorafenib7. Additionally, anti-angiogenic therapies may normalize tumor blood vessels8-10 , potentially enhancing drug delivery9-13 and immune infiltration and interferon response through reconstructing the TME6, 14, 15. Hence, the reintroduction of lenvatinib at a dose that is well-tolerated post-RFA is helpful at averting potential relapse, ultimately contributing to extended OS and PFS.

RFA, in addition to its primary role in volume reduction for HCC, may also exert a mild influence on the immune system to avert potential relapse. Through the release of tumor-specific antigens and the induction of proinflammatory cytokines, these immunomodulatory effects bring about changes in the TME, thereby activating immune responses16. The synergy between TKI and RFA, as observed by Qi et al., enhances anti-tumor immune responses, suppressing certain signaling pathways17. Activation of the immune system post-RFA extends beyond the primary tumor site, suppressing distant tumor growth in rodent models18, 19 . RFA has also been reported to reinforces host adaptive immunity through various pathways, such as up-regulating CD8+ T cells and dendritic cells while down-regulating regulatory T cells20. However, the potency of RFA-induced immune activation alone may not be sufficient for fully recurred tumor elimination21, necessitating exploration of synergistic mechanisms involved the anti-angiogenic benefits of lenvatinib and the changeable TME associated with RFA. Wang F et al. firstly validated the efficacy of lenvatinib RFA sequential therapy for intermediate-stage HCC patients that exceeded the up-to-seven criterion, demonstrating improved OS (median: 21.3 months, 95% CI:14.0-28.0) and PFS (median: 12.5 months, 95% CI: 9.3-20.7) over a median follow-up period of 17.2 (6.7-38.5) months22. With an extended follow-up duration

1．研究概要(2)
(median: 18.42 months, range: 1.81–61.38 months) and an expanded cohort that includes patients beyond the up-to-seven criteria in the present study, the lenvatinib RFA sequential treatment group exhibited relatively longer median OS (38.27, 95%CI, 21.62–54.92 months) and PFS (13.80 ± 3.67 months), further emphasizing the promising survival outcomes associated with lenvatinib RFA sequential therapy.

6)参考文献(References)

1Kudo M, Finn RS, Qin S, et al. Lenvatinib versus sorafenib in first-line treatment of patients with unresectable hepatocellular carcinoma: a randomised phase 3 non-inferiority trial. Lancet. 2018 Mar 24;391: 1163–73.
2Eso Y, Marusawa H. Novel approaches for molecular targeted therapy against hepatocellular carcinoma. Hepatol Res. 2018 Jul;48: 597–607.
3Numata K, Wang F. New developments in ablation therapy for hepatocellular carcinoma: combination with systemic therapy and radiotherapy. Hepatobiliary Surg Nutr. 2022 Oct;11: 766–9.
4Mawatari S, Tamai T, Kumagai K, et al. Clinical Effect of Lenvatinib Re-Administration after Transcatheter Arterial Chemoembolization in Patients with Intermediate Stage Hepatocellular Carcinoma. Cancers (Basel). 2022 Dec 13;14.
5Hoshi T, Watanabe Miyano S, Watanabe H, et al. Lenvatinib induces death of human hepatocellular carcinoma cells harboring an activated FGF signaling pathway through inhibition of FGFR-MAPK cascades. Biochem Biophys Res Commun. 2019 May 21;513: 1–7.
6Kato Y, Tabata K, Kimura T, et al. Lenvatinib plus anti-PD-1 antibody combination treatment activates CD8+ T cells through reduction of tumor-associated macrophage and activation of the interferon pathway. PLoS One. 2019;14: e0212513.
7Kimura T, Kato Y, Ozawa Y, et al. Immunomodulatory activity of lenvatinib contributes to antitumor activity in the Hepa1-6 hepatocellular carcinoma model. Cancer Sci. 2018 Dec;109: 3993–4002.
8Goel S, Wong AH, Jain RK. Vascular normalization as a therapeutic strategy for malignant and nonmalignant disease. Cold Spring Harb Perspect Med. 2012 Mar;2: a006486.
9Goel S, Duda DG, Xu L, et al. Normalization of the vasculature for treatment of cancer and other diseases. Physiol Rev. 2011 Jul;91: 1071–121.
10Liu Z-L, Chen H-H, Zheng L-L, Sun L-P, Shi L. Angiogenic signaling pathways and anti-angiogenic therapy for cancer. Signal Transduction and Targeted Therapy. 2023 2023/05/11;8: 198.
11Jain RK. Normalizing tumor microenvironment to treat cancer: bench to bedside to biomarkers. J Clin Oncol. 2013 Jun 10;31: 2205–18.
12Fu Z, Li X, Zhong J, et al. Lenvatinib in combination with transarterial chemoembolization for treatment of unresectable hepatocellular carcinoma (uHCC): a retrospective controlled study. Hepatol Int. 2021 Jun;15: 663–75.
13Ikeda M, Yamashita T, Ogasawara S, et al. Multicenter Phase II Trial of Lenvatinib plus Hepatic Intra-Arterial Infusion Chemotherapy with Cisplatin for Advanced Hepatocellular Carcinoma: LEOPARD. Liver Cancer. 2023: 1–10.
14Deng H, Kan A, Lyu N, et al. Dual Vascular Endothelial Growth Factor Receptor and Fibroblast Growth Factor Receptor Inhibition Elicits Antitumor Immunity and Enhances Programmed Cell Death-1 Checkpoint Blockade in Hepatocellular Carcinoma. Liver Cancer. 2020 Jun;9: 338–57.
15Choi Y, Jung K. Normalization of the tumor microenvironment by harnessing vascular and immune modulation to achieve enhanced cancer therapy. Experimental & Molecular Medicine. 2023 2023/11/01.
16Napoletano C, Taurino F, Biffoni M, et al. RFA strongly modulates the immune system and anti-tumor immune responses in metastatic liver patients. Int J Oncol. 2008 Feb;32: 481–90.
17Qi X, Yang M, Ma L, et al. Synergizing sunitinib and radiofrequency ablation to treat hepatocellular cancer by triggering the antitumor immune response. J Immunother Cancer. 2020 Oct;8.
18Dromi SA, Walsh MP, Herby S, et al. Radiofrequency ablation induces antigen-presenting cell infiltration and amplification of weak tumor-induced immunity. Radiology. 2009 Apr;251: 58–66.
19Erös de Bethlenfalva-Hora C, Mertens JC, Piguet AC, et al. Radiofrequency ablation suppresses distant tumour growth in a novel rat model of multifocal hepatocellular carcinoma. Clin Sci (Lond). 2014 Feb;126: 243–52.
20Ahmed M, Kumar G, Moussa M, et al. Hepatic Radiofrequency Ablation-induced Stimulation of Distant Tumor Growth Is Suppressed by c-Met Inhibition. Radiology. 2016 Apr;279: 103–17.
21Löffler MW, Nussbaum B, Jäger G, et al. A Non-interventional Clinical Trial Assessing Immune Responses After Radiofrequency Ablation of Liver Metastases From Colorectal Cancer. Front Immunol. 2019;10: 2526.
22Wang F, Numata K, Komiyama S, et al. Combination Therapy With Lenvatinib and Radiofrequency Ablation for Patients With Intermediate-Stage Hepatocellular Carcinoma Beyond Up-To-Seven Criteria and Child-Pugh Class A Liver function: A Pilot Study. Front Oncol. 2022;12: 843680.

2. 執筆論文 Publication of thesis ※記載した論文を添付してください。Attach all of the papers listed below.

論文名 1 Title	Lenvatinib radiofrequency ablation sequential therapy offers survival benefits for patients with unresectable hepatocellular carcinoma at intermediate stage and the liver reserve of Child-Pugh A category: A Multicenter Study					
掲載誌名 Published journal	Hepatology Research (under review)					
	年 月	巻(号)	頁 ～ 頁		言語 Language	英語
第1著者名 First author	Ying Zhang	第2著者名 Second author	Kazushi Numata	第3著者名 Third author		Kento Imajo
その他著者名 Other authors	Haruki Uojima, Akihiro Funaoka, Satoshi Komiyama, Katsuaki Ogushi, Makoto Chuma, Kuniyasu Irie, Shigehiro Kokubu, Masato Yoneda, Takashi Kobayashi, Hisashi Hidaka, Taito Fukushima, Satoshi Kobayashi, Manabu Morimoto,					
論文名 2 Title	Enhancing Deep-Seated Hepatocellular Carcinoma Detection: Assessing the Added Value of Additional High Mechanical Index Setting in Sonazoid-based Contrast-Enhanced Ultrasound during Post-Vascular Phase					
掲載誌名 Published journal	Journal of Ultrasound in Medicine (under review)					
	年 月	巻(号)	頁 ～ 頁		言語 Language	英語
第1著者名 First author	Ying Zhang	第2著者名 Second author	Kazushi Numata	第3著者名 Third author		Hiromi Nihonmatsu
その他著者名 Other authors	Akihiro Funaoka, Haruo Miwa, Ritsuko Oishi, Akito Nozaki, Shin Maeda					
論文名 3 Title	Contrast Agents for Hepatocellular Carcinoma Imaging: Value and Progression					
掲載誌名 Published journal	Frontiers in Oncology					
	2022 年 6 月	12 巻(号)	頁 ～ 頁		言語 Language	英語
第1著者名 First author	Ying Zhang	第2著者名 Second author	Kazushi Numata	第3著者名 Third author		Du Yuewu
その他著者名 Other authors	Shin Maeda					
論文名 4 Title						
掲載誌名 Published journal						
	年 月	巻(号)	頁 ～ 頁		言語 Language	
第1著者名 First author		第2著者名 Second author		第3著者名 Third author		
その他著者名 Other authors						
論文名 5 Title						
掲載誌名 Published journal						
	年 月	巻(号)	頁 ～ 頁		言語 Language	
第1著者名 First author		第2著者名 Second author		第3著者名 Third author		
その他著者名 Other authors						

3. 学会発表 Conference presentation ※筆頭演者として総会・国際学会を含む主な学会で発表したものを記載してください

※Describe your presentation as the principal presenter in major academic meetings including general meetings or international meetin

学会名 Conference							
演 題 Topic							
開催日 date	年 月 日		開催地 venue				
形式 method	□ 口頭発表 Oral	□ ポスター発表 Poster	言語 Language	□ 日本語	□ 英語	□ 中国語	
共同演者名 Co-presenter							
学会名 Conference							
演 題 Topic							
開催日 date	年 月 日		開催地 venue				
形式 method	□ 口頭発表 Oral	□ ポスター発表 Poster	言語 Language	□ 日本語	□ 英語	□ 中国語	
共同演者名 Co-presenter							
学会名 Conference							
演 題 Topic							
開催日 date	年 月 日		開催地 venue				
形式 method	□ 口頭発表 Oral	□ ポスター発表 Poster	言語 Language	□ 日本語	□ 英語	□ 中国語	
共同演者名 Co-presenter							
学会名 Conference							
演 題 Topic							
開催日 date	年 月 日		開催地 venue				
形式 method	□ 口頭発表 Oral	□ ポスター発表 Poster	言語 Language	□ 日本語	□ 英語	□ 中国語	
共同演者名 Co-presenter							

4. 受賞（研究業績） Award (Research achievement)

名 称 Award name				
	国名 Country		受賞年 Year of award	年 月
名 称 Award name				
	国名 Country		受賞年 Year of award	年 月

5. 本研究テーマに関わる他の研究助成金受給 Other research grants concerned with your resarch theme

受給実績 Receipt record	□ 有　■ 無
助成機関名称 Funding agency	
助成金名称 Grant name	
受給期間 Supported period	年　4　月 ～　2024　年　3　月
受給額 Amount received	円
受給実績 Receipt record	□ 有　■ 無
助成機関名称 Funding agency	
助成金名称 Grant name	
受給期間 Supported period	年　月 ～　年　月
受給額 Amount received	円

6. 他の奨学金受給 Another awarded scholarship

受給実績 Receipt record	■ 有　□ 無
助成機関名称 Funding agency	公益財団法人首藤奨学財団
奨学金名称 Scholarship name	首藤奨学財団奨学金
受給期間 Supported period	2023　年　4　月 ～　2024　年　3　月
受給額 Amount received	600,000 円

7. 研究活動に関する報道発表 Press release concerned with your research activities

※記載した記事を添付してください。Attach a copy of the article described below

報道発表 Press release	□ 有　■ 無	発表年月日 Date of release	
発表機関 Released medium			
発表形式 Release method	・新聞　・雑誌　・Web site　・記者発表　・その他(　　)		
発表タイトル Released title			

8. 本研究テーマに関する特許出願予定 Patent application concerned with your research theme

出願予定 Scheduled	□ 有　■ 無	出願国 Application	
出願内容(概要) Application contents			

9. その他 Others

指導責任者(記名)　Numata Kazushi

frontiers | Frontiers in Oncology

REVIEW
published: 02 June 2022
doi: 10.3389/fonc.2022.921667

Contrast Agents for Hepatocellular Carcinoma Imaging: Value and Progression

Ying Zhang[1,2,3], *Kazushi Numata*[2*], *Yuewu Du*[1] *and Shin Maeda*[3]

[1] Department of Medical Ultrasound, Ningbo Medical Centre Li Huili Hospital, Ningbo, China, [2] Gastroenterological Center, Yokohama City University Medical Center, Yokohama, Japan, [3] Department of Gastroenterology, Graduate School of Medicine, Yokohama City University, Yokohama, Japan

Hepatocellular carcinoma (HCC) has the third-highest incidence in cancers and has become one of the leading threats to cancer death. With the research on the etiological reasons for cirrhosis and HCC, early diagnosis has been placed great hope to form a favorable prognosis. Non-invasive medical imaging, including the associated contrast media (CM)-based enhancement scan, is taking charge of early diagnosis as mainstream. Meanwhile, it is notable that various CM with different advantages are playing an important role in the different imaging modalities, or even combined modalities. For both physicians and radiologists, it is necessary to know more about the proper imaging approach, along with the characteristic CM, for HCC diagnosis and treatment. Therefore, a summarized navigating map of CM commonly used in the clinic, along with ongoing work of agent research and potential seeded agents in the future, could be a needed practicable aid for HCC diagnosis and prognosis.

Keywords: ultrasound, MRI, CECT, hepatocellular carcinoma (HCC), contrast media (CM)

OPEN ACCESS

Edited by:
Kun Zhang,
Tongji University, China

Reviewed by:
Dan Zhao,
Hangzhou Red Cross Hospital, China
Chengcheng Niu,
Central South University, China

****Correspondence:***
Kazushi Numata
kz_numa@yokohama-cu.ac.jp

Specialty section:
This article was submitted to Radiation Oncology, a section of the journal Frontiers in Oncology

Received: *16 April 2022*
Accepted: *02 May 2022*
Published: *02 June 2022*

Citation:
Zhang Y, Numata K, Du Y and Maeda S (2022) Contrast Agents for Hepatocellular Carcinoma Imaging: Value and Progression. Front. Oncol. 12:921667. doi: 10.3389/fonc.2022.921667

INTRODUCTION

Hepatocellular carcinoma (HCC) has the third-highest incidence in cancers, along with the fourth leading cause of cancer death in 2020 globally. Moreover, cirrhosis, a major source of HCC, composed 2.4% of death with all causes in 2019 according to the WHO. Meanwhile, hepatitis B virus (HBV) and hepatitis C virus (HCV) infection, alcohol abuse, and non-alcoholic steatohepatitis (NASH) are dominating etiological reasons for cirrhosis and HCC. Modern medicine believes the small HCC is preventable and curable through early diagnosis and timely etiological treatment if screening and surveillance could be well conducted for cirrhosis (1). Therefore, non-invasive medical imaging techniques, such as MRI, ultrasound (US), and CT, have contributed to HCC patients' management (2–6).

For early diagnosis, treatment assessment, and follow-up, multiple medical imaging modalities were improved and adapted in every corner of HCC prevention and supervision. In the past decades, the diagnostic efficacy of medical imaging has been elevated through the improvement of imaging resolution and associated intravenous contrast agents. US elastography and MR elastography are recommended to supervise and assess hepatic fibrosis, which may gradually progress to cirrhosis without medical intervention (7). On the other hand, taking characteristic advantage of the dual blood supply of the liver, transvenous contrast agents depict the liver lesion by illustrating the tumorous

blood supply with characteristics of arterial enhancement (wash-in) and portal hypodensity or hyposignal (wash-out). The classical imaging findings of wash-in and wash-out were believed to have a sensitivity of approximately 60% and a specificity of 96%–100% for small HCCs with a size of 10–20 mm. Still, a biopsy is needed in 40% of these lesions. Along with a deeper investigation of clinical research, an experienced radiologist can achieve a much more satisfying diagnostic efficacy through guidelines like the American College of Radiology Liver Imaging Reporting and Data System (ACR LIRADS) (8, 9). As a result, contrast enhancement imaging, like dynamic MRI and contrast-enhanced CT (CECT), is recommended in mainstream guidelines for preoperative HCC diagnosis with certainty. Screening using the non-enhanced US is also recommended for patients at a higher risk of HCC every 6 months. When it comes to contrast-enhanced US (CEUS), though it is not recommended by the World Federation for Ultrasound in Medicine and Biology (WFUMB) guidelines for liver lesion detection due to the narrow window for arterial phase observation (10), some meta-analyses indicated it to be a promising diagnostic approach for HCC with a sensitivity of 93% (95% CI: 91%–95%) and a specificity of 90% (95% CI: 88%–92%) (11), as well as the diagnostic efficacy of 93% in small HCCs (≦2 cm) (12).

Contrast-enhanced imaging for the tumor is a tracer technique of contrast media (CM) in essence. The distribution and dynamic phases of the agent are analyzed for lesion detection and characterization for early diagnosis and possible prognosis prediction. Therefore, a summarized navigating map of CM commonly used in the clinic, along with ongoing work of agent research and potential seeded agents in the future, could be a needed reference work for both physicians and radiologists.

BLOOD POOL CONTRAST AGENTS

Ultrasound Contrast Agents

As early as the late 1960s, people found that the microbubbles (MBs) that provide many reflecting interfaces for echo are a good intravascular flow tracer for US imaging (13), and the hydrogen peroxide solution was launched for echocardiography thereafter. According to the inner gas of the MB, US contrast agent (UCA) could be classified into two generations. Air core with the polymeric coat is the so-called first-generation UCA, such as Levovist (Schering, Berlin-Wedding, Germany). The first-generation UCA is a milestone in the history of medical US imaging development, though it comes with defects like unstableness and unsafety (13). Thereafter, inert gas that is enveloped with a lipid shell at a diameter of approximately several micrometers is developed as the second-generation UCA, which is slightly smaller than that of the red blood cell. Taking advantage of materials science and technology development, the second-generation UCA with greater stability and biosafety can achieve a promising diagnostic efficacy for HCC (11, 12), along with the negligible report of anaphylaxis compared with CT and MRI, which means that UCA can be employed for the patients having iodine allergy, chronic kidney disease, hepatic function failure, asthma, and so on. Moreover, the bedside operation with a portable US machine could be performed in the emergency department (ED) and intensive care unit (ICU) as needed. However, concerning clinical practice, CEUS is not good at imaging the hepatic lesion located near the lung and behind the costal bone, due to the so-called shadow zone caused by the costal bone and lung. The other weakness is US attenuation in far-field of a fatty liver can lead to the indefinable hepatic situation.

Currently, sulfur hexafluoride (i.e., SonoVue, Bracco Imaging, Milan, Italy) is the most consumed in the global UCA market, followed by perfluorinated butane (i.e., Sonazoid, GE Healthcare, Oslo, Norway). The former is a pure blood pool agent, while the latter behaves similarly at the beginning but permeates into extravascular space soon after administration, which will be discussed in Section 3.

Iodinated Agents for Contrast-Enhanced CT

Many iodinated agents are pure blood pool agents, which are the widest and longest used CM for X-ray-based enhancement scans (i.e., CECT) (**Figure 1**). To date, the effort of optimizing small-molecule iodinated agents for contrast enhancement could be mainly classified into three eras, including four categories of compounds, from ionic to non-ionic, from monomers to dimers, from high-osmolality to iso-/low-osmolality, associating with decreasing toxicity and increasing bio-tolerability. Commercially available agents are abundant in the clinic, such as iohexol (Omnipaque, GE Healthcare), iopromide (Ultravist, Bayer Healthcare, Leverkusen, Germany), iodixanol (Visipaque, GE Healthcare), iopamidol (Isovue, Bracco Imaging, Milan, Italy), and iothalamate (Cysto-Conray II, Mallinckrodt Imaging, St. Louis, MO, USA). Moreover, novel agents, like iosimenol and GE-145, are on the way to commercialization with the improvements made on an existing basis. The diagnostic efficacy of CECT for HCC in terms of area under the receiver operating characteristic (ROC) curve (AUC), sensitivity, and specificity were reported to be 0.93, 93%, and 82%, respectively (14). For HCC patients, the most distinctive role that CT perfusion imaging has played is the transarterial chemoembolization (TACE) assessment (15). However, despite great improvements that have been made in the bone and cartilage tissue, iodinated contrast agents employed in parenchymal organs, like the liver, have not yet been largely renovated (16, 17).

The blood pool agent applied to MRI is mainly established for MR angiography rather than the liver tumor, which is beyond the scope of the present review article and will not be discussed herein.

EXTRACELLULAR CONTRAST AGENTS

Non-Specific Agents

For MRI, gadolinium-based micromolecule agents that have five or seven unpaired electrons could be stimulated to be paramagnetic under an external magnetic field. Those so-called paramagnetic contrast agents for dynamic MRI are developed

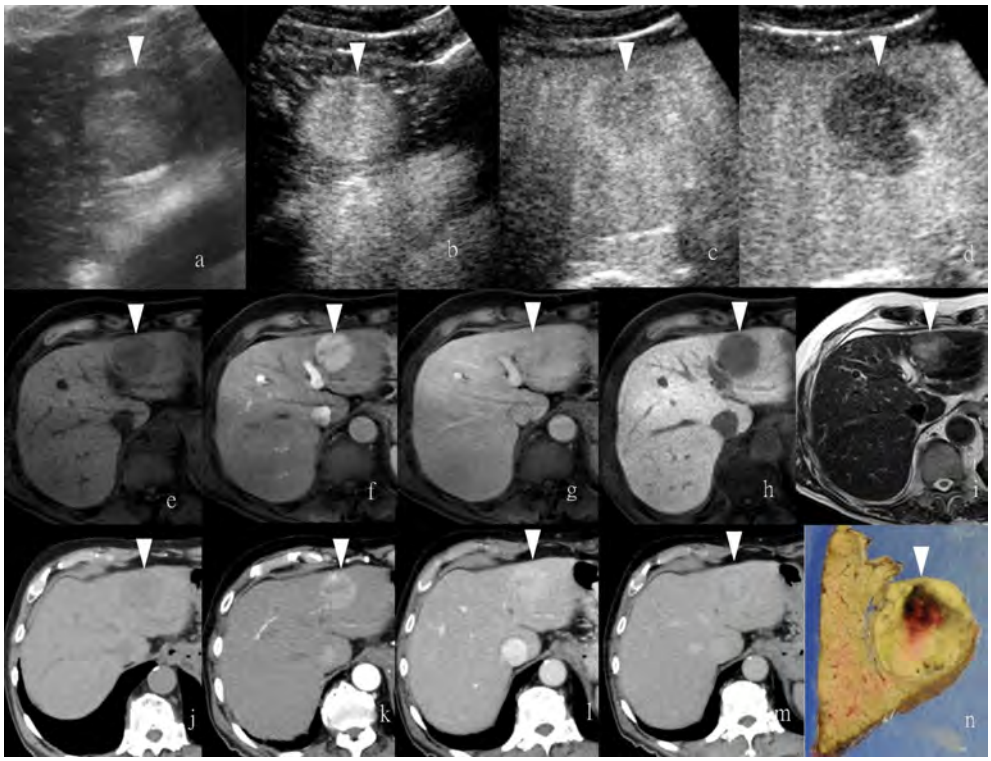

FIGURE 1 | Images of a man in his eighties with a pathological diagnosis of moderately differentiated hepatocellular carcinoma (HCC) and had a history of hepatitis **(C)** At the Sonazoid-enhanced ultrasound (US), the liver lesion at a size of 43 mm with a thin halo located at segment III was observed on B-mode US **(A)**. It was rapidly enhanced in the arterial phase (wash-in) **(B)**, started to fade (wash-out) in portal phase **(C)**, and was totally exhausted in the post-vascular phase **(D)**. At Gd-EOB-DTPA-enhanced MRI, the lesion was hypointense on T1-weighted image **(E)**, with the typical characteristics of wash-in and wash-out from arterial phase, portal phase, to delayed phase **(F–H)**. It showed hyperintensity on T2-weighted image **(I)**. At iodine agent-enhanced CT, it has low-density before enhancement **(J)**. It also showed wash-in and wash-out from arterial phase, portal phase, to delayed phase **(K–M)**. Finally, the gross specimen vividly reflected the morphological information of tumor **(N)**. Arrowheads indicate the margin of the HCC lesion.

and enriched (18). Gadolinium chelates (Gd-chelates) are clinically available mainstream for dynamic MRI on T1-weighted images, including Gd-DTPA (gadopentetic acid, Magnevist, Berlex, Berlin, Germany), Gd-DTPA-BMA (gadodiamide, Omniscan, Nycomed Amersham, Amersham, UK), Gd-HP-DO3A (gadoteridol, ProHance, Bracco Diagnostics, Milan, Italy), Gd-DTPA-BMEA (gadoversetamide, Optimark, Mallinckrodt, Staines-upon-Thames, UK), Gd-DOTA (gadoterate, meglumine, Dotarem Guerbet, Princeton, NJ, USA), and Gd-BT-DO3A (gadobutrol Gadovist, Schering Diagnostics, Berlin, Germany). These extracellular agents for non-specific liver MRI are commonly used worldwide because of the good patient tolerance and satisfying diagnostic efficacy (19). Thus, clinical recommendations from guidelines are almost based on the Gd-chelates (8, 9). Moreover, the informative images provided by contrast-enhanced MRI (CEMRI) also contribute to the therapy assessment (**Table 1**).

Reticuloendothelial System Endocytosis

Ferumoxytol, a kind of iron oxide nanoparticles (IONPs) approved by the Food and Drug Administration (FDA) as medicine for iron deficiency in adults, was recently reported to be feasible for MR angiography thanks to the characteristic of longer half-life in circulation and the advantage of superparamagnetism (20–23). The so-called negative contrast agents, containing iron oxide particles, darken the normal liver background on T2-weighted images to negatively enhance the target issue, in contrast with the so-called positive agents that brighten the target tissue on T1-weighted images, like Gd-chelates. The first commercially available reticuloendothelial system (RES)-specific contrast agent is ferumoxides (Feridex) (24), which makes lesions that contain negligible RES cells conspicuous on T2-weighted images since the normal liver background containing many RES cells can selectively take up iron oxide particulates to lower the T2 signal intensity (25). Iron oxide crystals coated with dextran or carboxydextran are named superparamagnetic iron oxide (SPIO), which is normally employed as T2 MR CM. With a sufficient infusion of SPIO, normal hepatocytes containing many Kupffer cells are supposed to catch most SPIO particles, leading to a dark area on T2-weighted images. By contrast, tumors, whether benign or malignant, primary or metastatic, that are deficient in Kupffer cells cannot exhibit SPIO uptake, shaping a relatively hyperintense area. However, focal nodular hyperplasia (FNH)

TABLE 1 | The categories of extracellular contrast agents in clinical practice.

Category	Specificity	Class	Classical agents	Featured purposes	Modality
Extracellular agent	Non-specific	Gadolinium chelates	Gadopentetic acid (Gd-DTPA)	Tumor imaging; blood pool imaging	T1 agent for MRI
Reticuloendothelial system (RES) agent (Kupffer cells included)	RES specific	Iron oxide	Ferucarbotran (Feridex)	Liver tumor imaging	T2 agent for MRI
		Microbubbles	Perfluorinated butane (Sonazoid)	Liver tumor imaging; blood pool imaging	Ultrasound contrast agent
Hepatobiliary agent	Hepatobiliary specific	Manganese-based compound	Mangafodipir (Mn-DPDP)	MR cholangiography; liver function indicator	T1 agent for MRI
			Gadobenate dimeglumine (Gd-BOPTA); gadoxetic acid (Gd-EOB-DTPA)	Liver tumor imaging	T1 agent for MRI

seems to be an exception, since SPIO particles may accumulate there and lead to a resultant isointense or even hypointense appearance (26, 27). Following SPIO, the derivative in terms of ultrasmall particulate iron oxides (USPIO) with advantages of convenient administration and striking prolonged plasma half-life that enables it also as a blood pool agent was developed thereafter (28, 29) (**Table 1**).

Regarding UCA, Sonazoid is an MB of perfluorobutane core wrapped by the shell of hydrogenated egg phosphatidylserine. At first, Sonazoid MBs were used as the blood pool contrast agent. As early as 1 min after the intravenous administration, the MBs start to diffuse into extravascular and intercellular space where they will be phagocytosed by the Kupffer cells in the normal liver sinusoids. Approximately 10 min later, once intravascular MBs are mostly eliminated, the remaining stable MBs endocytosed by resident macrophages in liver parenchyma will shape the so-called additional Kupffer phase or post-vascular phase, which can last to 2 h after injection (30–32) (**Table 1**). Moreover, in the classical enhancement features of wash-in and wash-out, HCC theoretically appears to be perfusion defects in the Kupffer phase or post-vascular phase because of Kupffer cell shortage (**Figures 1**, **2**). The characteristics of the additional post-vascular phase aid much in HCC detection and diagnosis. Recently, Sonazoid has been proven to be non-inferior to SonoVue in a retrospective clinical study for focal liver lesion (FLL) (33). However, if the lesion is isoechoic in the post-vascular phase, misdiagnosis can happen at a rate of approximately 17% (34). Worse still, owing to histological reasons of some well-differentiated HCC, the sign of perfusion defect in the Kupffer phase could be observed at a rate of only 69% among HCC patients (35). Also, some benign lesions that lack Kupffer cells have a chance to be misdiagnosed as a false-positive sign in the Kupffer phase (36). Therefore, the expected additional clinical benefit on diagnosis gained from the Kupffer phase has not yet been confirmed (37). As for HCC intervention, after US brings real-time monitoring for minimally invasive operations like lesion biopsy and regional ablation, CEUS is employed for more accurate guidance and unique immediate evaluation during therapy (38–43). Vascular-sensitive assessment makes CEUS an indispensable aid for effective

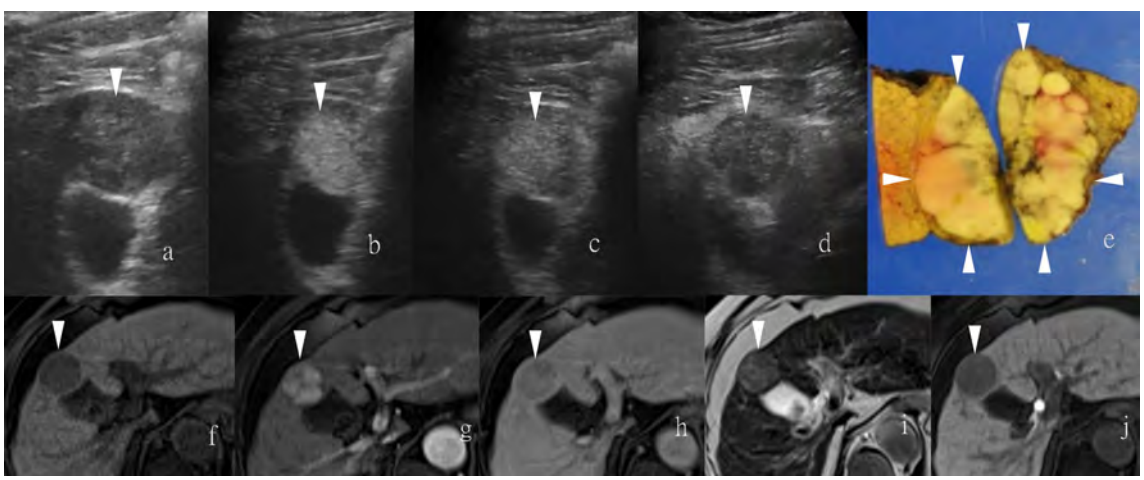

FIGURE 2 | Images of a man in his sixties with a pathological diagnosis of poorly to moderately differentiated hepatocellular carcinoma (HCC) and had a history of cirrhosis. At the Sonazoid-enhanced ultrasound (US), the liver lesion was heterogeneous hyperechoic with the indistinct margin on B-mode US **(A)**. It was rapidly enhanced in the arterial phase (wash-in) **(B)**, still iso-echoic in portal phase **(C)**, and was totally exhausted in the post-vascular phase **(D)**. At Gd-EOB-DTPA-enhanced MRI, the lesion was hypointense on T1-weighted image **(F)**, with uncharacteristic wash-in and delayed wash-out from arterial phase to delayed phase **(G, H)**. It showed hyperintensity on T2-weighted image **(I)**. The contrast media (CM) were totally exhausted till the hepatobiliary phase **(J)**. The gross specimen indicated the heterogeneous pathological differentiation of HCC **(E)**. Arrowheads indicate the margin of the HCC lesion.

radiofrequency (RF)/microwave (MV) ablation (44, 45). On the other hand, three-dimensional (3D) US can provide additional lateral and other viewing angles, and morphological information offers UCA another usable imaging modality (i.e., contrast-enhanced 3D US, CE 3D US) (46, 47) (**Figure 3**). Moreover, contrast enhancement is also employed in fusion imaging to reveal extra small liver lesions and biopsy navigation (48) (**Figure 4**).

Hepatocyte-Specific Uptake

Mangafodipir trisodium (Mn-DPDP) used to be a classical hepatocyte-selective contrast agent that was developed in the last century and has favorable contrast-to-noise measurements and lesion detection rate as compared to non-enhanced MRI (49, 50). It was high-profile at the beginning for the prolonged enhancement relative to the traditional T1 contrast agents (51). The uptake of Mn-DPDP occurs in hepatocytes, and its elimination is in the biliary tree. Thus, the metabolism process of Mn-DPDP can indicate hepatobiliary function (52, 53). Moreover, it is reported that the hepatocyte-selective contrast agent is correlative with the pathological differentiation degree of HCC (54). Since the uptake of Mn-DPDP strictly occurs in hepatocytes, the extrahepatic originated metastases can be negatively illustrated (55). However, in contrast to the question of how many normal hepatocytes are contained in a lesion, the question of whether a liver lesion is malignant or not will be the highest concern for patients.

By integrating the mechanisms of both hepatocyte-selective contrast agents and non-specific extracellular Gd-chelates, gadolinium-based hepatobiliary-specific agents were thereby developed, such as gadobenate dimeglumine (Gd-BOPTA) and gadoxetic acid (Gd-EOB-DTPA), which are worldwide commercially available and have become a promising MRI contrast agent for FLL (56–58). For HCC diagnostic imaging, the so-called hepatobiliary contrast agents achieve further detection in the early stage for primary, recurrent, and metastatic HCCs through usual dynamic imaging and additional hepatobiliary delayed phase (59–62) (**Figures 1**, **2**). Beyond diagnosis, uptake of Gd-EOB-DTPA of HCC lesions is reported to be a biomarker for prognosis (63), as well as the estimation of liver function (64). Concerning patients' tolerance, Gd-EOB-DTPA only requires a minimum injection dose to present a satisfying enhancement in the liver and smaller branch of the biliary tree relative to Gd-BOPTA (55) (**Table 1**).

MOLECULAR IMAGING AGENTS

For the diagnostic and therapeutic purpose of molecular imaging, by means of conjugating some antibody, peptide, or ligand, molecular imaging agents are artificially designed to anchor the targeted cellular and molecular hallmarks pathologically (65).

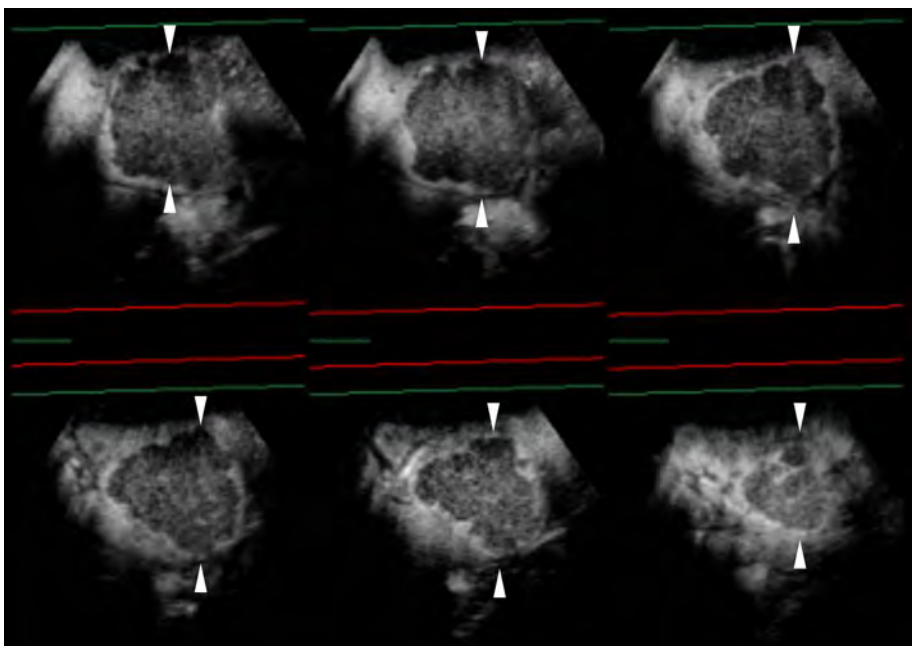

FIGURE 3 | Sonazoid-enhanced ultrasound (US) images of a man in his seventies with a pathological diagnosis of moderately differentiated hepatocellular carcinoma (HCC), who had a history of hepatitis C. The tumor was 70mm. Consecutive lateral images of the tumor remarkably illumed the irregular margin on the three-dimensional (3D) US, which was obtained by auto-sweep 3D scanning in the post-vascular phase. Tomographic ultrasound images in plane A, which can be translated from front to rear, with a slice distance of 4.8 mm. Arrowheads indicate the margin of the HCC lesion.

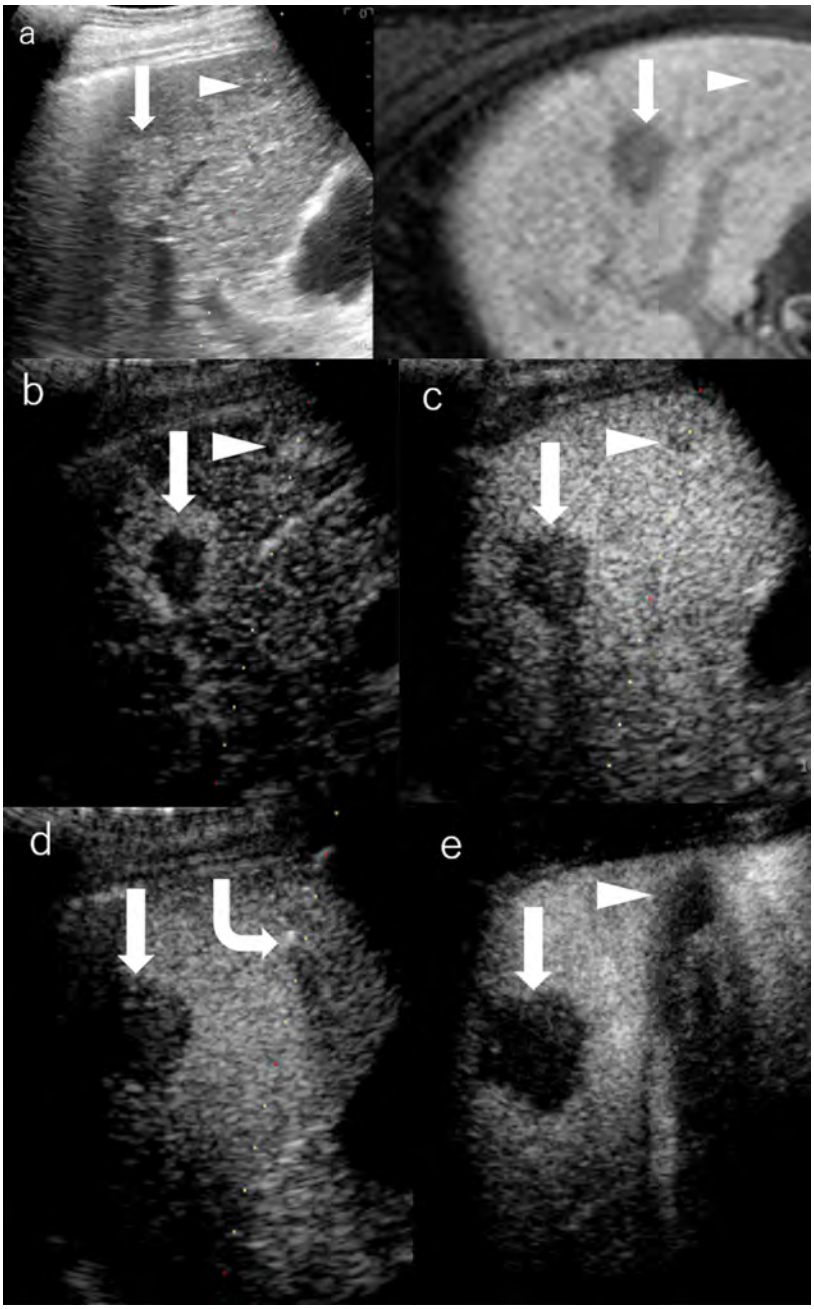

FIGURE 4 | Images of a man in his seventies with a pathological diagnosis of moderately differentiated hepatocellular carcinoma (HCC) and had a history of cirrhosis and HCC. The hepatobiliary phase of EOBMRI (right side), as the reference, was combined with conventional grayscale US (left side), displayed an 8-mm indistinctive hypointense area (the triangular arrow) in segment V on the same screen for the fusion imaging **(A)**. The extrasmall lesion was hypervascular in the arterial phase of Sonazoid-enhanced ultrasound (US) **(B)**, while the post-vascular phase indicated it to be a slightly hypoechoic area **(C)**. Pathway guidance was ready for radiofrequency ablation (RFA) needle manipulation on real-time US **(B–D)**, along with tracking for the metallic needle tip (the curved arrow) **(D)**. The contrast-enhanced US (CEUS) evaluated the target ablation area to be non-enhanced after RFA **(E)**. Arrows indicate the margin of the bigger HCC lesion, which was previously treated by RFA. And Arrowheads indicate the margin of the extrasmall HCC lesion.

Immune Molecular Anchoring

By means of immunoreaction, gadolinium-labeled reagents for liver tumor marking and monitoring of the MR modality are commonly employed in a tumor-bearing animal model for cancer research (66, 67). The molecular weight of reagents mainly ranges from dozens to hundreds of kDa. Likewise, the MBs or nanobubbles binding compounds marked with the tumor-specific immune molecule are also available for cancer research in the CEUS modality (66).

Stimulus-Responsive/Microenvironment-Dependent Contrast Agents

A T1/T2 switchable MR contrast agent was recently validated on a mouse model for HCC early diagnosis (68, 69). Previously, the diagnostic efficacy of IONP-based MRI was not as high as expected when it was simply employed as a liver-specific T2 agent (70). However, researchers recently found that IONP clusters could be accordingly disaggregated thanks to the acidic tumor microenvironment, which can generate a downstream tumor-specific T1 contrast agent. As a result, the IONP agents can additionally be employed to delineate HCC on T1-weighted images after switching to a downstream tumor-specific contrast agent. Based on IONP, agents decorated with functional small-molecular ligands through surface engineering are thereafter designed to be stimulus-responsive agents, pH-sensitive, and nanoscale distance-dependent (68, 71–75). Furthermore, concerning the aggregation phenomenon that commonly happened in nanoparticles with a large surface area/volume ratio, ultrafine nanoparticles could facilitate intratumoral homogeneous distribution of contrast agents (76). IONP at a diameter of 3.6 nm is supposed to be an optimal T1 agent *in vivo* (77). Moreover, core engineering of various designs of size, shape, composition, surface coating, molecular weight, and drug delivery has indicated IONP to be a hopeful T1 contrast agent (78–85). Beyond imaging, Yang et al. developed a novel nanoparticle that releases Fe^{2+} for the treatment of folic acid (FA) receptor-positive solid tumors through the ferroptosis pathway while being supervised through the Mn agent-enhanced imaging (86, 87). Also, Song et al. developed an assay of therapeutic natural killer cells (NK cells) conjugated with Sonazoid MB to make the antitumor process visible in real-time CEUS (88).

Scale-Dependent Particles

As nanomedicine was developed recently, emerging nanomaterials have been studied for contrast enhancement imaging. Some nanoscaled CM can permeate into tumor stroma through weak tumor vessels to depict the tumor with or without the assistance from functional parts equipped in advance (89). Moreover, sonoporation induced by external stimulation of focused US can reversibly increase the permeabilization of the cell membrane, leading to the potential visualization of HCC intracellular therapy in the future (90).

CLINICAL CHALLENGES AND PROSPECTS

As for the clinically commonly used contrast agents, Guang et al. performed a meta-analysis to compare the diagnostic value of CEUS, CT, and MRI in FLL. To rule out HCC from FLL, CECT has the highest sensitivity of 90% (95% CI: 88%–92%), followed by CEUS (88%) and CEMRI (86%). Both CEUS and CEMRI have a higher sensitivity of 81% than CECT (77%). However, all results have no statistical significance (16, 91). Moreover, Westwood et al. found that CEUS could be a cost-effective alternative for HCC diagnosis relative to CECT or CEMRI with similar diagnostic performance (92). Research about combined multimodal medical imaging (including Sonazoid-enhanced US, Gd-EOB-DTPA-enhanced MRI, and CECT) conducted by Masatoshi Kudo figured out that the sensitivity for HCC diagnosis is 72%, 74%, and 86% for CEUS, CECT, and Gd-EOB-DTPA-enhanced MRI, respectively, with no significance among the three imaging modalities. When combining US with MRI, the sensitivity soared as high as 90% (93).

Meanwhile, controversies still remain regarding the diagnostic efficacy of HCC. Despite that the hepatobiliary agent-enhanced MRI is believed to reach an early diagnosis for HCC that is still in the hypovascular stage (94), researchers analyzed the clinical trials that use different contrast agents for HCC diagnosis and found no significant difference in the diagnostic efficacy in terms of sensitivity and specificity between the MRI using extracellular agents and hepatobiliary agents (95, 96). Imbriaco et al. claimed that Gd-EOB-DTPA-enhanced MRI has a better diagnostic performance than CECT only for lesions that are smaller than 20 mm and patients with Child-Pugh class A (97). Moreover, for patients with cirrhosis, Kim et al. demonstrated better performance of hepatobiliary agent-enhanced MRI relative to routine US screening for surveillance of people at a higher risk of HCC (2). In addition, molecular imaging agents, like IONP-based MR agents, are still on the way to fulfilling the various clinical needs (98). On the other hand, although current CM has been deeply improved through materials science, biosafety is still the most crucial factor for patients having various allergies and metabolism troubles. Necessary reinjection of contrast agents for CT and MRI may come with a potential risk of side effects. Minimized dose of contrast agent that meets all clinical needs will be a future trend for CM research.

To sum up, the CM brings out the best diagnostic performance for suitable patients under appropriate conditions. Although Gd-DTPA-enhanced MRI and non-ionic iodinated agents-enhanced CT are usually recommended for HCC diagnosis by mainstream guidelines, liver-specific CM, like Gd-EOB-DTPA and Sonazoid, have already played an anticipated role in HCC diagnosis and prognosis prediction. Furthermore, the amelioration of molecular imaging agents has drawn a blueprint for future medical imaging.

AUTHOR CONTRIBUTIONS

Concept and design: KN and YZ. Manuscript writing: YZ. Figure presentation: KN. Reviewed the manuscript: all authors. All authors contributed to the article and approved the submitted version.

FUNDING

This work was partially supported by grants from the Natural Science Foundation of Ningbo (No. 2019A610313), Medical

Science and Technology Project of Zhejiang Province (No. 2021KY312), Ningbo Medical Science and Technology Project (No. 2019Y05), Ningbo Clinical Medicine Research Center Project (No. 2019A21003), Japan-China Sasakawa Medical Scholarship, and Young Talents Training Program of Ningbo Municipal Health Commission.

REFERENCES

1. Ferlay J, Colombet M, Soerjomataram I, Parkin DM, Piñeros M, Znaor A, et al. Cancer Statistics for the Year 2020: An Overview. *Int J Cancer* (2021).
2. Kim SY, An J, Lim YS, Han S, Lee JY, Byun JH, et al. MRI With Liver-Specific Contrast for Surveillance of Patients With Cirrhosis at High Risk of Hepatocellular Carcinoma. *JAMA Oncol* (2017) 3(4):456–63. doi: 10.1001/jamaoncol.2016.3147
3. Elsayes KM, Hooker JC, Agrons MM, Kielar AZ, Tang A, Fowler KJ, et al. Version of LI-RADS for CT and MR Imaging: An Update. *Radiographics* (2017) 37(7):1994–2017. doi: 10.1148/rg.2017170098
4. Marrero JA, Ahn J, Rajender Reddy K. ACG Clinical Guideline: The Diagnosis and Management of Focal Liver Lesions. *Am J Gastroenterol* (2014) 109(9):1328–47. doi: 10.1038/ajg.2014.213
5. Kudo M, Matsui O, Izumi N, Iijima H, Kadoya M, Imai Y, et al. JSH Consensus-Based Clinical Practice Guidelines for the Management of Hepatocellular Carcinoma: 2014 Update by the Liver Cancer Study Group of Japan. *Liver Cancer* (2014) 3(3-4):458–68. doi: 10.1159/000343875
6. Park J-W, Hyeok LJ, Lee JS, Tak TY, Bae SH, Yeon JE, et al. 2014 Korean Liver Cancer Study Group-National Cancer Center Korea Practice Guideline for the Management of Hepatocellular Carcinoma. *Korean J Radiol* (2015) 16 (3):465–522. doi: 10.3348/kjr.2015.16.3.465
7. Horowitz JM, Kamel IR, Arif-Tiwari H, Asrani SK, Hindman NM, Kaur H, et al. ACR Appropriateness Criteria(®) Chronic Liver Disease. *J Am Coll Radiol* (2017) 14(11s):S391–s405. doi: 10.1016/j.jacr.2017.08.045
8. American College of Radiology. *Liver Reporting and Data Systems (LI-RADS)* Available at: https://www.acr.org/Clinical-Resources/Reporting-and-Data-Systems/LI-RADS (Accessed June 4, 2019).
9. Marks RM, Masch WR, Chernyak V. LI-RADS: Past, Present, and Future, From the AJR Special Series on Radiology Reporting and Data Systems. *AJR Am J Roentgenol* (2021) 216(2):295–304. doi: 10.2214/AJR.20.24272
10. Dietrich CF, Nolsøe CP, Barr RG, Berzigotti A, Burns PN, Cantisani V, et al. Guidelines and Good Clinical Practice Recommendations for Contrast-Enhanced Ultrasound (CEUS) in the Liver-Update 2020 WFUMB in Cooperation With EFSUMB, AFSUMB, AIUM, and FLAUS. *Ultrasound Med Biol* (2020) 46(10):2579–604. doi: 10.1016/j.ultrasmedbio.2020.04.030
11. Friedrich-Rust M, Klopffleisch T, Nierhoff J, Herrmann E, Vermehren J, Schneider MD, et al. Contrast-Enhanced Ultrasound for the Differentiation of Benign and Malignant Focal Liver Lesions: A Meta-Analysis. *Liver Int* (2013) 33(5):739–55. doi: 10.1111/liv.12115
12. Niu Y, Huang T, Lian F, Li F. Contrast-Enhanced Ultrasonography for the Diagnosis of Small Hepatocellular Carcinoma: A Meta-Analysis and Meta-Regression Analysis. *Tumour Biol* (2013) 34(6):3667–74. doi: 10.1007/s13277-013-0948-z
13. Gramiak R, Shah PM. Echocardiography of the Aortic Root. *Invest Radiol* (1968) 3(5):356–66. doi: 10.1097/00004424-196809000-00011
14. Jia GS, Feng GL, Li JP, Xu HL, Wang H, Cheng YP, et al. Using Receiver Operating Characteristic Curves to Evaluate the Diagnostic Value of the Combination of Multislice Spiral CT and Alpha-Fetoprotein Levels for Small Hepatocellular Carcinoma in Cirrhotic Patients. *Hepatobiliary Pancreat Dis Int* (2017) 16(3):303–9. doi: 10.1016/S1499-3872(17)60018-3
15. Saake M, Lell MM, Eller A, Wuest W, Heinz M, Uder M, et al. Imaging Hepatocellular Carcinoma With Dynamic CT Before and After Transarterial Chemoembolization: Optimal Scan Timing of Arterial Phase. *Acad Radiol* (2015) 22(12):1516–21. doi: 10.1016/j.acra.2015.08.021
16. Kim KA, Kim MJ, Choi JY, Park MS, Lim JS, Chung YE, et al. Detection of Recurrent Hepatocellular Carcinoma on Post-Operative Surveillance: Comparison of MDCT and Gadoxetic Acid-Enhanced MRI. *Abdom Imaging* (2014) 39(2):291–9. doi: 10.1007/s00261-013-0064-y
17. Matoba M, Kitadate M, Kondou T, Yokota H, Tonami H. Depiction of Hypervascular Hepatocellular Carcinoma With 64-MDCT: Comparison of Moderate- and High-Concentration Contrast Material With and Without Saline Flush. *AJR Am J Roentgenol* (2009) 193(3):738–44. doi: 10.2214/AJR.08.2028
18. Gandhi SN, Brown MA, Wong JG, Aguirre DA, Sirlin CB. MR Contrast Agents for Liver Imaging: What, When, How. *Radiographics* (2006) 26 (6):1621–36. doi: 10.1148/rg.266065014
19. Bellin MF, Vasile M, Morel-Precetti S. Currently Used non-Specific Extracellular MR Contrast Media. *Eur Radiol* (2003) 13(12):2688–98. doi: 10.1007/s00330-003-1912-x
20. Bashir MR, Bhatti L, Marin D, Nelson RC. Emerging Applications for Ferumoxytol as a Contrast Agent in MRI. *J Magn Reson Imaging* (2015) 41 (4):884–98. doi: 10.1002/jmri.24691
21. Ersoy H, Jacobs P, Kent CK, Prince MR. Blood Pool MR Angiography of Aortic Stent-Graft Endoleak. *AJR Am J Roentgenol* (2004) 182(5):1181–6. doi: 10.2214/ajr.182.5.1821181
22. Hope MD, Hope TA, Zhu C, Faraji F, Haraldsson H, Ordovas KG, et al. Vascular Imaging With Ferumoxytol as a Contrast Agent. *AJR Am J Roentgenol* (2015) 205(3):W366–73. doi: 10.2214/AJR.15.14534
23. Huang Y, Hsu JC, Koo H, Cormode DP. Repurposing Ferumoxytol: Diagnostic and Therapeutic Applications of an FDA-Approved Nanoparticle. *Theranostics* (2022) 12(2):796–816. doi: 10.7150/thno.67375
24. Ros PR, Freeny PC, Harms SE, Seltzer SE, Davis PL, Chan TW, et al. Hepatic MR Imaging With Ferumoxides: A Multicenter Clinical Trial of the Safety and Efficacy in the Detection of Focal Hepatic Lesions. *Radiol* (1995) 196(2):481–8. doi: 10.1148/radiology.196.2.7617864
25. Tanimoto A, Kuribayashi S. Application of Superparamagnetic Iron Oxide to Imaging of Hepatocellular Carcinoma. *Eur J Radiol* (2006) 58(2):200–16. doi: 10.1016/j.ejrad.2005.11.040
26. Grazioli L, Morana G, Kirchin MA, Caccia P, Romanini L, Bondioni MP, et al. MRI of Focal Nodular Hyperplasia (FNH) With Gadobenate Dimeglumine (Gd-BOPTA) and SPIO (Ferumoxides): An Intra-Individual Comparison. *J Magn Reson Imaging* (2003) 17(5):593–602. doi: 10.1002/jmri.10289
27. Terkivatan T, van den Bos IC, Hussain SM, Wielopolski PA, de Man RA, IJzermans JNM. Focal Nodular Hyperplasia: Lesion Characteristics on State-of-the-Art MRI Including Dynamic Gadolinium-Enhanced and Superparamagnetic Iron-Oxide-Uptake Sequences in a Prospective Study. *J Magn Reson Imaging* (2006) 24(4):864–72. doi: 10.1002/jmri.20705
28. Zhao M, Liu Z, Dong L, Zhou H, Yang S, Wu W, et al. A GPC3-Specific Aptamer-Mediated Magnetic Resonance Probe for Hepatocellular Carcinoma. *Int J Nanomed* (2018) 13:4433–43. doi: 10.2147/IJN.S168268
29. Shan L. Superparamagnetic Iron Oxide Nanoparticles (SPION) Stabilized by Alginate. In: *Molecular Imaging and Contrast Agent Database (MICAD)*. Bethesda (MD: National Center for Biotechnology Information (US (2004).
30. Li P, Hoppmann S, Du P, Li H, Evans PM, Moestue SA, et al. Pharmacokinetics of Perfluorobutane After Intra-Venous Bolus Injection of Sonazoid in Healthy Chinese Volunteers. *Ultrasound Med Biol* (2017) 43 (5):1031–9. doi: 10.1016/j.ultrasmedbio.2017.01.003
31. Yanagisawa K, Moriyasu F, Miyahara T, Yuki M, Iijima H. Phagocytosis of Ultrasound Contrast Agent Microbubbles by Kupffer Cells. *Ultrasound Med Biol* (2007) 33(2):318–25. doi: 10.1016/j.ultrasmedbio.2006.08.008
32. Shunichi S, Hiroko I, Fuminori M, Waki H. Definition of Contrast Enhancement Phases of the Liver Using a Perfluoro-Based Microbubble Agent, Perflubutane Microbubbles. *Ultrasound Med Biol* (2009) 35 (11):1819–27. doi: 10.1016/j.ultrasmedbio.2009.05.013
33. Zhai HY, Liang P, Yu J, Cao F, Kuang M, Liu FY, et al. Comparison of Sonazoid and SonoVue in the Diagnosis of Focal Liver Lesions: A Preliminary Study. *J Ultrasound Med* (2019) 38(9):2417–25. doi: 10.1002/jum.14940
34. Kunishi Y, Numata K, Morimoto M, Okada M, Kaneko T, Maeda S, et al. Efficacy of Fusion Imaging Combining Sonography and Hepatobiliary Phase MRI With Gd-EOB-DTPA to Detect Small Hepatocellular Carcinoma. *AJR Am J Roentgenol* (2012) 198(1):106–14. doi: 10.2214/AJR.10.6039

35. Duisyenbi Z, Numata K, Nihonmatsu H, Fukuda H, Chuma M, Kondo M, et al. Comparison Between Low Mechanical Index and High Mechanical Index Contrast Modes of Contrast-Enhanced Ultrasonography: Evaluation of Perfusion Defects of Hypervascular Hepatocellular Carcinomas During the Post-Vascular Phase. *J Ultrasound Med* (2019) 38(9):2329–38. doi: 10.1002/jum.14926
36. Ishibashi H, Maruyama H, Takahashi M, Shimada T, Kamesaki H, Fujiwara K, et al. Demonstration of Intrahepatic Accumulated Microbubble on Ultrasound Represents the Grade of Hepatic Fibrosis. *Eur Radiol* (2012) 22 (5):1083–90. doi: 10.1007/s00330-011-2346-5
37. Barr RG, Huang P, Luo Y, Xie X, Zheng R, Yan K, et al. Contrast-Enhanced Ultrasound Imaging of the Liver: A Review of the Clinical Evidence for SonoVue and Sonazoid. *Abdom Radiol (NY)* (2020) 45(11):3779–88. doi: 10.1007/s00261-020-02573-9
38. Spârchez Z, Radu P, Kacso G, Spârchez M, Zaharia T, Al Hajjar N. Prospective Comparison Between Real Time Contrast Enhanced and Conventional Ultrasound Guidance in Percutaneous Biopsies of Liver Tumors. *Med Ultrason* (2015) 17(4):456–63. doi: 10.11152/mu.2013.2066.174.deu
39. Park HS, Kim YJ, Yu MH, Jung SI, Jeon HJ. Real-Time Contrast-Enhanced Sonographically Guided Biopsy or Radiofrequency Ablation of Focal Liver Lesions Using Perflurobutane Microbubbles (Sonazoid): Value of Kupffer-Phase Imaging. *J Ultrasound Med* (2015) 34(3):411–21. doi: 10.7863/ultra.34.3.411
40. Liu F, Yu X, Liang P, Cheng Z, Han Z, Dong B. Contrast-Enhanced Ultrasound-Guided Microwave Ablation for Hepatocellular Carcinoma Inconspicuous on Conventional Ultrasound. *Int J Hyperthermia* (2011) 27 (6):555–62. doi: 10.3109/02656736.2011.564262
41. Yan SY, Zhang Y, Sun C, Cao HX, Li GM, Wang YQ, et al. Comparison of Real-Time Contrast-Enhanced Ultrasonography and Standard Ultrasonography in Liver Cancer Microwave Ablation. *Exp Ther Med* (2016) 12(3):1345–8. doi: 10.3892/etm.2016.3448
42. Miyamoto N, Hiramatsu K, Tsuchiya K, Sato Y, Terae S, Shirato H. Sonazoid-Enhanced Sonography for Guiding Radiofrequency Ablation for Hepatocellular Carcinoma: Better Tumor Visualization by Kupffer-Phase Imaging and Vascular-Phase Imaging After Reinjection. *Jpn J Radiol* (2009) 27(4):185–93. doi: 10.1007/s11604-009-0317-4
43. Numata K, Morimoto M, Ogura T, Sugimori K, Takebayashi S, Okada M, et al. Ablation Therapy Guided by Contrast-Enhanced Sonography With Sonazoid for Hepatocellular Carcinoma Lesions Not Detected by Conventional Sonography. *J Ultrasound Med* (2008) 27(3):395–406. doi: 10.7863/jum.2008.27.3.395
44. Wiggermann P, Zuber-Jerger I, Zausig Y, Loss M, Scherer MN, Schreyer AG, et al. Contrast-Enhanced Ultrasound Improves Real-Time Imaging of Ablation Region During Radiofrequency Ablation: Preliminary Results. *Clin Hemorheol Microcirc* (2011) 49(1-4):43–54. doi: 10.3233/CH-2011-1456
45. Mauri G, Porazzi E, Cova L, Restelli U, Tondolo T, Bonfanti M, et al. Intraprocedural Contrast-Enhanced Ultrasound (CEUS) in Liver Percutaneous Radiofrequency Ablation: Clinical Impact and Health Technology Assessment. *Insights Imaging* (2014) 5(2):209–16. doi: 10.1007/s13244-014-0315-7
46. Luo W, Numata K, Morimoto M, Oshima T, Ueda M, Okada M, et al. Role of Sonazoid-Enhanced Three-Dimensional Ultrasonography in the Evaluation of Percutaneous Radiofrequency Ablation of Hepatocellular Carcinoma. *Eur J Radiol* (2010) 75(1):91–7. doi: 10.1016/j.ejrad.2009.03.021
47. Numata K, Luo W, Morimoto M, Kondo M, Kunishi Y, Sasaki T, et al. Contrast Enhanced Ultrasound of Hepatocellular Carcinoma. *World J Radiol* (2010) 2(2):68–82. doi: 10.4329/wjr.v2.i2.68
48. Kang TW, Lee MW, Song KD, Kim M, Kim SS, Kim SH, et al. Added Value of Contrast-Enhanced Ultrasound on Biopsies of Focal Hepatic Lesions Invisible on Fusion Imaging Guidance. *Korean J Radiol* (2017) 18(1):152–61. doi: 10.3348/kjr.2017.18.1.152
49. Bernardino ME, Young SW, Lee JK, Weinreb JC. Hepatic MR Imaging With Mn-DPDP: Safety, Image Quality, and Sensitivity. *Radiol* (1992) 183(1):53–8. doi: 10.1148/radiology.183.1.1549694
50. Young SW, Bradley B, Muller HH, Rubin DL. Detection of Hepatic Malignancies Using Mn-DPDP (Manganese Dipyridoxal Diphosphate) Hepatobiliary MRI Contrast Agent. *Magn Reson Imaging* (1990) 8(3):267–76. doi: 10.1016/0730-725X(90)90099-N
51. Rofsky NM, Earls JP. Mangafodipir Trisodium Injection (Mn-DPDP). A Contrast Agent for Abdominal MR Imaging. *Magn Reson Imaging Clin N Am* (1996) 4(1):73–85. doi: 10.1016/S1064-9689(21)00555-9
52. Mitchell DG, Alam F. Mangafodipir Trisodium: Effects on T2- and T1-Weighted MR Cholangiography. *J Magn Reson Imaging* (1999) 9(2):366–8. doi: 10.1002/(SICI)1522-2586(199902)9:2<366::AID-JMRI33>3.0.CO;2-E
53. Seale MK, Catalano OA, Saini S, Hahn PF, Sahani DV. Hepatobiliary-Specific MR Contrast Agents: Role in Imaging the Liver and Biliary Tree. *Radiographics* (2009) 29(6):1725–48. doi: 10.1148/rg.296095515
54. Murakami T, Baron RL, Peterson MS, Oliver JH3rd, Davis PL, Confer SR, et al. Hepatocellular Carcinoma: MR Imaging With Mangafodipir Trisodium (Mn-DPDP). *Radiol* (1996) 200(1):69–77. doi: 10.1148/radiology.200.1.8657947
55. Reimer P, Schneider G, Schima W. Hepatobiliary Contrast Agents for Contrast-Enhanced MRI of the Liver: Properties, Clinical Development and Applications. *Eur Radiol* (2004) 14(4):559–78. doi: 10.1007/s00330-004-2236-1
56. Vogl TJ, Kümmel S, Hammerstingl R, Schellenbeck M, Schumacher G, Balzer T, et al. Liver Tumors: Comparison of MR Imaging With Gd-EOB-DTPA and Gd-DTPA. *Radiol* (1996) 200(1):59–67. doi: 10.1148/radiology.200.1.8657946
57. Huppertz A, Balzer T, Blakeborough A, Breuer J, Giovagnoni A, Heinz-Peer G, et al. Improved Detection of Focal Liver Lesions at MR Imaging: Multicenter Comparison of Gadoxetic Acid-Enhanced MR Images With Intraoperative Findings. *Radiol* (2004) 230(1):266–75. doi: 10.1148/radiol.2301020269
58. Neri E, Bali MA, Ba-Ssalamah A, Boraschi P, Brancatelli G, Alves FC, et al. ESGAR Consensus Statement on Liver MR Imaging and Clinical Use of Liver-Specific Contrast Agents. *Eur Radiol* (2016) 26(4):921–31. doi: 10.1007/s00330-015-3900-3
59. Li XQ, Wang X, Zhao DW, Sun J, Liu JJ, Lin DD, et al. Application of Gd-EOB-DTPA-Enhanced Magnetic Resonance Imaging (MRI) in Hepatocellular Carcinoma. *World J Surg Oncol* (2020) 18(1):219. doi: 10.1186/s12957-020-01996-4
60. Yoo SH, Choi JY, Jang JW, Bae SH, Yoon SK, Kim DG, et al. Gd-EOB-DTPA-Enhanced MRI is Better Than MDCT in Decision Making of Curative Treatment for Hepatocellular Carcinoma. *Ann Surg Oncol* (2013) 20 (9):2893–900. doi: 10.1245/s10434-013-3001-y
61. Rimola J, Forner A, Sapena V, Llarch N, Darnell A, Díaz A, et al. Performance of Gadoxetic Acid MRI and Diffusion-Weighted Imaging for the Diagnosis of Early Recurrence of Hepatocellular Carcinoma. *Eur Radiol* (2020) 30(1):186–94. doi: 10.1007/s00330-019-06351-0
62. Kuwatsuru R, Kadoya M, Ohtomo K, Tanimoto A, Hirohashi S, Murakami T, et al. Comparison of Gadobenate Dimeglumine With Gadopentetate Dimeglumine for Magnetic Resonance Imaging of Liver Tumors. *Invest Radiol* (2001) 36(11):632–41. doi: 10.1097/00004424-200111000-00002
63. Yamashita T, Kitao A, Matsui O, Hayashi T, Nio K, Kondo M, et al. Gd-EOB-DTPA-Enhanced Magnetic Resonance Imaging and Alpha-Fetoprotein Predict Prognosis of Early-Stage Hepatocellular Carcinoma. *Hepatol* (2014) 60(5):1674–85. doi: 10.1002/hep.27093
64. Katsube T, Okada M, Kumano S, Hori M, Imaoka I, Ishii K, et al. Estimation of Liver Function Using T1 Mapping on Gd-EOB-DTPA-Enhanced Magnetic Resonance Imaging. *Invest Radiol* (2011) 46(4):277–83. doi: 10.1097/RLI.0b013e318200f67d
65. Burtea C, Laurent S, Vander Elst L, Muller RN. Contrast Agents: Magnetic Resonance. *Handb Exp Pharmacol* (2008) (185 Pt 1):135–65. doi: 10.1007/978-3-540-72718-7_7
66. Serkova NJ, Glunde K, Haney CR, Farhoud M, De Lille A, Redente EF, et al. Preclinical Applications of Multi-Platform Imaging in Animal Models of Cancer. *Cancer Res* (2021) 81(5):1189–200. doi: 10.1158/0008-5472.CAN-20-0373
67. Anani T, Rahmati S, Sultana N, David AE. MRI-Traceable Theranostic Nanoparticles for Targeted Cancer Treatment. *Theranostics* (2021) 11 (2):579–601. doi: 10.7150/thno.48811
68. Lu J, Sun J, Li F, Wang J, Liu J, Kim D, et al. Highly Sensitive Diagnosis of Small Hepatocellular Carcinoma Using pH-Responsive Iron Oxide Nanocluster Assemblies. *J Am Chem Soc* (2018) 140(32):10071–4. doi: 10.1021/jacs.8b04169
69. Lin J, Xin P, An L, Xu Y, Tao C, Tian Q, et al. Fe(3)O(4)-ZIF-8 Assemblies as pH and Glutathione Responsive T(2)-T(1) Switching Magnetic Resonance Imaging Contrast Agent for Sensitive Tumor Imaging *In Vivo*. *Chem Commun (Camb)* (2019) 55(4):478–81. doi: 10.1039/C8CC08943D

70. Yu MH, Kim JH, Yoon JH, Kim HC, Chung JW, Han JK, et al. Small (≤1-Cm) Hepatocellular Carcinoma: Diagnostic Performance and Imaging Features at Gadoxetic Acid-Enhanced MR Imaging. *Radiol* (2014) 271(3):748–60. doi: 10.1148/radiol.14131996
71. Choi JS, Kim S, Yoo D, Shin TH, Kim H, Gomes MD, et al. Distance-Dependent Magnetic Resonance Tuning as a Versatile MRI Sensing Platform for Biological Targets. *Nat Mater* (2017) 16(5):537–42. doi: 10.1038/nmat4846
72. Ling D, Park W, Park SJ, Lu Y, Kim KS, Hackett MJ, et al. Multifunctional Tumor pH-Sensitive Self-Assembled Nanoparticles for Bimodal Imaging and Treatment of Resistant Heterogeneous Tumors. *J Am Chem Soc* (2014) 136 (15):5647–55. doi: 10.1021/ja4108287
73. Kievit FM, Zhang M. Surface Engineering of Iron Oxide Nanoparticles for Targeted Cancer Therapy. *Acc Chem Res* (2011) 44(10):853–62. doi: 10.1021/ar2000277
74. Li F, Liang Z, Liu J, Sun J, Hu X, Zhao M, et al. Dynamically Reversible Iron Oxide Nanoparticle Assemblies for Targeted Amplification of T1-Weighted Magnetic Resonance Imaging of Tumors. *Nano Lett* (2019) 19(7):4213–20. doi: 10.1021/acs.nanolett.8b04411
75. Xiao S, Yu X, Zhang L, Zhang Y, Fan W, Sun T, et al. Synthesis Of PEG-Coated, Ultrasmall, Manganese-Doped Iron Oxide Nanoparticles With High Relaxivity For T(1)/T(2) Dual-Contrast Magnetic Resonance Imaging. *Int J Nanomed* (2019) 14:8499–507. doi: 10.2147/IJN.S219749
76. Wang L, Huang J, Chen H, Wu H, Xu Y, Li Y, et al. Exerting Enhanced Permeability and Retention Effect Driven Delivery by Ultrafine Iron Oxide Nanoparticles With T(1)-T(2) Switchable Magnetic Resonance Imaging Contrast. *ACS Nano* (2017) 11(5):4582–92. doi: 10.1021/acsnano.7b00038
77. Shen Z, Chen T, Ma X, Ren W, Zhou Z, Zhu G, et al. Multifunctional Theranostic Nanoparticles Based on Exceedingly Small Magnetic Iron Oxide Nanoparticles for T(1)-Weighted Magnetic Resonance Imaging and Chemotherapy. *ACS Nano* (2017) 11(11):10992–1004. doi: 10.1021/acsnano.7b04924
78. Khandhar AP, Wilson GJ, Kaul MG, Salamon J, Jung C, Krishnan KM. Evaluating Size-Dependent Relaxivity of PEGylated-USPIOs to Develop Gadolinium-Free T1 Contrast Agents for Vascular Imaging. *J BioMed Mater Res A* (2018) 106(9):2440–7. doi: 10.1002/jbm.a.36438
79. Tao C, Chen Y, Wang D, Cai Y, Zheng Q, An L, et al. Macromolecules With Different Charges, Lengths, and Coordination Groups for the Coprecipitation Synthesis of Magnetic Iron Oxide Nanoparticles as T(1) MRI Contrast Agents. *Nanomater (Basel)* (2019) 9(5). doi: 10.3390/nano9050699
80. Sherwood J, Rich M, Lovas K, Warram J, Bolding MS, Bao Y. T(1)-Enhanced MRI-Visible Nanoclusters for Imaging-Guided Drug Delivery. *Nanoscale* (2017) 9(32):11785–92. doi: 10.1039/C7NR04181K
81. Vangijzegem T, Stanicki D, Boutry S, Paternoster Q, Vander Elst L, Muller RN, et al. VSION as High Field MRI T(1) Contrast Agent: Evidence of Their Potential as Positive Contrast Agent for Magnetic Resonance Angiography. *Nanotechnology* (2018) 29(26):265103. doi: 10.1088/1361-6528/aabbd0
82. Yang L, Wang Z, Ma L, Li A, Xin J, Wei R, et al. The Roles of Morphology on the Relaxation Rates of Magnetic Nanoparticles. *ACS Nano* (2018) 12 (5):4605–14. doi: 10.1021/acsnano.8b01048
83. Tran HV, Ngo NM, Medhi R, Srinoi P, Liu T, Rittikulsittichai S, et al. Multifunctional Iron Oxide Magnetic Nanoparticles for Biomedical Applications: A Review. *Mater (Basel)* (2022) 15(2). doi: 10.3390/ma15020503
84. Reynders H, Van Zundert I, Silva R, Carlier B, Deschaume O, Bartic C, et al. Label-Free Iron Oxide Nanoparticles as Multimodal Contrast Agents in Cells Using Multi-Photon and Magnetic Resonance Imaging. *Int J Nanomed* (2021) 16:8375–89. doi: 10.2147/IJN.S334482
85. Zhang W, Liu L, Chen H, Hu K, Delahunty I, Gao S, et al. Surface Impact on Nanoparticle-Based Magnetic Resonance Imaging Contrast Agents. *Theranostics* (2018) 8(9):2521–48. doi: 10.7150/thno.23789
86. Yang B, Liu Q, Yao X, Zhang D, Dai Z, Cui P, et al. FePt@MnO-Based Nanotheranostic Platform With Acidity-Triggered Dual-Ions Release for Enhanced MR Imaging-Guided Ferroptosis Chemodynamic Therapy. *ACS Appl Mater Interfaces* (2019) 11(42):38395–404. doi: 10.1021/acsami.9b11353
87. Yang B, Dai Z, Zhang G, Hu Z, Yao X, Wang S, et al. Ultrasmall Ternary FePtMn Nanocrystals With Acidity-Triggered Dual-Ions Release and Hypoxia Relief for Multimodal Synergistic Chemodynamic/Photodynamic/Photothermal Cancer Therapy. *Adv Healthc Mater* (2020) 9(21):e1901634. doi: 10.1002/adhm.201901634
88. Song HW, Lee HS, Kim SJ, Kim HY, Choi YH, Kang B, et al. Sonazoid-Conjugated Natural Killer Cells for Tumor Therapy and Real-Time Visualization by Ultrasound Imaging. *Pharmaceutics* (2021) 13(10). doi: 10.3390/pharmaceutics13101689
89. Goertz DE, Todorova M, Mortazavi O, Agache V, Chen B, Karshafian R, et al. Antitumor Effects of Combining Docetaxel (Taxotere) With the Antivascular Action of Ultrasound Stimulated Microbubbles. *PloS One* (2012) 7(12): e52307. doi: 10.1371/journal.pone.0052307
90. Yin H, Sun L, Pu Y, Yu J, Feng W, Dong C, et al. Ultrasound-Controlled CRISPR/Cas9 System Augments Sonodynamic Therapy of Hepatocellular Carcinoma. *ACS Cent Sci* (2021) 7(12):2049–62. doi: 10.1021/acscentsci.1c01143
91. Guang Y, Xie L, Ding H, Cai A, Huang Y. Diagnosis Value of Focal Liver Lesions With SonoVue®-Enhanced Ultrasound Compared With Contrast-Enhanced Computed Tomography and Contrast-Enhanced MRI: A Meta-Analysis. *J Cancer Res Clin Oncol* (2011) 137(11):1595–605. doi: 10.1007/s00432-011-1035-8
92. Westwood M, Joore M, Grutters J, Redekop K, Armstrong N, Lee K, et al. Contrast-Enhanced Ultrasound Using SonoVue® (Sulphur Hexafluoride Microbubbles) Compared With Contrast-Enhanced Computed Tomography and Contrast-Enhanced Magnetic Resonance Imaging for the Characterisation of Focal Liver Lesions and Detection of Liver Metastases: A Systematic Review and Cost-Effectiveness Analysis. *Health Technol Assess* (2013) 17(16):1–243. doi: 10.3310/hta17160
93. Alaboudy A, Inoue T, Hatanaka K, Chung H, Hyodo T, Kumano S, et al. Usefulness of Combination of Imaging Modalities in the Diagnosis of Hepatocellular Carcinoma Using Sonazoid®-Enhanced Ultrasound, Gadolinium Diethylene-Triamine-Pentaacetic Acid-Enhanced Magnetic Resonance Imaging, and Contrast-Enhanced Computed Tomography. *Oncol* (2011) 81 Suppl 1:66–72. doi: 10.1159/000333264
94. Motosugi U, Bannas P, Sano K, Reeder SB. Hepatobiliary MR Contrast Agents in Hypovascular Hepatocellular Carcinoma. *J Magn Reson Imaging* (2015) 41 (2):251–65. doi: 10.1002/jmri.24712
95. Kim DW, Choi SH, Kim SY, Byun JH, Lee SS, Park SH, et al. Diagnostic Performance of MRI for HCC According to Contrast Agent Type: A Systematic Review and Meta-Analysis. *Hepatol Int* (2020) 14(6):1009–22. doi: 10.1007/s12072-020-10100-7
96. Zhao C, Dai H, Shao J, He Q, Su W, Wang P, et al. Accuracy of Various Forms of Contrast-Enhanced MRI for Diagnosing Hepatocellular Carcinoma: A Systematic Review and Meta-Analysis. *Front Oncol* (2021) 11. doi: 10.3389/fonc.2021.680691
97. Imbriaco M, De Luca S, Coppola M, Fusari M, Klain M, Puglia M, et al. Diagnostic Accuracy of Gd-EOB-DTPA for Detection Hepatocellular Carcinoma (HCC): A Comparative Study With Dynamic Contrast Enhanced Magnetic Resonance Imaging (MRI) and Dynamic Contrast Enhanced Computed Tomography (Ct). *Pol J Radiol* (2017) 82:50–7. doi: 10.12659/PJR.899239
98. Frtús A, Smolková B, Uzhytchak M, Lunova M, Jirsa M, Kubinová Š, et al. Analyzing the mechanisms of iron oxide nanoparticles interactions with cells: A road from failure to success in clinical applications. *J Control Release* (2020) 328:59–77. doi: 10.1016/j.jconrel.2020.08.036

Conflict of Interest: The authors declare that the research was conducted in the absence of any commercial or financial relationships that could be construed as a potential conflict of interest.

日中笹川医学奨学金制度＜学位取得コース＞評価書
課程博士：指導教官用

Supported by 日本財団 THE NIPPON FOUNDATION

第 43 期　　研究者番号：G4308　　作成日　：　2024 年 3 月 8 日

氏　名	葉 盛	YE SHENG	性別	M	生年月日　1982/03/19
所属機関（役職）	南京紅十字血液中心成分採血科（副主任医師）				
研究先（指導教官）	奈良県立医科大学大学院医学研究科　循環器システム医科学 （中川修教授、小亀浩市教授）				
研究テーマ	ADAMTS13 による VON WILLEBRAND 因子制御破綻がもたらす疾患の病態解析 Pathological analysis of diseases caused by the regulation failure of ADAMTS13 to von Willebrand factor				
専攻種別	□論文博士		☑課程博士		

研究者評価（指導教官記入欄）

成績状況	㊇　良　可　不可 学業成績係数=	取得単位数 ４／４
学生本人が行った研究の概要	von Willebrand 因子（VWF）は止血を担う血漿タンパク質であり、ADAMTS13 は VWF を切断して止血機能を抑制する。VWF と ADAMTS13 の機能的バランスが崩れると出血性あるいは血栓性の疾患につながる。von Willebrand 病は VWF の遺伝子異常に伴う出血性疾患であり、その診断や病型分類のためには遺伝子解析が重要であるが、VWF 遺伝子の特徴から、従来の解析方法では実施のハードルが高い。そこで、新しいロングリードシーケンシング法を工夫して VWF 遺伝子を効率よくかつ正確に解析することを目標とした。2022 年度は、遺伝子異常を正確に同定するためのワークフローを構築した。2023 年度は、患者 DNA 試料を解析して VWF 遺伝子のバリアントを同定し、その機能解析を進めた。	
総合評価	【良かった点】 研究に対する熱意はきわめて高く、常に向上心を持って取り組んだ。VWF 遺伝子全長の PCR とロングリードシーケンシングの実験条件検討にはかなりの労力を要したが、日々の計画をしっかり立て、アドバイスや自習を活かして着々と研究を進めた。当初の目的であった遺伝子解析方法の確立は達成したため、解析手法を広げ、多くの知識と技術を習得した。 【改善すべき点】 2022 年度には「新しい技術を習得する際、ミスを避けたい気持ちが強いため過度に慎重になることがある。ポイントを正確に把握することで、もう少し気持ちに余裕を持って実験を行うことができると研究能力が伸びると思われる。」と評価したが、2023 年度にはこれを理解し克服した。現在の意欲を維持し続けることが重要である。 【今後の展望】 この２年間で、新しい VWF 遺伝子解析方法の確立を達成し、さらに VWF タンパク質機能解析を開始するところまで進んだ。今後、病態との関連を明確にし、近いうちに原著論文として投稿する。	
学位取得見込	２年間の研究計画は順調に進んだ。論文投稿に向けた最終実験も進んでいるため、目標期間内（１年以内）に学位を取得できる見込みは大きい。	
	評価者（指導教官名）　　小亀浩市	

日中笹川医学奨学金制度<学位取得コース>報告書
研究者用

第43期　　研究者番号：G4308　　作成日：2024年3月1日

氏名	叶 盛	YE SHENG	性別	M	生年月日 1982/03/19
所属機関(役職)	南京紅十字血液中心成分採血科(副主任医師)				
研究先(指導教官)	奈良県立医科大学大学院医学研究科循環器システム医科学(中川修教授、小亀浩市教授)				
研究テーマ	ADAMTS13によるVON WILLEBRAND因子制御破綻がもたらす疾患の病態解析 Pathological analysis of diseases caused by the regulation failure of ADAMTS13 to von Willebrand factor				
専攻種別	論文博士	☐	課程博士	☑	

1．研究概要（1）

1）目的（Goal）

To establish a long-read sequencing method using Oxford Nanopore Technology (ONT) to overcome the difficulties in von Willebrand factor (VWF) gene analysis.

2）戦略（Approach）

The identification of causative variants in VWF is important for the diagnosis, classification, and clinical management of von Willebrand disease (VWD) and acquired von Willebrand syndrome (AVWS)[1]. In this study, we demonstrated an optimal solution by using long-range PCR and ONT sequencing[2]. Specific primers were designed and optimized to amplify ~15-kb PCR amplicons covering the entire VWF (175 kb), avoiding unwanted amplification due to repetitive sequences or pseudogene VWFP1[3]. All amplicons were subjected to DNA library preparation. ONT data were analyzed using dedicated software and identified candidate variants were verified by Sanger sequencing and expressed on HEK293 cells to investigate its impact on secretion and multimer distribution of VWF by multimer analysis and western blotting.

3）材料と方法（Materials and methods）

Patients and samples

One VWD patient and two AVWS patients registered in the NCVC Biobank were enrolled in this study[4], their genomic DNA (gDNA) samples were diluted to 50 ng/μL concentration for long-range PCR.

Mammalian cell cultures

HEK293 cells were cultured in D-MEM high glucose medium with 10% fetal bovine serum at 37℃ in 5% CO_2.

Long-range PCR

PCR primer pairs were basically designed by Primer-Blast on NIH with SNP handling, repeat and low complexity filters on. For 21~29 kb pseudogene-homology region, four verified primers were used[5]. All PCR amplicons subjected to library preparation were verified by 1.2% agarose gel electrophoresis then purified and quantified accordingly.

ONT sequencing and data analysis

The final 20 fmol DNA library was prepared using the ligation kit (SQK-LSK114). ONT sequencing performed on GridION sequencer were run for 5-12 hrs using R10.4 flow-cell. Variants were called using the Clair3 and Longshot. All identified candidate variants were verified by Sanger sequencing.

Expression of VWF mutant

Wild-type (wt) and mutant VWF were expressed on HEK293 cells using vector pcDNA3.1 and Avalanche Transfection Reagent (EZ Biosystems, Maryland, USA) according to the manufacturer's instructions. Forty-eight or seventy-two hours after the transfection, medium was collected and the expression level of recombinant VWF (rVWF) protein was measured by western blotting.

Multimers analysis

1.2% SDS-agarose gels were used, and the multimers were visualized by fluorescence luminescent-based imaging using HRP-polyclonal rabbit anti-human VWF antibody P0226 (Dako, Jena, Germany) and secondary goat anti-rabbit 800CW antibody (LI-COR Biosciences, Nebraska, USA).

Generation of high shear stress

Given enzyme called a disintegrin-like and metalloproteinase with thrombospondin type 1 motif 13 (ADAMTS13) can specially cleave VWF under shear, to examine the rVWF cleavage by ADAMTS13 at high shear stress, we created an original instrument with two syringes and one injection needle to generate high shear stress[6].

4）実験結果（Results）

Amplification of VWF gene using long-range PCR

According to the agarose check following the PCR, some primer pairs with low efficiency were redesigned to generate favorable DNA products for ONT sequencing. After several optimizations, forty-two primers were determined, and twenty-one 12~15 kb PCR amplicons covering entire VWF were produced despite yielding some minor nonspecific products.

ONT sequencing and variants calling

Total reads of 95.38k,128.13k, and 114.55k were generated from three samples by ONT sequencing, respectively. Using selected reads by quality score and size, over 200 variants (SNV and INDEL) were identified per sample. Although no candidate variant was found in VWD, among two AVWS, p.Gln2442His and g.6087520_6090118del were identified respectively.

１．研究概要（2）

4）実験結果（Results）

Variants validation using Sanger sequencing

p.Gln2442His was validated, however, g.6087520_6090118del was confirmed as an artifact derived from long-range PCR due to a special sequence called “direct repeats”[7]. Although this kind of sequence also exists in reference sequence of VWF gene, it only generated <1% deletion-amplicons. Nevertheless，eight heterozygous SNPs possessed by the third patient in the region of g.6087416-6087659 made it easily generate more deletion-amplicons than reference sequence (50% vs <1%).

Functional analysis of VWF SNV mutant identified in AVWS

Expression analysis showed that the level of rVWF-mutant protein is identical to rVWF-WT, suggesting this mutation may less disturb the synthesize and secretion of rVWF in HEK293 cell. Multimers patterns of secreted rVWF-mutant exhibited a similar profile to rVWF-WT, even with ADAMTS13 under high shear stress, that implied this mutation may not induce alterations in the VWF structure or domains related to ADAMTS13 cleavage.

5）考察（Discussion）

Here, we present a genetic analysis method to identify causative variants in VWF gene to overcome the difficulties usually faced by Sanger or short-read next-generation sequencing (NGS). ONT can measure the changes in electrical charges while DNA passing through biological nanopores, which offers exceptionally long reads that allows direct sequencing through regions like long repetitive sequences, pseudogene-homology regions, and complex gene loci[2]. We used long-range PCR to amplify the whole VWF gene sequence for subsequent library preparation and long-read sequencing, and the optimization of long-range PCR was mainly focused on DNA polymerase, primer design, template volume, and PCR microtubes.

For DNA polymerase, we used TaKaRa PrimeSTAR GXL DNA Polymerase, which performed superbly in our study. For primer design, it is necessary to exclude all primers that may contain known SNPs or be located in repetitive or low complexity regions. In addition to that, especially in VWFP1-homology region, we used four VWF-selective primers already verified and designed the corresponding reverse or forward primers outside the VWFP1-homology region[5]. The amount of gDNA template used in our PCR was determined as 100~200 ng after several attempts. Surprisingly, we noticed even PCR microtube can greatly influence the long-range PCR results. It seemed PCRs using microtubes with thinner plastic wall have superior performance. This emphasized the importance of selection of PCR microtubes for long-range PCR, which is in consistent of the implication showed by Chua et al.[8].

Direct repeats is one kind of non-B DNA motifs consisting of two copies of the repeated unit separated by a nonrepetitive spacer, which can lead to a slipped strand structure with looped out bases, just like we discovered in the third patient with AVWS[7]. This indicated that amplification of regions containing multiple repetitive sequences using long-range PCR remains a challenge. Therefore, more careful validation and confirmation of variants identified by this method is needed to avoid any associated misleading results. A research group investigated the molecular mechanisms behind the generation of PCR artifacts caused by repetitive sequences. They proposed using primers that anneal to locations far from the repeats to decrease artifact products and alleviate this issue[9]. Similarly, we also noticed that PCR using primer near these repetitive sequences produced fewer no-deletion reads, which may coincide with their findings.

Genetic defects in type 1 VWD have been reported to be located throughout the whole VWF gene, but new variants still may not necessarily cause disease due to the highly polymorphic nature of VWF gene[10]. Moreover, many studies reveled that not all patients of this type have a VWF genetic defect, the rate of genetic variants ranged from 45% to 68%, which may explain our result of the VWD patient[11, 12].

We identified p.Gln2442His, a C3 domain coding region SNV in a left ventricular assist device (LVAD) -associated AVWS patient. It was predicted be a deleterious mutation in Asian population[13]. This is the first report of it in clinical case, which may indicate some potential association with the onset risk of AVWS. Thus, we conducted a thorough investigation of its impact on VWF structure and functions. Although no significant correlation was found to the synthesize, secretion or ADAMTS13 cleavage yet, as a mutation near the binding site of platelet receptor glycoprotein (GP)IIb/IIIa, further work needs to be done to look into its impact on the binding of GPIIb/IIIa with appropriate approaches.

In general, we reported a novel VWF gene analysis method combining with ONT technology and long-range PCR which could be a powerful tool to investigate the pathogenetic mechanisms of VWF disorders.

6）参考文献（Reference）

1.James PD, Connell NT, Ameer B, et al. ASH ISTH NHF WFH 2021 guidelines on the diagnosis of von Willebrand disease. Blood Adv. 2021;5(1):280-300.
2.Lin B, Hui J, and Mao H. Nanopore Technology and Its Applications in Gene Sequencing. Biosensors (Basel). 2021;11(7).
3.Matsushita T. [The management strategy for von Willebrand disease]. Rinsho Ketsueki. 2021;62(5):435-444.
4.Guidelines for the Management of von Willebrand Disease 2021. Japanese Journal of Thrombosis and Hemostasis. 2021;32(4):413-481.
5.Mancuso DJ, Tuley EA, Westfield LA, et al. Human von Willebrand factor gene and pseudogene: structural analysis and differentiation by polymerase chain reaction. Biochemistry. 1991;30(1):253-69.
6.Hayakawa M, Kato S, Matsui T, et al. Blood group antigen A on von Willebrand factor is more protective against ADAMTS13 cleavage than antigens B and H. J Thromb Haemost. 2019;17(6):975-983.
7.Weissensteiner MH, Cremona MA, Guiblet WM, et al. Accurate sequencing of DNA motifs able to form alternative (non-B) structures. Genome Res. 2023;33(6):907-922.
8.Chua EW, Miller AL, and Kennedy MA. Choice of PCR microtube can impact on the success of long-range PCRs. Anal Biochem. 2015;477:115-7.
9.Hommelsheim CM, Frantzeskakis L, Huang M, and Ülker B. PCR amplification of repetitive DNA: a limitation to genome editing technologies and many other applications. Sci Rep. 2014;4:5052.
10.Flood VH, Garcia J, and Haberichter SL. The role of genetics in the pathogenesis and diagnosis of type 1 Von Willebrand disease. Curr Opin Hematol. 2019;26(5):331-5.
11.Yadegari H, Driesen J, Pavlova A, et al. Mutation distribution in the von Willebrand factor gene related to the different von Willebrand disease (VWD) types in a cohort of VWD patients. Thromb Haemost. 2012;108(4):662-71.
12.Flood VH, Christopherson PA, Gill JC, et al. Clinical and laboratory variability in a cohort of patients diagnosed with type 1 VWD in the United States. Blood. 2016;127(20):2481-8.
13.Wang QY, Song J, Gibbs RA, et al. Characterizing polymorphisms and allelic diversity of von Willebrand factor gene in the 1000 Genomes. J Thromb Haemost. 2013;11(2):261-9.

2. 執筆論文 Publication of thesis ※記載した論文を添付してください。Attach all of the papers listed below.

論文名 1 Title						
掲載誌名 Published journal						
	年　月	巻(号)	頁　～　頁	言語 Language		
第1著者名 First author		第2著者名 Second author		第3著者名 Third author		
その他著者名 Other authors						
論文名 2 Title						
掲載誌名 Published journal						
	年　月	巻(号)	頁　～　頁	言語 Language		
第1著者名 First author		第2著者名 Second author		第3著者名 Third author		
その他著者名 Other authors						
論文名 3 Title						
掲載誌名 Published journal						
	年　月	巻(号)	頁　～　頁	言語 Language		
第1著者名 First author		第2著者名 Second author		第3著者名 Third author		
その他著者名 Other authors						
論文名 4 Title						
掲載誌名 Published journal						
	年　月	巻(号)	頁　～　頁	言語 Language		
第1著者名 First author		第2著者名 Second author		第3著者名 Third author		
その他著者名 Other authors						
論文名 5 Title						
掲載誌名 Published journal						
	年　月	巻(号)	頁　～　頁	言語 Language		
第1著者名 First author		第2著者名 Second author		第3著者名 Third author		
その他著者名 Other authors						

3. 学会発表 Conference presentation ※筆頭演者として総会・国際学会を含む主な学会で発表したものを記載してください。

※Describe your presentation as the principal presenter in major academic meetings including general meetings or international meetings.

学会名 Conference	第45回日本血栓止血学会学術集会			
演 題 Topic	VWF遺伝子解析の困難性を克服するロングリードシーケンシング法の構築			
開催日 date	2023 年 6 月 15 日	開催地 venue	福岡県北九州市	
形式 method	☑ 口頭発表 Oral ☑ ポスター発表 Poster	言語 Language	☑ 日本語 ☐ 英語 ☐ 中国語	
共同演者名 Co-presenter	樋口（江浦）由佳、松本雅則、小亀浩市			
学会名 Conference	1st National Cerebral and Cardiovascular Center Annual Symposium			
演 題 Topic	Genetic analysis using long-read sequencing to overcome the difficulties in VWF gene			
開催日 date	2023 年 7 月 21 日	開催地 venue	大阪府吹田市	
形式 method	☐ 口頭発表 Oral ☑ ポスター発表 Poster	言語 Language	☐ 日本語 ☑ 英語 ☐ 中国語	
共同演者名 Co-presenter	Yuka Eura, Masanori Matsumoto, Koichi Kokame			
学会名 Conference	第46回日本血栓止血学会学術集会			
演 題 Topic	ロングリードシーケンシングでVWF遺伝子に同定したバリアントの検証と機能解析			
開催日 date	2024 年 6 月 13 日	開催地 venue	石川県金沢市	
形式 method	☑ 口頭発表 Oral ☐ ポスター発表 Poster	言語 Language	☑ 日本語 ☐ 英語 ☐ 中国語	
共同演者名 Co-presenter	樋口（江浦）由佳、松本雅則、小亀浩市			
学会名 Conference	The 32nd Congress of the International Society on Thrombosis and Haemostasis			
演 題 Topic	Genetic analysis using long-read sequencing to overcome the difficulties in VWF gene			
開催日 date	2024 年 6 月 22-26 日	開催地 venue	Bangkok, Thailand	
形式 method	☐ 口頭発表 Oral ☑ ポスター発表 Poster	言語 Language	☐ 日本語 ☑ 英語 ☐ 中国語	
共同演者名 Co-presenter	Yuka Eura, Masanori Matsumoto, Koichi Kokame			

4. 受賞（研究業績） Award (Research achievement)

名 称 Award name	第45回日本血栓止血学会学術集会優秀ポスター賞			
	国名 Country name	日本	受賞年 Year of award	2023 年 6 月
名 称 Award name				
	国名 Country name		受賞年 Year of award	年 月

5. 本研究テーマに関わる他の研究助成金受給 Other research grants concerned with your resarch theme

受給実績 Receipt record	□ 有 □ 無
助成機関名称 Funding agency	
助成金名称 Grant name	
受給期間 Supported period	年 月 ～ 年 月
受給額 Amount received	円
受給実績 Receipt record	□ 有 □ 無
助成機関名称 Funding agency	
助成金名称 Grant name	
受給期間 Supported period	年 月 ～ 年 月
受給額 Amount received	円

6. 他の奨学金受給 Another awarded scholarship

受給実績 Receipt record	□ 有 □ 無
助成機関名称 Funding agency	
奨学金名称 Scholarship name	
受給期間 Supported period	年 月 ～ 年 月
受給額 Amount received	円

7. 研究活動に関する報道発表 Press release concerned with your research activities

※記載した記事を添付してください。Attach a copy of the article described below

報道発表 Press release	□ 有 □ 無	発表年月日 Date of release	
発表機関 Released medium			
発表形式 Release method	・新聞 ・雑誌 ・Web site ・記者発表 ・その他( )		
発表タイトル Released title			

8. 本研究テーマに関する特許出願予定 Patent application concerned with your research theme

出願予定 Scheduled application	□ 有 □ 無	出願国 Application country	
出願内容(概要) Application contents			

9. その他 Others

指導責任者(記名) 小鬼 浩市

日中笹川医学奨学金制度(学位取得コース)評価書
課程博士：指導教官用

第 43 期　　研究者番号：G4309　　作成日　：2023 年 3 月 8 日

氏　名	王 喻	Wang Yu	性別	F	生年月日　1989.12.18
所属機関（役職）	京都大学大学院医学研究科医学専攻免疫ゲノム医学（大学院生）				
研究先（指導教官）	京都大学大学院医学研究科附属がん免疫総合研究センター（本庶 佑センター長）				
研究テーマ	PD-1 阻害による免疫賦活化異常疾患の研究 Studies on diseases caused by hyperimmune activities due to PD-1 blockade				
専攻種別	□論文博士		☑課程博士		

研究者評価（指導教官記入欄）

成績状況	優 学業成績係数=	取得単位数 26／30
学生本人が行った研究の概要	PD-1 阻害抗体治療を受けた 200-300 人のがん患者（複数のがん種）から収集した plasma を用いて、約 300 種類のメタボライトを測定した。臨床データーから統計解析を行い、irAE（自己免疫様副作用）を予測できる複数のメタボライト A を同定した。そのうちの一つはマウス自己免疫疾患モデルにおいても高値であることを発見した。さらにそのメタボライト A が結合するリガンドタンパクを同定した。	
総合評価	【良かった点】まさに寝食を忘れて実験に没頭できる優秀な学生である。コロナにより入国が遅れ 1 年少ないにもかかわらず確実に成果を出し、大きな論文として完成間近である。また礼儀正しく、正直で素直なため、新しい技術や知識に対する吸収力が非常に高い。それらを用いたアウトプットも正確に出すことができるため、データーに対する信用性も高い。Discussion も活発に行い、好奇心旺盛な学生である。新しい技術を他人教えることもでき、既にリーダー的存在である。 【改善すべき点】大変よく働く反面、体を壊さないか多少心配になることもある。ただその時は無理せず休むように勧めている。自分でよく考えよく実験を行うが、それらを他人にアピールする方法はまだ改善の余地がある。2 年の経験を経て、英語で理論的に論文作成する能力は確実に伸びたが、プレゼンテーションスライドを用いた発表技術等についてはまだ改善余地がある。 【今後の展望】王さんは、飲み込みが早く手技も正確なため、研究の方は予想以上に順調に進んでいる。また行っている研究はがん免疫治療分野においても非常に注目されつつあるテーマであり、早期に完成させることで世界に大きなインパクトを与えることができると確信している。	
学位取得見込	本奨学金終了後、おそらく 2 年以内に論文発表できると思われる。行っている研究内容も次の課題を生み出す末広がりなテーマであり、生理学の根源を開拓する良いテーマである。予測不能なことが起こらない限り、予定通り学位を取得できる見込みである。	
評価者（指導教官名）　本庶佑		

日中笹川医学奨学金制度(学位取得コース)報告書
研究者用

第43期　　研究者番号：G4309　　作成日：2023年3月 3 日

氏名	王 喻	Wang Yu	性別	F	生年月日 1989. 12. 18
所属機関(役職)	京都大学大学院医学研究科医学専攻免疫ゲノム医学(大学院生)				
研究先(指導教官)	京都大学大学院 医学研究科附属がん免疫総合研究センター(本庶 佑センター長)				
研究テーマ	PD-1阻害による免疫賦活化異常疾患の研究 Studies on diseases caused by hyperimmune activities due to PD-1 blockade				
専攻種別	論文博士	☐	課程博士	☑	

1．研究概要(1)

1)目的(Goal)

Cancer immunotherapy with immune checkpoint inhibitors (ICIs) represented by PD-1 blockade antibodies has prevailed in the world as the first line therapy these days. However, since the PD-1 molecule on lymphocytes serves as an immune brake, the administration of PD-1 blockade antibody sometimes induces adverse events called Immune-Related Adverse Events (irAEs), which resemble autoimmune diseases in cancer patients (Figure 1). IrAE is generated by the over-activation of T cell immunity, which is kind of off-target of ICI therapy (Ye, W.et al. Br J Cancer 124, 1661-1669 (2021)(1).The incidence of clinical irAEs is around 10 % among the ICI-treated patients, and 30-40% are severe (more than grade 3) among those who experienced irAEs at any level (Golnaz Moradet al.cell 184, October 14, 2021)(2). Mechanism investigation and biomarkers identification of irAEs is therefore important for better-personalized medicine, and prevention or earlier intervention of irAEs.(Jing, Y. Nat Commun 11, 4946 (2020)(3). Our laboratory has studied responsive and unresponsive mechanisms to PD-1 blockade cancer immunotherapy from the view of immune metabolism in order to develop combination therapy and biomarkers (Al-Hansi et al. Science, 378:eabj3510, 2022.)(4). However, solid metabolite biomarkers for irAE prediction have not been reported. In this project we explored the candidate of irAE biomarkers and the mechanisms involved in the found biomarker.

2)戦略(Approach) Our laboratory has studied immune metabolism in the field of cancer immunotherapy. Our group already published the prediction biomarker of ICI responsiveness using plasma metabolites which are related to microbiota (Hatae et al, JCI insight 5:e133501, 2020)(5). We will use similar methods to identify the prediction biomarkers of irAEs. Note that as plasma metabolites were identified using the patients' blood before the first ICI treatment, these metabolite markers could be predictive. After the identification of metabolite biomarkers, we investigated the physiological meaning and mechanism of the metabolite biomarkers using cross-disciplinary methods and technologies.

3)材料と方法(Materials and methods) Collaborated with Kyoto University hospital, we collected the plasma from 200-300 patients who suffered non-small cell lung cancer, renal cell carcinoma, and urothelial carcinoma. Around 200-300 metabolites were measured from the patient's plasma by liquid chromatography-mass spectrometry before the 1st injection of PD-1 blockade therapy. In order to identify the metabolites which discriminate between the patients with irAE and without irAE group, we compared each metabolite level between the patients with irAE and without irAE. To understand the physiological meaning of the identified metabolite markers, we tested the target metabolite in the autoimmune disease mouse models including NOD diabetes models and contact hypersensitivity models (CHS: skin inflammation model) which is one of the most frequent symptoms of irAE. To understand the function of the candidate metabolite biomarkers, we analyzed the inflamed tissues and the infiltrated immune cells, by integrating the latest technologies such as metabolomics, single-cell sequencing analysis. We collaborated with Tohoku University and further examined the regulation function and molular mechanisms of the metabolite by seahorse, confocal microscopy and super resolution microscopy, and molecular biology methods (Fig. 2 and 3).

4)実験結果(Results) By comparison of the plasma metabolites between patients with irAE and without irAE, we detected several metabolites which could predict irAE patients before starting the treatments. Among the candidates, metabolite A is prominently high in the irAE patients (Fig. 4). We found this metabolite was also upregulated in inflammatory ears in the CHS model (Fig. 5). Interestingly, when we intravenously injected the metabolite A, the skin inflammation of CHS was attenuated (Fig.6), indicating that metabolite A serves as an immune modulator and this might be evolved in a negative feedback system of inflammation. Sinle cell analysis demonstrated that the metabolite A modulated the immune cells populations (Fig.7), which is now under the detail analysis. Molecular biology analysis revealed that metabolite A could bind to a mitochondrial protein and promote the mitochondria respiration accompanying with the mitochondria fusion (Fig.8).

5)考察(Discussion) We successfully identified the candidate of metabolite biomarker for irAE patients before the treatment. This discovery should improve the diagnosis of cancer immunotherapy and personalized medicine. Molecular biology methods and single-cell sequencing analysis uncovered its molecular mechanism and functions which are very novel among previous studies of metabolite A. Based on these findings, we have hypothesized the mechanism as follows. 1) The patients who might develop irAE by the treatment have preexisting inflammatory diseases or microinflammation niches. 2) The systemic circulation of metabolite was upregulated to reduce these inflammatory niches but insufficient. 3) The exogenous metabolite A supplement can help to reduce the inflammation sufficiently. We will search more and complete this project in the next year utilizig the conditional KO mouse and transgenic mouse of the related genes to investigate the detail mechanisms in vivo. Thank you very much for the support of my scientific life. 日中笹川医学奨学金.

1．研究概要（2）

Figure 1: Immune regulation by PD-1

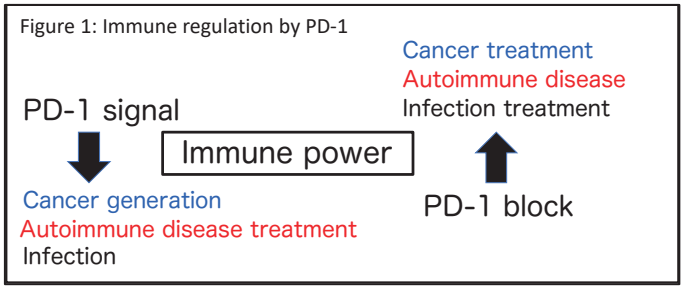

Figure 2: Analysis strategy

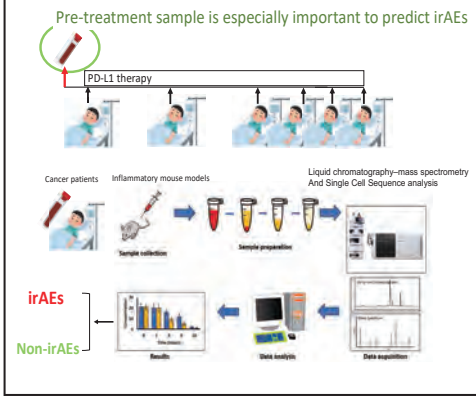

Figure 3: Graphic Hypothesis

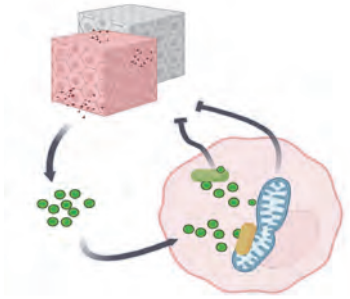

Figure 4

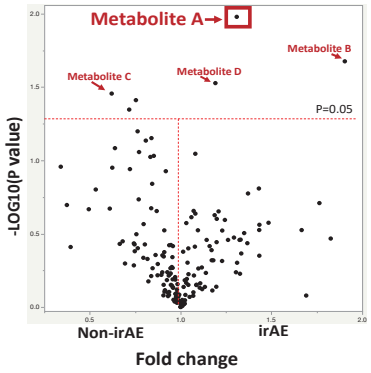

Figure

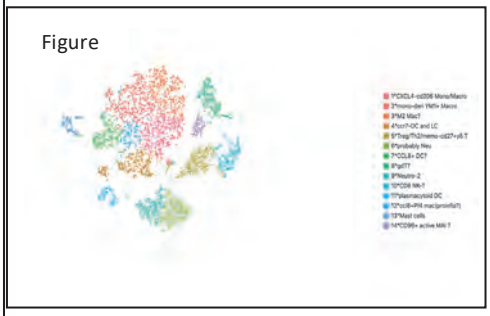

Figure

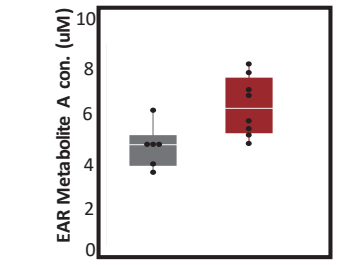

Figure

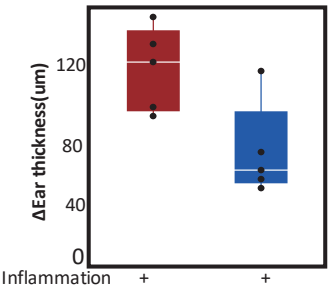

Figure

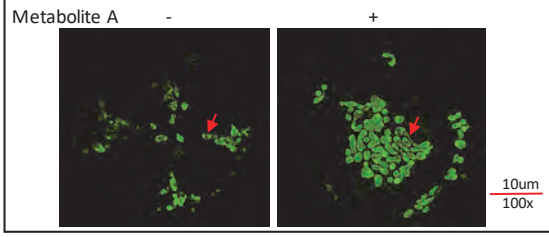

6）参考文献（References）

1.Ye, W., Olsson-Brown, A., Watson, R.A. et al. Checkpoint-blocker-induced autoimmunity is associated with favourable outcome in metastatic melanoma and distinct T-cell expression profiles. Br J Cancer 124, 1661–1669 (2021).
2. Golnaz Morad,Beth A. Helmink, Padmanee Sharma.et al.Hallmarks of response, resistance, and toxicity to immune checkpoint blockade.Cell 184, October 14, 2021 a 2021 Elsevier Inc.
3.Jing, Y., Liu, J., Ye, Y. et al. Multi-omics prediction of immune-related adverse events during checkpoint immunotherapy. Nat Commun 11, 4946 (2020).
4.Muna Al-Habsi,Kenji Chamoto, Tasuku Honjo,*et al.*Spermidine activates mitochondrial trifunctional protein and improves antitumor immunity in mice.Science.abj3510. Epub 2022 Oct 28.
5.Ryusuke Hatae, Toyohiro Hirai, Tasuku Honjo.et al.Combination of host immune metabolic biomarkers for the PD-1 blockade cancer immunotherapy. JCI Insight. 2020;5(2):e133501.

2. 執筆論文 Publication of thesis ※記載した論文を添付してください。Attach all of the papers listed below.

論文名 1 Title						
掲載誌名 Published journal						
	年　月	巻(号)	頁　～　頁	言語 Language		
第1著者名 First author		第2著者名 Second author		第3著者名 Third author		
その他著者名 Other authors						
論文名 2 Title						
掲載誌名 Published journal						
	年　月	巻(号)	頁　～　頁	言語 Language		
第1著者名 First author		第2著者名 Second author		第3著者名 Third author		
その他著者名 Other authors						
論文名 3 Title						
掲載誌名 Published journal						
	年　月	巻(号)	頁　～　頁	言語 Language		
第1著者名 First author		第2著者名 Second author		第3著者名 Third author		
その他著者名 Other authors						
論文名 4 Title						
掲載誌名 Published journal						
	年　月	巻(号)	頁　～　頁	言語 Language		
第1著者名 First author		第2著者名 Second author		第3著者名 Third author		
その他著者名 Other authors						
論文名 5 Title						
掲載誌名 Published journal						
	年　月	巻(号)	頁　～　頁	言語 Language		
第1著者名 First author		第2著者名 Second author		第3著者名 Third author		
その他著者名 Other authors						

3. 学会発表　Conference presentation　※筆頭演者として総会・国際学会を含む主な学会で発表したものを記載してください。

※Describe your presentation as the principal presenter in major academic meetings including general meetings or international meetings.

学会名 Conference					
演　題 Topic					
開催日 date	年　月　日		開催地 venue		
形式　method	□ 口頭発表　Oral	□ ポスター発表　Poster	言語　Language	□ 日本語	□ 英語　□ 中国語
共同演者名 Co-presenter					
学会名 Conference					
演　題 Topic					
開催日 date	年　月　日		開催地 venue		
形式　method	□ 口頭発表　Oral	□ ポスター発表　Poster	言語　Language	□ 日本語	□ 英語　□ 中国語
共同演者名 Co-presenter					
学会名 Conference					
演　題 Topic					
開催日 date	年　月　日		開催地 venue		
形式　method	□ 口頭発表　Oral	□ ポスター発表　Poster	言語　Language	□ 日本語	□ 英語　□ 中国語
共同演者名 Co-presenter					
学会名 Conference					
演　題 Topic					
開催日 date	年　月　日		開催地 venue		
形式　method	□ 口頭発表　Oral	□ ポスター発表　Poster	言語　Language	□ 日本語	□ 英語　□ 中国語
共同演者名 Co-presenter					

4. 受賞（研究業績）　Award (Research achievement)

名　称 Award name				
	国名 Country name		受賞年 Year of award	年　月
名　称 Award name				
	国名 Country name		受賞年 Year of award	年　月

5. 本研究テーマに関わる他の研究助成金受給 Other research grants concerned with your resarch theme

受給実績 Receipt record	□ 有 ■ 無
助成機関名称 Funding agency	
助成金名称 Grant name	
受給期間 Supported period	年 月 ～ 年 月
受給額 Amount received	円
受給実績 Receipt record	□ 有 ■ 無
助成機関名称 Funding agency	
助成金名称 Grant name	
受給期間 Supported period	年 月 ～ 年 月
受給額 Amount received	円

6. 他の奨学金受給 Another awarded scholarship

受給実績 Receipt record	□ 有 ■ 無
助成機関名称 Funding agency	
奨学金名称 Scholarship name	
受給期間 Supported period	年 月 ～ 年 月
受給額 Amount received	円

7. 研究活動に関する報道発表 Press release concerned with your research activities

※記載した記事を添付してください。Attach a copy of the article described below

報道発表 Press release	□ 有 ■ 無	発表年月日 Date of release	
発表機関 Released medium			
発表形式 Release method	・新聞 ・雑誌 ・Web site ・記者発表 ・その他（ ）		
発表タイトル Released title			

8. 本研究テーマに関する特許出願予定 Patent application concerned with your research theme

出願予定 Scheduled application	□ 有 ■ 無	出願国 Application country	
出願内容（概要） Application contents			

9. その他 Others

指導責任者（記名） 本庶 佑

日中笹川医学奨学金制度＜学位取得コース＞評価書
課程博士：指導教官用

第 43 期　　研究者番号：G4310　　作成日　：　2024 年 3 月 8 日

氏　名	孔 徳川	KONG DECHUAN	性別	M	生年月日　1987/09/13
所属機関（役職）	上海市疾病予防控制中心伝染病防治所急性伝染病防治科（医師）				
研究先（指導教官）	熊本大学大学院 医学教育部ヒトレトロウイルス学共同研究センター 感染免疫学分野（上野 貴将　教授、徳永 研三　客員教授）				
研究テーマ	新型コロナウイルスの複製を制御する宿主因子の同定と機能解析 — Identification and functional analysis of host factors that regulate SARS-CoV-2 replication				
専攻種別	□論文博士		☑課程博士		

研究者評価（指導教官記入欄）

成績状況	㊧　良　可　不可 学業成績係数= 90	取得単位数 取得単位数／取得すべき単位総数
学生本人が行った研究の概要	ウイルスの複製に関わる宿主因子の研究は特にレトロウイルス学において最先端で進んでいることから、まず HIV の複製を阻害する抗ウイルス宿主因子 MARCH8 の分子ウイルス学的研究に着手した。 HIV-1 エンベロープ糖タンパク質（HIV-1 Env）および水胞性口炎ウイルス G タンパク質（VSV-G）に対する動物種別 MARCH8 の抑制効果について検討した。サル、マウス、ウシの MARCH8 野生型および 2 種類の変異体を作製した。これらの抗ウイルス活性を検討するため、各 MARCH8 を HIV-1 Env 欠損型ルシフェラーゼレポーターウイルス DNA、HIV-1 Env 発現プラスミドまたは VSV-G 発現プラスミドと共にヒト胎児腎細胞株 293T にコトランスフェクションして、産生されたウイルスの感染性を検討した。その結果、ヒト MARCH8 と同様、サル、マウス、ウシ MARCH8 の野生型は HIV-1 Env と VSV-G に対する抑制能を保持し、一方で 2 種類の変異体はどちらも抑制活性を失っていた。このことから MARCH8 の抗ウイルスエンベロープ活性およびその機能領域は動物種間で高度に保存されていることが明らかになった。 次に、HIV-1 潜伏機構に関与する宿主側要因を探るべく潜伏感染細胞モデルの樹立を試みた。まず蛍光強度および光安定性において GFP より優れた新規蛍光タンパク質 StayGold およびルシフェラーゼの二つのレポーター遺伝子を挿入した HIV-1 ミニジーン（gag-pol、vif、vpr 遺伝子を欠損）を構築した。この HIV-1 ミニジーンのトランスフェクションで得られたウイルスを用いて感染実験を行った。その結果、感染後 4 週以内で StayGold および Luc2 の活性が徐々に低下したことから、最終的に潜伏感染細胞が樹立できることが確認できた。また一部の持続感染状態の細胞に Gag-Pol 発現プラスミドを再導入した後に産生されたウイルスが感染性を保持することも証明した。HIV-1 制御遺伝子 tat を標的とした CRISPR ノックアウトにより、潜伏感染細胞のプロウイルス DNA を効率よく破壊することができた。	
総合評価	【良かった点】 ・ウイルス学研究に対するモチベーションが高い。 ・真摯に実験に取り組み、失敗しても諦めずに何度もやり直す姿勢を持っている。 ・関連研究に関する情報を収集するべく、最新論文のチェックを細目に行っている。 【改善すべき点】 ・最初に研究指導を受ける際にメモを取りノートにまとめる習慣をつける。 ・試薬/消耗品を使い切って初めて発注要求したりせず、事前に誰かに伝える。 ・トラブルシューティングを全て自分で行おうとせず、悩む前に指導教官に相談する。 【今後の展望】 日常的に十分な実験量をこなしており、徐々に良質なデータが増えてきているので、更なる伸びしろは感じられる。	
学位取得見込	equal first author (3rd author)としての論文を現在投稿中である。それに加えて first author 論文用別の研究プロジェクトも進行中であり期限内の学位取得は可能である。	
	評価者（指導教官名）　徳永　研三	

日中笹川医学奨学金制度<学位取得コース>報告書
研究者用

Supported by 日本財団 THE NIPPON FOUNDATION

第43期　　研究者番号：G4310　　作成日：2024年3月 8日

氏名	孔 徳川	KONG DECHUAN	性別	M	生年月日 1987/09/13
所属機関(役職)	上海市疾病予防控制中心伝染病防治所急性伝染病防治科（医師）				
研究先（指導教官）	熊本大学大学院 医学教育部ヒトレトロウイルス学共同研究センター 感染免疫学分野（上野 貴将 教授、徳永 研三 客員教授）				
研究テーマ	新型コロナウイルスの複製を制御する宿主因子の同定と機能解析 Identification and functional analysis of host factors that regulate SARS-CoV-2 replication				
専攻種別	論文博士	☐	課程博士	☑	

1．研究概要(1)

1)目的(Goal)： 過去4年間に渡り、全世界を席巻した新型コロナウイルス（SARS-CoV-2）はようやく世界各地で収束しつつある。現在のオミクロン変異株JN.1の場合でも、mRNAワクチンの繰返し接種のおかげで、たとえ感染はしても重症化することはなくなり、インフルエンザと変わらぬ風邪ウイルスの一種と見なせるほど制御可能となってきた。こうした感染防御の役割を担うのは、ワクチン接種や感染後に得られる獲得免疫やそれらに即座に反応する自然免疫だけでなく、第三の免疫と呼ばれる「内因性免疫」が挙げられる。この働きを担うタンパク質としてヒト細胞が有する抗ウイルス宿主因子のいくつかが、SARS-CoV-2やHIV-1を始めとする種々の病原性ウイルスに対しても有効であることがこれまで数多く報告されている。こうした宿主因子によるウイルス感染防御に関する知見を得るとともに、将来的な感染再拡大に対する予防戦略を構築することを目的とする。

2)戦略(Approach)： ウイルスの複製に関わる宿主因子の研究が最先端レベルで進んでいるレトロウイルス学に着手して、分子ウイルス学的研究手法および宿主因子に関する知見について学ぶ。指導教官である徳永研三先生のチームが2015年に発見してNature Medicine誌 (1) に報告した後に関連研究 (2-5) を次々と展開してきた「**(A)抗ウイルス宿主因子MARCH8**」について、さらなる機能解析に取り組んだ。また同時にウイルス複製に関わる宿主因子研究の一環として、HIV-1潜伏感染の制御機構を探るべく「**(B) 潜伏感染細胞モデルの樹立**」を試みた。

3)材料と方法(Materials and methods)

i) 細胞：

(A) ヒト胎児腎細胞293T (6) をトランスフェクション用に、MAGIC5細胞 (7) をウイルス感染用に使用した。サル（Rhesus macaque）、マウス、ウシMARCH8発現プラスミド作製用にRT-PCRの鋳型として必要な細胞RNAの抽出のために、それぞれアカゲザル網膜内皮細胞RF/6A (8)、マウス繊維芽細胞 NIH3T3 (9)、ウシ腎臓細胞MDBK (10)を用いた。

(B) トランスフェクション用に293Tを、ウイルス感染用に293T細胞、MAGIC5細胞およびMOLT-4細胞 (11)を使用した。

ii) プラスミドDNA：

(A) シュードウイルス作製用にHIV-1エンベロープ糖タンパク質（Env）発現プラスミド pC-NLenv (1)、水胞性口炎ウイルスGタンパク質（VSV-G）発現プラスミド pC-VSVg (1)、HIV-1 Env欠損型ルシフェラーゼレポーターウイルスDNA pNL-Luc2-IN/HiBiT-E(-)Fin (12)を用いた。またヒトMARCH8発現プラスミドとしてpC-MARCH8 (1)、RING-CH変異型MARCH8発現プラスミド pC-MARCH8-W114A (1)、チロシンモチーフ変異型MARCH8発現プラスミド pC-MARCH8-222AxxL225 (2)を用いた

(B) シュードウイルス作製用に水胞性口炎ウイルスGタンパク質（VSV-G）発現プラスミド pC-VSVg (4)、Gag-Pol発現HiBiT-tagプラスミドpsPAX2-IN/HiBiT (5)を、HIV-1ミニジーン作製用にHIV-1 Env欠損型ルシフェラーゼレポーターウイルスDNA pNL-Luc2-IN/HiBiT-E(-)Fin (5) を、用いた。CRISPR/Cas9によるノックアウトには Tat標的型pLentiCRISPRv2-tat3 (6) を用いた。

iii) プラスミド構築：

(A) RF/6A、NIH3T3、およびMDBK細胞からReliaprep RNA Cell Miniprep system (Promega; Z6010)を用いて細胞RNAを抽出し、PrimeScript One Step RT-PCR Kit Ver. 2（Takara; RR057A） によりRT-PCR増幅を行った。得られたDNA断片を電気泳動後にアガロースゲルから切り出してQIAquick PCR Purification Kit（QIAGEN; 28104）を用いて精製した。さらに制限酵素 KpnI/XhoI で処理した最終断片を同じく KpnI/XhoI で処理した哺乳類細胞発現プラスミドpCAGGSに挿入した。各々のRING-CH変異体およびチロシンモチーフ変異体を作製するため、3種類の動物由来の野生型MARCH8を鋳型に乗換えPCRを行い、増幅した KpnI/XhoI 断片をpCAGGSに挿入した。またこれら全てのN末HA-tag版も作製した。作製した全ての発現プラスミドはGenewiz遺伝子解析サービスにより遺伝子配列の確認を行った。

(B) StayGold（SG）発現プラスミドまたはEGFP発現プラスミドを鋳型に、それぞれSG遺伝子またはEGFP遺伝子のPCR増幅を行った。得られたDNA断片を電気泳動後にアガロースゲルから切り出してQIAquick PCR Purification Kit（QIAGEN; 28104）を用いて精製した。さらに制限酵素 NotI/XhoI で処理した最終断片を、同じく NotI/XhoI で処理したHiBiTタグ付加全長HIV-1プロウイルスLuc2レポーターDNA pNL-Luc2-IN/HiBiT-E(-)Fin (12) のLuc2遺伝子と置換した。また前者からgag-pol-vif-vpr領域を一挙に欠損させVpu遺伝子開始コドンを潰すことにより構造遺伝子envと制御遺伝子tat-revのみ発現するHIV-1遺伝子を作製し初代HIV-1ミニジーンとした。それを基にSG遺伝子下流にIRES-Luc2遺伝子を挿入したプラスミドを第2世代HIV-1ミニジーンとし、さらにCD4陽性細胞で感染させる場合のCD4によるEnvト発現抑制を回避するためにnef/vpuを復活させたプラスミドを第3世代HIV-1ミニジーンとした。また第3世代は元のNL-Env型（CXCR4指向性 [X4]）に加えADA-ENV型（CCR5指向性 {R5}）も作製した。構築した全ての発現プラスミドの遺伝子配列の確認はGenewiz遺伝子解析サービスにより行った。

iv) トランスフェクション：

(A) pC-NLenvまたはpC-VSVg（20 ng）をpNL-Luc2-IN/HiBiT-E(-)Fin（500 ng）と各動物由来の野生型または変異型MARCH8発現プラスミド（0、60、120 ng）、さらに空プラスミドpCAGGS（480、420、360 ng）と共に、FuGENE6 Transfection Reagent（Promega; E2691）を用いて2.5×10^5個の293T細胞にコトランスフェクションした。

(B) SGレポーターHIV-1プラスミドまたはレポーターHIV-1プラスミド（500 ng）をpC-VSVg（20 ng）と空プラスミド（480 ng）と共に、第1世代ミニジーンpNL-TatRevEnv-SG、または第2世代（450 ng）をGag-Pol発現HiBiT-tagプラスミドpsPAX2-IN/HiBiT（450 ng）とpC-VSVg（20 ng）と空プラスミドpCAGGS（80 ng）と共に、FuGENE6 Transfection Reagent（Promega; E2691）を用いて2.5×10^5個の293T細胞にコトランスフェクションした。または第3世代HIV-1-X4ミニジーンあるいはHIV-1-R5ミニジーン（500 ng）をpsPAX2-IN/HiBiT（500 ng）と共に、同細胞数の293T細胞にFuGENE6でコトランスフェクションした。CRISPRノックアウト用にpLentiCRISPRv2-tat3またはコントロール（450 ng）、psPAX2-IN/HiBiT（450 ng）、pC-VSVg（20 ng）と空プラスミドpCAGGS（80 ng）を同細胞数の293T細胞にFuGENE6でコトランスフェクションした。

1．研究概要(2)
3)材料と方法(Materials and methods) つづき
v) ウイルス定量:
(A, B) トランスフェクションの16時間後に293T細胞をPBSで洗浄して、更に24時間後に7.5 U/ml DNase I (Roche Applied Science; 11284932001)で処理した培養上清またはp24量が既知の標準ウイルス25 μLを、等量のHiBiT Lytic Substrate (1:50) in Nano-Glo HiBiT Lytic Buffer(Nano-Glo HiBiT Lytic Detection System; Promega; N3030)と混合して、10分間室温静置した後、Centro LB960 luminometer (Berthold)を用いてHiBiTルシフェラーゼ活性を測定した。
vi) 感染性アッセイ:
(A, B)各培養上清のHiBiTルシフェラーゼ活性をp24量に換算した後、1ng p24相当のウイルスを、(A)の実験または第2世代HIV-1ミニジーン由来VSVシュードウイルスまでは1.2 x 10^4個の293T細胞に、第3世代ADA-Envウイルスは1 x 10^4個のMAGIC5細胞に、また第3世代NL-Envウイルスでは1 x 10^4個のMAGIC5細胞およびCD4陽性T細胞株MOLT-4(2 x 10^4個)に感染させた。それぞれのウイルスを各細胞に感染させた後、第1世代HIV-1ミニジーン由来ウイルスまでは蛍光顕微鏡Fluoview FV1000-IX81 (Olympus)により経時的(2、24、26、36日)に蛍光観察のみを行った。第2世代以降は、蛍光顕微鏡観察に加えて、経時的に感染細胞を100 μLの One-Glo Luciferase Assay Reagent (Promega; E6110).で溶解してホタルルシフェラーゼ活性を Centro LB960ルミノメーター(Berthold)によって測定した。
vii) ウエスタンブロッティング:
(Aのみ) 各N末HA-tag付加MARCH8発現プラスミド(500 ng)と 空プラスミドpCAGGS(500 ng)を、FuGENE6を用いて2.5×105個の293T細胞にトランスフェクションした。48時間後に200 μLの細胞溶解液を加えてSDS-PAGEを行った後、PVDF膜に転写した。抗HA単クローン抗体 (Sigma; H9658)または抗β-actin単クローン抗体 (Sigma; A5316)を反応させ、Western ECL Substrate(Biorad; 1705061)で可視化した後、LAS-3000 imaging system (FujiFilm)で検出した。
vii) インテグレーション確認のためのDNA PCR:
(Bのみ) 経時的に感染細胞を回収し、DNeasy Blood & Tissue Kit(QIAGEN; 69504)により抽出した細胞DNAを鋳型に、StayGold遺伝子を標的としたPCRをPrimeSTAR Max Premix (Takara;R045Q)を用いて行い、アガロースの電気泳動によりHIV-1プロウイルスDNAの有無を確認した。
viii) CRISPRノックアウト:
(Bのみ) 第3世代HIV-1ミニジーン由来ウイルスを感染させたMAGIC5に対し、Tatを標的とするTat3-CRISPRレンチウイルスベクターまたはコントロールのCRISPRレンチウイルスベクターを用いてトランスダクションを行った。ノックアウト効率を検証するため、蛍光顕微鏡観察およびルシフェラーゼアッセイを実施した。
4)実験結果(Results)
(A) トランスフェクションおよびウエスタンブロッティング実験により、今回新たに作製したMARCH8発現プラスミドは全て同レベルで正常に発現していることが確認できた。動物種別MARCH8のHIV-1 EnvおよびVSV-Gに対する抑制効果について、感染性アッセイにより検討した結果、ヒトMARCH8と同様、サル、マウス、およびウシMARCH8の野生型はHIV-1 EnvとVSV-Gに対する量依存的な抑制能を保持していた。その一方でRING-CH変異型およびチロシンモチーフ変異型MARCH8はどちらも抑制活性を失っていた。
(B) SG発現ウイルスとEGFP発現ウイルスのMAGIC5細胞への感染後の蛍光比較において、SG発現ウイルスの方がEGFP発現ウイルスよりも圧倒的な蛍光強度と光安定性を示すことが明らかになった。次にHIV-1から全てのアクセサリー遺伝子とgag-pol領域を取り除いた第1世代HIV-1ミニジーン由来ウイルスの感染実験において、蛍光顕微鏡観察を行った結果、感染後4週間程度かけて徐々に蛍光レベルが低下していくことが分かった。また簡易に感染後の遺伝子発現を定量化できるようにLuc2遺伝子を導入した第2世代ウイルス、およびCD4陽性細胞株に対する感染を行った第3世代ウイルスでは、蛍光レベルに加えてルシフェラーゼ活性の経時的低下も確認できた。また細胞DNAのPCRにより、蛍光及びルシフェラーゼ活性が消失した後も、HIV-1プロウイルスDNAが確かに存在することを明らかにした。また持続感染細胞に対するTatを標的としたCRISPRノックアウトは非常に効率よくHIV-1プロウイルスDNAを破壊できることが明らかになった。
5)考察(Discussion)
(A) MARCH8の抗ウイルスエンベロープ活性およびその機能領域は、異なる動物種間(ヒト、サル、マウス、およびウシ)で高度に保存されていることが明らかになった。
(B) 本研究において、完全長のHIV-1ではなく、HIV-1ミニジーンを利用した潜伏感染実験系を組むことにより、よりHIV-1の潜伏状態をsimplifyするとともに、新規蛍光タンパク質SGを用いることで更に潜伏状態を容易に可視化することが可能となった。この潜伏状態を制御する宿主側の要因を探るために、今後CRISPRライブラリーを用いたスクリーニングによって関連因子の同定を試みたい。またCRISPRノックアウトによるHIV-1破壊効率は良いものの、完全ではないことから、挿入箇所特異的なノックアウト効率の違いが認められるか否かについて今後検討する。さらに今後、HIV-1 LTRを標的とした活性化型CRISPRにより潜伏感染細胞を再活性化させ、それによって発現するEnvを認識して排除するシステムの構築に取り組みたい。
6)参考文献(References)
1. Tada, T., Zhang, Y., Koyama, T., Tobiume, M., Tsunetsugu-Yokota, Y., Yamaoka, S. et al. (2015) MARCH8 inhibits HIV-1 infection by reducing virion incorporation of envelope glycoproteins Nat Med 21:1502-1507.
2. Zhang, Y., Tada, T., Ozono, S., Kishigami, S., Fujita, H., and Tokunaga, K. (2020) MARCH8 inhibits viral infection by two different mechanisms Elife 9:e57763.
3. Tada, T., Zhang, Y., Fujita, H., and Tokunaga, K. (2022) MARCH8: the tie that binds to viruses FEBS J 289:3642-3654.
4. Zhang, Y., Ozono, S., Tada, T., Tobiume, M., Kameoka, M., Kishigami, S. et al. (2022) MARCH8 Targets Cytoplasmic Lysine Residues of Various Viral Envelope Glycoproteins Microbiol Spectr 10:e0061821.
5. Zhang, Y., Tada, T., Ozono, S., Yao, W., Tanaka, M., Yamaoka, S. et al. (2019) Membrane-associated RING-CH (MARCH) 1 and 2 are MARCH family members that inhibit HIV-1 infection J Biol Chem 294:3397-3405.
6. Pear, W. S., Nolan, G. P., Scott, M. L., and Baltimore, D. (1993) Production of high-titer helper-free retroviruses by transient transfection Proc Natl Acad Sci U S A 90:8392-8396.
7. Hachiya, A., Aizawa-Matsuoka, S., Tanaka, M., Takahashi, Y., Ida, S., Gatanaga, H. et al. (2001) Rapid and simple phenotypic assay for drug susceptibility of HIV-1 using CCR5-expressing HeLa/CD4(+) cell clone 1-10 (MAGIC-5) Antimicrob Agents Chemother 45:495-501.
8. Hu, F., Mah, K., andTeramura, D. J. (1986) Gossypol effects on cultured normal and malignant melanocytes In Vitro Cell Dev Biol 22:583-588.
9. Todaro, G. J., and Green, H. (1963) Quantitative studies of the growth of mouse embryo cells in culture and their development into established lines J Cell Biol 17:299-313.
10. Madin, S. H., andDarby, N. B., Jr. (1958) Established kidney cell lines of normal adult bovine and ovine origin Proc Soc Exp Biol Med 98:574-576.
11. Minowada, J., Onuma, T., and Moore, G. E. (1972) Rosette-forming human lymphoid cell lines. I. Establishment and evidence for origin of thymus-derived lymphocytes J Natl Cancer Inst 49:891-895.
12. Ozono, S., Zhang, Y., Tobiume, M., Kishigami, S., and Tokunaga, K. (2020) Super-rapid quantitation of the production of HIV-1 harboring a uminescent peptide tag J Biol Chem 295:13023-13030.

2. 執筆論文 Publication of thesis ※記載した論文を添付してください。Attach all of the papers listed below.

論文名 1 Title	Repetitive mRNA vaccination is required to improve the quality of broad-spectrum anti-SARS-CoV-2 antibodies in the absence of CXCL13. Sci. Adv. 9:eadg2122. 2023.					
掲載誌名 Published journal	Science Advances					
	2023 年 8 月	9 巻(号)	eadg2122頁 ～ 頁	言語 Language	English	
第1著者名 First author	Azarias Da Silva, M.	第2著者名 Second author	Nioche, P.	第3著者名 Third author	Soudaramourty, C.	
その他著者名 Other authors	Bull-Maurer, A., Tiouajni, M., Kong, D., Zghidi-Abouzid, O., Picard, M., Mendes-Frias, A., Santa-Cruz, A., Carvalho, A., Capela, C., Pedrosa, J., Castro A.G., Loubet, P., Sotto, A., Muller, L., Lefrant, J.Y., Roger, C., Claret, P.G., Duvnjak, S., Tran, T.A., Tokunaga, K., Silvestre, R., Corbeau, P., Mammano, F., Estaquier, J.					
論文名 2 Title						
掲載誌名 Published journal						
	年 月	巻(号)	頁 ～ 頁	言語 Language		
第1著者名 First author		第2著者名 Second author		第3著者名 Third author		
その他著者名 Other authors						
論文名 3 Title						
掲載誌名 Published journal						
	年 月	巻(号)	頁 ～ 頁	言語 Language		
第1著者名 First author		第2著者名 Second author		第3著者名 Third author		
その他著者名 Other authors						
論文名 4 Title						
掲載誌名 Published journal						
	年 月	巻(号)	頁 ～ 頁	言語 Language		
第1著者名 First author		第2著者名 Second author		第3著者名 Third author		
その他著者名 Other authors						
論文名 5 Title						
掲載誌名 Published journal						
	年 月	巻(号)	頁 ～ 頁	言語 Language		
第1著者名 First author		第2著者名 Second author		第3著者名 Third author		
その他著者名 Other authors						

3. 学会発表 Conference presentation ※筆頭演者として総会・国際学会を含む主な学会で発表したものを記載してください

※Describe your presentation as the principal presenter in major academic meetings including general meetings or international meetin

学会名 Conference	第70回日本ウイルス学会				
演 題 Topic	The development of in vitro HIV-1 latency models using a viral minigene system.				
開催日 date	2023 年 9 月 27 日	開催地 venue	仙台		
形式 method	□ 口頭発表 Oral ☑ ポスター発表 Poster	言語 Language	□ 日本語 ☑ 英語 □ 中国語		
共同演者名 Co-presenter	Seiya Ozono, Masanori Kameoka, Takamasa Ueno, and Kenzo Tokunaga				
学会名 Conference	24th Kumamoto AIDS Seminar				
演 題 Topic	HIV-1 minigene system to establish an in vitro latency model.				
開催日 date	2023 年 11 月 6 日	開催地 venue	熊本		
形式 method	□ 口頭発表 Oral ☑ ポスター発表 Poster	言語 Language	□ 日本語 ☑ 英語 □ 中国語		
共同演者名 Co-presenter	Seiya Ozono, Masanori Kameoka, Takamasa Ueno, and Kenzo Tokunaga				
学会名 Conference					
演 題 Topic					
開催日 date	年 月 日	開催地 venue			
形式 method	□ 口頭発表 Oral □ ポスター発表 Poster	言語 Language	□ 日本語 □ 英語 □ 中国語		
共同演者名 Co-presenter					
学会名 Conference					
演 題 Topic					
開催日 date	年 月 日	開催地 venue			
形式 method	□ 口頭発表 Oral □ ポスター発表 Poster	言語 Language	□ 日本語 □ 英語 □ 中国語		
共同演者名 Co-presenter					

4. 受賞（研究業績） Award (Research achievement)

名 称 Award name				
	国名 Country		受賞年 Year of award	年 月
名 称 Award name				
	国名 Country		受賞年 Year of award	年 月

5. 本研究テーマに関わる他の研究助成金受給 Other research grants concerned with your resarch theme

受給実績 Receipt record	☐ 有　☐ 無
助成機関名称 Funding agency	
助成金名称 Grant name	
受給期間 Supported period	年　月 ～　年　月
受給額 Amount received	円
受給実績 Receipt record	☐ 有　☐ 無
助成機関名称 Funding agency	
助成金名称 Grant name	
受給期間 Supported period	年　月 ～　年　月
受給額 Amount received	円

6. 他の奨学金受給 Another awarded scholarship

受給実績 Receipt record	■ 有　☐ 無
助成機関名称 Funding agency	熊本大学
奨学金名称 Scholarship name	熊本大学大学院博士課程奨学金給付制度（KDS）（私費留学生枠）
受給期間 Supported period	2021 年 4 月 ～ 2022 年 4 月
受給額 Amount received	1,054,600 円

7. 研究活動に関する報道発表 Press release concerned with your research activities

※記載した記事を添付してください。Attach a copy of the article described below

報道発表 Press release	☐ 有　☐ 無	発表年月日 Date of release	
発表機関 Released medium			
発表形式 Release method	・新聞　・雑誌　・Web site　・記者発表　・その他（　　）		
発表タイトル Released title			

8. 本研究テーマに関する特許出願予定 Patent application concerned with your research theme

出願予定 Scheduled	☐ 有　☐ 無	出願国 Application	
出願内容（概要） Application contents			

9. その他 Others

JSTさくらサイエンスオンラインプログラム（2022年11月29日～12月3日）におけるZoom講演
「Exchange and share experiences in daily life as a doctoral course student in Tokyo, Japan.」

指導責任者（記名）　徳永　研三

CORONAVIRUS

Repetitive mRNA vaccination is required to improve the quality of broad-spectrum anti–SARS-CoV-2 antibodies in the absence of CXCL13

Marne Azarias Da Silva[1], Pierre Nioche[1,2], Calaiselvy Soudaramourty[1], Anne Bull-Maurer[3], Mounira Tiouajni[1,2], Dechuan Kong[4,5], Ouafa Zghidi-Abouzid[6], Morgane Picard[1], Ana Mendes-Frias[7,8], André Santa-Cruz[7,8,9], Alexandre Carvalho[7,8,9], Carlos Capela[7,8,9], Jorge Pedrosa[7,8], António Gil Castro[7,8], Paul Loubet[10], Albert Sotto[10], Laurent Muller[11], Jean-Yves Lefrant[11], Claire Roger[11], Pierre-Géraud Claret[12], Sandra Duvnjak[13], Tu-Anh Tran[14], Kenzo Tokunaga[5], Ricardo Silvestre[7,8], Pierre Corbeau[15,16], Fabrizio Mammano[1,3]†, Jérôme Estaquier[1,6]†*

Since the initial spread of severe acute respiratory syndrome coronavirus 2 infection, several viral variants have emerged and represent a major challenge for immune control, particularly in the context of vaccination. We evaluated the quantity, quality, and persistence of immunoglobulin G (IgG) and IgA in individuals who received two or three doses of messenger RNA (mRNA) vaccines, compared with previously infected vaccinated individuals. We show that three doses of mRNA vaccine were required to match the humoral responses of preinfected vaccinees. Given the importance of antibody-dependent cell-mediated immunity against viral infections, we also measured the capacity of IgG to recognize spike variants expressed on the cell surface and found that cross-reactivity was also strongly improved by repeated vaccination. Last, we report low levels of CXCL13, a surrogate marker of germinal center activation and formation, in vaccinees both after two and three doses compared with preinfected individuals, providing a potential explanation for the short duration and low quality of Ig induced.

INTRODUCTION

Since the initial SARS-CoV-2 (severe acute respiratory syndrome coronavirus 2) pandemic related to the Wuhan strain (*1*), several viral variants have emerged. These variants, particularly Beta (B.1.351), Delta (B.1.617.2), and, more recently, diverse Omicron subtypes, represent a major challenge for immune control, especially in the context of vaccination. Most of the mutations that differentiate these strains from the original isolate are localized in the two domains of the spike (S) protein shown to be targeted by neutralizing antibodies (*2*–*4*): the receptor binding domain (RBD) that interacts with the angiotensin II (ACE2) receptor and the N-terminal domain (NTD).

Current vaccines, such as those manufactured by Pfizer/BioNTech (BNT162b2) and by Moderna/National Institute of Allergy and Infectious Diseases (mRNA-1273), encode for an S protein whose sequence is similar to the early Wuhan-Hu viral isolate. The emergence of viral variants has consequently challenged vaccine effectiveness. Initial reports have shown lower levels of recognition of Beta and Delta variants, even after the second dose of vaccine (*5*–*8*). The recently emerged Omicron variants were reported to be less efficiently neutralized than the Wuhan-Hu strain by immunoglobulin G (IgG) from vaccinated individuals even after a third dose (*9*–*15*) and by therapeutic neutralizing antibodies (*16*–*18*).

Beyond neutralizing antibody, it has been shown that Fc effector mechanisms including antibody-dependent complement deposition, antibody-dependent neutrophil phagocytosis, and antibody-dependent cellular cytotoxicity responses may contribute in the control of viral dissemination by clearing viral-infected cells and limiting disease severity (*19*, *20*). We recently demonstrated that the amount of IgG capable to recognize the Wuhan-Hu S-protein on cell surface of transfected cells are lower in patients with severe coronavirus 2019 (COVID-19), and this was associated with frequent CD4 T cell apoptosis (*21*, *22*). Furthermore, it has been suggested that antibody cellular effector functions induced by mRNA vaccine are preserved despite the loss of Omicron neutralization, indicating a disconnection between the requirements for quantity and quality of antibodies for the two functions (*23*). An incomplete natural immunity against variants has been also reported in convalescent individuals (*24*), who displayed lower quality of Fc-mediated antibody responses compared to individuals vaccinated with two

[1]INSERM-U1124, Université Paris Cité, Paris, France. [2]Structural and Molecular Analysis Platform, BioMedTech Facilities INSERM US36-CNRS UMS2009, Université Paris Cité, Paris, France. [3]Université de Tours, INSERM, UMR1259 MAVIVH, Tours, France. [4]Joint Research Center for Human Retrovirus Infection, Kumamoto University, Kumamoto, Japan. [5]Department of Pathology, National Institute of Infectious Diseases, Tokyo, Japan. [6]CHU de Québec-Université Laval Research Center, Québec City, Québec, Canada. [7]Life and Health Sciences Research Institute (ICVS), School of Health Sciences, University of Minho, Braga, Portugal. [8]ICVS/3B's-PT Government Associate Laboratory, Braga/Guimarães, Portugal. [9]Department of Internal Medicine, Hospital of Braga, Braga, Portugal. [10]Service des Maladies Infectieuses et Tropicales, CHU de Nîmes, Nîmes, France. [11]Service de Réanimation Chirugicale, CHU de Nîmes, Nîmes, France. [12]Urgences Médico-Chirugicales Hospitalisation, CHU de Nîmes, Nîmes, France. [13]Service de Gérontologie et Prévention du Vieillissement, CHU de Nîmes, Nîmes, France. [14]Service de Pédiatrie, CHU de Nîmes, Nîmes, France. [15]Institut de Génétique Humaine, UMR9002 CNRS-Université de Montpellier, Montpellier, France. [16]Laboratoire d'Immunologie, CHU de Nîmes, Nîmes, France.
*Corresponding author. Email: jerome.estaquier@crchudequebec.ulaval.ca
†These authors contributed equally to this work.

doses of mRNA-1273 (*25*). Nevertheless, convalescents individuals boosted with vaccine are better protected against reinfection than vaccinated alone with two doses of vaccine (*26*–*28*).

While most of the studies have assessed the role of neutralizing IgG, little is known about mucosal humoral response induced by vaccines. Studies including ours have shown that, early after SARS-CoV-2 infection, a dominant IgA humoral response is induced against the nucleocapsid (N) and S proteins (*29*, *30*). The presence of IgA in vaccinated individuals would be extremely important in the event of further contact with the virus, particularly during the first days of infection. The IgA in the mucosal tissue could limit viral dissemination and disease outcome, but little is known on the delay and durability of this response in individuals, with or without previous infection, who have received a vaccine boost.

Although the beneficial effect of vaccination is well established (*31*, *32*) and vaccinees mount a competent humoral response against SARS-CoV-2 (*33*–*37*), repetitive vaccination campaigns have been necessary to maintain an efficient humoral response capable of preventing severe forms and hospitalization. The requirement for repetitive doses to improve humoral response and cross-reactivity suggests a short half-life of the antibodies induced in the absence of boost and probably a low avidity response. Paradoxically, few studies have determined the avidity of Ig in vaccinated individuals, which reflect antibody maturation following germinal center (GC) formation (*38*, *39*). In this context, measuring the level of chemokine (C-X-C motif) ligand 13 (CXCL13) in the blood may represent an interesting biomarker of GC activation in humans associated with protective humoral response following vaccination (*40*–*42*).

In this study, we evaluated the humoral response of vaccinated individuals, some of whom had also been infected during the first wave of SARS-CoV-2 in 2020, before vaccines became available. By analyzing both the quantity and quality of IgG and IgA, our results demonstrated that the amount and persistence of Ig were higher in individuals previously exposed to the virus and boosted with vaccine compared to vaccinated-only individuals. Three doses of mRNA vaccine were required to improve the quantity, quality, and cross-reactivity against Beta and Omicron variants. We found difference in recognition among Omicron subtypes, between vaccinees only and preinfected individuals. Thus, mRNA vaccine induced Ig capable to recognize variant S proteins expressed on cell surface that is of major importance for Fc-mediated function by vaccines. While CXCL13 levels are high during the acute phase of SARS-CoV-2 infection, vaccine administration, even after the third dose, has no impact on the levels of CXCL13 detected in the plasma. This result may help to explain why booster vaccination induces a potent humoral response in previously infected patients compared with vaccinated-only individuals who require at least three doses of vaccine to reach similar levels of humoral response. Thus, our work provides a framework to explain the need for repeated immunizations to provide stronger and longer-lasting humoral responses, which might contribute to controlling viral dissemination even against variants of concern.

RESULTS

Three mRNA vaccinations are required for IgG and IgA responses similar to those of convalescent and boosted individuals

To determine the impact of mRNA vaccination boosts, we analyzed humoral responses in different groups of donors (Fig. 1A). Individuals included (i) nonvaccinated convalescent individuals, from whom samples were collected 6 months after SARS-CoV-2 infection (Pre; n = 17); (ii) convalescent individuals vaccinated with BNT162b2 (1 to 3 months after vaccination, Pre + V; n = 15), so called hybrid immune responders; and (iii) individuals only vaccinated with two doses (n = 9, samples collected at two time points: V2,1-3M, 1 to 3 months after vaccination and V2,4-6M, 4 to 6 months after vaccination) or (iv) with three doses of mRNA vaccines (1 to 2 months after vaccination, V3,1-2M; n = 13) and a group of naïve individuals as a negative control (naïve, n = 31). All convalescent individuals were infected between March and December 2020, when only the original strain and the Alpha variant were circulating in Europe. As indicated in Table 1, five individuals received the Moderna vaccine for their third dose, whereas all the others only received the Pfizer formulation. We first assessed the levels of specific antibodies against the S1 and N antigens by ELISA (enzyme-linked immunosorbent assay) as previously described (*16*). This latter antigen was used as a marker to follow individuals that may have been infected with SARS-CoV-2. The optical density (OD) values of the ELISA performed with patients' plasma are shown in Fig. 1 (B to E). As expected, anti-N IgG were detected in convalescent individuals irrespective of their vaccination status but not in vaccinated-only individuals (Fig. 1B) nor in the naïve group. Although the OD values of anti-N IgG antibodies were significantly different (P = 0.048), the levels of anti-S1 IgG were clearly higher in convalescents boosted with a vaccine dose (hybrid immunity, Pre + V: 3.37 ± 0.22) compared with nonvaccinated convalescent individuals (Pre: 1.57 ± 0.43, P < 0.0001) both at

Table 1. Characteristics of individuals included in this study. M, male; F, female.

Groups/vaccine	*N*	Pfizer (BNT162b2)	Moderna (mRNA-1273)	Age, years Median [Range]	Gender	
					M	F
Pre: Convalescents 6 months after infection	17			67 [52–87]	11	6
Pre + V: Convalescents + vaccine (1 to 3 months after vaccination)	15	15		56 [25–81]	5	10
V2,1-3M: Vaccinated two doses (1 to 3 months after vaccination)	9	9		46 [12–85]	5	4
V2,4-6M: Vaccinated two doses (4 to 6 months after the vaccination)	9	9		57 [28–85]	4	5
V3,1-2M: Vaccinated three doses (1 to 2 months after the vaccination)	13	8	5	54 [12–85]	7	6

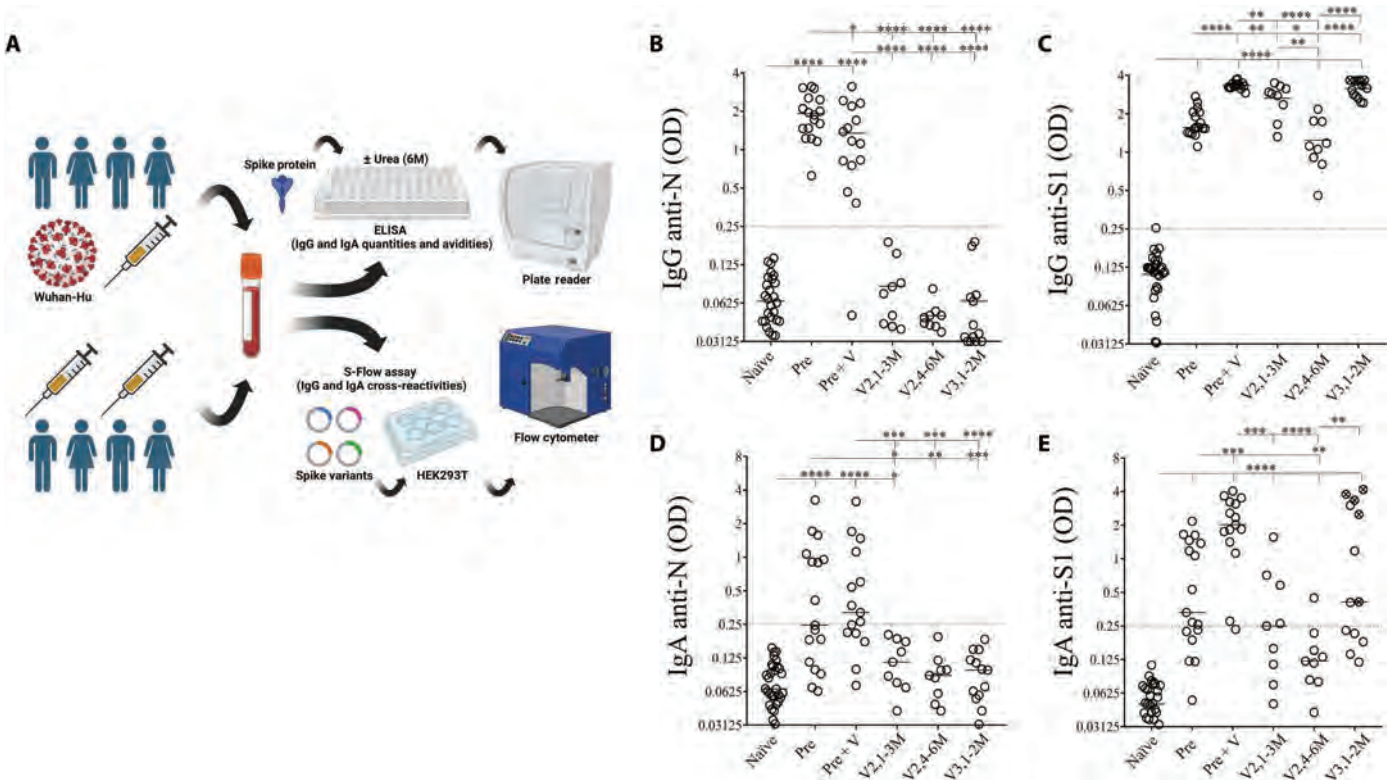

Fig. 1. IgG response against the N and spike proteins in convalescents and vaccinated individuals. (**A**) Plasma from healthy donors (naïve) convalescent individuals (Pre), convalescent individuals boosted with vaccine (Pre + V), vaccinees after two doses either at months 1 to 3 (V2,1-3M) or months 4 to 6 (V2,4-6M), and after three doses at months 1 to 2 (V3,1-2M) were diluted to 1/400. (**B** to **E**) Plasma from healthy donors (naïve) convalescent individuals (Pre), convalescent individuals boosted with vaccine (Pre + V), vaccinees after two doses either at months 1 to 3 (V2,1-3M) or months 4 to 6 (V2,4-6M), and after three doses at months 1 to 2 (V3,1-2M) were diluted to 1/400. (B) and (C) Specific immunoglobulin G (IgG) and (D) and (E) IgA were tested against the nucleocapsid (N) and spike (S1) proteins. Optical density (OD) is shown. Each circle represents one individual. Lines represent median values. Dashed lines represent antibody specificity (OD = 0.25) in comparison with IgG and IgA from healthy donors. Statistical analysis was performed using a Mann-Whitney *U* test (*$P < 0.05$; **$P < 0.01$; ***$P < 0.001$; ****$P < 0.0001$). (C) and (E) Symbols with a cross represent individuals who received at least one dose of mRNA-1273, whereas open symbols represent individuals who only received BNT162b2 in the vaccination scheme.

1/400 (Fig. 1C) and 1/800 dilutions (fig. S1). This difference may in part be due to the longer time after exposure of the convalescent individuals (6 months) as compared to convalescent and vaccinated individuals (1 to 3 months). Only one individual had anti-N IgG antibodies below the positive threshold. Notably, the levels of specific anti-S1 IgG, 1 to 3 months after the second dose, remained lower (V2,1-3M: 2.88 ± 0.73) than those observed in convalescents receiving one dose of vaccine (Pre + V: 3.37 ± 0.22, $P = 0.0035$; Fig. 1C). The OD values of anti-S1 IgG were lower 4 to 6 months after the second dose (V2,4-6M: 1.12 ± 0.54) and increased again, boosted by the third dose (V3,1-2M: 3.24 ± 0.48).

Having observed differences in the IgG response between vaccinated individuals and those previously infected with SARS-CoV-2, we then compared their IgA responses. We and others have shown that humoral response against the S protein also includes IgA (*21*, *43*–*45*). Furthermore, IgA were reported to dominate the early antibody response to SARS-CoV-2 (*21*, *29*). The presence of IgA, boosted by the mRNA vaccine, could be of importance, since IgA is the most abundant antibody isotype in the mucosa, where these antibodies provide the first line of immune defense against pulmonary viral infections (*46*). Like IgG, specific IgA were assessed by ELISA at the same dilution in plasma (1/400). In convalescent individuals (Pre), we found specific IgA against the N (8 of 17) and S1 (10 of 17) proteins (Fig. 1, D and E, respectively). The OD values of IgA (Fig. 1, D and E) were significantly lower than those observed for the IgG (Fig. 1, B and C). This was observed both for Ig anti-N (Pre, $P < 0.0001$ and Pre + V, $P = 0.0209$) and for anti-S (Pre, $P = 0.0002$ and Pre + V, $P = 0.0027$). IgA response against S was improved by mRNA boost (hybrid patients, Pre + V: 1.93 ± 1.20) compared to convalescent individuals without vaccination (Pre, 0.33 ± 0.69; Fig. 1E). Our results highlighted that two doses of mRNA induce low levels of IgA against S1 (V2,1-3M: 4 of 10 individuals were responders), which declined after 4 to 6 months (V2,4-6M: 1 of 10 individuals were responders). After the third dose, more than half of vaccinated individuals (8 of 13) developed high level IgA responses (Fig. 1E). Of interest, IgA levels were higher in individuals who received one dose of mRNA-1273 compared to individuals who received only BNT162b2 (OD, 3.35 ± 1.5 and 0.22 ± 1.1, respectively, $P = 0.01$), whereas this difference was lower for IgG response (OD: mRNA-1273, 3.63 ± 0.14 and BNT162b2, 2.8 ± 0.41, $P = 0.01$). Together, our results confirm the need for repeated administration of mRNA vaccines, with at least three doses to induce a humoral response against S like that seen in individuals previously infected by SARS-CoV-2 and boosted with mRNA vaccine.

Repeated mRNA vaccinations improve IgG and IgA responses to recognize viral variants although Beta and Omicron BA.1 remain of concern

In addition to neutralization, antibodies contribute to clearing viral-infected cells through different mechanisms limiting viral dissemination and have recently been described as participating in immune defense against SARS-CoV-2 (*19*). To assess the recognition of viral proteins by antibodies present in patients′ plasma, the S-Flow assay relies on transfected cells expressing the S protein on the cell surface using flow cytometry (*16*, *47*). Transfection of plasmids encoding the S protein does not require biosafety level 3 confinement and allows to test recent isolates without the need for replication-competent virus isolation. Before using transfected cells, we assessed whether antibodies present in the plasma of vaccinees and convalescent individuals were capable to recognize viral antigens on the surface of Wuhan-Hu infected cells (fig. S2). Whereas we clearly detected infected cells compared to uninfected cells, one cannot formally assume that S was the sole antigen present on cell surface.

We then analyzed the ability of IgG to cross-recognize viral variants by expressing S proteins on the cell surface upon transfection. To normalize the data for each variant, the results were expressed as the percentages of cells recognized by the patient′s plasma, while a specific monoclonal antibody recognizing transfected cells against S2 was used as a positive control and attributed a value of 100% (fig. S3). Figure 2 shows the specific detection of S proteins by flow cytometry. Plasma from a healthy donor (Fig. 2A) did not recognize transfected cells, whereas plasma from a vaccinated convalescent individual recognized the S proteins of four viral variants, expressed on the cell surface (Fig. 2B). As expected, plasma from all convalescent individuals recognized the Wuhan-Hu strain (Pre: 75.5 ± 12.3%; Fig. 2C), whereas the percentages of S-Flow decreased for Delta (Pre: 68 ± 21%; Fig. 2D) and were extremely low for Beta and Omicron BA.1 (Pre: 7.6 ± 13.1 and 21 ± 18.2%, respectively; Fig. 2, E and F). Thus, convalescent individuals displayed low cross-reactivity. In contrast, convalescent individuals boosted with the mRNA vaccine (Pre + V) developed IgG that recognized all variants including Beta and Omicron. Vaccinated-only individuals demonstrated specific IgGs against the Wuhan-Hu (84.5 ± 19.5%) and Delta (65 ± 17.3%) after the second dose (V2,1-3M; Fig. 2, C and D). The percentages of S-Flow were lower for Beta (15 ± 20.1%) and BA.1 (37 ± 27.3%) compared to convalescent vaccinated individuals (Fig. 2, E and F). However, IgG reactivity markedly decreased at months 4 to 6 (V2,4-6M), including for the Wuhan-Hu strain, and was particularly low for Beta and BA.1 (17.5 ± 9.3 and 13 ± 7.9%, respectively; Fig. 2, E and F). Boosting humoral response with a third dose not only increased the levels of specific IgG against Wuhan-Hu and Delta (Fig. 2, C and D) but also induced significantly higher humoral responses against Beta and BA.1 (Fig. 2, E and F). Patients having received a dose of mRNA-1273 vaccine were better responders against BA.1 than those who received only three doses of BTN162b2 vaccine (S-Flow, 96 ± 5.3 versus 52.7 ± 18.6%, respectively, $P = 0.004$).

We had the opportunity to obtain sequential samples over more than 1 year after vaccination from three individuals (Fig. 3) including one convalescent individual who had been vaccinated (panel A), one vaccinated individual who was infected after the third dose (panel B), and a third one who had received four doses of the mRNA vaccine (panel C). For the three individuals, we found high levels of IgG after two exposures (natural or vaccine). After the third exposure, the levels of specific IgG antibodies plateaued for at least 6 months and were boosted in the third individual after an additional dose.

Assessing variant recognition, we found that, in the individual preinfected with SARS-CoV-2 and boosted with one dose of vaccine, IgGs were capable of recognizing all four viral strains (Fig. 3D). However, the levels of antibodies capable of recognizing Beta and BA.1 markedly decreased in comparison to Wuhan-Hu and Delta until the booster (Fig. 3D). The second dose improved humoral response against the four strains, although IgGs recognizing Beta remained lower. Likewise, in the second individual (Fig. 3E), IgG induced by vaccination recognized Wuhan-Hu and Delta strains, whereas the cross-reactivity of IgG against Beta and BA.1. rapidly declined. The third dose improved cross-reactivity against all four strains, although recognition of Beta was lower compared to the other strains. In this individual, who was infected after vaccination, recognition of the BA.1 variant rose markedly and reached the same level as for the Delta variant, which had been predominant before (Fig. 3E). Last, in the third individual (Fig. 3F), two doses of vaccine were not enough to generate IgG capable of recognizing the Beta strain (Fig. 3F). After the third dose, an increase was observed but Beta and BA.1 recognition declined over the 6-month interval (Fig. 3F). Despite an additional dose (Fig. 3F), IgG did not reach higher levels against Beta, and the percentages of cross-reactivity against Beta, Delta, and BA.1 remained lower compared to Wuhan-Hu and did not exceed 50% (Fig. 3F).

We then assessed IgA cross-reactivity (Fig. 4). In some convalescent individuals and in most of those who received a boost (10 of 14), IgA recognized the Wuhan-Hu (Fig. 4A). However, while individuals with two doses of mRNA vaccine had low levels of IgA, half of the vaccinees who had received a third dose (V3,1-2M) developed specific IgA (Fig. 4A). We then assessed variant cross-reactivities in this subgroup of IgA responders. Overall, we observed a low cross-reactivity with some individuals, either convalescents boosted with the vaccine (Pre + V) or vaccinees who had received three doses (V3,1-2M), maintained a cross-reactivity against Delta (Fig. 4B), but very few recognized Beta and BA.1 (Fig. 4, C and D). IgA from convalescents (Pre) were unable to recognize Delta, Beta, or BA.1.

Thus, these results demonstrated the efficacy that can be reached by repeated administrations of mRNA vaccine to induce IgG and IgA that may contribute to the elimination of infected cells. However, without natural infection, specific IgG do not persist for long time, low levels of IgA are produced, and one of the main concerns is the low recognition of Beta and BA.1 variants.

Structural analysis of RBD and NTD reveals potential regions in variants that may impact antibody recognition

Several studies have previously described the impact of mutations on viral infectivity and escape from recognition by monoclonal antibodies (mAbs) used in therapy, suggesting the importance of the RBD as well as the NTD (Fig. 5A) (*2*–*4*). Delta RBD mutations, which do not include N501Y, are L452R and T478K, and Omicron (BA.1) has seven mutations that map to the ACE2 binding footprint (K417N, S477N, Q493R, G496S, Q498R, N501Y, and Y505H; Fig. 5B, amino acids are indicated by an "*"). These mutations are mainly conserved in the other BA.2 variants of concern. Beta has only three mutations in the RBD compared to

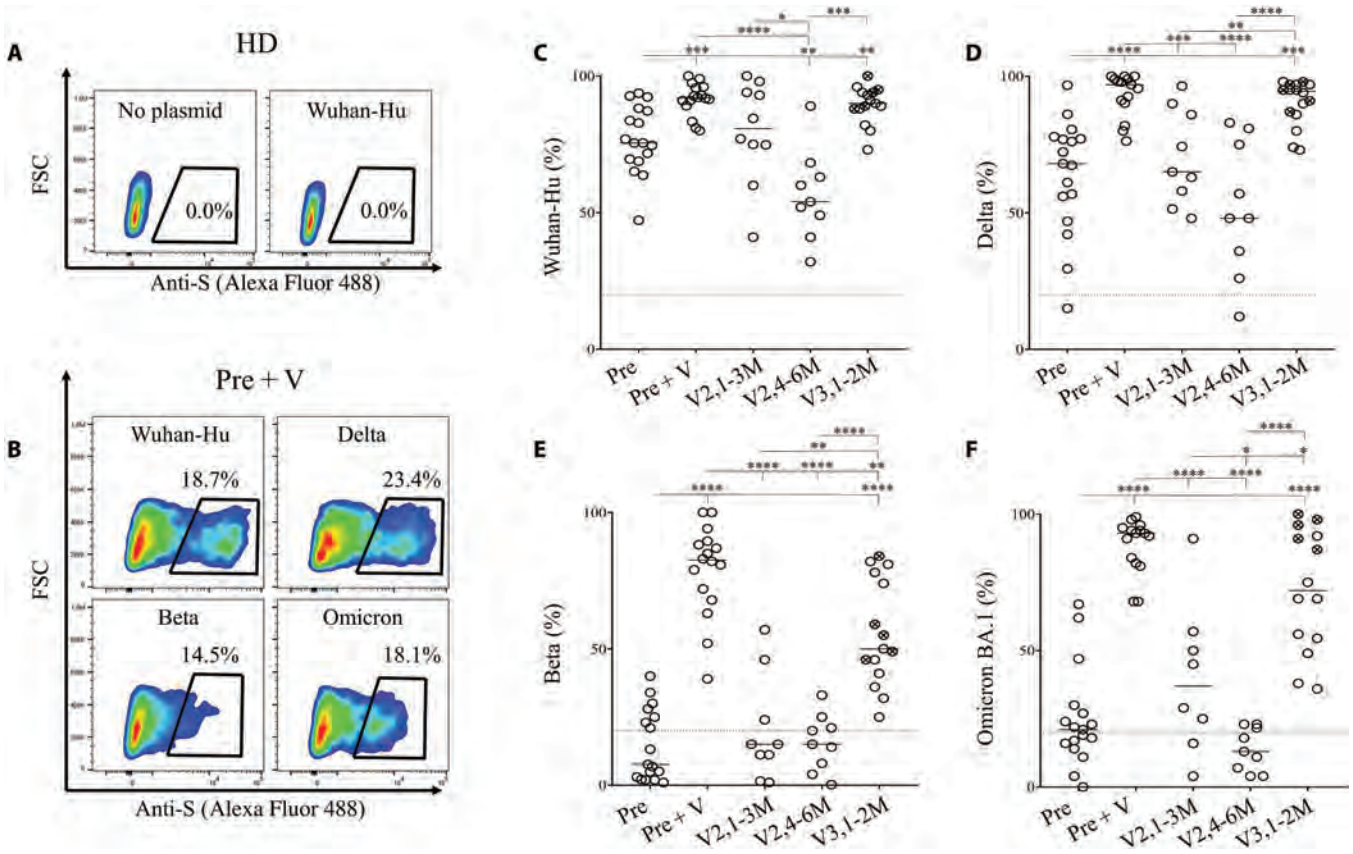

Fig. 2. IgG cross-reactivity against viral variants in convalescents and vaccinees. (**A** and **B**) Representative S-Flow assay. HEK293T cells either nontransfected or transfected with a plasmid encoding for the S protein were either labeled with (A) plasma from a healthy donor (HD) or (B) with plasma from a convalescent individual boosted with a vaccine dose (Pre + V). The percentages of cells recognized by specific IgG were detected by flow cytometry are shown for each variant. (**C** to **F**) Plasma from individuals, assessed in Fig. 1, were monitored for their capacity to recognize the different S variants including (C) Wuhan-Hu, (D) Delta, (E) Beta, and (F) Omicron. Relative percentages were calculated as follows: (% of IgG from plasma individuals − % of secondary IgG alone/% of anti-S2 mAbs − % of secondary IgG alone)*100. Each circle represents one individual. Lines represent median values. Statistical analysis was performed using a Mann-Whitney *U* test (*$P < 0.05$; **$P < 0.01$; ***$P < 0.001$; ****$P < 0.0001$). Symbols with a cross represent individuals who received at least one dose of mRNA-1273, whereas open symbols represent individuals who only received BNT162b2 in the vaccination scheme. Dot plots show forward size scatter (FSC) against anti-S detection.

Wuhan-Hu (K417N, E484K, and N501Y; Fig. 5B), which are also present in the Omicron subtypes. These minimal differences in the Beta RBD have been previously reported to substantially decrease neutralization by class I and class II monoclonal antibodies (*16*, *48*, *49*). By superimposing the variant structures onto the Wuhan-Hu RBD structure in the down state (not interacting with ACE2), the structural differences are centered around amino acids 365 and 380 (Fig. 5, C and D). These variations almost disappear entirely when the RBD is in the "up" conformation and interacting with the ACE2 receptor (fig. S4, A and B). The lower capacity of IgG to recognize Beta in comparison to Wuhan-Hu spike proteins in transfected cells is unlikely to be due to the differences in the RBD alone. The NTD region is the second most variable domain in which a supersite was reported flanked by glycans that also contribute in neutralizing SARS-CoV-2 infection (*6*, *50*–*53*). Whereas no insertion or deletion of amino acids have been observed within RBD in any variants so far, they have been observed in the NTD (Fig. 5E). These deletions affect the main solvent-exposed loops in the Beta (due to a deletion localized inside the structure affecting the five external loops) and in the Omicron variants (Fig. 5F) compared to the Wuhan-Hu and Delta strains (Fig. 5F). All the BA.2 variants compared to BA.1 contained a deletion in the N1 loop as well the absence of a glycan (NxT/S sequence is replaced by NxI) (Fig. 5E). The variation in the Delta structure was only observed around the single insertion at amino acids E156 and F157. This was further confirmed by plotting the root mean square (RMS) deviation of those six superimpositions compared to the insertion/deletion positions (fig. S4, C to F). On the other hand, insertion and/or deletion in the Beta and Omicron variants that induced large structural variations on external loops (Fig. 5F) could alter IgG recognition of the S protein expressed on cell surface.

We assessed in the S-Flow assay (*21*) the impact of such conformational changes using a mAb that recognizes the NTD domain. This mAb recognized cells expressing the Wuhan-Hu strain (fig. S5A). On the other hand, cells expressing Delta were not recognized by this clone (4A8) due to the deletion in the mAb binding site. Consistent with the notion that mutations/deletions in the NTD affect cross-reactivity, neither Beta- nor BA.1-expressing cells were recognized by this mAb (fig. S5). Therefore, considering that

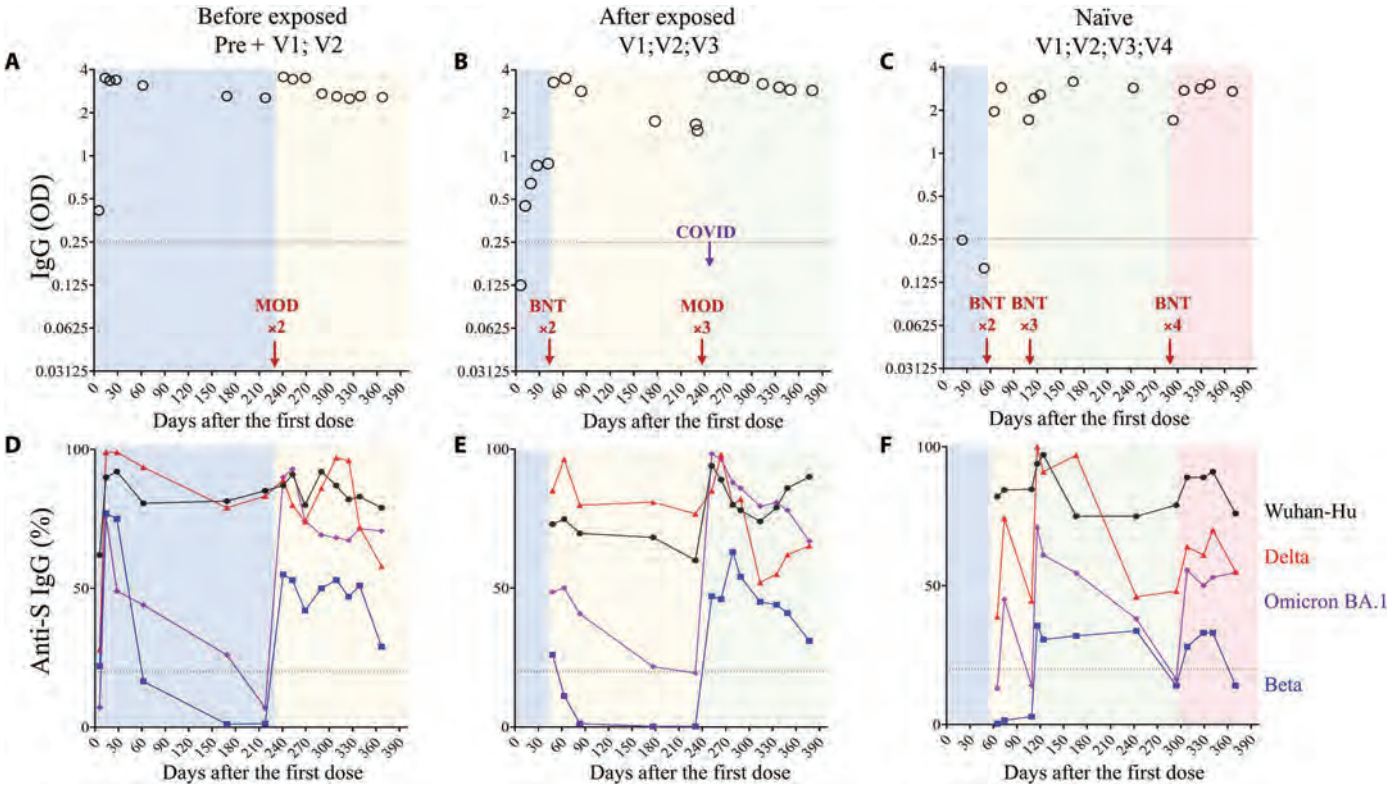

Fig. 3. Longitudinal analysis of IgG response either in convalescents boosted with mRNA vaccine or vaccinees. (**A** to **C**) ELISA was used to assess specific IgG response against S protein. Plasma were diluted to 1/400. Circles represent blood samplings at different time points after vaccination (first dose). Red arrows represent dates of vaccine boosts [BioNTech (BNT): BNT162b2 or Moderna (MOD): mRNA-1273]. In (B), the date of severe acute respiratory syndrome coronavirus 2 (SARS-CoV-2) infection is indicated. In (C), uninfected SARS-CoV-2 individual (naive) is shown. OD is shown. Dashed lines represent antibody specificity (0.25). COVID, coronavirus disease. (**D** to **F**) S-Flow assay was used to detect specific IgG cross-reactivity against viral variants. Thus, plasma from the same individuals at the same time points were tested against transfected cells expressing either the Wuhan-Hu spike strain (black circles), Delta variant (red triangles), Beta variant (blue squares), or Omicron variant (violet diamonds). Results are expressed as the percentages of specific IgG recognizing transfected cells by flow cytometry.

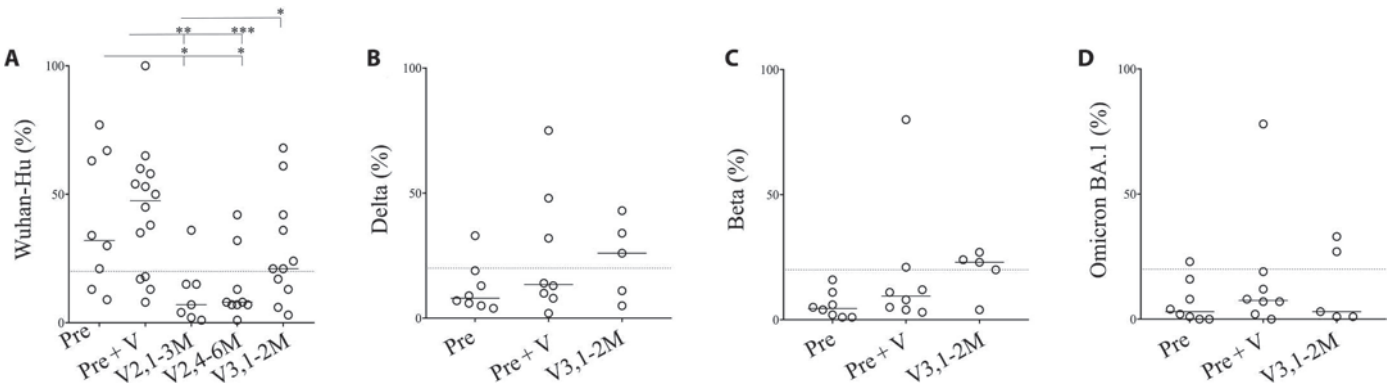

Fig. 4. IgA cross-reactivity against viral variants in convalescents and vaccinees. (**A**) Wuhan-Hu, (**B**) Delta, (**C**) Beta and (**D**) Omicron. Percentages of specific IgA detecting variants by flow cytometry (S-Flow assay) are shown. Plasma from V2 were not tested against Delta, Beta, and Omicron due the low levels of IgA detected by ELISA. In (B) to (D), only IgA responders against Wuhan-Hu were tested. Relative percentages were calculated as follows: (% of IgA from plasma individuals − % of secondary IgA alone/% of anti-S2 mAbs − % of secondary IgA alone)*100. Each circle represents one individual. Lines represent median values. Statistical analysis was performed using a Mann-Whitney *U* test (*$P < 0.05$; **$P < 0.01$; ***$P < 0.001$).

the main differences of BA.2 subtypes compared to BA.1 are related to the N1, N2, and N3 loops of the NTD (Fig. 5F), we hypothesized that such differences may provide a support for immune escape. Analyses of humoral response against BA.2 sublineages (BA.4/5, BA.2.12.1, and BA.2.75) revealed that IgG from vaccinees (V3,1-2M) were less capable to recognize BA.2 than BA.1 variant

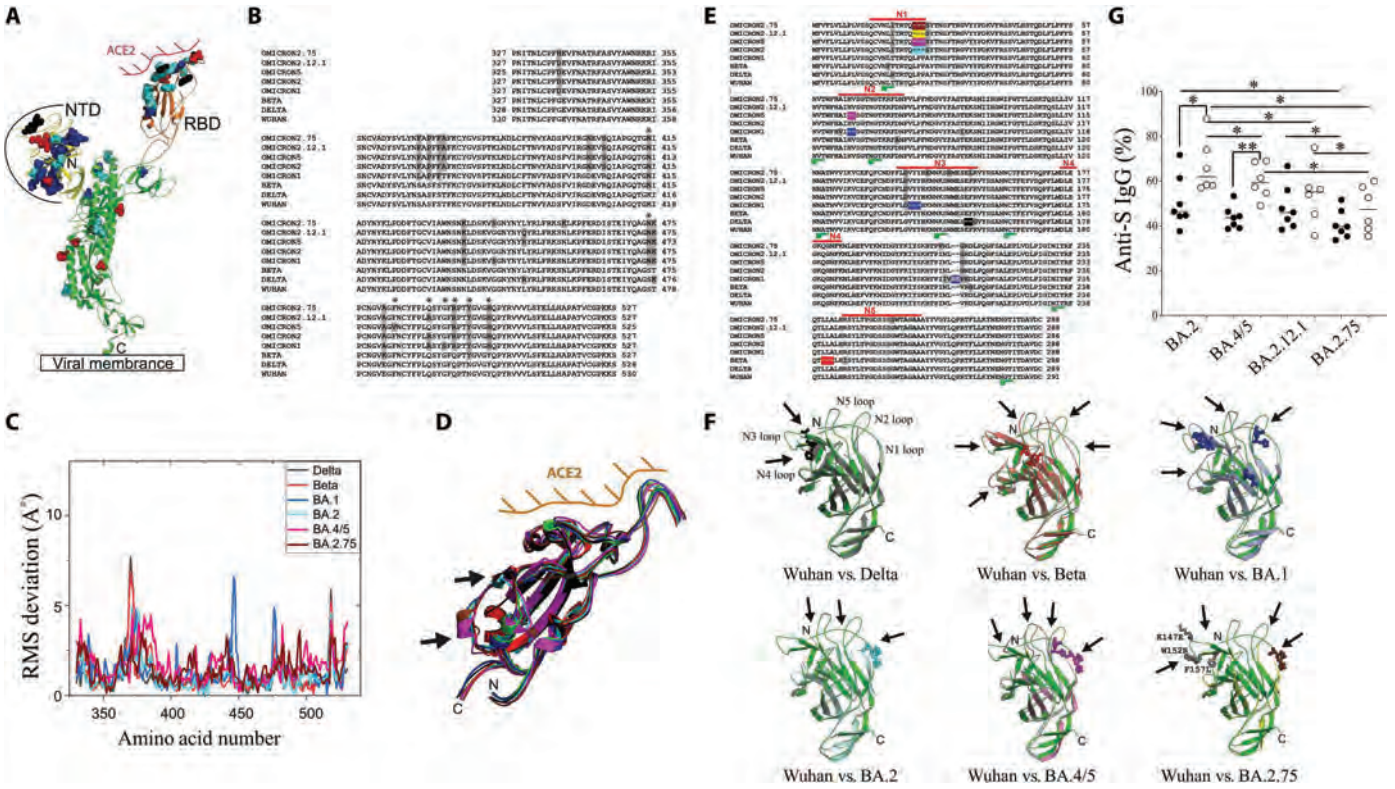

Fig. 5. Structural comparison of SARS-CoV-2 variants and Omicron BA.2 subtype IgG cross reactivities. (**A**) One monomer of S protein where the angiotensin II (ACE2) interaction with the receptor binding domain (RBD) is indicated in pink and N-terminal domain (NTD) area exposed to the solvent is indicated by a black line. (**B**) Sequence alignment of the RBD domains where mutations in viral variants are indicated in gray in comparison to the Wuhan sequence. (**C**) Root mean square (RMS) deviation from the RBD structural alignment against the Wuhan-Hu structure [Protein Data Bank identifier (PDB ID): 7L2E]. All RBD structures are in the down state (PDB ID used: 7Q9I, Beta; 7SO9, Delta; 7TM0, Omicron BA.1; 7UB0, Omicron BA.2; 7XNS Omicron BA.4/5; and 7YR1, Omicron BA.2.75). The structure from Omicron BA.2.12.2 was not yet validated. (**D**) Structural superimposition of the Wuhan RBD with the different variants. The main differences are indicated by arrows. (**E**) Sequence alignment of the NTD where insertion/deletion in the Omicron variants are in color. The other mutations are indicated in gray. (**F**) Superimposition of the Wuhan-Hu NTD with Delta, Beta, Omicron BA.1, Omicron BA.2, Omicron BA.4/5, or Omicron BA.2.75 NTDs. Arrows indicate large structural variations of solvent exposed loops. (**G**) IgG cross-reactivity against Omicron BA.2 subtypes. Plasma from either preexposed vaccinated individuals (Pre + V; open circles) or individuals vaccinated either with three doses of vaccine (V3,1-2M; black circles) were monitored for their capacity to recognize the Omicron BA.2 variants. The relative percentages were calculated as described in Fig. 2. Each circle represents one individual. Statistical analysis was performed using a Mann-Whitney *U* test (*$P < 0.05$; **$P < 0.01$).

expressed on the cell surface of transfected cells (BA.2, 50.8 ± 11% and BA.1, 71.6 ± 23%, $P = 0.03$, respectively; Figs. 2F and 5G). We also observed that IgG from convalescents boosted with the vaccine (Pre + V) recognized less efficiently BA.2 than BA.1 (66.8 ± 12 and 88.5 ± 10%, $P = 0.007$, respectively; Figs. 2F and 5G). Recent works suggest that Omicron BA.2 variants are more resistant to neutralization than BA.2 (*54*, *55*). Comparing BA.2 subtypes, BA.4/5 are less recognized than BA.2 by IgG from vaccinees than individuals preinfected and vaccinated (BA.2: V3,1-2M, 50.8 ± 11% versus Pre + V, 66.8 ± 12%, $P = 0.02$ and BA.4/5: V3,1-2M, 43.7 ± 5% versus Pre + V, 60 ± 8%, $P = 0.001$, respectively; Fig. 5G). However, BA.2.12.1 and BA.2.75 sublineages are the main variants of concern even for preinfected vaccinees (Pre + V). Thus, these percentages decreased to 53.9 ± 13 and 47.8 ± 10% in this group and were not significantly different from those observed in vaccinees (V3,1-2M, 48.2 ± 10 and 40.7 ± 6%; Fig. 5G).

Our results support the idea that mRNA vaccines induce IgG whose recognition is also affected by the structural modifications in the NTD region, which, in addition to the RBD, is the most variable regions in SARS-CoV-2. Note that BA.2.75, which displays three additional mutations in the third loop of the supersite (*51*), is the least recognized BA.2 sublineage. This may be indicative of immune pressure and represent one possible mechanism of immune escape. The lower recognition of the S proteins expressed on cell surface would limit cellular effector functions mediated by antibodies and reduce the control of SARS-CoV-2 variants, particularly in the context of BA.2.12.2 and BA.2.75 variants that recently emerged worldwide.

Three mRNA vaccinations allow to produce antibodies with similar affinities as those from convalescent and boosted individuals

The progressive loss in the levels and cross-reactivities of specific IgG and IgA requiring repeat vaccinations to maintain their efficacy prompted us to explore the avidity of Ig induced by the mRNA vaccine. The avidity of antibodies reflects the quality and strength of the antibody-antigen complex resulting from the Ig maturation process (*38*, *56*). However, little attention has been paid to the avidity of anti-S antibodies during COVID-19 vaccination. Figure 6A shows the avidity index (AI) of IgG against the

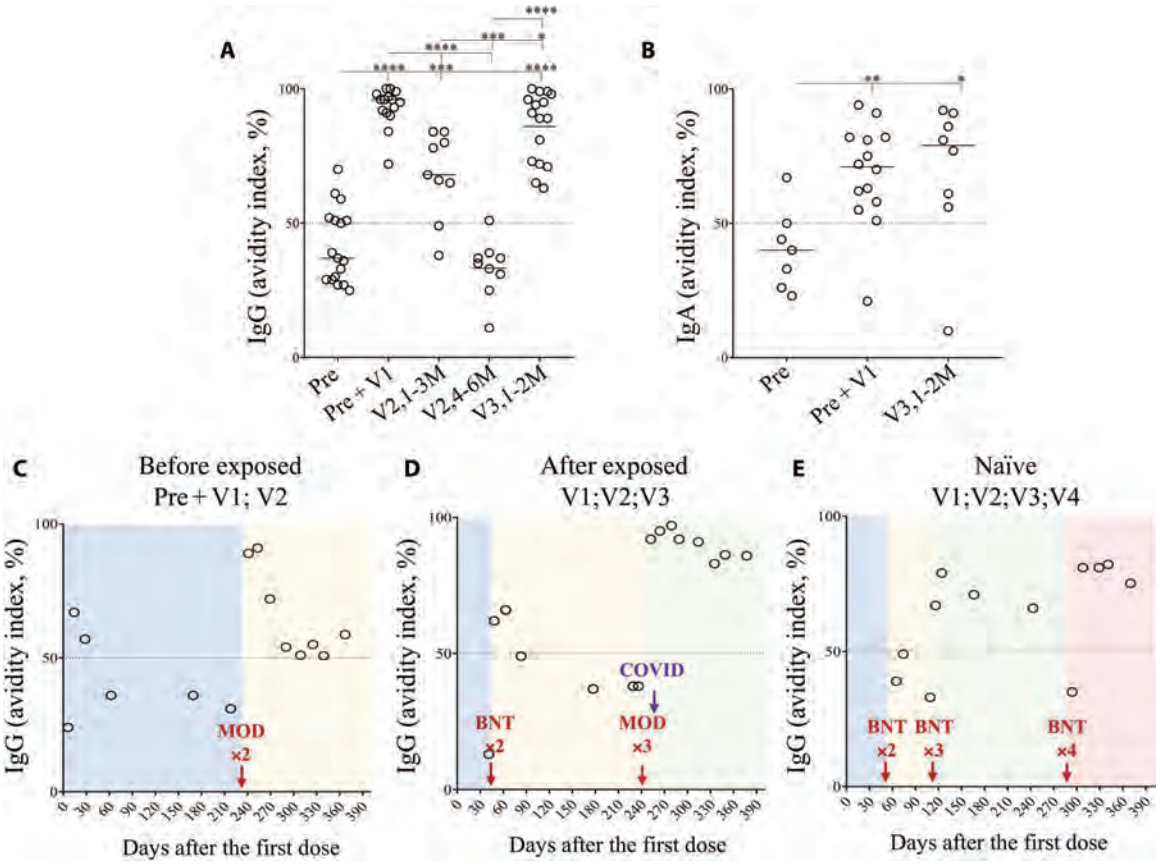

Fig. 6. Avidity of IgG and IgA against the spike protein in convalescents and vaccinated individuals. The avidity index (AI; OD with 6M urea/OD without urea × 100) was assessed by ELISA from plasma of individuals as described in Fig. 1. Plasma are diluted to 1/400. Thus, the AIs of (**A**) specific IgG and (**B**) IgA are shown. Dashed lines represent high avidity levels (indexes with a value above 50% are considered to be high, those between 31 and 49% was considered as intermediate, and values below 30% are considered to be low). Lines represent median values. (**C** to **E**). AIs of IgG from plasma of individuals described in Fig. 3 were measured longitudinally. Statistical analysis was performed using a Mann-Whitney *U* test (*$P < 0.05$; **$P < 0.01$; ***$P < 0.001$; ****$P < 0.0001$).

Wuhan-Hu S1 protein using a denaturing urea treatment (6M). The AIs of antibodies with values more than 50% are considered as high (*56*). Our results highlighted that a vaccine boost markedly improves the AI of IgG (Pre + V, 95.4 ± 7.1%) compared to IgG from convalescent individuals (Pre, 37 ± 13.9%; Fig. 6A). In vaccinees, the AI of IgG from individuals receiving three doses of vaccine (V3,1-2M: 90 ± 13%) was very high, reaching the same level of convalescent and boosted individuals. This index was higher compared to IgG from individuals receiving only two doses of vaccine either early after vaccination (V2,1-3M: 68 ± 16%) or later (V2,4-6M: 35 ± 10.8%; Fig. 6A).

By plotting the AIs against the percentages of S-Flow recognition, we found a strong association in individuals previously infected and boosted with vaccine (Pre + V; fig. S6). Only a subgroup of individuals demonstrated, despite high AIs, lower level of Beta detection (<70% of S-Flow; fig. S6). In individuals vaccinated with three doses (V3,1-2M), the ones who displayed greater IgG cross-reactivity against variants were those with the higher AIs (fig. S7). Of interest, vaccinees who received one dose of mRNA-1273 developed IgG with stronger avidity capable to recognize better Omicron than those who received only three doses of BNT162b2 (fig. S7).

For IgA, individuals with two doses were not tested due to the low levels of IgA (Fig. 1D). We found that the IgA AI was high in convalescent individuals boosted with the vaccine (Pre + V: 71 ± 18.9%) compared to convalescents (Pre: 40 ± 15.2%; Fig. 6B). The AIs of vaccinees with three doses are high (79 ± 27.3%) and similar to those observed in convalescents with a boost (Fig. 6B).

Our results from the longitudinal follow-up of the three individuals indicated that IgG avidity declined soon after vaccination, even in individuals who had been previously infected or after two doses (Fig. 6, C to E). Thus, an additional boost was required to improve the avidity. The avidity was similar after three or four doses (Fig. 6E). Thus, these data indicated that the AI decreases rapidly despite repeated vaccinations.

Ig affinity maturation depends on the formation of GC and requires the interaction of B and T cells in B cell follicles (*57*). CXCL13 represents in humans a surrogate marker of GC activation and is associated with neutralizing antibodies with high avidity (*40*–*42*), while humoral response occurring in the extrafollicular zones generates short-lived B cells and Ig with low avidity (*58*, *59*). Furthermore, type I interferon (IFN) may also contribute to the induction of CXCL13 (*60*). Thus, we assessed the levels of CXCL13 in vaccinees from whom samples were obtained within 2 weeks after vaccination including preexposed individuals (Pre + V) and in individuals acutely infected (SARS-CoV-2), compared to healthy individuals (naïve; Fig. 7A). In the analysis of individuals receiving

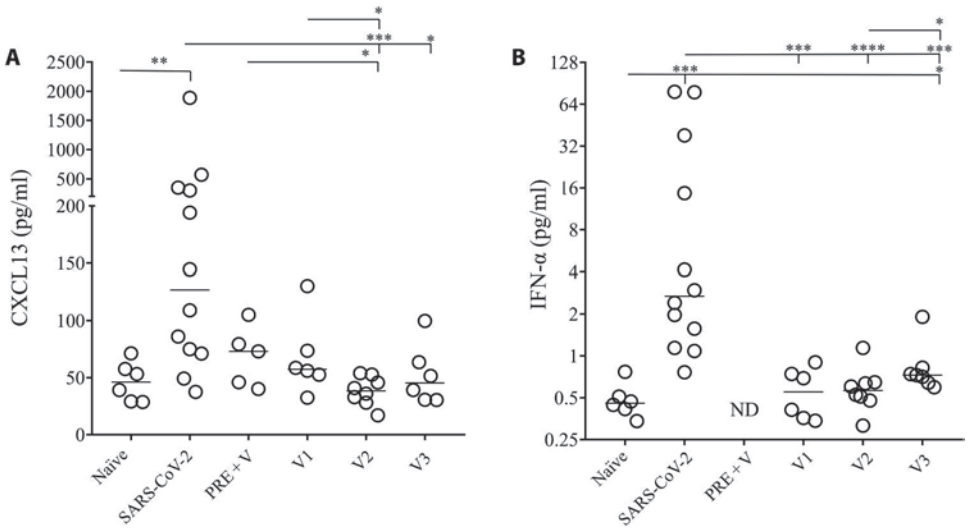

Fig. 7. Plasma levels of CXCL13 and type I IFN measurement in healthy donors, acute SARS-CoV-2–infected individuals, and vaccinees. (**A**) CXCL13 and (**B**) interferon-α (IFN-α) levels in the plasma of either healthy donors (naïve), acutely infected individuals (SARS-CoV-2), preexposed vaccinated individuals (Pre + V) and individuals vaccinated with one dose (V1), two doses (V2), or three doses (V3) of vaccine. Blood was collected 15 days after vaccination or infection. Each dot represents one individual. Lines represent median values. Statistical analysis was performed using a Mann-Whitney *U* test (*$P < 0.05$; **$P < 0.01$; ***$P < 0.001$; ****$P < 0.0001$). ND, not done.

one (V1, 57.3 ± 13.7 pg/ml), two (V2, 38.5 ± 4.4 pg/ml), or three doses (V3, 51.5 ± 10.8 pg/ml), the levels of CXCL13 were similar to those of healthy donors, whereas their levels were higher in acutely infected patients (Fig. 7A). Although not significantly different, the levels of CXCL13 were lower in healthy individuals (46.1 ± 6.9 pg/ml) compared to preexposed individuals boosted by mRNA vaccine (Pre + V, 73.02 ± 11.8 pg/ml). However, because of the limited number of individuals tested, this difference deserves to be further addressed. Similarly, we found that IFN-α levels were low in vaccinees compared to those of acutely infected individuals (Fig. 7B). Therefore, the low levels of CXCL13 are associated with the low avidity observed in vaccinees, suggesting suboptimal GC induction.

Together, these results indicate that boosts are required to improve the avidity of specific IgG, in particular, in individuals whose immunity is only due on vaccination and is associated with low CXCL13 levels. They also suggest that loss of avidity may contribute to the loss of cross-reactivity against the different variants that we observed in vaccinees compared to previously infected individuals and boosted with the vaccine.

DISCUSSION

Overall, our results indicate that individuals previously infected with SARS-CoV-2 and boosted with mRNA vaccines developed a strong humoral response, whereas multiple doses of vaccines are required to induce similar responses in nonexposed individuals. The immune response induced by the mRNA vaccine has valuable cross-reactivity against the different viral variants, although Beta and the more recent Omicron BA.2 sublineages are of major concern in this perspective, since their lower recognition on the cell surface will also reduce Fc effector functions. Therefore, in the absence of previous infection, repeated administrations of mRNA vaccine are required and can be boosted by a fourth dose, providing a possible explanation for their increased preventive effect on the development of severe disease by different variants (*61*). Unlike IgG, the presence of IgA may also be beneficial in providing protection at the mucosal viral entry (*62*). IgA antibodies were induced only after the third dose. However, unfortunately, because of their short half-life and their low avidity, IgA may confer a protection of limited duration, especially regarding SARS-CoV-2 variants.

Considering the half-life and low avidity of antibodies and the requirement for repeated vaccinations, the low levels of CXCL13 probably indicate suboptimal GC activations and extrafollicular B cells maturation in vaccinated individuals. B cell maturation and Ig avidity leading to high neutralizing antibodies depend on B and T cell interaction, and CXCL13 in the plasma is a surrogate marker of GC activation (*40*–*42*). It has been shown by Samanovic *et al.* (*63*) that the levels of CXCL13 remain low after two doses of vaccine. We confirm this finding and show that, even after three doses of vaccine, they remain similar to those of healthy donors and lower than the levels observed in individuals infected by SARS-CoV-2. This is also consistent with the general absence of hyperplasia of draining lymph nodes following mRNA vaccination (less than 0.3% of the recipients) (*32*). Of interest, other vaccines have been reported to increase the levels of CXCL13 in individuals having received either yellow fever vaccine or Ad5/HIV vaccine (*40*). The absence of type I IFN after BNT162b2 vaccination is consistent with vaccine manufacturing in which RNA has been modified to markedly reduced innate immune sensing and inflammation (*64*) Thus, consistent with the earlier theory of P. Matzinger in 90s as "the danger theory of immunity" (*65*), the absence of innate sensing may require repetitive vaccination for maintaining high levels of antibody. A previous report, using fine needle aspirates of draining axillary lymph nodes, has indicated the presence of GC B cells in vaccinees for 2 months after the boost (*66*); however, this cannot exclude the detection of extrafollicular B cells. Our follow-up study showed that the avidity decreases after

2 months. Kim *et al.* (*67*), performing bone marrow aspirates in individuals vaccinated 6 months earlier with two doses of BNT162b2, have observed that the frequency of bone marrow plasma cells against the S protein was at least 20-fold lower compared to those induced by the 2019-2020 influenza virus vaccine. One limitation of our study is the absence of draining lymph nodes data from vaccinees that may help to elucidate lymphoid organization and GC development, as we previously described for other infectious diseases (*68*, *69*).

In the past, the level and persistence of antibodies were demonstrated as being low, even with repeated immunizations, in the absence of T cell help and associated with extrafollicular B cells (*70*–*72*). Thus, short-lived B cell immunity was counteracted by associating a "carrier," as a T cell dominant epitope to improve B cell immunity. Moreover, one possibility of improving mRNA vaccines could be to use cytokines such as interleukin-12 that boosts GC formation and could be considered for longer-lasting immune response (*73*). Of interest, in individuals previously infected and boosted with vaccine, the humoral response was extremely rapid and stronger in quantity and quality compared to individuals having received two doses of vaccine. This indicates an imprinting of SARS-CoV-2 immunity in hybrid responders. These results are consistent with the presence of activated memory B cells described by Rodda *et al.* (*74*) in hybrid immunity. This persistence of memory B cells could reflect larger amounts of antigen present after infection and longer ongoing B cell follicle activation contributing to the imprinting, which is consistent with the levels of CXCL13 detected in the plasma of SARS-CoV-2–infected individuals during the acute phase.

We also demonstrated that the avidity of Ig decreased rapidly even after repetitive boosts. This is of importance, because, generally, avidity is associated with the neutralizing capacity of antibodies (*75*). Furthermore, the lower ability of plasma from vaccines to recognize Beta and Omicron variants might also be related to the lower avidity of antibodies induced by vaccination alone. Our results, using the S-Flow assay, are indicative of a lower capacity to recognize the variants, which may also have consequences for humoral response related to cell-mediated cytotoxicity. The ability to eliminate infected cells might contribute to limiting the duration of infection and/or viral dissemination (*76*). In this context, it cannot be excluded that viral spread through cell-to-cell transmission can evade neutralizing antibodies. This is well known in HIV infections (*77*, *78*) and was recently demonstrated in SARS-CoV-2 (*79*). Consistent with a previous report (*25*), we found that convalescent individuals in the absence of a vaccine boost displayed low quality of antibodies capable to recognize the S protein on the surface of cells, as compared to vaccinated individuals. However, our results highlighted that once vaccinated, convalescent individuals develop a strong humoral response with broader IgG cross-reactivities against SARS-CoV-2 variants. Nevertheless, of particular concern is the low recognition of the S protein from Beta and BA.2 Omicron sublineages (BA.2.12.1 and BA.275) by vaccinees' plasma. Previous reports, on the basis of neutralizing assay using both pseudoviruses and viruses, showed that BA.1 (certainly related to the higher number of mutations in the RBD) was more resistant compared to Beta (*80*, *81*). In contrast, the S-Flow assay indicated that Beta is less recognized than BA.1 Omicron. Our longitudinal analysis also suggests that the quality of antibody is declining after the third dose, over the 6 months of follow-up, particularly regarding the Beta and Omicron variants. Although limited to one individual, we have observed that despite a fourth dose, Beta recognition declined again. Therefore, additional studies deserve to be conducted analyzing the effect of an additional boost or even after viral exposure on the duration of the humoral response. A fourth dose was described to improve protection as compared to three doses of vaccine (*61*). Thus, our results suggest the importance to also assess the capacity of Ig to recognize SARS-CoV-2 variants on cell surface highlighting the role of deletions in the NTD region of new Omicron variants as a virus strategy to escape from the immune response.

There are some additional limitations in our study. Whereas we have observed that if the third vaccination was performed with mRNA-1271, then it induced IgA and improved the quality of IgG recognizing Omicron as compared with BNT162b2 vaccinees only; this was performed on a limited number of individuals. A recent report, however, also suggested a beneficial effect of mRNA-1273 to induce IgA compared to BNT162b2 (*82*). Given the role of mucosal immunity against such viral infection, future studies in larger cohorts are needed.

Despite these limitations, our data provided evidence for potential differences in the quantity and quality of the humoral responses in hybrid immune responders compared to individuals having received three doses of mRNA vaccine and highlighted the interest for analyzing immune response directed against S variant proteins expressed on the cell surface. In conclusion, in the context of the generalized third dose of vaccination, our study provides novel findings regarding the levels of protection and the impact of vaccine strategy to control the dynamics of COVID variants.

MATERIALS AND METHODS

Study design and participants

The bioclinical features of patients recruited are given in Table 1. This study was approved by the Ethics Committee of the Île-de-France (EudraCT/IDRCB 2020-A00875-34 and Clinical Trials: NCT04351711, Nîmes University Hospital) and from the Clinical Board and Ethics Committee (ref 69/2020, Hospital de Braga, Portugal). All patients had provided written informed consent. We also analyzed samples obtained longitudinally at different time points after vaccination. Blood was collected, and plasma was obtained after centrifugation was frozen to −80°C.

IgA and IgG humoral responses

Antibody production was monitored by measuring specific Igs via ELISA against N and S1 proteins as previously described (*16*). Briefly, NUNC MaxiSorp well plates were coated with antigens (0.5 μg/ml in tris-HCl, pH 9.6) overnight. After saturation with bovine serum albumin (BSA), plasmas were diluted to 1:400 and 1:800 and incubated for 90 min. Plates were then washed and incubated with goat anti-human IgG (Fc-specific) peroxidase (A0170, MilliporeSigma) and goat anti-human IgA (Fc-specific) peroxidase (SAB3701229, MilliporeSigma) for 45 min. These antibodies were highly specific to the Fc fragments not recognizing the kappa and lambda chains of the Ig. After several washings, substrate reagent solution (R&D Systems) was added and incubated for 30 min. The reactions were stopped using sulfuric acid (1 N). The plate was read on a Thermo Scientific Varioskan reader at wavelengths of 450 and 540 nm.

SARS-COV-2 spike avidity assay

Like for ELISA, NUNC MaxiSorp ELISA plates were coated with S1 antigen to monitor the avidity of IgA and IgG. Once incubated in the presence of 1:400 dilution of plasma, plates were washed with phosphate-buffered saline (PBS) and then incubated for 30 min at 37°C in the absence (PBS) or presence of 6M urea. Thereafter, similarly specific IgA and IgG were detected with secondary antibodies and revealed with substrate reagent solution (R&D Systems). The AI was calculated as follows: AI% = (OD value of urea-treated sample/OD of untreated sample)*100. Indexes with values more than 50% were considered as high IgG avidity, 31 to 49% was considered as intermediate IgG avidity, and values below 30% were considered as low IgG avidity.

S-Flow assay

The assay was conducted in two settings, using SARS-CoV-2–infected or SARS-CoV-2–transfected cells. The day before infection, 4×10^6 Vero-E6 cells were seeded in 75-cm^2 cell culture flasks in Dulbecco's minimum essential medium (DMEM) supplemented with 10% heat-inactivated fetal bovine serum (FBS) and penicillin and streptomycin solution (100 μg/ml) and incubated at 37°C and 5% CO_2. On the day of infection, the cell monolayer was 90% confluent. Medium was removed, cells were washed once with medium, and different flasks were inoculated with: SARS-CoV-2 Wuhan-Hu strain (Global Initiative on Sharing All Influenza Data accession no. EPI_ISL_16833248) at a multiplicity of infection of 0.01. Cells were incubated for 1 hour at 37°C with shaking. The inoculum was then replaced with DMEM containing 2% FBS. Two days after inoculation, cells were harvested with trypsin (Gibco) and centrifuged for 3 min at 900*g*. In the other setting, 293T cells were transfected using Lipofectamine 2000 (Life Technologies) and plasmids encoding the full length of the SARS-CoV-2 S variants (*47*). The Wuhan-Hu S-expressing plasmid was provided by O. Schwartz, whereas Beta and Delta were purchased from InvivoGen (Spike pseudotyping plasmid, plv-spike-v3 and plv-spike-v8, respectively), and the Omicron S protein (BA.1 and BA.2 sublineages) plasmids were produced in-house. After transfection and overnight culture, the cells were detached using PBS-EDTA and transferred into U-bottom 96-well culture plates (200,000 cells per well). For both infected and transfected cells, the cellular pellets were saturated with 10% FBS at 4°C for 10 min and incubated with the patients' plasma (1:300 dilution) in PBS containing 0.5% BSA for 30 min at 4°C. Cells were then washed and stained for 30 min at 4°C using the same antibodies as described for ELISA but labeled with fluorescein isothiocyanate (Sigma-Aldrich). After washing, cells were fixed with 2% paraformaldehyde. Furthermore, we used two mAbs as controls in this study: anti-spike (S2) (GeneTex, clone 1A9) and anti-NTD mAb (ProteoGenix, clone 4A8). The mAbs were diluted to 1:1000 and revealed using specific Alexa Fluor 488–labeled secondary antibodies. Cells were analyzed on an Attune NxT flow cytometer using FlowJo software (Tree Star Inc.).

Quantification of CXCL13 and IFN-α

The amounts of CXCL13 and IFN-α in the plasma were quantified by ELISA (R&D Systems). Plates were read at a reference wavelength of 490 nM.

Statistical analyses

Statistics were calculated using GraphPad Prism software. A non-parametric Mann-Whitney *U* test and Student's *t* test were used for comparison. *P* values indicate significant differences ($^*P < 0.05$; $^{**}P < 0.01$; $^{***}P < 0.001$; $^{****}P < 0.0001$). Correlations were assessed using the Spearman test. A chi-square test was used to compare frequency.

Supplementary Materials

This PDF file includes:

Figs. S1 to S7

REFERENCES AND NOTES

1. P. Zhou, X. L. Yang, X. G. Wang, B. Hu, L. Zhang, W. Zhang, H. R. Si, Y. Zhu, B. Li, C. L. Huang, H. D. Chen, J. Chen, Y. Luo, H. Guo, R. D. Jiang, M. Q. Liu, Y. Chen, X. R. Shen, X. Wang, X. S. Zheng, K. Zhao, Q. J. Chen, F. Deng, L. L. Liu, B. Yan, F. X. Zhan, Y. Y. Wang, G. F. Xiao, Z. L. Shi, A pneumonia outbreak associated with a new coronavirus of probable bat origin. *Nature* **579**, 270–273 (2020).
2. L. Piccoli, Y. J. Park, M. A. Tortorici, N. Czudnochowski, A. C. Walls, M. Beltramello, C. Silacci-Fregni, D. Pinto, L. E. Rosen, J. E. Bowen, O. J. Acton, S. Jaconi, B. Guarino, A. Minola, F. Zatta, N. Sprugasci, J. Bassi, A. Peter, A. De Marco, J. C. Nix, F. Mele, S. Jovic, B. F. Rodriguez, S. V. Gupta, F. Jin, G. Piumatti, G. Lo Presti, A. F. Pellanda, M. Biggiogero, M. Tarkowski, M. S. Pizzuto, E. Cameroni, C. Havenar-Daughton, M. Smithey, D. Hong, V. Lepori, E. Albanese, A. Ceschi, E. Bernasconi, L. Elzi, P. Ferrari, C. Garzoni, A. Riva, G. Snell, F. Sallusto, K. Fink, H. W. Virgin, A. Lanzavecchia, D. Corti, D. Veesler, Mapping neutralizing and immunodominant sites on the SARS-CoV-2 spike receptor-binding domain by structure-guided high-resolution serology. *Cell* **183**, 1024–1042.e21 (2020).
3. A. J. Greaney, A. N. Loes, K. H. D. Crawford, T. N. Starr, K. D. Malone, H. Y. Chu, J. D. Bloom, Comprehensive mapping of mutations in the SARS-CoV-2 receptor-binding domain that affect recognition by polyclonal human plasma antibodies. *Cell Host Microbe* **29**, 463–476.e6 (2021).
4. Z. Wang, F. Muecksch, A. Cho, C. Gaebler, H.-H. Hoffmann, V. Ramos, S. Zong, M. Cipolla, B. Johnson, F. Schmidt, J. DaSilva, E. Bednarski, T. Ben Tanfous, R. Raspe, K. Yao, Y. E. Lee, T. Chen, M. Turroja, K. G. Milard, J. Dizon, A. Kaczynska, A. Gazumyan, T. Y. Oliveira, C. M. Rice, M. Caskey, P. D. Bieniasz, T. Hatziioannou, C. O. Barnes, M. C. Nussenzweig, Analysis of memory B cells identifies conserved neutralizing epitopes on the N-terminal domain of variant SARS-Cov-2 spike proteins. *Immunity* **55**, 998–1012.e8 (2022).
5. W. Dejnirattisai, J. Huo, D. Zhou, J. Zahradník, P. Supasa, C. Liu, H. M. E. Duyvesteyn, H. M. Ginn, A. J. Mentzer, A. Tuekprakhon, R. Nutalai, B. Wang, A. Dijokaite, S. Khan, O. Avinoam, M. Bahar, D. Skelly, S. Adele, S. A. Johnson, A. Amini, T. G. Ritter, C. Mason, C. Dold, D. Pan, S. Assadi, A. Bellass, N. Omo-Dare, D. Koeckerling, A. Flaxman, D. Jenkin, P. K. Aley, M. Voysey, S. A. C. Clemens, F. G. Naveca, V. Nascimento, F. Nascimento, C. F. da Costa, P. C. Resende, A. Pauvolid-Correa, M. M. Siqueira, V. Baillie, N. Serafin, G. Kwatra, K. Da Silva, S. A. Madhi, M. C. Nunes, T. Malik, P. J. M. Openshaw, J. K. Baillie, M. G. Semple, A. R. Townsend, K. A. Huang, T. K. Tan, M. W. Carroll, P. Klenerman, E. Barnes, S. J. Dunachie, B. Constantinides, H. Webster, D. Crook, A. J. Pollard, T. Lambe, N. G. Paterson, M. A. Williams, D. R. Hall, E. E. Fry, J. Mongkolsapaya, J. Ren, G. Schreiber, D. I. Stuart, G. R. Screaton, SARS-CoV-2 Omicron-B.1.1.529 leads to widespread escape from neutralizing antibody responses. *Cell* **185**, 467–484.e15 (2022).
6. M. McCallum, A. De Marco, F. A. Lempp, M. A. Tortorici, D. Pinto, A. C. Walls, M. Beltramello, A. Chen, Z. Liu, F. Zatta, S. Zepeda, J. di Iulio, J. E. Bowen, M. Montiel-Ruiz, J. Zhou, L. E. Rosen, S. Bianchi, B. Guarino, C. S. Fregni, R. Abdelnabi, S. C. Foo, P. W. Rothlauf, L. M. Bloyet, F. Benigni, E. Cameroni, J. Neyts, A. Riva, G. Snell, A. Telenti, S. P. J. Whelan, H. W. Virgin, D. Corti, M. S. Pizzuto, D. Veesler, N-terminal domain antigenic mapping reveals a site of vulnerability for SARS-CoV-2. *Cell* **184**, 2332–2347.e16 (2021).
7. C. Davis, N. Logan, G. Tyson, R. Orton, W. T. Harvey, J. S. Perkins, G. Mollett, R. M. Blacow; COVID-19 Genomics UK (COG-UK) Consortium, T. P. Peacock, W. S. Barclay, P. Cherepanov, M. Palmarini, P. R. Murcia, A. H. Patel, D. L. Robertson, J. Haughney, E. C. Thomson, B. J. Willett; COVID-19 DeplOyed VaccinE (DOVE) Cohort Study investigators, Reduced neutralisation of the Delta (B.1.617.2) SARS-CoV-2 variant of concern following vaccination. *PLOS Pathog.* **17**, e1010022 (2021).
8. V.-V. Edara, B. A. Pinsky, M. S. Suthar, L. Lai, M. E. Davis-Gardner, K. Floyd, M. W. Flowers, J. Wrammert, L. Hussaini, C. R. Ciric, S. Bechnak, K. Stephens, B. S. Graham, E. Bayat Mokhtari, P. Mudvari, E. Boritz, A. Creanga, A. Pegu, A. Derrien-Colemyn, A. R. Henry, M. Gagne, D. C. Douek, M. K. Sahoo, M. Sibai, D. Solis, R. J. Webby, T. Jeevan, T. P. Fabrizio, Infection

and vaccine-induced neutralizing-antibody responses to the SARS-CoV-2 B.1.617 variants. *N. Engl. J. Med.* **385**, 664–666 (2021).

9. I. Nemet, L. Kliker, Y. Lustig, N. Zuckerman, O. Erster, C. Cohen, Y. Kreiss, S. Alroy-Preis, G. Regev-Yochay, E. Mendelson, M. Mandelboim, Third bnt162b2 vaccination neutralization of SARS-CoV-2 omicron infection. *N. Engl. J. Med.* **386**, 492–494 (2022).
10. W. F. Garcia-Beltran, K. J. St Denis, A. Hoelzemer, E. C. Lam, A. D. Nitido, M. L. Sheehan, C. Berrios, O. Ofoman, C. C. Chang, B. M. Hauser, J. Feldman, A. L. Roederer, D. J. Gregory, M. C. Poznansky, A. G. Schmidt, A. J. Iafrate, V. Naranbhai, A. B. Balazs, mRNA-based COVID-19 vaccine boosters induce neutralizing immunity against SARS-CoV-2 Omicron variant. *Cell* **185**, 457–466.e4 (2022).
11. A. Muik, B. G. Lui, A. K. Wallisch, M. Bacher, J. Mühl, J. Reinholz, O. Ozhelvaci, N. Beckmann, R. C. Güimil Garcia, A. Poran, S. Shpyro, A. Finlayson, H. Cai, Q. Yang, K. A. Swanson, Ö. Türeci, U. Şahin, Neutralization of SARS-CoV-2 Omicron by BNT162b2 mRNA vaccine-elicited human sera. *Science* **375**, 678–680 (2022).
12. J. M. Carreño, H. Alshammary, J. Tcheou, G. Singh, A. J. Raskin, H. Kawabata, L. A. Sominsky, J. J. Clark, D. C. Adelsberg, D. A. Bielak, A. S. Gonzalez-Reiche, N. Dambrauskas, V. Vigdorovich, K. Srivastava, D. N. Sather, E. M. Sordillo, G. Bajic, H. van Bakel, V. Simon, F. Krammer, Activity of convalescent and vaccine serum against SARS-CoV-2 Omicron. *Nature* **602**, 682–688 (2022).
13. S. Miyamoto, T. Arashiro, Y. Adachi, S. Moriyama, H. Kinoshita, T. Kanno, S. Saito, H. Katano, S. Iida, A. Ainai, R. Kotaki, S. Yamada, Y. Kuroda, T. Yamamoto, K. Ishijima, E. S. Park, Y. Inoue, Y. Kaku, M. Tobiume, N. Iwata-Yoshikawa, N. Shiwa-Sudo, K. Tokunaga, S. Ozono, T. Hemmi, A. Ueno, N. Kishida, S. Watanabe, K. Nojima, Y. Seki, T. Mizukami, H. Hasegawa, H. Ebihara, K. Maeda, S. Fukushi, Y. Takahashi, T. Suzuki, Vaccination-infection interval determines cross-neutralization potency to SARS-CoV-2 Omicron after breakthrough infection by other variants. *Med* **3**, 249–261.e4 (2022).
14. L. Liu, S. Iketani, Y. Guo, J. F. W. Chan, M. Wang, L. Liu, Y. Luo, H. Chu, Y. Huang, M. S. Nair, J. Yu, K. K. H. Chik, T. T. T. Yuen, C. Yoon, K. K. W. To, H. Chen, M. T. Yin, M. E. Sobieszczyk, Y. Huang, H. H. Wang, Z. Sheng, K.-Y. Yuen, D. D. Ho, Striking antibody evasion manifested by the Omicron variant of SARS-CoV-2. *Nature* **602**, 676–681 (2022).
15. E. Cameroni, J. E. Bowen, L. E. Rosen, C. Saliba, S. K. Zepeda, K. Culap, D. Pinto, L. A. VanBlargan, A. De Marco, J. di Iulio, F. Zatta, H. Kaiser, J. Noack, N. Farhat, N. Czudnochowski, C. Havenar-Daughton, K. R. Sprouse, J. R. Dillen, A. E. Powell, A. Chen, C. Maher, L. Yin, D. Sun, L. Soriaga, J. Bassi, C. Silacci-Fregni, C. Gustafsson, N. M. Franko, J. Logue, N. T. Iqbal, I. Mazzitelli, J. Geffner, R. Grifantini, H. Chu, A. Gori, A. Riva, O. Giannini, A. Ceschi, P. Ferrari, P. E. Cippà, A. Franzetti-Pellanda, C. Garzoni, P. J. Halfmann, Y. Kawaoka, C. Hebner, L. A. Purcell, L. Piccoli, M. S. Pizzuto, A. C. Walls, M. S. Diamond, A. Telenti, H. W. Virgin, A. Lanzavecchia, G. Snell, D. Veesler, D. Corti, Broadly neutralizing antibodies overcome SARS-CoV-2 Omicron antigenic shift. *Nature* **602**, 664–670 (2022).
16. D. Planas, N. Saunders, P. Maes, F. Guivel-Benhassine, C. Planchais, J. Buchrieser, W.-H. Bolland, F. Porrot, I. Staropoli, F. Lemoine, H. Péré, D. Veyer, J. Puech, J. Rodary, G. Baele, S. Dellicour, J. Raymenants, S. Gorissen, C. Geenen, B. Vanmechelen, T. Wawina-Bokalanga, J. Martí-Carreras, L. Cuypers, A. Sève, L. Hocqueloux, T. Prazuck, F. A. Rey, E. Simon-Loriere, T. Bruel, H. Mouquet, E. André, O. Schwartz, Considerable escape of SARS-CoV-2 Omicron to antibody neutralization. *Nature* **602**, 671–675 (2022).
17. M. Hoffmann, N. Krüger, S. Schulz, A. Cossmann, C. Rocha, A. Kempf, I. Nehlmeier, L. Graichen, A. S. Moldenhauer, M. S. Winkler, M. Lier, A. Dopfer-Jablonka, H. M. Jäck, G. M. N. Behrens, S. Pöhlmann, The Omicron variant is highly resistant against antibody-mediated neutralization: Implications for control of the COVID-19 pandemic. *Cell* **185**, 447–456.e11 (2022).
18. Y. Cao, J. Wang, F. Jian, T. Xiao, W. Song, A. Yisimayi, W. Huang, Q. Li, P. Wang, R. An, J. Wang, Y. Wang, X. Niu, S. Yang, H. Liang, H. Sun, T. Li, Y. Yu, Q. Cui, S. Liu, X. Yang, S. Du, Z. Zhang, X. Hao, F. Shao, R. Jin, X. Wang, J. Xiao, Y. Wang, X. S. Xie, Omicron escapes the majority of existing SARS-CoV-2 neutralizing antibodies. *Nature* **602**, 657–663 (2022).
19. E. S. Winkler, P. Gilchuk, J. Yu, A. L. Bailey, R. E. Chen, Z. Chong, S. J. Zost, H. Jang, Y. Huang, J. D. Allen, J. B. Case, R. E. Sutton, R. H. Carnahan, T. L. Darling, A. C. M. Boon, M. Mack, R. D. Head, T. M. Ross, J. E. Crowe Jr., M. S. Diamond, Human neutralizing antibodies against SARS-CoV-2 require intact Fc effector functions for optimal therapeutic protection. *Cell* **184**, 1804–1820.e16 (2021).
20. Y. C. Bartsch, S. Fischinger, S. M. Siddiqui, Z. Chen, J. Yu, M. Gebre, C. Atyeo, M. J. Gorman, A. L. Zhu, J. Kang, J. S. Burke, M. Slein, M. J. Gluck, S. Beger, Y. Hu, J. Rhee, E. Petersen, B. Mormann, M. de St Aubin, M. A. Hasdianda, G. Jambaulikar, E. W. Boyer, P. C. Sabeti, D. H. Barouch, B. D. Julg, E. R. Musk, A. S. Menon, D. A. Lauffenburger, E. J. Nilles, G. Alter, Discrete SARS-CoV-2 antibody titers track with functional humoral stability. *Nat. Commun.* **12**, 1018 (2021).
21. S. André, M. Azarias da Silva, M. Picard, A. Alleaume-Buteau, L. Kundura, R. Cezar, C. Soudaramourty, S. C. André, A. Mendes-Frias, A. Carvalho, C. Capela, J. Pedrosa, A. Gil Castro, P. Loubet, A. Sotto, L. Muller, J.-Y. Lefrant, C. Roger, P.-G. Claret, S. Duvnjak, T.-A. Tran, O. Zghidi-Abouzid, P. Nioche, R. Silvestre, P. Corbeau, F. Mammano, J. Estaquier, Low quantity and quality of anti-spike humoral response is linked to CD4 T-cell apoptosis in COVID-19 patients. *Cell Death Dis.* **13**, 741 (2022).
22. S. André, M. Picard, R. Cezar, F. Roux-Dalvai, A. Alleaume-Butaux, C. Soundaramourty, A. S. Cruz, A. Mendes-Frias, C. Gotti, M. Leclercq, A. Nicolas, A. Tauzin, A. Carvalho, C. Capela, J. Pedrosa, A. G. Castro, L. Kundura, P. Loubet, A. Sotto, L. Muller, J. Y. Lefrant, C. Roger, P. G. Claret, S. Duvnjak, T. A. Tran, G. Racine, O. Zghidi-Abouzid, P. Nioche, R. Silvestre, A. Droit, F. Mammano, P. Corbeau, J. Estaquier, T cell apoptosis characterizes severe Covid-19 disease. *Cell Death Differ.* **29**, 1486–1499 (2022).
23. Y. C. Bartsch, X. Tong, J. Kang, M. J. Avendaño, E. F. Serrano, T. García-Salum, C. Pardo-Roa, A. Riquelme, Y. Cai, I. Renzi, G. Stewart-Jones, B. Chen, R. A. Medina, G. Alter, Omicron variant Spike-specific antibody binding and Fc activity are preserved in recipients of mRNA or inactivated COVID-19 vaccines. *Sci. Transl. Med.* **14**, eabn9243 (2022).
24. E. C. Sabino, L. F. Buss, M. P. S. Carvalho, C. A. Prete Jr., M. A. E. Crispim, N. A. Fraiji, R. H. M. Pereira, K. V. Parag, P. da Silva Peixoto, M. U. G. Kraemer, M. K. Oikawa, T. Salomon, Z. M. Cucunuba, M. C. Castro, A. A. de Souza Santos, V. H. Nascimento, H. S. Pereira, N. M. Ferguson, O. G. Pybus, A. Kucharski, M. P. Busch, C. Dye, N. R. Faria, Resurgence of COVID-19 in Manaus, Brazil, despite high seroprevalence. *Lancet* **397**, 452–455 (2021).
25. P. Kaplonek, S. Fischinger, D. Cizmeci, Y. C. Bartsch, J. Kang, J. S. Burke, S. A. Shin, D. Dayal, P. Martin, C. Mann, F. Amanat, B. Julg, E. J. Nilles, E. R. Musk, A. S. Menon, F. Krammer, E. O. Saphire, C. Andrea, G. Alter, mRNA-1273 vaccine-induced antibodies maintain Fc effector functions across SARS-CoV-2 variants of concern. *Immunity* **55**, 355–365.e4 (2022).
26. L. J. Abu-Raddad, H. Chemaitelly, H. H. Ayoub, H. M. Yassine, F. M. Benslimane, H. A. Al Khatib, P. Tang, M. R. Hasan, P. Coyle, Z. Al Kanaani, E. Al Kuwari, A. Jeremijenko, A. H. Kaleeckal, A. N. Latif, R. M. Shaik, H. F. Abdul Rahim, G. K. Nasrallah, M. G. Al Kuwari, A. A. Butt, H. E. Al Romaihi, M. H. Al-Thani, A. Al Khal, R. Bertollini, Association of prior SARS-CoV-2 infection with risk of breakthrough infection following mRNA vaccination in Qatar. *JAMA* **326**, 1930–1939 (2021).
27. S. Gazit, R. Shlezinger, G. Perez, R. Lotan, A. Peretz, A. Ben-Tov, E. Herzel, H. Alapi, D. Cohen, K. Muhsen, G. Chodick, T. Patalon, Severe Acute Respiratory Syndrome Coronavirus 2 (SARS-CoV-2) Naturally acquired immunity versus vaccine-induced immunity, reinfections versus breakthrough infections: A retrospective cohort study. *Clin. Infect. Dis.* **75**, e545–e551 (2022).
28. Y. Goldberg, M. Mandel, Y. M. Bar-On, O. Bodenheimer, L. S. Freedman, N. Ash, S. Alroy-Preis, A. Huppert, R. Milo, Protection and waning of natural and hybrid immunity to SARS-CoV-2. *N. Engl. J. Med.* **386**, 2201–2212 (2022).
29. D. Sterlin, A. Mathian, M. Miyara, A. Mohr, F. Anna, L. Claër, P. Quentric, J. Fadlallah, H. Devilliers, P. Ghillani, C. Gunn, R. Hockett, S. Mudumba, A. Guihot, C. E. Luyt, J. Mayaux, A. Beurton, S. Fourati, T. Bruel, O. Schwartz, J. M. Lacorte, H. Yssel, C. Parizot, K. Dorgham, P. Charneau, Z. Amoura, G. Gorochov, IgA dominates the early neutralizing antibody response to SARS-CoV-2. *Sci. Transl. Med.* **13**, eabd2223 (2021).
30. F. N. Zervou, P. Louie, A. Stachel, I. M. Zacharioudakis, Y. Ortiz-Mendez, K. Thomas, M. E. Aguero-Rosenfeld, SARS-CoV-2 antibodies: IgA correlates with severity of disease in early COVID-19 infection. *J. Med. Virol.* **93**, 5409–5415 (2021).
31. L. R. Baden, H. M. El Sahly, B. Essink, K. Kotloff, S. Frey, R. Novak, D. Diemert, S. A. Spector, N. Rouphael, C. B. Creech, J. McGettigan, S. Khetan, N. Segall, J. Solis, A. Brosz, C. Fierro, H. Schwartz, K. Neuzil, L. Corey, P. Gilbert, H. Janes, D. Follmann, M. Marovich, J. Mascola, L. Polakowski, J. Ledgerwood, B. S. Graham, H. Bennett, R. Pajon, C. Knightly, B. Leav, W. Deng, H. Zhou, S. Han, M. Ivarsson, J. Miller, T. Zaks, Efficacy and safety of the mRNA-1273 SARS-CoV-2 vaccine. *N. Engl. J. Med.* **384**, 403–416 (2020).
32. F. P. Polack, S. J. Thomas, N. Kitchin, J. Absalon, A. Gurtman, S. Lockhart, J. L. Perez, G. Pérez Marc, E. D. Moreira, C. Zerbini, R. Bailey, K. A. Swanson, S. Roychoudhury, K. Koury, P. Li, W. V. Kalina, D. Cooper, R. W. Frenck, L. L. Hammitt, Ö. Türeci, H. Nell, A. Schaefer, S. Ünal, D. B. Tresnan, S. Mather, P. R. Dormitzer, U. Şahin, K. U. Jansen, W. C. Gruber, Safety and efficacy of the BNT162b2 mRNA covid-19 vaccine. *N. Engl. J. Med.* **383**, 2603–2615 (2020).
33. D. Steensels, N. Pierlet, J. Penders, D. Mesotten, L. Heylen, Comparison of SARS-CoV-2 antibody response following vaccination with BNT162b2 and mRNA-1273. *JAMA* **326**, 1533–1535 (2021).
34. P. Naaber, L. Tserel, K. Kangro, E. Sepp, V. Jürjenson, A. Adamson, L. Haljasmägi, A. P. Rumm, R. Maruste, J. Kärner, J. M. Gerhold, A. Planken, M. Ustav, K. Kisand, P. Peterson, Dynamics of antibody response to BNT162b2 vaccine after six months: A longitudinal prospective study. *Lancet Reg. Health Eur.* **10**, 100208 (2021).
35. J. Wei, N. Stoesser, P. C. Matthews, D. Ayoubkhani, R. Studley, I. Bell, J. I. Bell, J. N. Newton, J. Farrar, I. Diamond, E. Rourke, A. Howarth, B. D. Marsden, S. Hoosdally, E. Y. Jones, D. I. Stuart, D. W. Crook, T. E. A. Peto, K. B. Pouwels, D. W. Eyre, A. S. Walker; COVID-19 Infection Survey team, Antibody responses to SARS-CoV-2 vaccines in 45,965 adults from the general population of the United Kingdom. *Nat. Microbiol.* **6**, 1140–1149 (2021).
36. P. B. Gilbert, D. C. Montefiori, A. B. McDermott, Y. Fong, D. Benkeser, W. Deng, H. Zhou, C. R. Houchens, K. Martins, L. Jayashankar, F. Castellino, B. Flach, B. C. Lin, S. O'Connell, C. McDanal, A. Eaton, M. Sarzotti-Kelsoe, Y. Lu, C. Yu, B. Borate, L. W. P. van der Laan,

N. S. Hejazi, C. Huynh, J. Miller, H. M. El Sahly, L. R. Baden, M. Baron, L. De La Cruz, C. Gay, S. Kalams, C. F. Kelley, M. P. Andrasik, J. G. Kublin, L. Corey, K. M. Neuzil, L. N. Carpp, R. Pajon, D. Follmann, R. O. Donis, R. A. Koup, Immune correlates analysis of the mRNA-1273 COVID-19 vaccine efficacy clinical trial. *Science* **375**, 43–50 (2022).

37. D. S. Khoury, D. Cromer, A. Reynaldi, T. E. Schlub, A. K. Wheatley, J. A. Juno, K. Subbarao, S. J. Kent, J. A. Triccas, M. P. Davenport, Neutralizing antibody levels are highly predictive of immune protection from symptomatic SARS-CoV-2 infection. *Nat. Med.* **27**, 1205–1211 (2021).
38. M. H. Korhonen, J. Brunstein, H. Haario, A. Katnikov, R. Rescaldani, K. Hedman, A new method with general diagnostic utility for the calculation of immunoglobulin G avidity. *Clin. Diagn. Lab. Immunol.* **6**, 725–728 (1999).
39. G. J. Thorbecke, A. R. Amin, V. K. Tsiagbe, Biology of germinal centers in lymphoid tissue. *FASEB J.* **8**, 832–840 (1994).
40. C. Havenar-Daughton, M. Lindqvist, A. Heit, J. E. Wu, S. M. Reiss, K. Kendric, S. Bélanger, S. P. Kasturi, E. Landais, R. S. Akondy, H. M. McGuire, M. Bothwell, P. A. Vagefi, E. Scully, G. D. Tomaras, M. M. Davis, P. Poignard, R. Ahmed, B. D. Walker, B. Pulendran, M. J. McElrath, D. E. Kaufmann, S. Crotty, M. A. Price, J. Gilmour, P. Fast, A. Kamali, E. J. Sanders, O. Onzala, S. Allen, E. Hunter, E. Karita, W. Kilembe, S. Lakhi, M. Inambao, CXCL13 is a plasma biomarker of germinal center activity. *Proc. Natl. Acad. Sci. U.S.A.* **113**, 2702–2707 (2016).
41. J. M. Mabuka, A.-S. Dugast, D. M. Muema, T. Reddy, Y. Ramlakhan, Z. Euler, N. Ismail, A. Moodley, K. L. Dong, L. Morris, B. D. Walker, G. Alter, T. Ndung'u, Plasma CXCL13 but Not B cell frequencies in acute HIV infection predicts emergence of cross-neutralizing antibodies. *Front. Immunol.* **8**, 1104 (2017).
42. F. Moukambi, H. Rabezanahary, Y. Fortier, V. Rodrigues, J. Clain, G. Benmadid-Laktout, O. Zghidi-Abouzid, C. Soundaramourty, M. Laforge, J. Estaquier, Mucosal T follicular helper cells in SIV-infected rhesus macaques: Contributing role of IL-27. *Mucosal Immunol.* **12**, 1038–1054 (2019).
43. Q. X. Long, B. Z. Liu, H. J. Deng, G. C. Wu, K. Deng, Y. K. Chen, P. Liao, J. F. Qiu, Y. Lin, X. F. Cai, D. Q. Wang, Y. Hu, J. H. Ren, N. Tang, Y. Y. Xu, L. H. Yu, Z. Mo, F. Gong, X. L. Zhang, W. G. Tian, L. Hu, X. X. Zhang, J. L. Xiang, H. X. Du, H. W. Liu, C. H. Lang, X. H. Luo, S. B. Wu, X. P. Cui, Z. Zhou, M. M. Zhu, J. Wang, C. J. Xue, X. F. Li, L. Wang, Z. J. Li, K. Wang, C. C. Niu, Q. J. Yang, X. J. Tang, Y. Zhang, X. M. Liu, J. J. Li, D. C. Zhang, F. Zhang, P. Liu, J. Yuan, Q. Li, J. L. Hu, J. Chen, A. L. Huang, Antibody responses to SARS-CoV-2 in patients with COVID-19. *Nat. Med.* **26**, 845–848 (2020).
44. K. Röltgen, A. E. Powell, O. F. Wirz, B. A. Stevens, C. A. Hogan, J. Najeeb, M. Hunter, H. Wang, M. K. Sahoo, C. Huang, F. Yamamoto, M. Manohar, J. Manalac, A. R. Otrelo-Cardoso, T. D. Pham, A. Rustagi, A. J. Rogers, N. H. Shah, C. A. Blish, J. R. Cochran, T. S. Jardetzky, J. L. Zehnder, T. T. Wang, B. Narasimhan, S. Gombar, R. Tibshirani, K. C. Nadeau, P. S. Kim, B. A. Pinsky, S. D. Boyd, Defining the features and duration of antibody responses to SARS-CoV-2 infection associated with disease severity and outcome. *Sci. Immunol.* **5**, eabe0240 (2020).
45. C. A. Pierce, P. Preston-Hurlburt, Y. Dai, C. B. Aschner, N. Cheshenko, B. Galen, S. J. Garforth, N. G. Herrera, R. K. Jangra, N. C. Morano, E. Orner, S. Sy, K. Chandran, J. Dziura, S. C. Almo, A. Ring, M. J. Keller, K. C. Herold, B. C. Herold, Immune responses to SARS-CoV-2 infection in hospitalized pediatric and adult patients. *Sci. Transl. Med.* **12**, eabd5487 (2020).
46. P. Brandtzaeg, F.-E. Johansen, Mucosal B cells: Phenotypic characteristics, transcriptional regulation, and homing properties. *Immunol. Rev.* **206**, 32–63 (2005).
47. L. Grzelak, S. Temmam, C. Planchais, C. Demeret, L. Tondeur, C. Huon, F. Guivel-Benhassine, I. Staropoli, M. Chazal, J. Dufloo, D. Planas, J. Buchrieser, M. M. Rajah, R. Robinot, F. Porrot, M. Albert, K. Y. Chen, B. Crescenzo-Chaigne, F. Donati, F. Anna, P. Souque, M. Gransagne, J. Bellalou, M. Nowakowski, M. Backovic, L. Bouadma, L. Le Fevre, Q. Le Hingrat, D. Descamps, A. Pourbaix, C. Laouénan, J. Ghosn, Y. Yazdanpanah, C. Besombes, N. Jolly, S. Pellerin-Fernandes, O. Cheny, M. N. Ungeheuer, G. Mellon, P. Morel, S. Rolland, F. A. Rey, S. Behillil, V. Enouf, A. Lemaitre, M. A. Créach, S. Petres, N. Escriou, P. Charneau, A. Fontanet, B. Hoen, T. Bruel, M. Eloit, H. Mouquet, O. Schwartz, S. van der Werf, A comparison of four serological assays for detecting anti-SARS-CoV-2 antibodies in human serum samples from different populations. *Sci. Transl. Med.* **12**, eabc3103 (2020).
48. P. Wang, M. S. Nair, L. Liu, S. Iketani, Y. Luo, Y. Guo, M. Wang, J. Yu, B. Zhang, P. D. Kwong, B. S. Graham, J. R. Mascola, J. Y. Chang, M. T. Yin, M. Sobieszczyk, C. A. Kyratsous, L. Shapiro, Z. Sheng, Y. Huang, D. D. Ho, Antibody resistance of SARS-CoV-2 variants B.1.351 and B.1.1.7. *Nature* **593**, 130–135 (2021).
49. T. Zhou, L. Wang, J. Misasi, A. Pegu, Y. Zhang, D. R. Harris, A. S. Olia, C. A. Talana, E. S. Yang, M. Chen, M. Choe, W. Shi, I. T. Teng, A. Creanga, C. Jenkins, K. Leung, T. Liu, E. D. Stancofski, T. Stephens, B. Zhang, Y. Tsybovsky, B. S. Graham, J. R. Mascola, N. J. Sullivan, P. D. Kwong, Structural basis for potent antibody neutralization of SARS-CoV-2 variants including B.1.1.529. *Science* **376**, eabn8897 (2022).
50. F. Amanat, M. Thapa, T. Lei, S. M. S. Ahmed, D. C. Adelsberg, J. M. Carreño, S. Strohmeier, A. J. Schmitz, S. Zafar, J. Q. Zhou, W. Rijnink, H. Alshammary, N. Borcherding, A. G. Reiche, K. Srivastava, E. M. Sordillo, H. van Bakel, J. S. Turner, G. Bajic, V. Simon, A. H. Ellebedy, F. Krammer, SARS-CoV-2 mRNA vaccination induces functionally diverse antibodies to NTD, RBD, and S2. *Cell* **184**, 3936–3948.e10 (2021).
51. G. Cerutti, Y. Guo, T. Zhou, J. Gorman, M. Lee, M. Rapp, E. R. Reddem, J. Yu, F. Bahna, J. Bimela, Y. Huang, P. S. Katsamba, L. Liu, M. S. Nair, R. Rawi, A. S. Olia, P. Wang, B. Zhang, G. Y. Chuang, D. D. Ho, Z. Sheng, P. D. Kwong, L. Shapiro, Potent SARS-CoV-2 neutralizing antibodies directed against spike N-terminal domain target a single supersite. *Cell Host Microbe* **29**, 819–833.e7 (2021).
52. N. Suryadevara, S. Shrihari, P. Gilchuk, L. A. VanBlargan, E. Binshtein, S. J. Zost, R. S. Nargi, R. E. Sutton, E. S. Winkler, E. C. Chen, M. E. Fouch, E. Davidson, B. J. Doranz, R. E. Chen, P. Y. Shi, R. H. Carnahan, L. B. Thackray, M. S. Diamond, J. E. Crowe Jr., Neutralizing and protective human monoclonal antibodies recognizing the N-terminal domain of the SARS-CoV-2 spike protein. *Cell* **184**, 2316–2331.e15 (2021).
53. W. N. Voss, Y. J. Hou, N. V. Johnson, G. Delidakis, J. E. Kim, K. Javanmardi, A. P. Horton, F. Bartzoka, C. J. Paresi, Y. Tanno, C.-W. Chou, S. A. Abbasi, W. Pickens, K. George, D. R. Boutz, D. M. Towers, J. R. McDaniel, D. Billick, J. Goike, L. Rowe, D. Batra, J. Pohl, J. Lee, S. Gangappa, S. Sambhara, M. Gadush, N. Wang, M. D. Person, B. L. Iverson, J. D. Gollihar, J. M. Dye, A. S. Herbert, I. J. Finkelstein, R. S. Baric, J. S. McLellan, G. Georgiou, J. J. Lavinder, G. C. Ippolito, Prevalent, protective, and convergent IgG recognition of SARS-CoV-2 non-RBD spike epitopes. *Science* **372**, 1108–1112 (2021).
54. Q. Wang, Y. Guo, S. Iketani, M. S. Nair, Z. Li, H. Mohri, M. Wang, J. Yu, A. D. Bowen, J. Y. Chang, J. G. Shah, N. Nguyen, Z. Chen, K. Meyers, M. T. Yin, M. E. Sobieszczyk, Z. Sheng, Y. Huang, L. Liu, D. D. Ho, Antibody evasion by SARS-CoV-2 Omicron subvariants BA.2.12.1, BA.4 and BA.5. *Nature* **608**, 603–608 (2022).
55. E. Takashita, S. Yamayoshi, V. Simon, H. van Bakel, E. M. Sordillo, A. Pekosz, S. Fukushi, T. Suzuki, K. Maeda, P. Halfmann, Y. Sakai-Tagawa, M. Ito, S. Watanabe, M. Imai, H. Hasegawa, Y. Kawaoka, Efficacy of antibodies and antiviral drugs against omicron BA.2.12.1, BA.4, and BA.5 subvariants. *N. Engl. J. Med.* **387**, 468–470 (2022).
56. J. Gutiérrez, C. Maroto, Are IgG antibody avidity assays useful in the diagnosis of infectious diseases? A review. *Microbios* **87**, 113–121 (1996).
57. I. C. MacLennan, A. Gulbranson-Judge, K. M. Toellner, M. Casamayor-Palleja, E. Chan, D. M. Sze, S. A. Luther, H. A. Orbea, The changing preference of T and B cells for partners as T-dependent antibody responses develop. *Immunol. Rev.* **156**, 53–66 (1997).
58. T. Defrance, M. Taillardet, L. Genestier, T cell-independent B cell memory. *Curr. Opin. Immunol.* **23**, 330–336 (2011).
59. S. Fagarasan, T. Honjo, T-Independent immune response: New aspects of B cell biology. *Science* **290**, 89–92 (2000).
60. A. E. Denton, S. Innocentin, E. J. Carr, B. M. Bradford, F. Lafouresse, N. A. Mabbott, U. Mörbe, B. Ludewig, J. R. Groom, K. L. Good-Jacobson, M. A. Linterman, Type I interferon induces CXCL13 to support ectopic germinal center formation. *J. Exp. Med.* **216**, 621–637 (2019).
61. Y. M. Bar-On, Y. Goldberg, M. Mandel, O. Bodenheimer, O. Amir, L. Freedman, S. Alroy-Preis, N. Ash, A. Huppert, R. Milo, Protection by a fourth dose of BNT162b2 against Omicron in Israel. *N. Engl. J. Med.* **386**, 1712–1720 (2022).
62. M. Bemark, D. Angeletti, Know your enemy or find your friend?—Induction of IgA at mucosal surfaces. *Immunol. Rev.* **303**, 83–102 (2021).
63. M. I. Samanovic, A. R. Cornelius, S. L. Gray-Gaillard, J. R. Allen, T. Karmacharya, J. P. Wilson, S. W. Hyman, M. Tuen, S. B. Koralov, M. J. Mulligan, R. S. Herati, Robust immune responses are observed after one dose of BNT162b2 mRNA vaccine dose in SARS-CoV-2–experienced individuals. *Sci. Transl. Med.* **14**, eabi8961 (2022).
64. K. Karikó, H. Muramatsu, F. A. Welsh, J. Ludwig, H. Kato, S. Akira, D. Weissman, Incorporation of pseudouridine into mrna yields superior nonimmunogenic vector with increased translational capacity and biological stability. *Mol. Ther.* **16**, 1833–1840 (2008).
65. P. Matzinger, Tolerance, danger, and the extended family. *Annu. Rev. Immunol.* **12**, 991–1045 (1994).
66. J. S. Turner, J. A. O'Halloran, E. Kalaidina, W. Kim, A. J. Schmitz, J. Q. Zhou, T. Lei, M. Thapa, R. E. Chen, J. B. Case, F. Amanat, A. M. Rauseo, A. Haile, X. Xie, M. K. Klebert, T. Suessen, W. D. Middleton, P.-Y. Shi, F. Krammer, S. A. Teefey, M. S. Diamond, R. M. Presti, A. H. Ellebedy, SARS-CoV-2 mRNA vaccines induce persistent human germinal centre responses. *Nature* **596**, 109–113 (2021).
67. W. Kim, J. Q. Zhou, S. C. Horvath, A. J. Schmitz, A. J. Sturtz, T. Lei, Z. Liu, E. Kalaidina, M. Thapa, W. B. Alsoussi, A. Haile, M. K. Klebert, T. Suessen, L. Parra-Rodriguez, P. A. Mudd, S. P. J. Whelan, W. D. Middleton, S. A. Teefey, I. Pusic, J. A. O'Halloran, R. M. Presti, J. S. Turner, A. H. Ellebedy, Germinal centre-driven maturation of B cell response to mRNA vaccination. *Nature* **604**, 141–145 (2022).
68. V. Rodrigues, M. Laforge, L. Campillo-Gimenez, C. Soundaramourty, A. Correia-de-Oliveira, R. J. Dinis-Oliveira, A. Ouaissi, A. Cordeiro-da-Silva, R. Silvestre, J. Estaquier, Abortive T follicular helper development is associated with a defective humoral response in Leishmania infantum-infected macaques. *PLOS Pathog.* **10**, e1004096 (2014).
69. F. Moukambi, H. Rabezanahary, V. Rodrigues, G. Racine, L. Robitaille, B. Krust, G. Andreani, C. Soundaramourty, R. Silvestre, M. Laforge, J. Estaquier, Correction: Early loss of splenic Tfh cells in SIV-infected rhesus macaques. *PLOS Pathog.* **12**, e1005393 (2016).

70. D. H. Katz, B. Benacerraf, in *Advances in Immunology*, F. J. Dixon, H. G. Kunkel, Eds. (Academic Press, 1972), vol. 15, pp. 1–94.
71. N. A. Mitchison, The carrier effect in the secondary response to hapten-protein conjugates. II. Cellular cooperation. *Eur. J. Immunol.* **1**, 18–27 (1971).
72. N. W. Palm, R. Medzhitov, Immunostimulatory activity of haptenated proteins. *Proc. Natl. Acad. Sci. U.S.A.* **106**, 4782–4787 (2009).
73. N. Schmitt, R. Morita, L. Bourdery, S. E. Bentebibel, S. M. Zurawski, J. Banchereau, H. Ueno, Human dendritic cells induce the differentiation of interleukin-21-producing T follicular helper-like cells through interleukin-12. *Immunity* **31**, 158–169 (2009).
74. L. B. Rodda, P. A. Morawski, K. B. Pruner, M. L. Fahning, C. A. Howard, N. Franko, J. Logue, J. Eggenberger, C. Stokes, I. Golez, M. Hale, M. Gale Jr., H. Y. Chu, D. J. Campbell, M. Pepper, Imprinted SARS-CoV-2-specific memory lymphocytes define hybrid immunity. *Cell* **185**, 1588–1601.e14 (2022).
75. D. Pichler, M. Baumgartner, J. Kimpel, A. Rössler, L. Riepler, K. Bates, V. Fleischer, D. von Laer, W. Borena, R. Würzner, Marked increase in avidity of SARS-CoV-2 antibodies 7-8 months after infection is not diminished in old age. *J Infect Dis* **224**, 764–770 (2021).
76. A. T. Tan, M. Linster, C. W. Tan, N. Le Bert, W. N. Chia, K. Kunasegaran, Y. Zhuang, C. Y. L. Tham, A. Chia, G. J. D. Smith, B. Young, S. Kalimuddin, J. G. H. Low, D. Lye, L. F. Wang, A. Bertoletti, Early induction of functional SARS-CoV-2-specific T cells associates with rapid viral clearance and mild disease in COVID-19 patients. *Cell Rep.* **34**, 108728 (2021).
77. M. Malbec, F. Porrot, R. Rua, J. Horwitz, F. Klein, A. Halper-Stromberg, J. F. Scheid, C. Eden, H. Mouquet, M. C. Nussenzweig, O. Schwartz, Broadly neutralizing antibodies that inhibit HIV-1 cell to cell transmission. *J. Exp. Med.* **210**, 2813–2821 (2013).
78. I. A. Abela, L. Berlinger, M. Schanz, L. Reynell, H. F. Günthard, P. Rusert, A. Trkola, Cell-cell transmission enables HIV-1 to evade inhibition by potent CD4bs directed antibodies. *PLOS Pathog.* **8**, e1002634 (2012).
79. C. Zeng, J. P. Evans, T. King, Y.-M. Zheng, E. M. Oltz, S. P. J. Whelan, L. J. Saif, M. E. Peeples, S.-L. Liu, SARS-CoV-2 spreads through cell-to-cell transmission. *Proc. Natl. Acad. Sci. U.S.A.* **119**, e2111400119 (2022).
80. R. Kotaki, Y. Adachi, S. Moriyama, T. Onodera, S. Fukushi, T. Nagakura, K. Tonouchi, K. Terahara, L. Sun, T. Takano, A. Nishiyama, M. Shinkai, K. Oba, F. Nakamura-Uchiyama, H. Shimizu, T. Suzuki, T. Matsumura, M. Isogawa, Y. Takahashi, SARS-CoV-2 Omicron-neutralizing memory B cells are elicited by two doses of BNT162b2 mRNA vaccine. *Sci. Immunol.* **7**, eabn8590 (2022).
81. B. L. Sievers, S. Chakraborty, Y. Xue, T. Gelbart, J. C. Gonzalez, A. G. Cassidy, Y. Golan, M. Prahl, S. L. Gaw, P. S. Arunachalam, C. A. Blish, S. D. Boyd, M. M. Davis, P. Jagannathan, K. C. Nadeau, B. Pulendran, U. Singh, R. H. Scheuermann, M. B. Frieman, S. Vashee, T. T. Wang, G. S. Tan, Antibodies elicited by SARS-CoV-2 infection or mRNA vaccines have reduced neutralizing activity against Beta and Omicron pseudoviruses. *Sci. Transl. Med.* **14**, eabn7842 (2022).
82. P. Kaplonek, D. Cizmeci, S. Fischinger, A. R. Collier, T. Suscovich, C. Linde, T. Broge, C. Mann, F. Amanat, D. Dayal, J. Rhee, M. de St Aubin, E. J. Nilles, E. R. Musk, A. S. Menon, E. O. Saphire, F. Krammer, D. A. Lauffenburger, D. H. Barouch, G. Alter, mRNA-1273 and BNT162b2 COVID-19 vaccines elicit antibodies with differences in Fc-mediated effector functions. *Sci. Transl. Med.* **14**, eabm2311 (2022).

Acknowledgments: K.T. thanks the Japan Society for the Promotion of Science (KAKENHI, 21K07060) and J.E. thanks the Canada Research Chair program for their financial support. J.E. and P.C. also thank AbbVie France and AbbVie Canada for supporting this COVID-19 study. We are grateful to T. Sawyers, Medical Writer at the BESPIM, Nîmes University Hospital, France, for critical reading of the manuscript. **Funding:** This work was supported by a grant to J.E. from the Fondation pour la Recherche Médicale and the Agence nationale de la recherche (COVID-I^{2}A) as well as by a grant to P.C. from Nîmes University Hospital (NIMAO/2020/COVID/PC-01). This work was also funded by a grant to R.S. from the Foundation for Science and Technology (FCT), project UIDB/50026/2020 and UIDP/50026/2020; and by the NORTE-01-0145-FEDER-000013 and NORTE-01-0145-FEDER-000023 projects, supported by North Portugal Regional Operational Programme (NORTE 2020), under the PORTUGAL 2020 Partnership Agreement, through the European Regional Development Fund (ERDF) and FCT contracts 2021.07836.BD to A.M.-F. and CEECIND/00185/2020 to R.S. M.A. thanks the ANRS | Maladies infectieuses emergentes for his fellowship. This work was also supported by the Clinical Academic Centers (2CA-Braga) through the grant 2017 2CACOVID-AIR. **Author contributions:** Conceived and designed the experiments: M.A.D.S., P.N., K.T., R.S., P.C., F.M., and J.E. Performed the experiments: M.A.D.S., P.N., C.S., A.B.-M., M.T., D.K., O.Z.-A., and M.P. Patients' recruitment and clinics: A.M.-F., A.S.-C., A.C., C.C., J.P., A.G.C., P.L., A.S., L.M., J.-Y.L., C.R., P.-G.C., S.D., T.-A.T., and P.C. Analyzed the data: M.A.D.S., P.N., K.T., R.S., P.C., F.M., and J.E. Wrote the paper: M.A.D.S., P.N., K.T., R.S., P.C., F.M., and J.E. **Competing interests:** The authors declare that they have no competing interests. **Data and materials availability:** All data needed to evaluate the conclusions in the paper are present in the paper and/or the Supplementary Materials.

Submitted 9 December 2022
Accepted 5 July 2023
Published 4 August 2023
10.1126/sciadv.adg2122

公益財団法人日中医学協会
TEL 03-5829-9123
FAX 03-3866-9080
E-MAIL iryo@jpcnma.or.jp
〒101-0032 東京都千代田区岩本町 1-4-3
住泉KMビル6階
URL：https://www.jpcnma.or.jp/